COALESCENCE IN OIL/WATER SYSTEMS

COALESCENCE IN OIL/WATER SYSTEMS

By

KENNETH A. BURRILL, B.Eng.Sc.

M.Eng.

A Thesis

Submitted to the School of Graduate Studies

in Partial Fulfilment of the Requirements

for the Degree

Doctor of Philosophy

McMaster University

January, 1970

Acknowledgements

If this list of acknowledgements was to be exhaustive, it would be very long indeed. I therefore content myself with acknowledging a special gratitude to those people who had a direct interest in this work.

First, I thank Dr. Tom Hodgson, who introduced me to coalescence, and who patiently submitted to a constant bombardment of questions during the first eight months of this work. Secondly, I wish to thank Mr. Peter Groeneweg and Mr. Albert Liem for their critical evaluation of ideas presented to them during informal discussions.

From a technical point of view, I wish to acknowledge the special assistance of Mr. Uldis Golts of the Engineering Photography Dept., Mr. Zenon Kaptur of the University Electronic Shop, and Mr. Robert Dunn of the Chemical Engineering Machine Shop for their excellent work and advice.

I would like to thank Dr. R. B. Anderson and Dr. A. E. Hamielec of the Chemical Engineering Department, and Dr. P. Dawson and Dr. O. E. Hileman of the Chemistry Department for their helpful discussions on particular points brought up during the course of this work.

Finally, I acknowledge a special debt to two people, my wife Gayle, and my research supervisor, Dr. D. R. Woods, for their patience, advice, and constant encouragement. In

addition, my wife deserves a special thanks for typing this thesis.

Financial Acknowledgement:

I wish to thank the National Research Council for awarding a Studentship, which covered the three year period of this work, and for awarding Research Grant A2101 to finance this work.

K. A. Burrill

K. A. Burrill

Hamilton, January, 1970.

DOCTOR OF PHILOSOPHY (1970) McMASTER UNIVERSITY
(Chemical Engineering) Hamilton, Ontario.

TITLE: Coalescence in Oil/Water Systems

AUTHOR: Kenneth A. Burrill, B.Eng.Sc. (U.W.O.)
M.Eng. (McMaster University)

SUPERVISOR: Professor D. R. Woods

NUMBER OF PAGES: xxii , 436

SCOPE AND CONTENTS:

A theoretical and experimental study is presented of the effect of oil/water system physical properties, surfactant concentration, and drop size on the drop rest-time and lamella behaviour.

The work has three distinct parts. The first part is based on the assumption that the dynamic pressure distribution in the lamella can be described by a simple three term polynomial. Equations for the relative lamella thickness profile are derived and are shown to accurately describe experimental lamella thickness profiles measured both in this work and by other investigators.

The second part presents and discusses the experimentally measured drop rest-times and simultaneously observed lamella behaviour for the range of variables studied. Five mechanisms are proposed to account for the observed lamella behaviour.

The third part derives equations to describe the lamella drainage, the interfacial distribution of adsorbed surfactant for a lamella undergoing drainage, and the dynamic lamella pressure distribution. The solution of the lamella drainage equation is then compared with experimentally determined profiles of the relative lamella thickness for both the complex model and a simple model based on a parallel disc lamella.

Table of Contents

List of Tables

List of Figures

CHAPTER 1. INTRODUCTION

1. Introduction To Coalescence

Taking a stoppered glass bottle, half full of water and half full of an immiscible oil, and shaking it often results in swarms of droplets in both phases. When the bottle is then held still, the droplets congregate at both sides of the oil/water bulk interface. Gradually, the two liquids become clear again as the droplets enter their respective phases.

If the progress of one droplet in the bottle is followed, it approaches the bulk interface, rests at this interface for a length of time and then disappears into its phase, often leaving behind a small drop in its place. For purposes of discussion, the author assumes that the oil is lighter than the water, that the drop is oil and that the large horizontal oil/water interface is called the bulk interface. Since the drop is oil, the oil phase is termed the discontinuous phase, and water the continuous phase. Merging of the droplet with its own phase is called coalescence, and the sequence of events leading up to and including this coalescence is termed the coalescence process.

The time consuming step in the coalescence process is often the resting of the droplet at the oil/water bulk interface. A film or lamella of continuous phase liquid is trapped between the droplet and the bulk interface. The rest-time of the drop at the interface is determined by the time taken for the lamella to drain to a critical thickness. At

this thickness a hole suddenly and inexplicibly forms in the lamella, the contents of the drop flow into the discontinuous phase liquid, and coalescence is complete.

1.1. The Importance of Coalescence

A study of coalescence is important from both a fundamental and a practical point of view.

The study of thin liquid films such as those that occur in liquid/liquid and gas/liquid (soap films) systems allows the strength of forces operating between interfaces to be measured.

Coalescence is intimately connected with the stability of thin liquid films. The existence of foams in lakes and rivers, printer's ink, distillation columns, and automobile engine oil is of great interest. The existence of emulsions and dispersions (unstable emulsions) in liquid/liquid extraction, water purification of industrial wastes, emulsion polymerization, and decantation is also important for design of these processes.

Since decantation is a common, important chemical engineering operation, it is considered as an example. A dispersion which yields large rest-times of droplets at the bulk interface means that when it is fed to a decanter, the decanter must be large enough to give long phase residence times so coalescence can occur. From a decanter design point of view, then, it would be advantageous to be able theoretically to predict droplet rest-times. Before looking at methods

of studying the coalescence problem, a short discussion of the variables that appear to affect coalescence will be considered. This will aid in understanding the difficulties of the methods of study.

1.1-1 Coalescence Variables

A major difficulty in studying coalescence is the vast array of variables that must be controlled. There are three types of variables in coalescence; physical property variables inherent in a choice of the liquid/liquid system, variables that are externally controllable which may interact with the liquid/liquid system variables, and external variables over which the experimenter has little contol and can only minimize or be aware of their influence. These three groups are discussed in turn.

Physical property variables that directly affect coalescence are density difference between the phases, phase viscosities, and interfacial tension. Another property is the phase dipole moment. This property determines how well an electrostatic field will be conducted through the phase.

Various properties of the drop and bulk interfaces may affect coalescence. Diffusion of molecules adsorbed at the interfaces may affect the ease with which an interface will move. Also, if the surface-adsorbed molecules (surface active molecules) attract one another strongly enough, another phase may be formed at the interface. This phase may give the interface a larger viscosity than either of the bulk phases.

Another effect of this deliberately added surface active agent or surfactant is often to set up a repulsion force between two interfaces which are very close together. The presence of ionic surfactant molecules at each interface ressembles a layer of charge at each interface, and if the phase separating the two interfaces is capable of conducting an electrostatic field, the two charged layers repell one another. Often, the interfaces are close enough that van der Waals attractive force opposes the "double-layer" repulsive force, so the lamella thins until the two opposing forces are equal.

Addition of electrolyte to the electrostatically conducting phase, usually water, allows the surface charges to be almost neutralized. The lamella may then get thin enough for rupture to occur, before the double layer force becomes appreciable.

Other variables which may be controlled are temperature, drop size, the distance the drop must travel from the point where the drop is formed to the interface, and interface curvature.

Often the experimenter has little control over some variables which may influence coalescence. Vibration of the interface, initial purity of the liquids, earth magnetic field fluctuation, and cosmic disturbances have, at one time or another, been suspect.

With this brief survey of the coalescence variables, different methods of studying coalescence suggest themselves.

1.1-2 Methods of Study

Two main methods may be used to study coalescence: large scale semi-industrial studies, and idealized single drop studies. For example, large scale studies could determine the effect of different liquids, surface active agent, electrolyte, temperature, drop size, etc., on the ability to separate a mixture into two 'pure' streams. This yields empirical correlations usually for drop rest-times or coalescence band thickness versus the variables for each system. There are many difficulties with this approach, such as the purity in large systems (> 1 litre volume). Drop size must be accurately measured, and the influence of drop internal circulation and surrounding droplets should be known to make accurate prediction possible. This approach also yields little insight into the actual mechanisms of the coalescence process.

A simpler idealized approach is to consider only a single drop and the bulk interface, or another drop. The influence of surrounding droplets is removed, purity can be more closely guarded in a smaller apparatus, and variables such as drop size and distance of drop fall may be controlled. Simple rest-time versus drop size plots yield information on the various parameters.

However, the behaviour of the lamella of continuous phase liquid is of ultimate importance since it determines rest-times. The thickness of the lamella may be measured in

two ways: by viewing the lamella parallel to the interface, or using light interference by viewing the lamella perpendicular to the interface. These two methods are outlined in Figure (1.1).

When viewing the lamella parallel to the interface, the prime prerequisite is that both liquids have very nearly the same refractive index. Only lamella thicknesses greater than 10^{-3} cm. can be observed using this technique. Another restriction is that the lamella may only be seen along a two dimensional slice. Behaviour of the lamella that may affect coalescence may be occuring in regions other than that being viewed.

The light interference technique requires the discontinuous phase liquid to have a refractive index close to that of glass and requires a large difference in refractive indices of the two liquids (> 0.10). Again, the interface is observed in only two dimensions, but here all the lamella within the barrier ring is within view and the thickness of the lamella can be determined from the interference colour, so, in essence, a three dimensional view is accorded.

Interpretation of the interference pattern can be difficult, especially when using monochromatic light. This method is limited to less than 3×10^{-4} cm. lamella thickness with white light, although there is really no upper limit when pure monochromatic light is used. A more complete discussion of this technique is given in Appendix A 3.

The emphasis of a review of past work is on the

Figure 1. Two Methods of Lamella Thickness Measurement

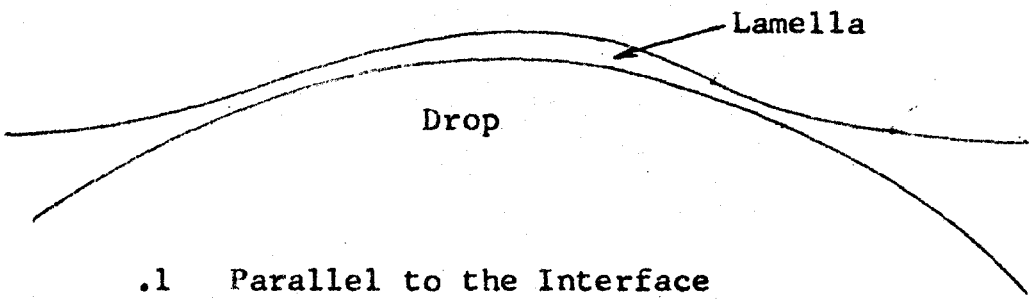

.1 Parallel to the Interface

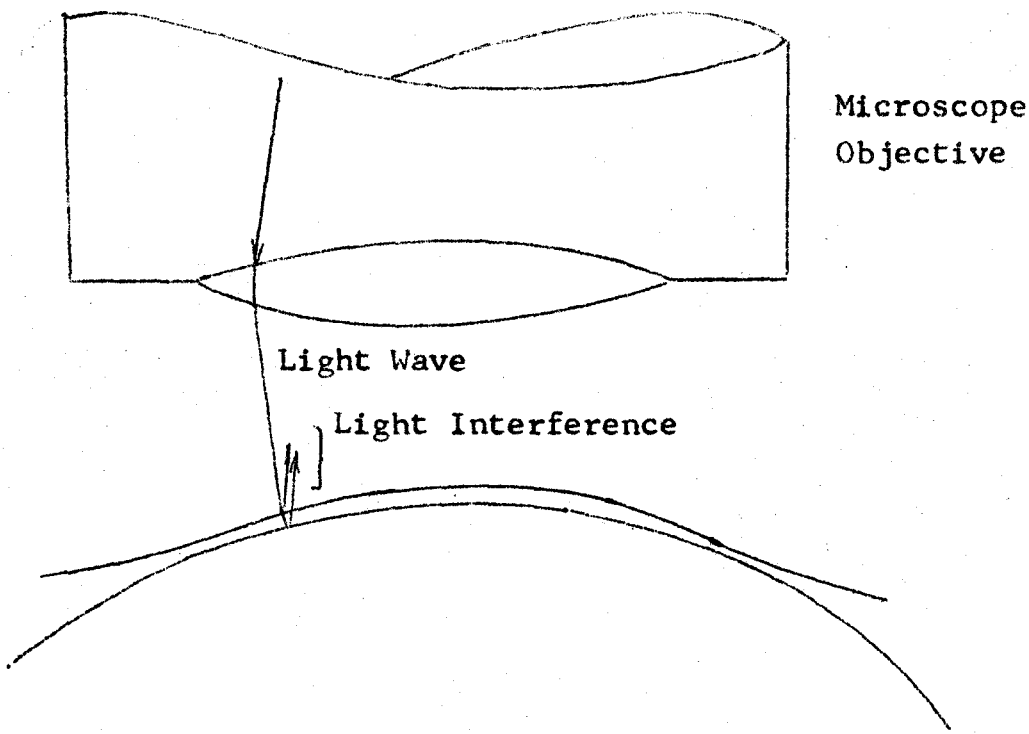

.2 Perpendicular to the Interface

idealized single drop studies. This review will consider how these two techniques have been used by the various investigators, give some of their more pertinent findings, and some criticism of their methods. When the coalescence field is then in perspective, the object and scope of this thesis are presented.

1.2. Historical Review

Most of the early work was concerned only with the rest-time of single droplets at an interface. Then the light interference technique was applied to the measurement of lamella thickness. Recently, the "through-the-side" study of lamella thickness has been used.

Each of these methods is considered in turn.

1.2.1. Rest-Time Measurement Only

There have been essentially two approaches made to the study of single drops at a bulk phase interface. One approach was concerned with only pure oil/water systems. The other approach studied the influence of added surface active agents on the drop rest-time.

With pure systems, researchers always found that drop rest-times were distributed randomly, with rest-times ranging from about one second to perhaps thirty seconds (1 - 14). These distributions of rest-time with drops observed were neither normally nor log-normally distributed. Extreme measures were often taken to attempt to ensure cleanliness of

apparatus and purity of compounds; interface cleaning procedures, such as surface impurity absorption with talc, "spilling" the interface, and suction with a capillary were used. Since systems were then supposed pure, any scatter in rest-times was attributed to uncontrollable external factors, such as mechanical vibration, kinetic temperature fluctuation, and unavoidable interfacial tension variation caused by thermal convection currents in the cell.

When surface active impurities were deliberately added to the liquid/liquid system, randomly distributed rest-times were again observed. However, the marked influence of a change in surfactant concentration overwhelmed the random fluctuations enough to allow trends in mean rest-times to be observed. The explanations for the influence of the surfactants included suggesting the existence of a double layer repulsion force for ionic surfactants, and a consideration of surface "wettability" when insoluble protein layers were present at the interface.

With the addition of only electrolytes to the pure system, the change in rest-time distributions was attributed to an electroviscous effect (13). The evidence on which these workers based this conclusion is deemed by the author to be insufficient when the results of later light interference studies are considered.

However, in 1966, Hodgson (4) developed experimental techniques that clarified earlier observations and

indeed opened up the coalescence field for renewed investigation. He devised a drop forming technique that allowed a simple Agla syringe to be used to form any size droplet easily and reproducibly. Practically, the technique is limited only by the volume of the capillary of the syringe. More significantly, a simple interface cleaning procedure was devised which showed that drop rest-times were a function of bulk interface age from time of cleaning, both with and without surfactants in the system. Considerable scatter in the rest-times was removed, and hence reproducibility of rest-times was excellent. Theoretically, Hodgson introduced qualitative and quantitative analysis to the sequence of events that must be occurring at the interfaces bounding the lamella. One of the most important results of his work is that interfaces in a pure system are unable to withstand any shear stress and will move in the direction of the shear. Pure systems give very short rest-times (< 1 second) for this reason. This shows that the systems used in past work were not pure enough, despite the elaborate and time consuming equipment and material cleaning procedures used by workers prior to 1966. As discussed by Hodgson and Lee (4) the older methods of interface cleaning may actually introduce contaminants or work so inefficiently that surface contamination is still present.

It is interesting to note that rest-time data from Hodgson's work still yield sigmoidal curves when plotted as cumulative drops versus cumulative observed rest-time, but

the spread of the curve is much narrower than in past work. The difficulty with Hodgson's work, however, is that the interpretation of rest-time data is limited in scope because of the lack of experimental knowledge about lamella shape and its behaviour. Consequently, data are interpreted in terms of a very simple mathematical model which cannot adequately describe lamella shape. Since lamella shape partially determines rest-time behaviour, the shape must be known.

1.2.2. Rest-Time Measurement and Light Interference

Once again there are two approaches. Few researchers have been concerned with the relationship between the drainage pattern revealed by interference measurements and the drop rest-time. Most have used the light interference technique to measure the rate of lamella thinning, the lamella thickness at rupture, and the lamella thickness when double layer repulsion balances van der Waals attractive force (15 - 32).

Both observation of lamella behaviour and measurement of rest-times are valuable in trying to predict drop rest-times. This is especially true if mathematical models can be found to accurately describe lamella thinning. Until recently, the modelling approach has not proved useful because the models have not been adequate.

Studies of rest-times have primarily been of bubbles or drops rather than one drop at an interface. Lindbald (18) studied the effect of humidity, electrostatic charge and

presence of surfactant on rest-time when two drops were shoved together. Scheludko (24) was not solely concerned with the rest-time of the gas bubbles he studied. He did reach the significant conclusion, as did Hodgson, that lamella drainage is hindered by the immobility of the surfactant-bearing interface because this interface can set up a gradient in interfacial tension to balance the shear stress caused by flow from the lamella.

Charles, Allan and Mason (20) studied nitrogen bubbles in a viscous liquid and reported the influence of surfactants on mean rest-time. MacKay and Mason (19) studied coalescence in liquid/liquid systems. Their systems generally contained no surfactants, and they were more concerned with lamella thinning than with rest-time.

Hodgson and Woods (17) were essentially the first to employ a study of drainage patterns in an attempt to simplify the problem of predicting rest-times. They showed that rest-times are quite different for even and uneven drainage, that trace quantities of deliberately added surfactant immensely affect the drainage patterns, identified four distinctly different drainage patterns, and proposed a simple mathematical model which predicted drop rest-times, in most cases of even drainage, to within a factor of two of the observed rest-time, for one of four observed lamella drainage patterns. This model is a two-dimensional approximation. The data used to evaluate the model were limited to two systems, anisole/water

and toluene/water, and for a small range of sodium lauryl sulfate concentrations of 10^{-6} to 10^{-4} grams/litre.

1.2.3. "Through-the-Side" Approach

Hartland (26 - 30) has studied coalescence of large drops of viscous liquids by observing coalescence parallel to the interface. He has been concerned mainly with drop-interface shape, and has attempted to predict the change in lamella shape with time for his systems. He paid little attention to drop rest-times, and his use of very viscous systems all but negates work done using surfactants since the large viscosities and drop and bulk phase circulation patterns should restrict any motion caused by the small forces acting at the surfactant-bearing interface. Purity of viscous systems is also a problem since most of the conventional interface cleaning techniques (including Hodgson's) will not function well with viscosities of the order of 30 cp.

The main advantage of this technique is the direct observation of the lamella. The main disadvantage is that the lamella is seen only in two dimensions. Drainage may seem to be even in one vertical plane, while in another vertical plane perpendicular to it uneven drainage may be taking place.

1.2.4. Evaluation of the Literature

Past workers often assumed that simple mathematical models, such as Reynolds' parallel discs model, should describe lamella thinning. This resulted in many explanations

as to why the data did not agree with the model, rather than attempts to derive new models that more closely describe the physical situation.

Use of the light interference technique to observe lamella drainage while measuring drop rest-times seems to be the most promising approach in collecting meaningful data on drop rest-times.

New theoretical insight and good data from the experimental technique of Hodgson and Woods seem to be the keys to understanding the coalescence process and to the accurate prediction of rest-times.

1.3. Object and Scope of This Thesis

The object of this thesis is to investigate the coalescence process with the aid of the light interference technique. Contributions of this thesis should be new understanding of the sequence of events extant in the lamella, the formulation of additional mathematical models to interpret experimental data, production of reproducible accurate data on lamella thickness and drop rest-time, and extension of the range of surfactant concentration and liquid/liquid system physical properties.

Experimentally, the work is limited to the study of small (<0.35 cm.) diameter oil droplets in water, with the oil lighter than the water. An ionic surfactant, sodium lauryl sulfate, and electrolyte, potassium chloride, were added to the water in varying quantities to influence the coalescence

process. Variables studied were:

1. Drop diameter
2. Distance of drop rise
3. Surfactant concentration
4. Electrolyte concentration
5. System physical properties

All other variables were either controlled, measured, or minimized where possible.

Thesis organization is based on a paper type structure since the work done is easily ordered into three distinct sections. Each paper will constitute a chapter. Experimental data, ideas, and additional work not included in the chapters, but relevant to this thesis, are included in appendices at the end of the thesis.

Bibliography

1. Cockbain, E. G. and T. S. McRoberts, J. Colloid Sci. 8 440-451 (1953).

2. Biswas, B. and D. A. Haydon, 3rd Int'l Congress on SAA, Vol. IV pg. 580-584.

3. Biswas, B. and D. A. Haydon, Kolloid Zeit. 185 31-38 (1962).

4. Hodgson, T. D. and J. C. Lee, J. Colloid and Int. Sci. 30 (1) 94-108 (1969).

5. Hawksley, J. L. and G. V. Jeffreys, A.I.Ch.E.J. 11 (3) 413-424 (1965).

6. Lawson, G. A. B. and G. V. Jeffreys, Trans. Inst. Chem. Engrs 43 T294-8 (1965).

7. Mahajan, A. D., Kolloid Zeit. 69 (1) 16-21 (1934).

8. Charles, G. E. and S. G. Mason, J. Colloid Sci. 15 (3) 235-267 (1960).

9. Neilsen, L. E., R. Wall and G. Adams, J. Colloid Sci. 13 441-458 (1958).

10. Gillespie, T. and E. K. Rideal, Trans Fara. Soc. 52 173-183 (1956).

11. Miura, M. and C. Uno, J. Sci. Hiroshima Univ. 20A (3) 171-176 (1957).

12. Weatherford, W. D. Jr., Private communication (1968).

13. Elton, G. A. H. and K. G. Picknett, 2nd Int'l Congress on SA London (1957) Vol. I pg. 288-294.

14. Watanabe, T., Bull. Chem. Soc. Japan 31 (2) 236-243 (1958).

15. Derjaguin, B. V. et al, J. Colloid Sci. 19 113-135 (1964).

16. Derjaguin, B. V. and A. S. Titievskaya, 2nd Int'l Congress on SA (London) Vol. II 211-219 (1957).

17. Hodgson, T. D. and D. R. Woods, J. Colloid and Int. Sci. 30 (4) 429-446 (1969).

18. Lindblad, N. R., J. Colloid Sci. 19 729-743 (1964).

19. MacKay, G. D. M. and S. G. Mason, J. Colloid Sci. 18 674-683 (1963).

20. Charles, G. E., R. S. Allan, and S. G. Mason, J. Colloid Sci. 16 (2) 150-165 (1961).

21. MacKay, G. D. M. and S. G. Mason, Can. J. Chem. Eng. 41 203-212 (1963).

22. Platikanov, D., J. Phys. Chem. 68 (12) 3619-3624 (1964).

23. Platikanov, D. and E. Manev, Proc. IV Int'l Congress on SAS (2) 1189-1197 (1964).

24. Scheludko, A., Kolloid Zeit. 155 39 (1957).

25. van den Temple, M., J. Colloid Sci. 13 125-133 (1958).

26. Hartland, S., Trans. Inst. Chem. Engrs (London) 45 T97-T114 (1967).

27. ibid, Chem. Eng. Sci. 24 987-995 (1969).

28. ibid, Trans. Inst. Chem Engrs 46 T275-T282 (1968).

29. ibid, Chem. Eng. Sci. 22 1675-1687 (1967).

30. ibid, J. Colloid and Int. Sci. 26 (4) 383-394 (1968).

31. Burrill, K. A. and D. R. Woods, J. Colloid and Int. Sci. 30 (4) 511-524 (1969).

32. Frankel, S. and K. J. Mysels, "Soap Films" Pergamon, London (1959).

CHAPTER 2.

LAMELLA PRESSURE DISTRIBUTION AND INTERFACE SHAPE

ABSTRACT

A method has been developed to calculate the hydrodynamic pressure distribution in a liquid film for a drop at a liquid/liquid interface. This method uses the relative thickness data obtained from light interference measurements made on the liquid film.

Once the hydrodynamic pressure distribution is known, the three-dimensional or absolute drop and bulk interface shapes can be calculated.

1. Introduction

The coalescence of liquid dispersions is important in such diverse industrial operations as waste water treatment and liquid/liquid extraction. To understand coalescence in multidroplet systems, fundamental studies have been made on single drops coalescing at a planar interface. Investigators have often used light interference or electrical conductivity methods to study the thickness of the trapped film of continuous phase fluid that prevents for a short rest time the dispersed phase droplet from coalescing.

For liquid/liquid coalescence of a single drop at an interface, both the drop and the bulk interfaces deform so that the shapes of these interfaces, bounding the trapped film, are difficult to predict. To fully understand the coalescence mechanism, the fluid flow from and in the neighborhood of the film together with the shapes of the interfaces bounding the film should be known. Information about the hydrodynamic pressure distribution in the trapped liquid film would aid in predicting both the flow and the interface shapes.

Little is known about the pressure distribution in the film for a deformable drop at a deformable interface. Hartland (1) has studied the approach of a large (1.265 cm. diameter) solid sphere to a liquid/liquid interface using an electrical conductivity method and photography. However, his film thicknesses are relatively large, greater than 10^{-3} cm., and he does not attempt to relate his calculated pressure

distribution to either film or interface shapes.

Princen (2), and Princen and Mason (3) predicted and confirmed interface shapes for a gaseous bubble at a gas/liquid interface for the case when double-layer repulsion prevents further thinning (equilibrium conditions). These authors therefore assumed no pressure distribution in the trapped film.

Jeffreys and Hawksley (4) photographed a water drop at a benzene/water interface and then calculated the film pressure distribution from the shape of the drop. This method is not accurate at small film thicknesses ($<10^{-3}$cm).

This chapter uses relative film thickness data obtained by a light interface technique to calculate the hydrodynamic pressure distribution in the film. Results of this approach are then used to predict three-dimensional drop and bulk interface shapes.

2. Experimental Part

To study film thinning for a single liquid drop at a liquid/liquid interface, the same all-glass coalescence cell used by Hodgson and Woods (5) was used. This is shown in Fig. (1).

The system studied was toluene drops in distilled water. The toluene was freshly distilled. Solutions of doubly distilled water (1 to 2 micromho resistivity) with 10^{-6} gm/liter of laboratory grade sodium lauryl sulfate and 0.01 N. potassium chloride were used. The latter chemical was added

to minimize double-layer repulsion.

To form a drop, the entire syringe assembly was moved upward until the capillary penetrated the interface. A micrometer was used to meter in a slug of 0.005 ml. of toluene into the capillary, and the syringe assembly was then lowered into position. The toluene was slowly forced from the capillary and allowed to rise to the interface as a drop. The distance of rise of the drops was less than 1 mm, and the drop was usually less than 10 seconds old when it reached the interface.

The special technique developed by Hodgson (6) of cleaning the interface and the extreme care taken to ensure cleanliness resulted in reproducible data in studying the effect of surfactants on film thinning.

The change in film thickness with time was observed and photographed through an Olympus Model MR metallurgical microscope and using a 30-watt tungsten light source. Immersion oil of the same refractive index as the glass plate was placed between the microscope lens and the glass plate to prevent reflection from the plate.

Drops usually coalesced within 10 seconds and were released at 1-minute intervals until no further changes were observed in the interference patterns for successive drops.

3. Theory

If the pressure distribution in the trapped fluid film were known as a function of time, then the change in

dimple shape could be found as a function of time, and absolute bulk and drop interface shapes could also be determined.

Normally, to determine the pressure distribution in the trapped fluid film at any instant, either the velocity distribution in the film or the absolute interface shape must be known. Film velocity distributions are not easily measured, and accurate determinations of the three-dimensional interface shapes are very difficult to obtain for small diameter drops. The photographic technique used by Hartland (7) is not sensitive enough for the region of interest in this work.

The procedure adopted in this chapter is to semiempirically describe the pressure distribution in the film. The form of the polynomial pressure correlation equation is dictated by realistic fluid dynamical boundary conditions. Equations describing the shapes of the bounding surfaces can then be written in terms of the pressure distribution. The constant required in the pressure distribution equation can then be determined by trial and error by comparing the experimental relative film shape, found from light interference measurements, with the predicted relative film shape.

3.1. The Form of the Pressure Distribution Equation

A generalized sketch of the drop and bulk interface shapes is shown in Fig. (3); a typical relative film thickness profile (dimple) is shown in Fig. (2).

Although a multi-term polynomial expression could be used to describe the film pressure distribution, a simple form

can be selected because of the hydrodynamic pressure boundary conditions. These are shown in Fig. (2) At an unknown radial distance R the pressure is zero and $\partial p/\partial r = 0$. At the centre, $r = 0, \partial p/\partial r = 0$.

An equation of the form:

$$P_r = a - br^x + cr^y \qquad \ldots.1$$

is sufficient to satisfy the boundary conditions of the pressure distribution. To further simplify this expression, let $y = x + 1$.

The fourth boundary condition to be imposed is that the pressure force must balance the drop buoyancy force. This is written:

$$\int_0^R 2\pi r P_r \, dr = Wg. \qquad \ldots.2$$

(The volume of that portion of the drop lying above or below the horizontal reference axis for drops rising or falling, respectively, does not decrease the drop buoyancy force significantly for small drops, and so is not considered. This analysis also assumes that acceleration of the interfaces is approximately zero; thus $\Sigma F \simeq 0$.)

Use of all four boundary conditions means that the constants a, b and c can be determined as functions of x and R.

Thus:

$$b = \frac{(x + 1)a}{R^x}$$

$$c = \frac{xa}{R^{x+1}}$$

and

$$a = \frac{Wg}{2\pi\eta R^2},$$

where

$$\eta = \left[\frac{1}{2} - \frac{(x + 1)}{(x + 2)} + \frac{x}{(x + 3)} \right].$$

Equations must now be derived that give the film thickness as a function of the pressure distribution.

3.2. Central Bulk Interface

It is convenient to divide the drop and bulk interfaces into the three parts shown in Fig. (3). The drop interface extends between 1 and 2, the central bulk interface between 4 and 5, and the bulk interface tail from 5 to 3, where point 3 lies at infinity. The lower "free surface" portion of the drop interface will not be considered.

The coordinate system used is also shown in Fig. (3). The horizontal axis coincides with the bulk interface tail at infinity. Let the position of the central bulk interface zenith be given by H_2 (i.e., at $r = 0$) and the height is k at any radius r. For the central bulk interface, the hydrostatic head of liquid in the film may or may not be important. If the hydrostatic head is included, a force balance on the central

bulk interface yields:

$$\gamma\left(\frac{1}{\beta_1} + \frac{1}{\beta_2}\right) - \Delta\rho gk = -P_r \,, \qquad \ldots.3$$

where β_1 and β_2 are the radii of curvature of the bulk interface, and are given by:

$$\frac{1}{\beta_1} = \frac{d^2k/dr^2}{\left[1 + (dk/dr)^2\right]^{3/2}} \,;$$

$$\frac{1}{\beta_2} = \frac{dk/dr}{r\left[1 + (dk/dr)^2\right]^{1/2}} \,.$$

To keep the analysis tractable, neglect $(dk/dr)^2$ relative to 1. This is a reasonable assumption since we find later on that:

$$\frac{dk}{dr} = 0\ (0.01)$$

and so

$$(dk/dr)^2 = 0\ (10^{-4}).$$

With this simplification and with the use of Eq. (1), Eq. (3) becomes:

$$\frac{d^2k}{dr^2} + \frac{1}{r}\frac{dk}{dr} - \frac{\Delta\rho gk}{\gamma} = -\frac{a}{\gamma} + \frac{br^x}{\gamma} - \frac{cr^{x+1}}{\gamma} \,. \qquad \ldots.3a$$

The complementary function to this ordinary second-order linear differential equation is:

$$k_c = AI_0(m) + BK_0(m),$$

where A and B are integration constants, I_0 and K_0 are modified Bessel functions of zero order, of the first and second kind, respectively, and:

$$m = re = r\sqrt{\frac{\Delta\rho g}{\gamma}}.$$

The method of variation of parameters was then used and the complete solution to Eq. (3) found to be:

$$k = AI_0(m) + BK_0(m) - I_0(m)\int_0^m \frac{K_0(m)\,\Psi(m)\,dm}{E} - K_0(m)\int_0^m \frac{-I_0(m)\,\Psi(m)\,dm}{E} \quad \ldots.3b$$

where:

$$\Psi(m) = \frac{a}{e^2} - \frac{bm^x}{e^{x+2}\gamma} + \frac{cm^{x+1}}{e^{x+3}\gamma};$$

$$E = I_0(m)K_1(m) - I_1(m)K_0(m); \quad \ldots.4$$

and I_1 and K_1 are modified Bessel functions of the first order, of the first and second kind, respectively.

Two boundary conditions can be used to determine A and B.

B.C.1: k is finite, m = 0; since $K_0 \longrightarrow +\infty$ as $m \rightarrow 0$; then $B = 0$.

B.C.2: $k = +H_2$; $m = 0$; then $A = +H_2$

since both integrals approach 0 as $m \rightarrow 0$.

The central bulk interface shape can thus be determined if x, K, and H_2 are known.

On the other hand if the hydrostatic head is neglected, a force balance on the central bulk interface yields:

$$\gamma \left(\frac{1}{\beta_1} + \frac{1}{\beta_2} \right) = -P_r \; ; \qquad \ldots.5$$

this can be written as:

$$\frac{d^2k}{dr^2} + \frac{1}{r}\frac{dk}{dr} = -\frac{a}{\gamma} + \frac{br^x}{\gamma} - \frac{cr^{x+1}}{\gamma} \; . \qquad \ldots.5a$$

This is an ordinary second-order linear differential equation, solved by reducing it to a first-order equation and integrating with the use of an integrating factor. The result is then integrated again to give:

$$k = -\frac{ar^2}{4\gamma} + \frac{br^{x+2}}{(x+2)^2\gamma} - \frac{cr^{x+3}}{(x+3)^2\gamma} + C_1 \ln r + C_2 \; , \qquad \ldots.5b$$

where C_1 and C_2 are integration constants. The two boundary conditions are as before:

B.C.1: k is finite; $r \rightarrow 0$; therefore $C_1 = 0$.

B.C.2: $k = +H_2$; $r = 0$; therefore $C_2 = +H_2$.

These two solutions for the inclusion and neglect of the hydrostatic head for the central bulk interface will

be compared later.

3.3. Drop Interface

To describe the drop interface shape, let the coordiate system be set up again as in Fig. (3). Let the position of the drop zenith be given by the distance H_1, relative to the horizontal axis, and let the drop interface height at any radius r be h, relative to the horizontal axis.

The drop is assumed small enough that it does not deform significantly because of gravity forces. This permits the use of the undeformed drop radius for calculating the relative drop internal pressure. Again, the hydrostatic head of liquid in the film may or may not be neglected. If the hydrostatic head (relative to the r - axis) is included in a force balance on the drop interface, the balance yields:

$$\gamma\left(\frac{1}{\beta_1^*}+\frac{1}{\beta_2^*}\right)+\Delta\rho gh-P_r=-\frac{2\gamma}{d}\,, \qquad \ldots.6$$

where $1/\beta_1^*$ and $1/\beta_2^*$ are now written in terms of h, the drop interface height relative to the horizontal reference axis. (This equation can be solved using the same techniques as for the central bulk interface, Eq. (3).)

If the hydrostatic head is neglected the force balance on the drop interface yields:

$$\gamma\left(\frac{1}{\beta_1^*}+\frac{1}{\beta_2^*}\right)-P_r=-\frac{2\gamma}{d}\,. \qquad \ldots.7$$

Equation (7) simplifies to :

$$\frac{d^2h}{dr^2} + \frac{1}{r}\frac{dh}{dr} = -\frac{2}{d} + \frac{a}{\gamma} - \frac{br^x}{\gamma} + \frac{cr^{x+1}}{\gamma} \quad \text{....7a}$$

This equation is integrated to give the final result:

$$h = -\frac{r^2}{2d} + \frac{ar^2}{4\gamma} - \frac{br^{x+2}}{(x+2)^2\gamma} + \frac{cr^{x+3}}{(x+3)^2\gamma} + C_3 \ln r + C_4, \quad \text{....7b}$$

where C_3 and C_4 are integration constants. The two boundary conditions are:

B.C.1 $\frac{dh}{dr} = 0$

$r = 0$ therefore $C_3 = 0$.

B.C.2 $h = H_1$

$r = 0$ therefore $C_4 = +H_1$.

The drop interface shape can thus be determined if x, R, and H_1 are known.

3.4. Bulk Interface Tail

To locate the central bulk interface segment, the location of its zenith H_2 must be determined. Whereas the value of H_2 depends on the pressure distribution in the film, we next show how the absolute position of the complete bulk interface can be determined if H_2 is known.

To do this, the shape of the bulk interface tail

needs to be determined. A force balance on the bulk interface tail yields:

$$\gamma\left(\frac{1}{\beta_1 r}+\frac{1}{\beta_2 r}\right) = \Delta\rho g k. \qquad \ldots.8$$

Simplifying the radii of curvature as before gives:

$$\frac{d^2k}{dr^2}+\frac{1}{r}\frac{dk}{dr}-\frac{\Delta\rho g k}{\gamma} = 0$$

Letting $m = er$, we get:

$$m^2\frac{d^2k}{dm^2}+m\frac{dk}{dm}-m^2k = 0. \qquad \ldots.8a$$

Equation (8a) is the modified form of Bessel's equation of order zero. Its solution is:

$$k = CI_0(m) + DK_0(m), \qquad \ldots.8b$$

where C and D are integration constants, and I_0 and K_0 are modified Bessel functions of order zero, of the first and second kind, respectively.

For the first boundary condition,

B.C.1: $k \to 0$; $m \to \infty$. Then $C = 0$ since $I_0(m) \to \infty$ as $m \to \infty$. The solution to Eq. (8) becomes:

$$k = DK_0(m). \qquad \ldots.9$$

At this point, we see that if x and R were known (pressure distribution known) the slope of the central bulk interface at $r = R$ can be approximated since $H_2I_0(m)$ is relatively constant. Thus the second boundary condition

is that

$$dk/dm \text{ is known at } m = eR$$

$$D = -\frac{dk/dm}{K_1(m)} ,$$

where K_1 is the modified Bessel function of the first order and the second kind.

Therefore, as the pressure distribution is known, the bulk interface shape and position relative to the horizontal reference axis are absolutely determined.

3.5. Film Shape

For a given pressure distribution, the absolute shapes of the drop and bulk interfaces can be calculated. By simply positioning the drop interface at any arbitrary location relative to the bulk interface (arbitrary H_1), a dimple is produced. The film thickness is then given by the equation:

$$\Delta = k - h. \qquad \ldots.10$$

Thus the pressure distribution is determined by comparing the experimental and calculated film thickness until they agree. The pressure distribution depends on three variables, a, x, and R, only two of which are independent.

However, Hodgson (9) has derived a set of equations which allow the dimple pressure at $r = 0$ to be determined from the experimental dimple shape. With reference to Fig. (4), if R_1 and R_2 are the radii of curvature of the drop and bulk

interfaces, respectively, and if Δ_0 and Δ_ϵ are the experimental film thicknesses at $r = 0$ and $r = \epsilon$, respectively, then simple geometry indicates:

$$R_1^2 = \epsilon^2 + (R_1 - Z_1)^2 . \qquad ....11$$

This may be written:

$$Z_1 = \frac{\epsilon^2}{2R_1}, \quad \text{if } Z_1 \ll R_1,$$

$$\text{and similarly, } Z_2 = \frac{\epsilon^2}{2R_2} .$$

The geometry also indicates:

$$\Delta_\epsilon = \Delta_0 + Z_1 - Z_2 . \qquad ....12$$

Now, a pressure balance at the film center yields:

$$\left(\frac{1}{R_1} + \frac{1}{R_2}\right) = \frac{1}{d} . \qquad ....13$$

Equations (12) and (13) can be solved simultaneously to yield values for R_1 and R_2, and so the film pressure at the center is then given by:

$$a = \frac{2\gamma}{R_2} . \qquad ....14$$

The above derivation assumes no pressure drop in the film between $r = 0$ and $r = \epsilon$.

4. Results and Discussion

The type of data obtainable is first presented.

Then, several assumptions made in the derivation of the preceding equations are justified. Pressure distributions are then derived from representative dimple shapes and for more restrictive geometries.

4.1. Data Obtained

Symmetric dimples are formed for interface ages less than 1 hour, for 10^{-6} grams/liter of sodium lauryl sulfate plus 0.01 N KCl. The dimple formed, for an interface age t = 16 minutes and for drop-at-interface times of θ = 0.79 second and θ = 8.7 seconds, is shown in Fig.(5).

4.2. Checking of Assumptions From Absolute Bulk and Drop Shapes

To check the assumptions used in deriving the preceding equations, absolute drop and bulk interface shapes were first calculated. A simple pressure distribution with x = 2 and R = 0.030 cm was chosen arbitrarily, and the absolute interface shapes were calculated using an I.B.M. 7040 digital computer for both force balances as expressed by Eq.(3) and Eq.(5). The resulting bulk interface shape and details are given in Table(1) for a toluene drop at a toluene/water interface.

Table(I) shows that including the hydrostatic head in the force balance has only a very slight effect on the absolute shape of the bulk interface. In evaluating the slope of the central bulk interface at m = eR, it was assumed that $H_2I_0(eR)$ was constant. The slope is found to be less than 1%

in error if this assumption is made. If greater accuracy is desired, a trial-and-error approach is necessary to locate the bulk interface more accurately.

The assumption that $dk/dr \ll 1$ was used to simplify the expressions for radii of curvature. Table (I) data show that the slopes are less than 0.01 and hence this assumption is reasonable.

The absolute bulk and drop interface shapes are also shown in Fig. (6). Here it is assumed that the hydrostatic head is negligible and that $H_2 - H_1 = 25 \times 10^{-4}$ cm. Notice that since the film pressure exceeds the drop internal pressure, the drop is dimpled.

4.3. Determining the Film Hydrodynamic Pressure Distribution From Film Thickness Data

To illustrate the applicability and ease in using the approach outlined in this chapter, dimple shapes at the opposite extremes of behavior are considered; a deep or pronounced dimple and a shallow, almost parallel disc dimple. The mathematical procedure was to determine the film pressure, a, at the center from Eq. (14) and search for the best value of x to satisfy Eq. (10) at at least 10 radial locations. To obtain accurate fits of the data in the region of the barrier ring, weighting factors were arbitrarily selected to emphasize that region, since the central region of the dimple is easily fitted.

This approach was programmed for a CDC 6400 digital computer. A simple grid search technique was used to find the

value of x which minimized the weighted difference sum of squares between calculated and experimental dimple shapes. The experimental dimple shapes used are given in Fig. (5). The results of the search techniques are given in Tables (2) and (3). Greater accuracy in the search is not warranted because the light interference technique is partially subjective, and so thicknesses could be in error up to 20%. This is especially true for the shallow dimple in Table (3).

The depth of the dimple is determined by the pressure a at the centre, and changes in x produce dimples of varying width, as shown in Fig. (7). The barrier ring radius also changes slightly as x is changed.

It can be seem from these data that the method provides an accurate representation of shapes that is flexible enough to handle the extremes of behavior.

4.4. Application to More Restrictive Geometries

This method can also be applied to aid in the understanding of specialized examples of the film thinning phenomena. As an indirect means of evaluating our approach, it is interesting to examine specialized cases. For example, Hartland (1) considered a solid sphere approaching a deformable liquid/liquid interface, and MacKay and Mason (11) and Hartland (10) photographed a dimpled drop at a solid plane surface. The approach of this chapter will now be used to qualitatively predict the dimple shapes these authors observed.

4.4.1. Deformable Drop at a Solid Plane Surface

If we neglect the hydrostatic force, a force balance on the drop interface near the flat plate yields:

$$\gamma\left(\frac{1}{\beta_1}+\frac{1}{\beta_2}\right)+P_r=\frac{2\gamma}{d}.$$

For the most general case, this can be solved to give:

$$h=\frac{r^2}{2d}-\frac{ar^2}{4\gamma}+\frac{br^{x+2}}{(x+2)^2\gamma}-\frac{cr^{x+2}}{(x+3)^2\gamma}+H, \qquad \ldots.15$$

where h is the height of the drop interface above the flat plate at any radius r, and H is the height of the drop interface centre above the flat plate (r = 0).

To calculate the dimple shape, consider the simplest pressure distribution. Let x = 2 and R = 0.030 cm. Then for a 0.005 ml toluene drop in water, the results are:

W_g = 0.652 dyne;

η = 3/20;

with

a = 768.3 dynes/cm^2;

b = 2.561 X 10^6 dynes/cm^4;

c = 5.691 X 10^7 dynes/cm^5;

d = 0.106 cm.

Let H be arbitrarily selected as $+1.0 \times 10^{-4}$ cm. Then the shape of the drop can be calculated, and is given in Fig. (8). This is similar to the shape of the drop interface shown both in MacKay and Mason's and in Hartland's papers.

4.4.2. A Solid Sphere at a Deformable Liquid/Liquid Interface

To see what the film shape may be for this case, let the toluene drop used in our analysis be undeformable.

With the hydrostatic force neglected, a force balance on the bulk interface yields:

$$-\gamma\left(\frac{1}{\beta_1}+\frac{1}{\beta_2}\right) = +P_r \,.$$

The general solution is:

$$k = \frac{-ar^2}{4\gamma} + \frac{br^{x+2}}{(x+2)^2\gamma} - \frac{cr^{x+3}}{(x+3)^2\gamma} + H_2 \,. \qquad \ldots.16$$

The sphere surface can be described by:

$$s = -d + \sqrt{d^2 - r^2} + H_1 \,,$$

where s is the distance of the sphere surface above the horizontal axis, d is the radius of the undeformed sphere, and H_1 is the height of the sphere zenith above the reference axis at $r = 0$.

If we use the same pressure distribution as in part (1) and let $H_2 - H_1 = 8 \times 10^{-5}$ cm, the dimple shape is then

given in Fig. (8). This dimple is similar in shape to those found by Hartland. Whereas Hartland attributed the dimple minimum in the centre to the hydrostatic force, this analysis indicates that this minimum is the result of having one surface of constant curvature (solid sphere) and one surface of varying curvature (curvature dependent on the hydrodynamic pressure distribution), since the secondary minimum at the center was obtained when the hydrostatic force was neglected.

4.5. Application to Larger Drops

The major restriction to the foregoing analysis is that the slopes of the drop and bulk interfaces are much smaller than unity. The application of this analysis to larger drops (0.5 ml) may be in considerable error, but it is interesting to note that dimples may be calculated which agree reasonably well with those given by Hartland (7) for large drops.

Results of hand calculations are given in Fig. (9), which shows the dimple for a 0.5 ml. glycerol drop after it has rested for 20 seconds at the glycerol/paraffin interface. Whereas the calculated hydrodynamic pressure distribution giving the agreement in Fig. (9) may be in error, the simple three-term polynomial form used for the pressure distribution appears to be flexible enough to account for this seemingly complex dimple shape. Also, since the hydrostatic head was neglected in calculating this dimple shape, the calculated pressure distribution probably more closely approximates the

the total pressure distribution in the film rather than just the hydrodynamic pressure.

4.6. General Application of This Approach

The method is very simple, requiring only an estimate of the dimple pressure at the center and an x value. The dimple pressure distribution has been determined successfully for drop diameters in the range 1.6 mm to 10 mm. The pressure distribution information is vital to the prediction of interface shapes and of subsequent thinning behavior. This latter topic is discussed in detail in Chapters 3 and 4.

Initially in this work, a Rosenbrock search technique was used to find optimum values of a and x to fit the experimental dimple shapes. However, the one-variable x approach was capable of giving as good results since the value of a changed by less than 1% of the initial value in the Rosenbrock search approach.

5. Conclusions

1. The pressure distribution within a fluid film can be determined from fundamental fluid dynamics and light interference data showing the relative thickness of the film.

2. The method requires the empirical determination from the experimental data of only one parameter, the power of variable used in the polynomial for the pressure distribution $P = a - br^x + cr^{x+1}$.

3. The pressure at the centre of the film can be

satisfactorily determined from a theoretical treatment by Hodgson. If this were not so, then the empirical correlation discussed in conclusion 2 would require two parameters, a and x.

4. The pressures do not fall to zero at the barrier ring; there is a significant pressure gradient beyond the barrier ring.

5. The absolute shapes of the interfaces can be predicted by this technique.

6. The effect of the hydrostatic head on the pressure distribution is negligible for drops of diameter 1.6 to 10 mm.

7. Film shapes of other authors can be reproduced from this technique, and this in turn gives a knowledge of the pressure distribution for these data.

8. For a solid sphere at a deformable interface a double dimple can occur even when the hydrostatic forces are negligible.

NOMENCLATURE

a = film pressure at center, dynes/cm^2.

d = drop radius, cm.

e = physical property parameter, cm^{-1} $\sqrt{\frac{\Delta \rho g}{\gamma}}$

g = 980 dynes/gram.

h = drop interface height of any radius r, cm.

H_1 = drop zenith position relative to the horizontal reference axis.

H_2 = central bulk interface zenith.

k = bulk interface height at any radius r.

P_r = film pressure at any radius r, dynes/cm^2.

r = any radial distance.

R = radius at which $P = 0$.

t = bulk interface age, minutes.

V_D = drop volume, cm^3.

W = drop weight, grams.

x = index used in pressure distribution.

Z = any vertical distance.

β = radius of curvature.

ϵ = arbitrary radius used in derivation of central film pressure.

γ = interfacial tension, dynes/cm.

Δ = film height, cm or A.

$\Delta\rho$ = density difference, grams/cm^3.

θ = elapsed time of drop at bulk interface, seconds.

PHYSICAL PROPERTIES OF TOLUENE/WATER SYSTEM

(Values taken from literature for 25°C)

$\rho_{water} = 1.0$ gm/ml.

$\rho_{toluene} = 0.867$ gm/ml.

$\gamma = 32.9$ dynes/cm.

Biblography

1. Hartland, S., J. Colloid Sci. 26 (4) 383-394 (1968).
2. Princen, H. M., J. Colloid Sci. 18 178-195 (1963).
3. Princen, H. M., and S. G. Mason, J. Colloid Sci. 25 (2) 156-172 (1965).
4. Jeffreys, G. V., and J. L. Hawksley, A.I.Ch.E.J. 11 (3) 413-424 (1965).
5. Hodgson, T. D. and D. R. Woods, J. Colloid and Int. Sci. 30 (4) 429-446 (1969).
6. Hodgson, T. D., Ph.D. Thesis, Swansea, (1966).
7. Hartland, S., Trans. Inst. Chem. Engrs. (London) 45 T97-T114 (1967).
8. Jenson, V. G. and G. V. Jeffreys, "Mathematical Methods in Chemical Engineering", pp. 56-57, Academic Press, London, (1963).
9. Hodgson, T. D., personal communication.
10. Hartland, S., Chem. Eng. Sci. 22 1675-1687 (1967).
11. MacKay, G. D. M. and S. G. Mason, Can. J. Chem. Eng. 41 203-212 (1963).

Table 1. Calculated Bulk Interface Shape

r (cm.)	Hydrostatic Head Included k (cm. x 10^2)	Hydrostatic Head Neglected k (cm. x 10^2)
0	1.2309	1.2301
0.005	1.2169	1.2158
0.010	1.1771	1.1759
0.015	1.1196	1.1181
0.020	1.0541	1.0523
0.025	0.9899	0.9877
0.030	0.9334	0.9306
0.05	0.7723	0.7700
0.10	0.5579	0.5562
0.50	0.1340	0.1336
1.0	0.0362	0.0361
1.5	0.0111	0.0110
2.0	0.0036	0.0035
2.5	0.0012	0.0012
3.0	0.0004	0.0004

Drop Diameter 0.212 cm. (0.005 ml. volume)

Toluene drop in water. Pressure distribution used was:

$$p = a - br^2 + cr^3$$

$a = 768.3$ dynes/cm.^{2}

$b = 2.561 \times 10^6$ dynes/cm.^{4}

$c = 5.691 \times 10^7$ dynes/cm.^{5}

$x = 2$

$R = 0.030$ cm.

Table 2. Experimental and Calculated Relative Lamella Shape for Large Dimple

r (cm.)	Δ (A°) Experimental	Δ (A°) Calculated	Weighting Factor λ
0	11000	11000	1
0.0025	10800	10797	4
0.0050	10000	10188	9
0.0075	9100	9173	16
0.0100	7700	7763	25
0.0125	6000	5995	36
0.0150	4400	3984	49
0.0175	2500	2002	64
0.0200	1000	586	81
0.0225	500	659	100

1. Calculated a is 332 dynes/cm.^{2}
2. Best x value based on weighted difference sum of squares is 6.1 .
3. Weighted difference sum of squares (for ten points) $= \sum \left[\left(A^{\circ}_{expt'l} - A^{\circ}_{cal'd} \right) \lambda \right]^2$

Table 3. Experimental and Calculated Relative Lamella Shape for Small Dimple

r(cm.)	Δ (A°) Experimental	Δ (A°) Calculated	Weighting Factor λ
0	1600	1600	1
0.0025	1550	1563	4
0.0050	1490	1450	9
0.0075	1200	1264	16
0.0100	950	1015	25
0.0125	600	740	36
0.0150	400	551	49
0.0175	600	693	64
0.0200	1450(est.)	1637	81
0.0225	4000(est.)	4169	100

1. Calculated a is 314.5 dynes/cm.^{2}
2. Best x value is 5.8 .
3. (est.) means that the experimental thicknesses have been estimated, since the interference rings were close together.

Figure 1. The Coalescence Cell

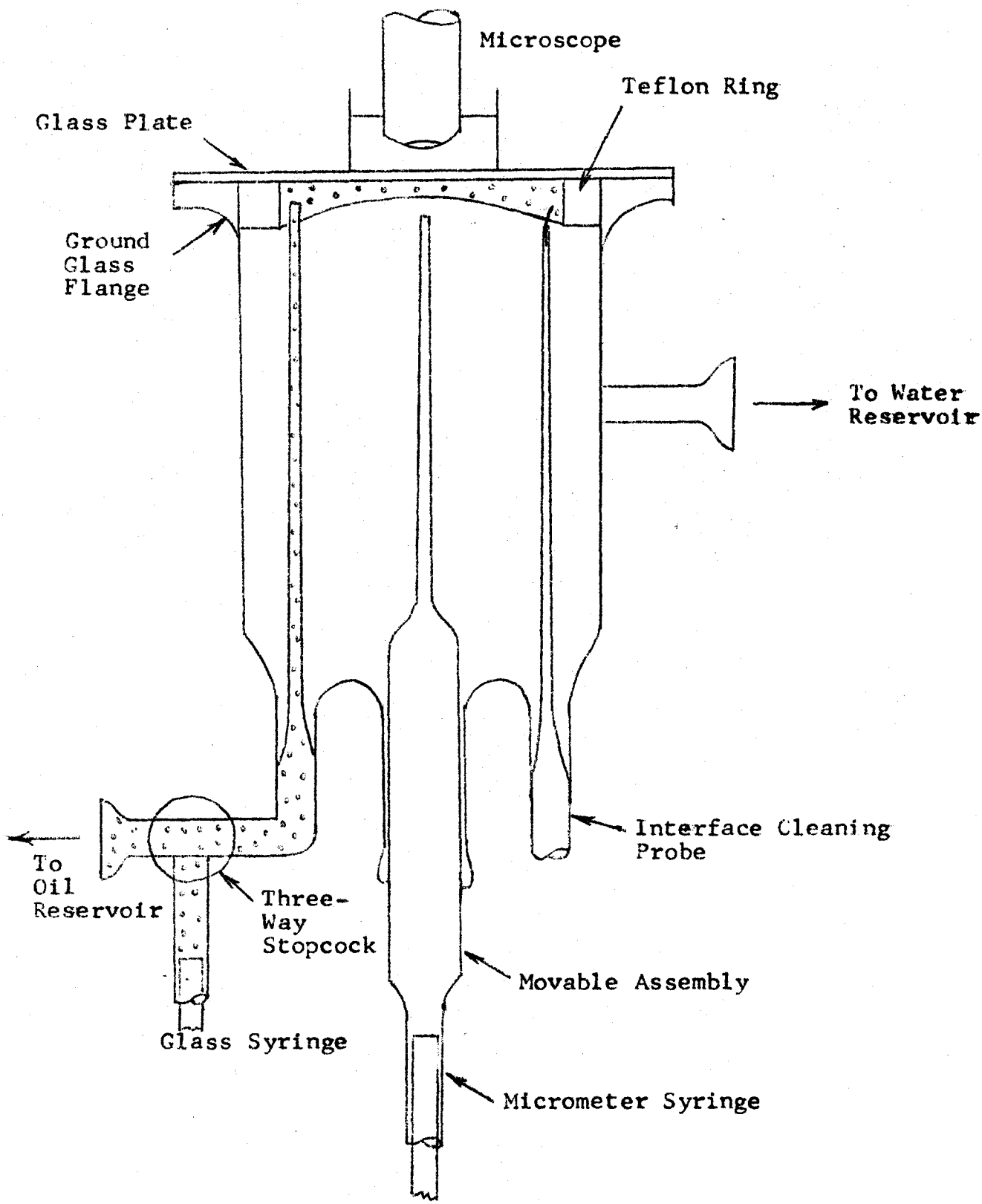

Figure 2. Typical Dimple Shape, with Boundary Conditions for Lamella Hydrodynamic Pressure Distribution

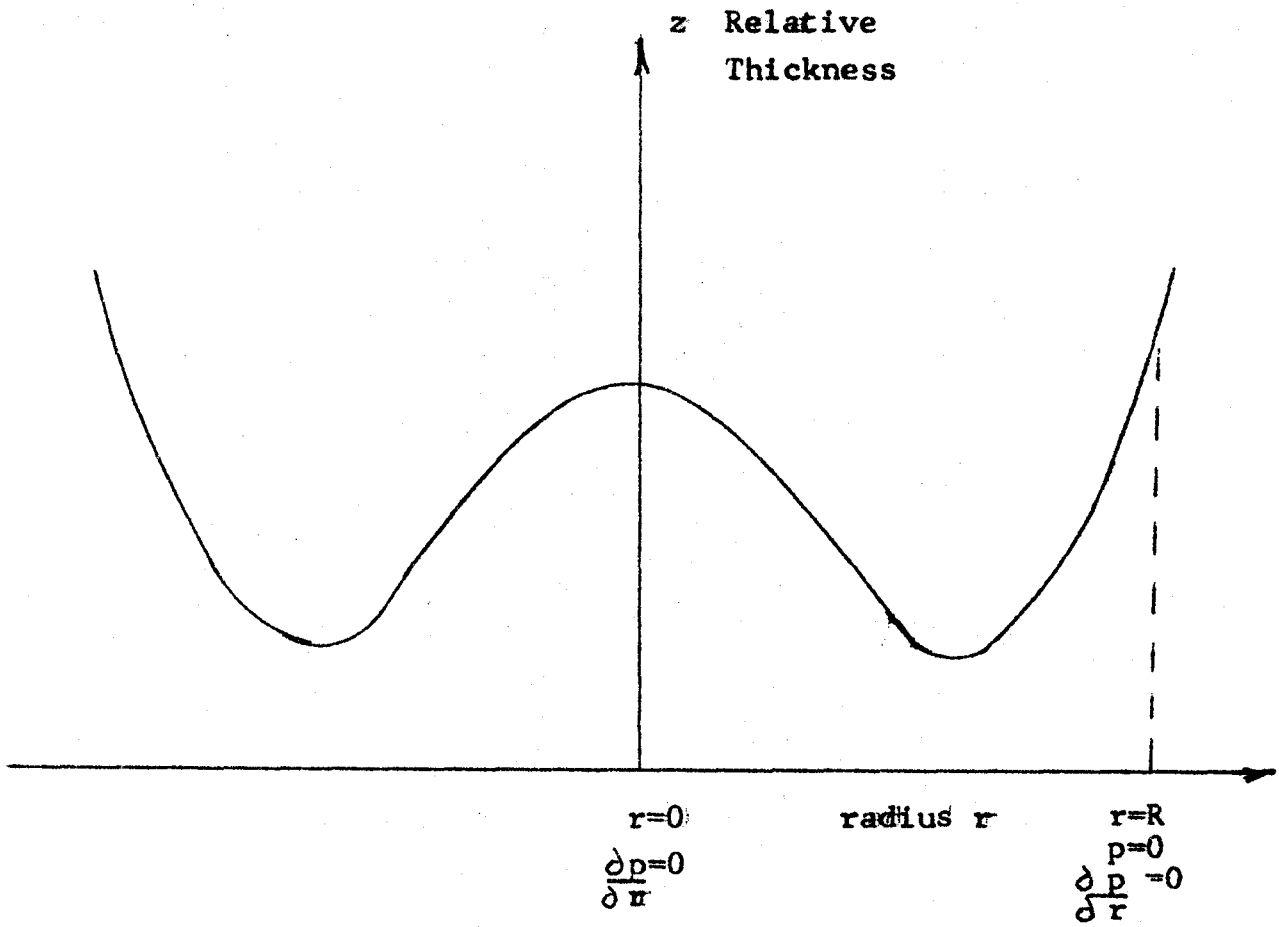

Figure 3. Drop and Bulk Interface Notation and Co-ordinate System

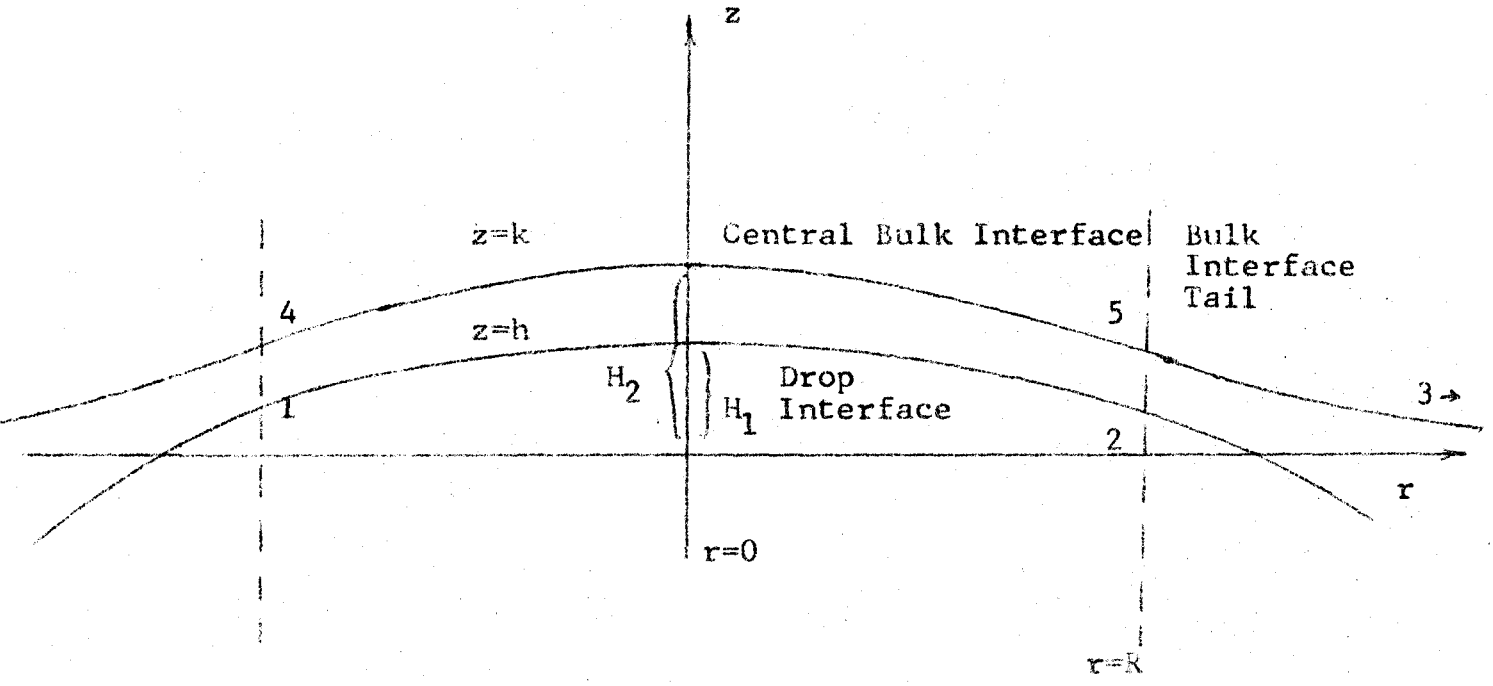

Figure 4. Geometry to Determine the Central Lamella Pressure "a"

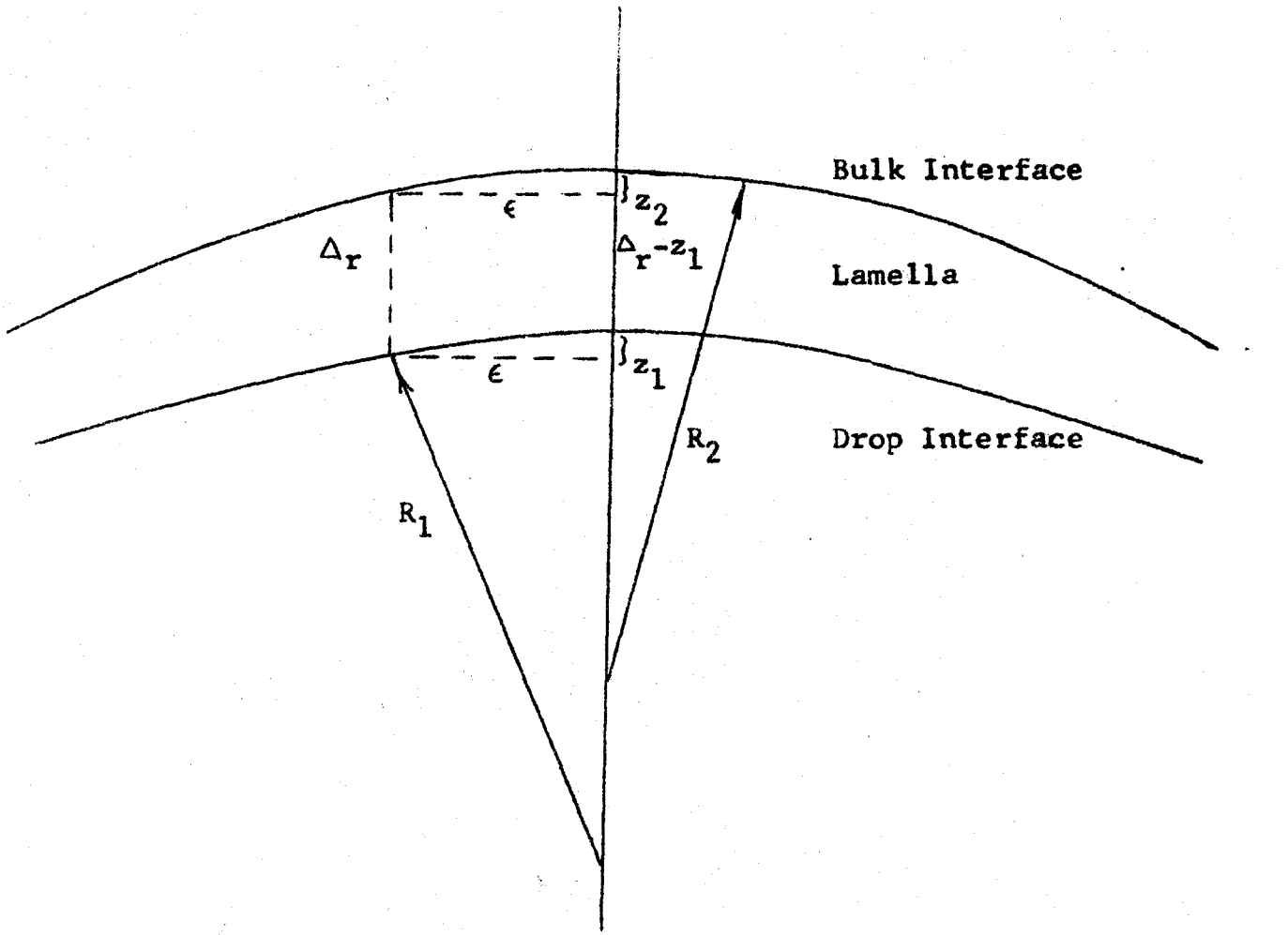

Figure 5. Experimental Relative Lamella Shapes

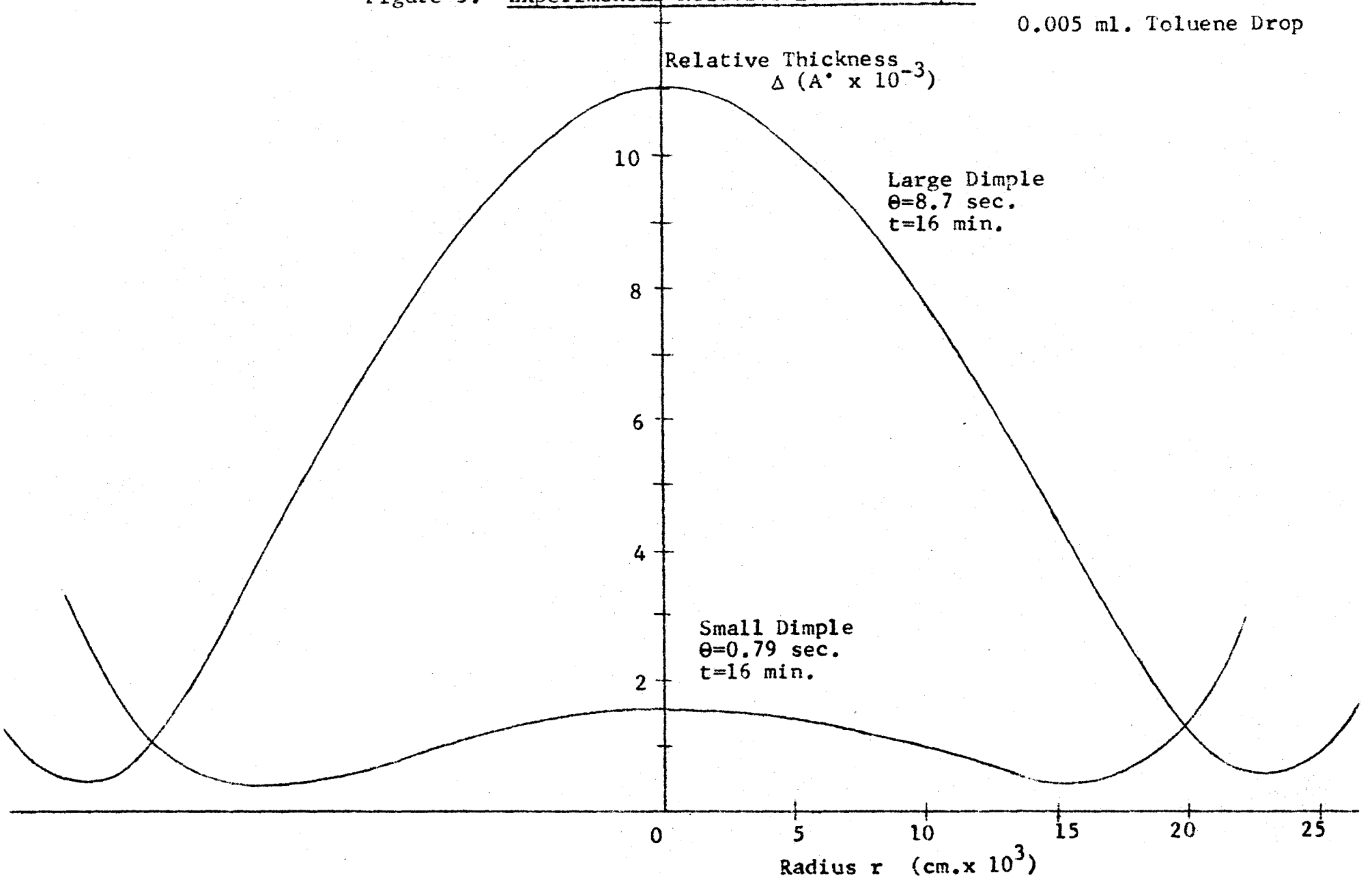

Figure 6. Three Dimensional Bulk and Drop Interface Shapes

(Axial Symmetry)

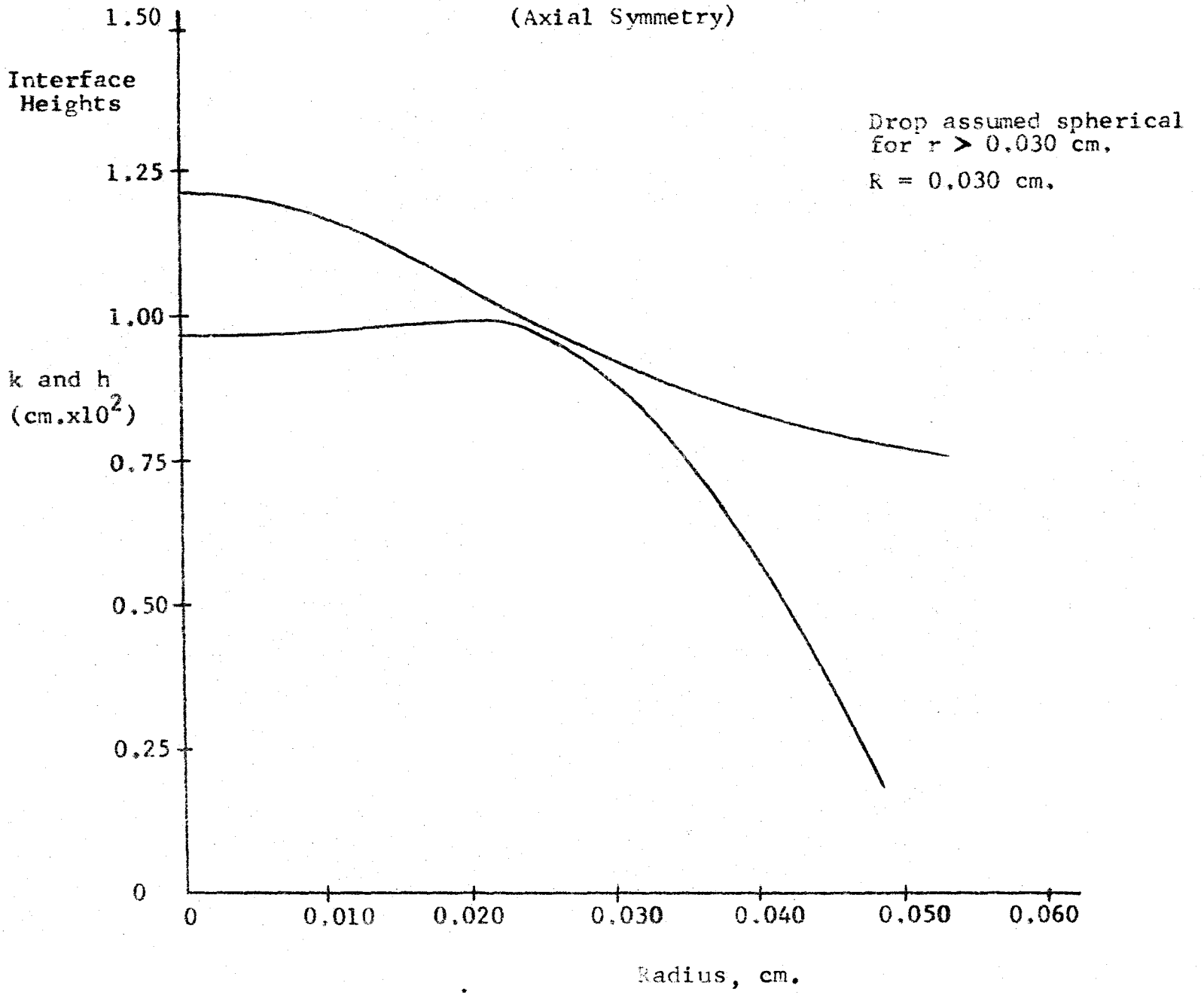

Figure 7. Effect of "x" on Dimple Shape for Given "a" and "R"

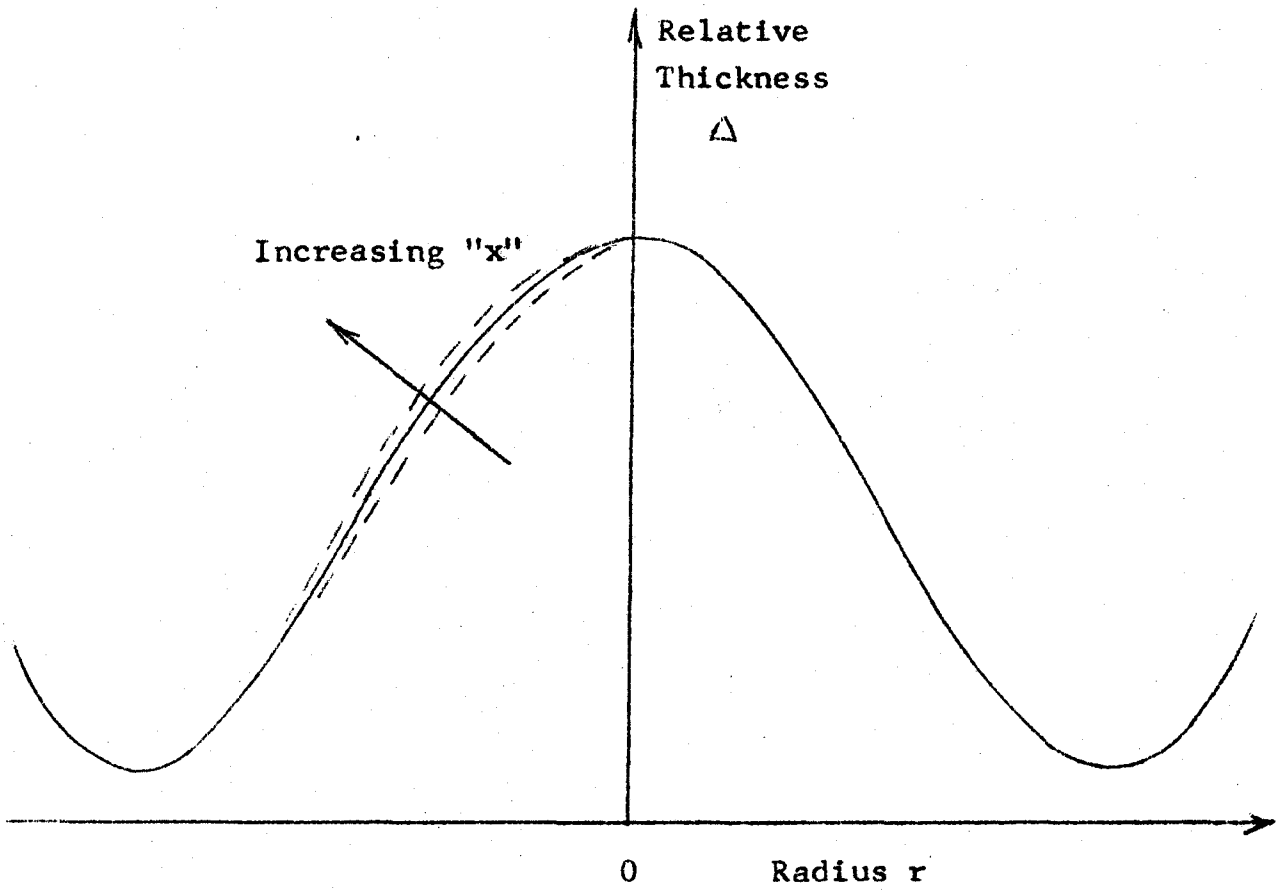

Figure 8. Drop Shape at a Flat Plate, and Relative Lamella Shape for a Solid Sphere at a Deformable Interface

(Hydrostatic Head Neglected)

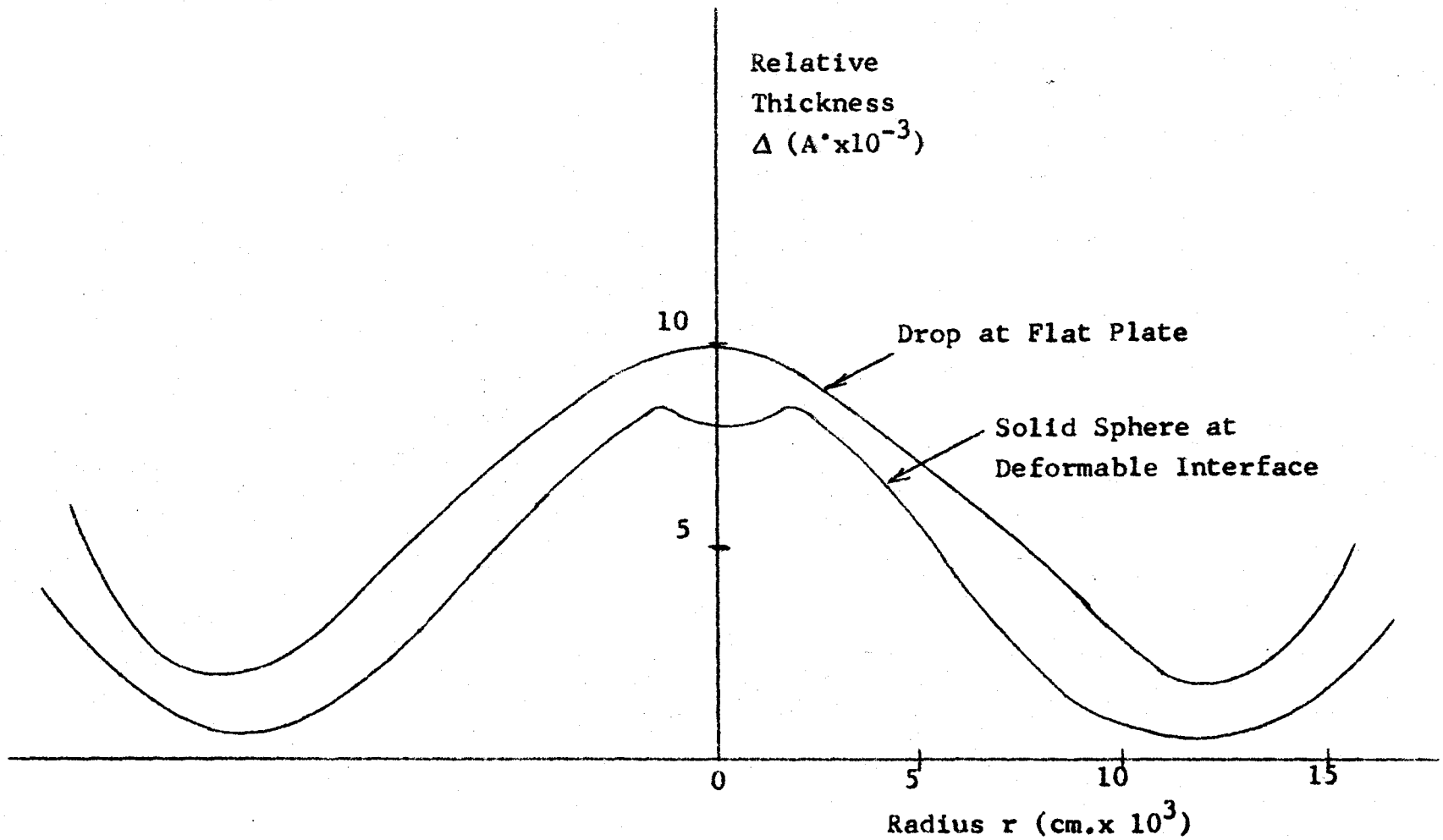

Figure 9. Calculated and Experimental Lamella Shapes for a Large (0.5 ml.) Drop

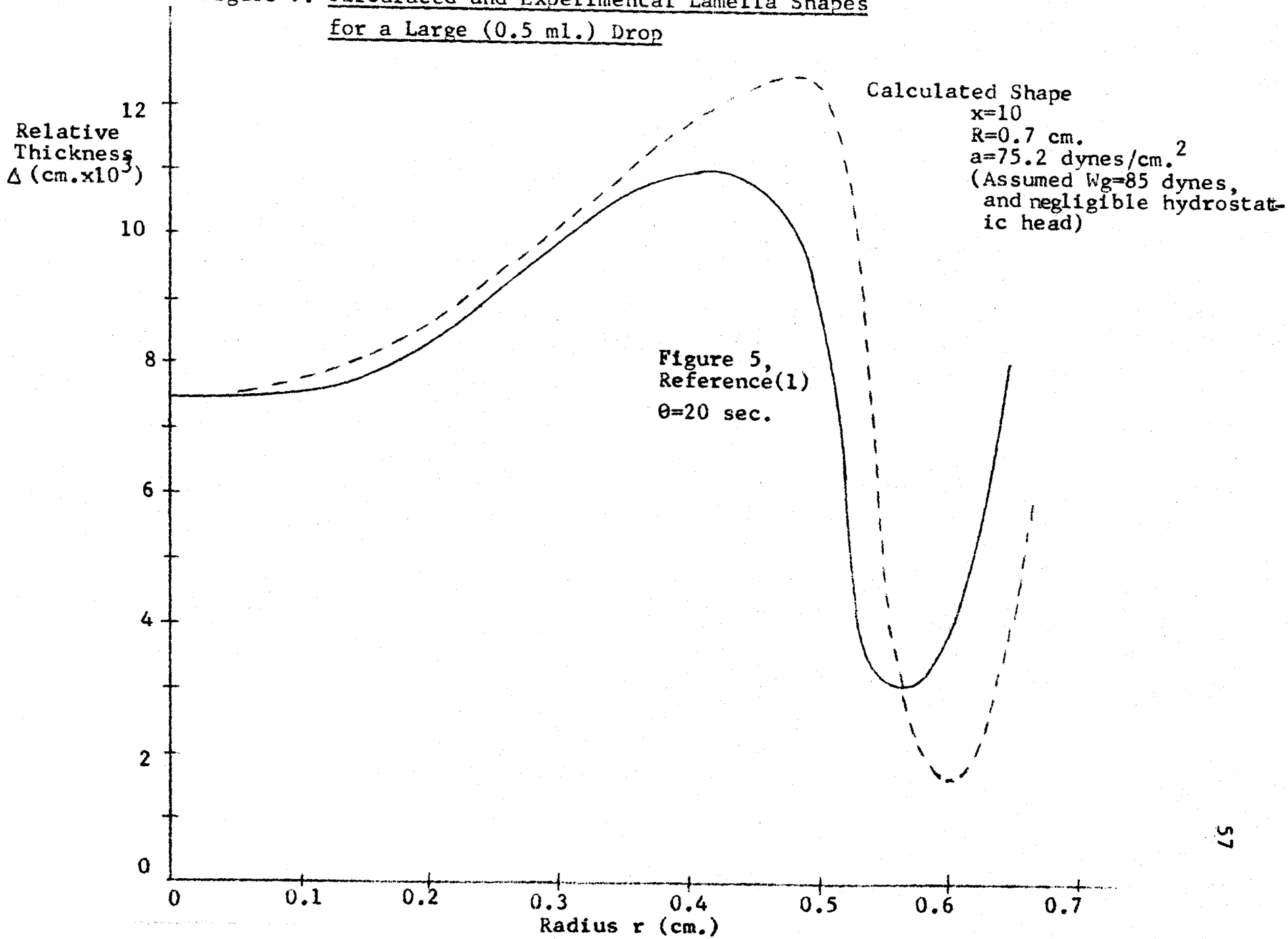

CHAPTER 3

AN INTERPRETATION OF LAMELLA BEHAVIOUR AND DROP REST-TIMES

ABSTRACT

The coalescence of single oil drops at an oil/water interface was studied with the use of a light inteference technique. Sodium lauryl sulfate, a surfactant, was deliberately added to the aqueous phase. The bulk oil/water interface could also be cleaned and the drop rest-time could then be measured as a function of the interface age from the time of cleaning. The oils used in this study were toluene, anisole, cyclohexanol, and a cyclohexane-anisole mixture. The use of these oils resulted in a variation of the oil/water density difference from 0.0097 to 0.133 gram/cm^3, a variation in the interfacial tension from 3.93 to 35.0 dynes/cm., and a variation in the discontinuous oil phase viscosities from 0.59 cp. to 32.8 cp., at 25°C. The aqueous phase concentration of the surfactant was varied from 0 to 10^{-2} grams/l. for the toluene/water system, and from 10^{-6} to 10^{-4} grams/l. for the other three systems. Sufficient KCl electrolyte was used to minimize double layer repulsion. The drop volumes used in the determination of the rest-times ranged from 0.001 to 0.020 ml. for the four oil/water systems.

The drop rest-times and the light interference patterns produced by the thin lamella formed between the drop and bulk interfaces were observed simultaneously. Consequently, the drop rest-time could be characterized by the additional observation

of whether even or uneven drainage of the lamella was observed. The appearance of even or uneven lamella drainage for a particular drop was found to be a function of the interfacial concentration of the adsorbed surfactant. Distinct patterns in the type of lamella drainage were observed for different interfacial concentrations of adsorbed surfactant, for each of the four oil/water systems studied.

All of the light interference patterns that were observed in this work could be decomposed into five distinct mechanisms for the lamella behaviour. These mechanisms were: the rapid approach mechanism , dimple formation, slow even thinning, uneven thinning, and lamella rupture. Each mechanism was interpreted in terms of the flow of water in the lamella and the movement of the bulk interface as affected by the interfacial concentration of adsorbed surfactant. An hypothesis for the cause of uneven drainage was formulated and was used to interpret the complex light interference patterns that were produced by the cyclohexanol/water system. These mechanisms were then employed to interpret the rest-time data.

The observed rest-times were also correlated using simple equations based on the Hodgson/Woods and parallel disc models. The former model consistently over-estimated the rest-time data by a maximum difference of +30%, and the latter model consistently under-estimated the rest-time data by a maximum difference of -70%. These correlations were based on rest-time data for only even lamella drainage, and, if possible, the same

interfacial concentration of adsorbed surfactant.

Coloured ciné photographs were taken of the interference patterns produced when the lamella was illuminated with white light for all four oil/water systems. When light intensity measurements were made on the gray-black region of the light interference pattern, the lamella thickness at rupture was estimated to be 200 - 400 A°.

1. Introduction

In most coalescence studies, only drop rest-times have been measured. These drop rest-times were observed for both pure liquid/liquid systems, and for systems which contained deliberately added surfactant (1-14). An interpretation of the rest-time data was often attempted through an analogy between coalescence and chemical kinetics (1). This analogy was successful in the correlation of the data of some investigators, but usually was not sufficient.

The light interference technique has been employed to observe the change in the lamella thickness with time. In past studies, the lamella thickness data were compared with models of lamella thinning, such as the parallel disc model. Despite the complexity of the light interference patterns produced by the lamella, no attempts were made by previous workers (15-25) to categorize the different patterns.

With the development of a method to clean the interface efficiently (4), the drop rest-time could be measured as a function of the interface age from the time of cleaning. The simultaneous observation of drop rest-times as a function of interface age and of the light interference patterns produced by the lamella has been done by Hodgson and Woods (17). These authors studied the light interference patterns produced by lamellae of the toluene/water and anisole/water systems. Four types of

lamella behaviour were observed. These types were dependent on the interfacial concentration of surfactant adsorbed at the bulk oil/water interface and on the oil/water system used.

In this chapter, the work of Hodgson and Woods has been repeated and extended to include two new oil/water systems. A wider range of the aqueous concentration of sodium lauryl sulfate, the surfactant, was used in the study of the toluene/water system, and drop rest-times and lamella behaviour were observed for various drop volumes.

2. Experimental Part

The experimental procedures used in this work may be divided into three parts. These parts are the cleaning of the coalescence cell, the operation of the cell and the method of data collection, and the microscope and the interpretation of the light interference colours and patterns. Each part will be discussed in turn.

2.1. Cleaning The Coalescence Cell

The apparatus was the same as that employed by Hodgson and Woods (17) and Burrill and Woods (27). A photograph of the equipment is shown in Figure (1a), a drawing of the equipment is shown in Figure (1b), and a detailed drawing of the cell only is shown in Figure (1c).

All the components of the cell that contacted the oil/water system were cleaned before the cell was assembled. These glass and teflon components were first degreased with acetone,

and were then immersed in fresh chromic acid for 24 hours. After the components were removed from the chromic acid, they were rinsed first with 1 micromho distilled water, then with phosphoric acid, and finally with 1 micromho distilled water. The components were then dried in a drying oven at 100°C for several hours. When the components were dry, they were rapidly assembled to seal the cell interior from the surrounding air.

The distilled water was at least triply distilled, once from alkaline potassium permanganate (except for the toluene/water study), and the final distillation was done in an all-quartz still. The water had then an electrical conductivity of about 1 micromho, and was stored in tightly-sealed polyethylene containers until used.

All chemicals were Fisher Reagent grade. The sodium lauryl sulfate surfactant (S.L.S.) was not purified further because of its extremely high surface activity. All the oils were distilled in a packed glass distillation column before use, and were then saturated with water and stored in stoppered glass volumetric flasks. The physical properties of the four oil/water systems are given in Table (1).

Aqueous S.L.S. solutions were made by first weighing 0.1 gram of S.L.S. and adding this to one litre of distilled water. Smaller aqueous concentrations of S.L.S. could then be made when 1 to 20 ml. volumes of the concentrated solution were pipetted into measured volumes of distilled water.

A small quantity of the oil being used in the study was poured onto the surface of the aqueous surfactant solution in the cell reservoir. The contents of the reservoir were then shaken to saturate the aqueous phase with oil. This oil remained in the reservoir during the course of the experiment. Also, once the cell was filled with the oil and the aqueous S.L.S. solution, the oil/water system remained in contact for the rest of the study.

2.2. The Cell Operation and Data Collection

Two unique features of the cell were the interface cleaning probe and the drop-forming syringe.

The construction of the interface cleaning probe has been described by Hodgson and Lee (4). To clean the interface, the cleaning probe was opened for a 2 to 3 minute period, and about 5 ml. of a 50/50 volume mixture of oil and water were forced out of the cell by hydrostatic pressure.

The construction of the drop-forming syringe has been described by Hodgson and Woods (17). Figure (1c) shows the essential details of the syringe assembly. To form a drop, the syringe assembly was raised until the ground-glass tip of the capillary pierced the interface to a depth of 2 to 3 mm. By the use of a micrometer attached to the syringe, the volume of oil withdrawn into the capillary could be measured. The assembly was then lowered into position. A drop was formed when the oil was slowly forced out of the capillary. No

satellite drops were formed when the droplet was detached from the capillary tip because the oil did not wet the clean glass capillary.

To obtain data on the drop rest-time as a function of interface age, the interface was cleaned and drops were released at fixed intervals and their rest-times were measured. The interface age was measured from the instant that the probe was closed. Normally, 10 to 15 seconds elapsed after the probe was closed before the first drop was forced from the capillary and allowed to rise about 1 mm. to the interface. The drop rest-time was measured from the instant of the first appearance of a light interference pattern in the microscope until the instant that the pattern ceased at lamella rupture.

Immediately after the rupture of the lamella, oil was again metered into the capillary, and the interface was then allowed to remain quiescent for 30 to 45 seconds. The oil was again forced from the capillary and a new rest-time measurement was made. This procedure was repeated every minute, if possible, and was continued until the rest-times showed little further change as the interface was aged.

Once reproducible rest-time data had been obtained for a particular oil/water system and for a particular aqueous concentration of S.L.S., the cell and the aqueous solution reservoir were emptied. If the rest-time study was begun with the smallest S.L.S. concentration, a new, more concentrated

solution could be added to the cell immediately, without repeating the cleaning of the cell.

2.3. The Microscope and Interpretation of the Light Interference Patterns

An Olympus model MR metallurgical microscope was employed in this work. It was converted to use a 25 watt Galileo tungsten light source. Normally, in metallurgical use, light would reflect from an opaque metal specimen and return to the microscope. In the present application to oil/water systems, only about 5% of the light incident on the oil/water interface was reflected because of the small difference in the refractive indices of the two liquids. By using oils with approximately the same refractive index as the glass plate, and by using a viscous immersion oil between the plate and the objective of the microscope, no reflection occurred except at the interface.

Two light rays will be reflected from a lamella because there are two interfaces. Since one light ray has traversed the lamella twice, and the rays have the same light source, but different path lengths, a condition for light interference exists. Thus, the metallurgical microscope functions as an interference microscope since the lamella provides the necessary path difference, instead of a second mirror as in the usual interference microscope. Also, since the light produced by a tungsten filament contains the entire spectrum of visible electromagnetic radiation, the light interference pattern produced by variations in the lamella thickness will be coloured. For monochromatic

light, there would be only alternately light and dark regions in the interference pattern.

The drop volume is an important variable in both the rest-time study and in the use of a microscope. Small drops of volume 0.001 to 0.020 ml. were used because they are almost spherical, are of practical industrial interest, can be measured accurately with a micrometer syringe, and provide no experimental difficulty when the drop forming technique is used. A force balance between the buoyancy force of a drop almost completely formed and the interfacial tension force yields an expression for the maximum radius of a drop which can be formed with this drop-forming technique. For a capillary of radius r', the result is:

$$d = \left| \frac{3 \gamma r'}{2 \Delta \rho g} \right|^{1/3} \qquad \ldots\ldots(1)$$

The choice of drop volume must also be consistent with the microscope optics. The field of view needed for the microscope is determined by the radius of the lamella and may be estimated by doing a force balance between the drop buoyancy force and the lamella pressure. The radius of the lamella is estimated from the equilibrium model (44) to be:

$$R = 2 d^2 \sqrt{\frac{\Delta \rho g}{3 \gamma}} \qquad \ldots\ldots(2)$$

Since the lamella is bounded by curved interfaces, as shown in Figure (2a), the depth of field of the microscope objective must

be large enough to permit all the interference fringes produced by the lamella to be in focus. Also, the distance from the top surface of the glass plate to the lamella must be less then the focal length of the microscope objective to permit fine focussing adjustments of the microscope. This distance was about 1 cm. for the cell used. To satisfy these various criteria, the microscope was used with a 10 x objective and 7 x eye-pieces.

Colour ciné 16 mm. photographs were made of the light interference patterns produced by the lamella. These photographs contained a permanent record of the change in the light interference patterns as a function of the elapsed time of the drop at the interface, and were made for each oil/water system and for each aqueous concentration of S.L.S.

To convert from an interference colour to the lamella thickness, equation (3) from Lawrence (28) was used. This equation is:

$$\mu'\theta' = \frac{n_i \lambda_o}{4} \qquad \ldots\ldots(3)$$

Equation (3) expresses an optical path length, $\mu'\theta'$, in terms of a fraction of the wavelength, λ_o. The optical path must be equal between lamella liquids whose refractive indices are different, but have the same interference colour. The right hand side of equation (3) may be interpreted in terms of an interference colour. Interference colours for white light illuminating a soap film of refractive index 1.40 are given by Lawrence.

If θ_1' is the soap film thickness, θ_2' the water lamella thickness, and if μ_1' equals 1.40 and μ_2' equals 1.33, the following equation may be used to apply Lawrence's soap film thicknesses to a water lamella. The equation is:

$$\mu_1' \theta_1' = \mu_2' \theta_2'$$

$$\therefore \quad \theta_2' = \frac{1.40}{1.33} \theta_1'$$

There is no difficulty in the conversion of an interference colour produced by white light to a lamella thickness because, for lamella thicknesses up to 8000 A°, the sequence and intensity of light interference colours is irregular and well-known. However, at thicknesses larger than 8000 A°, only red and green colours appear. To evaluate a lamella thickness greater than 8000 A°, the order of the colour must be known.

Figure (3) shows a typical light interference pattern for even drainage of the lamella. The slightly black colour at the edge of the pattern in the third photograph indicates an extremely thin local lamella thickness. From the edge of the pattern to the center, the pattern colours are interpreted to produce a dimple, as is shown below the photographs. There is no reason for the assumption of a regular increase in the lamella thickness. For example, Hartland (26) has shown cases of "double dimples" for large 0.5 ml. volume drops. However, the assumption of a single form of the dynamic pressure

distribution in the lamella, such as was done in Chapter (2), leads to an equation which predicts double dimples for 0.5 ml. drops, but only a single dimple for a small 0.005 ml. toluene drop in water. This suggests that the interpretation of the light interference pattern is correct. Furthermore, the colour sequences produced by lamellae whose thicknesses are less than 8000 A° clearly indicate that double dimpling does not occur in this range of lamella thickness.

To interpret the light interference pattern produced by the uneven drainage of a lamella, the line of symmetry must be defined which divides the pattern into two, mirror-image, semi-circular halves. This has been done for the six sequential photographs of the unsymmetrical patterns shown in Figure (4).

At a lamella thickness of about 1000 A°, there is no light interference, and the colour of the pattern is white. With further decreasing lamella thicknesses, the colour becomes gray and eventually becomes black. The thickness of the lamella when rupture occurs may provide information on the rupture mechanism. If the light intensity of the black colour is measured using a photocell, equation (4) may be used to calculate the lamella thickness (29). The equation is:

$$\frac{I}{I_o} = \text{sine}^2\left(\frac{y}{y_o} \frac{\pi}{2} \right) \qquad \text{.....(4)}$$

Equation (4) is applicable for measurements made with monochromatic light. Since white light appears to behave monochromatically

at less than 1000 A° thickness, equation (4) was applied to light intensity measurements made in this work. The maximum light intensity, I_o, was assumed to occur for a lamella thickness, y_o, of 1000 A°. Light intensity measurements were made from the ciné photographs. These photographs were projected in a dark room onto a screen that had a small hole. A photosensitive transistor protruded through the hole and a short plastic tube slid over the sides of the transistor to allow only light from a very small solid angle to enter the tube and enter the transistor. The current produced by the transistor was amplified and passed through a resistor. The voltage drop across the resistor was measured and recorded on a strip chart recorder.

A projector speed of 1 to 4 frames per second was used. When measurements were begun at an amber colour for a lamella of about 1600 A° thickness, the light intensity reached a maximum as lamella thinning progressed at about 1000 A° thickness, for a white interference colour. The light intensity then gradually decreased toward zero. Since I, I_o, and y_o are known, the lamella thickness, y, at any instant can be calculated from equation (4).

3. Theoretical Insight

In this section, the lamella behaviour is shown to be a function of both the flow of water in the lamella and of the motion of the bulk interface, and a function of the interfacial

concentration of surfactant. These two factors will be discussed in turn.

3.1. Flow in the Lamella

The analysis of the flow of water in the lamella may be simplified if the two dimensional representation of the lamella shape shown in Figure (2a) is changed to the shape shown in Figure (2b). This figure shows that the drop interface has arbitrarily been straightened, and that the vertical scale is expanded by a factor of one-hundred, relative to the horizontal scale.

Several terms must be defined. The two possible types of lamella drainage are shown in Figures (4) and (5). The symmetrical light interference pattern shown in Figure (5) is caused by even drainage of the lamella. Even drainage results when there is no variation in the flow of water at different angular locations, for each radial distance in the lamella. Uneven drainage will result in an unsymmetrical light interference pattern, as shown in Figure (4). Uneven drainage results when there is an angular variation in the flow of water from the lamella, for each radial location.

A surface is defined to exist at the boundary between a liquid and a gas when the gas is the liquid's vapour. Therefore, only one component is at the surface. An interface is defined to exist at a liquid/liquid boundary. Therefore, two components must be present to form an interface.

A lamella is defined to exist between two interfaces that are separated by only a thin layer of one phase. In this work, a lamella is arbitrarily defined to have a thickness of less than 10 microns.

The barrier ring is defined as that radial location where the lamella thickness is a minimum. Therefore, a lamella is "dimpled" if the barrier ring radius is not zero. This definition impliesthat the thickness of the lamella at the center is greater than at the barrier ring.

To simplify the discussion, the drop is oil and the continuous phase is water. The oil is less dense than the water. Since the buoyancy of the drop forces it against the bulk interface, a pressure exists in the lamella and water is forced to flow radially outward. The lamella drainage exerts an outward directed surface shear stress on both the drop and bulk interfaces. Pure gas/liquid and liquid/liquid interfaces cannot oppose a surface shear stress and will therefore move in the direction that the surface shear stress is applied. An interface which moves is termed "mobile", and one which is stationary is termed "immobile". The motion of the interfaces causes oil molecules immediately adjacent to the interface to move also, though less freely because of the viscosity of the oil. Therefore, a velocity gradient will exist in the oil phase.

The magnitude of the surface shear stress, S, is defined by the product of the liquid viscosity, μ, and the gradient of

the radial velocity in the z direction, $\frac{\partial u}{\partial z}$. Therefore, S is defined as:

$$S = -\mu \frac{\partial u}{\partial z}\Bigg|_{\text{interface}} \qquad \ldots\ldots(5)$$

If the viscosities of the oil and water are unequal, the velocity gradients at the interface are also unequal. Figure (2b) shows typical velocity gradients that must exist for the above case.

The two boundary conditions on the velocity gradients may be written:

B.C.1. $z = 0$

$$\mu_{\text{oil}} \frac{\partial \bar{v}}{\partial z}\Big|_{\text{oil}}\Bigg|_{z=0} = \mu_{\text{water}} \frac{\partial \bar{v}}{\partial z}\Big|_{\text{water}}\Bigg|_{z=0}$$

and,

B.C.2. $z = y$

$$\mu_{\text{oil}} \frac{\partial \bar{v}}{\partial z}\Big|_{\text{oil}}\Bigg|_{z=y} = \mu_{\text{water}} \frac{\partial \bar{v}}{\partial z}\Big|_{\text{water}}\Bigg|_{z=y}$$

where $\bar{v}$ is the velocity of the oil or water, parallel to the $z = 0$ or $z = y$ interface. These boundary conditions are exact, compared to the approximate form expressed by equation (5), because the radial velocity, u, is not necessarily parallel to an interface. However, u is approximately equal to $\bar{v}$ and is used in this work since the curvature of the lamella is small.

An interfacial tension exists in the interface because

of the force of attraction between molecules. When a surfactant diffuses to the interface, it reduces the interfacial tension of the pure interface by an amount proportional to its interfacial concentration. For a pure interface, the interfacial tension is constant, regardless of the variation with radius of the velocity of the interface. If the interface now contains adsorbed surfactant and a surface shearing stress is applied on the interface, the interface initially moves at different radial velocities at different radial locations because the radial velocity of the water flowing from the lamella also varies with radius. The interfacial concentration of surfactant may therefore increase or decrease at various radial locations. Since the interfacial tension varies inversely with the interfacial concentration of surfactant, for small interfacial concentrations, there may now be an interfacial tension gradient along the interface. This additional force is now applied on the interface together with the viscous shear force previously discussed.

In this discussion, only the drop interface is assumed to contain no surfactant. Therefore, the z-direction gradient of the radial velocity in the continuous and discontinuous oil phases will be different. If the oil is inviscid, then the radial velocity U of the bulk interface will be less than that for the drop interface, since the bulk interfacial tension gradient resists expansion of the circular interface. This is shown in Figure (2c).

If both the mass and radial acceleration of the bulk interface are assumed small, then no inertial force will oppose the change in the radial velocity U of the interface. Therefore, for an inviscid oil phase, the surface shear stress caused by the flow of water from the lamella must equal the interfacial tension gradient in the bulk interface. This is written:

$$\frac{d\gamma}{dr} = \mu_{water} \left.\frac{\partial u}{\partial z}\right|_{interface} \qquad .....(6)$$

Equation (6) is assumed to be valid even for small changes in U. If the velocity gradient $\frac{\partial u}{\partial z}$ decreases, $\frac{\partial \gamma}{dr}$ must also decrease. Since the interfacial concentration of surfactant, Γ, must increase with radial distance because an interfacial tension gradient exists, the bulk interface must contract to reduce $\frac{d\gamma}{dr}$; the surfactant is less widely distributed. Therefore, the bulk interface velocity U may be directed inward. If the contraction is large, there may be no net outflow from regions of the lamella where U is negative; indeed there may be a net inflow.

The redistribution of the surfactant in the bulk interface may also take place by surface diffusion of surfactant molecules toward the lamella center, and by the desorption/adsorption process. These two mechanisms of redistribution are discussed in Appendix A2 and are assumed unimportant in the surfactant redistribution which is discussed in this chapter.

Two other concepts are useful. These concepts are considered in the next section, along with a mathematical analysis

to allow the calculation of the values of the important variables.

3.2. The Radial Distribution of Surfactant Adsorbed in the Bulk Interface

In the previous section, the interfacial concentration of surfactant was dependent on radial location. To analyze this radial distribution, a modified form of the pressure polynomial derived in Appendix A2 is used. This polynomial satisfies the additional boundary condition, $\frac{\partial^2 p}{\partial r^2} = 0, \quad r = R.$

The polynomial is: $p = a_0 + a_2 r^2 + a_4 r^4 + a_6 r^6$ .....(7)

The coefficients, a_i, are known functions of the center lamella pressure p_o, and hence if p_o is calculated from an experimental profile of relative lamella thickness, the lamella pressure and its radial gradient may be calculated.

The simplified equation of motion, for cylindrical coordinates, in the r-direction (3) is:

$$\frac{\partial^2 u}{\partial z^2} = \frac{1}{\mu} \frac{\partial p}{\partial r} \qquad .....(8)$$

This equation applies to the flow of the water in the lamella. Equation (8) may be integrated to yield:

$$\mu \frac{\partial u}{\partial z} = \frac{\partial p}{\partial r} \; z \qquad .....(9)$$

where $\frac{\partial u}{\partial z} = 0$, $z = 0$, for the drop interface. The negative value of the left-hand-side of equation (9) was defined as the

shear stress. Equation (9) will be used to describe the surface shear stress acting on the bulk interface.

Since surfactant adsorbed at an interface lowers the interfacial tension by a degree dependent on the interfacial concentration of surfactant, for very small interfacial concentrations, a linear adsorption isotherm is assumed. This equation is written:

$$\gamma = \gamma_o - k'\Gamma \qquad \ldots\ldots(10)$$

where k' is a constant and Γ is the total concentration of interfacial surfactant molecules. Since the concentration of surfactant molecules in the aqueous phase is small relative to the interfacial concentration, for a three dimensional interface, Γ is approximately equal to the excess interfacial concentration of surfactant, as defined by Gibbs (see (40)). When the surface shear stress is balanced by the interfacial tension gradient in the bulk interface, equation (10) may be differentiated with respect to r and equated to equation (9), written for z = y. The result is:

$$\frac{d\gamma}{dr} = -k'\frac{\partial\Gamma}{\partial r} = y\frac{\partial p}{\partial r} \qquad \ldots\ldots(11)$$

Values for the pressure gradient obtained from equation (7) may be substituted into equation (11). If p_o is specified for a particular lamella shape, equation (11) may then be integrated to yield:

$$\Gamma = \Gamma_o - \frac{2}{k'} F(r) \qquad \ldots\ldots(12)$$

where $F(r) = \sum \frac{c_i r^i}{i}$, $(i = 2,4,\ldots 14)$,

Γ_o is the interfacial surfactant concentration at $r = 0$, and the coefficients, c_i, are known functions of p_o. Details are given in Appendix A2.

The radial distribution of interfacial surfactant can be calculated from equation (12) if Γ_o is known. The curve in Figure (6) shows the variation in the interfacial tension with radius, and the curve in Figure (7) shows the corresponding interfacial distribution of surfactant.

Figure (7) shows that the interfacial concentration of surfactant at $r = R$, Γ_{max}, exceeds the overall average interfacial concentration of surfactant, Γ_t, that has adsorbed at the undisturbed bulk interface, t minutes after the interface was cleaned of surfactant. To illustrate this point with a calculation done on experimental data, Figure (8) shows the experimentally observed relative lamella thickness profiles for 10^{-6} gm/l of S.L.S. + 0.01 N. KCl for a 0.020 ml. anisole drop at the bulk interface, 5 minutes after the interface was cleaned. At $\theta = 4.05$ seconds, the lamella began to drain unevenly, but at $\theta = 7.45$ seconds, the angular variation in the relative lamella thickness was sufficiently small to allow a symmetrical lamella to represent the observed lamella thickness profiles. Figure (9) shows the calculated radial distributions of the interfacial surfactant concentration for the profiles in

Figure (8). The profiles in Figure (8) were fitted with the polynomial described in chapter (2). In the calculation of Γ as a function of r, the value $\Gamma_o = 0$ was used for each profile. The calculation of Γ_t was made with the Ward-Tordai relationship (36). This latter equation should be reasonably accurate, far from equilibrium adsorption. However, the unknown hydrodynamics of interface cleaning, and the unknown influence of the drop syringe on the interfacial surfactant concentration when the syringe punctures the interface may result in a considerable error in the estimation of Γ_t. It is possible, therefore, that Γ_{max} is always greater than Γ_t for all θ, for even drainage.

If the calculations had been done with $\Gamma = \Gamma_t$ at $r = R$, then the interfacial surfactant concentration may become negative near the lamella center. The interface would be mobile in this region because no surfactant was present and there would be little radial variation in the lamella pressure. This lack of a radial pressure gradient would result in relative lamella thickness profiles which could not be described by the pressure polynomial discussed in Chapter (2). Since this is not the case, the boundary condition $\Gamma_o = 0$ was used, together with its implied conclusion that Γ_{max} is greater than Γ_t for some of the profiles.

The calculation of the radial variation in Γ is also dependent upon the accuracy of the linearized forms of the radii

of curvature, as derived in Chapter (2). Calculations for toluene/water and anisole/water are given in Appendix A2. These calculations show that the difference between the more accurately calculated relative lamella thickness profile and the profile calculated from the linearized expression is 1 - 3% at r = R. This difference is too small to affect the conclusion that Γ_{max} is greater than Γ_t for some of the profiles of Figure (8).

The large imbalance in interfacial tension that must exist in the bulk interface near r = R must necessarily cause bulk interface expansion in this region. This expansion would reduce the difference between Γ_{max} and Γ_t. Surfactant should also be lost from the stressed region of the bulk interface at a rate dependent upon the magnitude of the imbalance, expressed as $(\Gamma_{max} - \Gamma_t)$.

The loss of surfactant from the stressed region of the bulk interface leads to the concept of a minimum number of surfactant molecules, SM, needed in the bulk interface to balance the surface shear stress. This minimum may be calculated if Γ_o equals zero and if the surface shear stress is known. Equation (12) may be used to evaluate the sum. The result is:

$$SM = \sum_{r=0}^{R} \Gamma_r \, 2 \pi r \, \Delta r$$

The value of SM for each of the lamella profiles in Figure (8) is shown in Figure (10). Since lamella drainage decreases the

lamella thickness, especially in the region outside the barrier ring, less surfactant is required in the stressed region of the bulk interface to balance the surface shear stress, even though a dimple may form.

Therefore, surfactant is being lost from the stressed region of the bulk interface, but less surfactant is needed in the bulk interface to balance the decreasing surface shear stress. This concept is further discussed in section 4.2.

The effects of the oil/water system physical properties, drop radius, and relative lamella thickness on the values of Γ_{max}, SM, and the difference ($\Gamma_{max} - \Gamma_t$) are summarized in Table (2). In the calculations, the independent variables are the drop volume or radius d, the interfacial tension γ, the density difference $\Delta\rho$, and the center lamella pressure p_o. The value of the center lamella height, y_o, was constant at 2×10^{-4} cm.

The effect of p_o on the relative lamella thickness should first be discussed. Previous work done on the calculation of relative lamella thickness profiles has shown that, if $p_o = \frac{\gamma}{d}$, the barrier ring is at the lamella center. This relative lamella thickness profile approximates the parallel disc geometry. The lamella thickness slowly increases near the lamella center, and then increases more rapidly as the radial distance is increased. The barrier ring will occur at a non-zero radius if p_o is greater than $\frac{\gamma}{d}$. Therefore, the

anisole/water rows in Table (2) have two values for p_o, for each set of the other independent variables. The first entry of p_o in the row for anisole/water is for p_o equal to $\frac{\gamma}{d}$, and the second entry is for the arbitrary value $p_o = \frac{\gamma}{d} + 10.$ dyne/cm^2. There is no simple exact relationship to allow the calculation of the barrier ring height y_c or the depth of the dimple $y_o - y_c$. However, an approximate equation may be derived if the polynomial description of lamella thickness is used.

A polynomial which will be derived in Chapter (4) may be used to express y_c as a function of y_o and p_o. The first three terms of this polynomial may be written as:

$$y_c \doteq y_o + \left(\frac{1}{d} - \frac{p_o}{\gamma}\right)\frac{c^2}{2} + \frac{\pi p_o^2}{8\gamma W_g} c^4$$

where c is the barrier ring radius. The value of the barrier ring radius may be obtained by differentiating the above polynomial (written in r) with respect to r. When $\frac{dy}{dr} = 0$ for $r = c$, the expression for the barrier ring radius may be written:

$$c^2 = \frac{2\gamma W_g}{\pi p_o^2}\left(\frac{p_o}{\gamma} - \frac{1}{d}\right)$$

This expression is approximate only, and it is not very useful, since p_o must be known. By setting $p_o = \frac{\gamma}{d} + 10.$, and by substituting for c^2 and c^4 into the expression for y_c, it is found that:

$$y_o - y_c = \frac{50}{\gamma \pi p_o^2}$$

where $p_o = \frac{\gamma}{d} + 10.$

This expression shows that a small drop will be less dimpled than a large drop, because p_o increases as the drop volume decreases. The value of p_o may be used to vary the shape of the relative lamella thickness profile.

Column two of Table (2) contains the radius R at which the dynamic lamella pressure falls to zero. The value of R is calculated from an expression derived for the series type polynomial presented in Appendix A2. The dynamic lamella pressure is assumed only to have an effect on the interfacial distribution of adsorbed surfactant at a radius less than R.

Column three contains an arithmatic average for the surface shear stress which is exerted on the bulk interface. This average was not weighted to take into account the changing area over which the surface shear stress acts as radius increases, but attempts to show only that the surface shear stress for small drops is, in general, larger than for large drops.

Column four contains the minimum quantity of surfactant required in the bulk interface to balance the surface shear stress for the particular lamella shape being used in these calculations. Small drops require less surfactant than do large drops, despite the higher surface shear stress caused by small drops.

Column five contains the maximum interfacial surfactant

concentration, Γ_{max}, which occurs at r = R.

Column six contains the average interfacial surfactant concentration, Γ_t, which is required at the bulk interface for the minimum quantity of surfactant, SM, to be present. The data in this column show that the toluene/water system requires the largest Γ_t if the bulk interface is to be immobile for the particular lamella shape considered. The CA/water system requires an intermediate interfacial surfactant concentration, and the anisole/water system requires the smallest Γ_t.

For the anisole/water system, a small increase in p_o of 10 dyne/cm has a smaller effect on Γ_t for small drops than the increase does for larger drops. This is because the lamella thickness is less sensitive to a change in p_o for small drops than for large drops. Also, for the anisole/water system, a slight change in p_o (the relative lamella thickness profile) results in the large drop requiring a smaller interfacial surfactant concentration, Γ_t, than does a small drop, if the surface shear stress is balanced. Therefore, while the Γ_t for large drops is larger than the Γ_t for a small drops for approximately a parallel disc lamella, a slight change in the lamella shape of the larger drop is capable of reversing this dependence of Γ_t on drop size. There is, therefore, a weak dependence of Γ_t on drop size. The dependence of Γ_t on the relative lamella thickness profile is more important, especially

if large drops are considered.

Column seven contains the value of the driving force ($\Gamma_{max} - \Gamma_t$) that is postulated to exist if the polynomial accurately describes the interfacial distribution of adsorbed surfactant. If surfactant is lost from the stressed region of the bulk interface, $0 \leq r \leq R$, at a rate dependent on the magnitude of ($\Gamma_{max} - \Gamma_t$), then surfactant is lost most rapidly for the toluene/water system, more slowly lost for the CA/water system, and finally lost most slowly for the anisole/water system. This rating for the ease of loss of surfactant is for drop volumes of the three systems which give approximately the same light interference pattern radius. These volumes are marked with an asterisk in Table (2).

Conclusions reached after a consideration of Table (2) may be listed as follows:

(1) The driving force ($\Gamma_{max} - \Gamma_t$), for the loss of surfactant from the stressed region of the bulk interface, is smaller for small drops than for large drops. This dependence is shown by the calculations for the anisole/water system.

(2) There is only a small dependence of the minimum interfacial surfactant concentration, Γ_t, on drop size when compared with a change in system physical properties. The lamellae formed by small drops require a smaller Γ_t than do the lamellae for large drops, for a parallel disc type lamella thickness profile. However, a slight change in the lamella thickness profile for large drops can reverse the dependence

of Γ_t on drop size. Therefore, the dependence of bulk interface mobility on drop size cannot be determined because of the large effect that the lamella thickness profile has on Γ_t for large drops.

These conclusions depend upon the accuracy of several assumptions made in the calculation of the Table (2) values. The main assumption that was made is that the series type polynomial used in equation (12) describes the lamella pressure distribution. This assumption is considered further in Chapter (4).

With these concepts of an interfacial tension gradient balancing the surface shear stress, of the interfacial concentration of surfactant exceeding the "quiescent" interfacial surfactant Γ_t at $r = R$, and of the minimum quantity of surfactant required in the stressed region of the bulk interface to set up the balancing interfacial tension gradient, experimental observations of drop rest-times and of the lamella light interference patterns will now be considered.

4. Presentation and Analysis of Results

Three aspects of the data are discussed separately. First, the drop rest-times are interpreted as functions of the surfactant concentration, interface age, and drop volume. Secondly, the light interference patterns produced by the lamellae are interpreted to provide the lamella behaviour and then decomposed into mechanisms. Finally, an interpretation of the

rest-time data is attempted.

4.1. Drop Rest-times as a Function of Interface Age

Figures (11) to (27) show the drop rest-times that were observed as a function of the interface age and of drop size, for all the oil/water systems, and for various aqueous concentrations of S.L.S. The drops were not aged on the capillary for these data. Additional data for a non-ionic surfactant and for drop aging are given in Appendix A1.

Only the data for the toluene/water system will be described in detail here. A summary of the pertinent aspects of each figure is given in Tables (3a,b) for two separate aqueous surfactant concentrations 10^{-6} and 10^{-4} gm/l. of sodium lauryl sulfate. These Tables will be discussed in detail after the discussion of the toluene rest-time data has been completed.

Figure (11) shows the rest-time data for the "pure" toluene/water system as a function of interface age. The addition of KCl to the water was necessary since rest-times usually became very large after a short period of small rest-times for the completely pure toluene/water system. These large rest-times may be caused by double layer repulsion. The data in Figure (11) show that rest-times were almost zero for interface ages up to four minutes. For smaller drops of volume 0.0025 ml., this period of short rest-times could be extended up to an interface age of seven minutes.

At a certain critical interface age, termed t_c, the rest-times shown in Figure (11) become very large. Lamella drainage was uneven. Also, the large rest-times appear to be independent of interface age.

Figure (12a) shows the rest-time data for 10^{-6} gm/l. of S.L.S. + 0.01 N. KCl in the aqueous phase. The rest-time behaviour is similar to the data in Figure (11), only t_c is now one minute. The values of the rest-times pass through a maximum time, τ_{max}, equal to about 12 seconds. Rest-times then decrease to values of about eight seconds and do not appear to change further, even for very long interface ages. The lamella drains evenly for short interface ages and unevenly at large interface ages. For each interface age, the net rest-time, $\Delta\tau = \tau - \tau'$, excluding the time to form the dimple, τ', is relatively constant, as shown in Figure (12b). The constant value of $\Delta\tau$ indicates that the maximum in drop rest-time is caused by a longer time taken to form the lamella dimple at a small interface age, and that while water is flowing into the lamella, there is no decrease in thickness at the barrier ring. Slow, even lamella drainage must therefore begin at approximately the same lamella thickness each time. The light interference data support this conclusion.

Figure (13) shows the data obtained for an aqueous concentration of 10^{-5} gm/l. S.L.S. + 0.01 N. KCl. For these data, there is no period of short rest-times, hence $t_c = 0$.

The rest-times begin at a maximum value of τ_{max}, equal to 12 seconds, and decrease until the interface age is about fifteen minutes. At this interface age, the lamella drainage changes from even to uneven. No rest-time measurements were made at long interface ages for this particular concentration of surfactant.

Figure (14) presents rest-time data for 10^{-4} gm/l. S.L.S. + 0.10 N. KCl. Once again, there is no period of very short rest-times, and only the first drop at a zero interface age drained completely evenly. All other drops drained unevenly, with rest-times quickly falling to a constant value of about five seconds at an interface age greater than five minutes. At very long interface ages, drainage remained uneven and rest-times were extremely short at a value of about two seconds. The rest-times given in Figures (11) to (14) show a trend toward smaller rest-times as the aqueous surfactant concentration is increased, provided sufficient electrolyte is present in the aqueous solution to limit double layer repulsion to very small lamella thicknesses so that double layer effects do not interfere with the observations. For a further increase in the aqueous phase surfactant concentration to 10^{-3} gm/l. S.L.S. + 0.10 N. KCl, Figure (15) rest-times fall rapidly to a constant value and lamella drainage is always uneven. Rest-times become constant at one second for t equal to eight minutes, and there is no change at large interface ages. This suggests that

adsorption of surfactant rapidly reaches equilibrium near t equal to eight minutes.

Little change from the rest-time distribution of Figure (15) occurs for a further ten-fold increase in the aqueous surfactant concentration, provided more electrolyte is added to limit double layer repulsion. Rest-times become infinitely long if double layer repulsion can balance the drop buoyancy force at lamella thicknesses greater than 1000A°.

For the three other oil/water systems, only aqueous phase concentrations of 10^{-6} and 10^{-4} gm/l. of S.L.S. plus the necessary electrolyte were used; the purpose in the use of these systems was to study the dependence of rest-times on the physical properties of the system at the same aqueous phase surfactant concentrations and at approximately the same interfacial concentrations. The data of Figures (11) to (25) were analyzed using several criteria which are dependent on interface age; the results are shown in Tables (3a) and (3b).

Column two of Tables (3a,b) shows the range of drop size used for the data presented. Toluene drops of 0.005 ml. volume produced light interference patterns that filled the microscope field of view. The patterns were large enough to be accurately analyzed when photographs were taken and magnified. Anisole drops of 0.020 ml., cyclohexanol drops of 0.001 ml., and the cyclohexane/anisole mixture drops of 0.005 ml produced patterns of approximately the same size as the 0.005 ml.

toluene drops. Calculations and data for the light interference pattern radius are given in Table (4).

For purposes of rest-time prediction, the data may therefore be correlated on the basis of the drop volume which produced the same radius of the light interference patterns, among all the systems, or correlated on a constant drop volume basis for three of the systems.

Column three shows the range of interface ages during which rest-times were approximately zero. Rest-times were generally about 0.1 seconds and, in effect, the drop did not rest at the interface at all.

Column four shows the interface age when the maximum rest-time, $\tau_{max.}$, was observed near the beginning of rest-time measurements. Rest-times may become longer than $\tau_{max.}$ at larger interface ages, but the data in column four allow the rest-time distribution to be described more accurately at small interface ages. Column five shows the type of drainage observed when rest-times first become greater than 0.1 seconds. A discussion of the rest-times and drainage patterns data given by Tables (3a) and (3b) will be given in Section 4.3.

Column six shows whether there was a change in the drainage pattern at interface ages larger than t_c, but less than very long ages, t_∞. The rest-time distributions become more complex for the 10^{-4} gm/l. case. Column seven contains an average of the rest-times that were observed for interfaces several hours old, and column eight contains an approximate average of

the observed rest-times for the range of interface age studied. There is little difference in the magnitude of the rest-times for three of the oil/water systems. The viscous cyclohexanol/water system has a much higher average rest-time. Since the change in water viscosity with dissolved cyclohexanol is small, an increase in water viscosity only partially accounts for the larger rest-times for this system.

One final graphical summary of the data may be made. All of the rest-time data in this work were measured as a function of interface age. The interface age indirectly measures the interfacial concentration of surfactant. When equilibrium exists for the adsorbed surfactant, the interface age is very large. The equilibrium interfacial concentrations of surfactant may be calculated for the various aqueous S.L.S. concentrations used. These equilibrium concentrations are summarized in Table (5).

If 10^{-3} gm/l. of S.L.S. in the aqueous phase is chosen as a reference and if the interface is cleaned, then, for this aqueous concentration, the interfacial surfactant concentration will attain a series of values which, at different interface ages, will correspond to each of the equilibrium interfacial surfactant concentrations reached for the smaller aqueous phase concentrations of S.L.S. Table (6) summarizes these calculated interface ages. For example, at an interface age of 0.005 min., the interfacial surfactant concentration for adsorption from an

aqueous solution containing 10^{-3} gm/l. of S.L.S. will correspond to the equilibrium interfacial surfactant concentration that was reached for adsorption from a 10^{-6} gm/l. solution. Equilibrium adsorption is reached for t equal to five minutes, for 10^{-3} gm/l.

The rest-time data for different aqueous phase surfactant concentrations may now be placed on one graph. The data in Figures (12) to (27) are summarized in Figures (28a-f). The data of Figure (11) are not included for reasons to be discussed in sections 4.3-1 and 5.2. No attempt has been made to locate all the rest-time data accurately with respect to the abscissa time scale. Only rest-times which were measured for equilibrium adsorption are located accurately. Therefore, the slopes of the τ - t curves are arbitrary between the two points.

The calculations in Table (6) are for the same electrolyte concentration that was used for the toluene/water system. A 0.05 N. KCl. concentration for 10^{-4} gm/l. of S.L.S. was used for the other oil/water systems, but this change in KCl normality does not significantly change the times given in Table (6).

Two important points are clarified by this summary. The first point is that a researcher measuring drop rest-times, but not employing an interface cleaning probe, should observe only one drop rest-time if his interface is free of dust and dirt, and contains only an equilibrium adsorbed quantity of S.L.S. This rest-time may be found from Figure (28) if the

researcher's equilibrium concentration of interfacial surfactant can be related to the interface age required for the same interfacial surfactant concentration to adsorb from a 10^{-3} gm/l. S.L.S. + 0.10 N. KCl solution.

The second point clarified by the summary is the complexity of the rest-time data. The toluene/water system rest-times show a change from even to uneven drainage as the interfacial surfactant concentration is increased. The anisole/water system rest-times show a trend from uneven to even, and then to uneven drainage for small drops, and even-uneven-even-uneven for the large drop. The CA/water system data show the same even-uneven-even-uneven drainage changes as does the large 0.020 ml. anisole drop.

The complexity of the rest-time data may be reduced by a consideration of the lamella behaviour. This will be done in the next section.

4.2. Light Interference Patterns and Lamella Drainage: Mechanisms and Hypotheses

The observations of the light interference patterns produced by thousands of drops under varying conditions of interfacial surfactant concentration, drop size, distance of rise to the interface, and physical properties, added no new "drainage types" to those already mentioned by Hodgson and Woods (17). However, all the interference patterns could be decomposed into five distinct "mechanisms" for the lamella behaviour. These

mechanisms were: (1) rapid approach of the drop to the interface, (2) dimple formation in the lamella, (3) slow even thinning, (4) uneven thinning, and (5) lamella rupture. The success of this approach may be judged by the insight which these mechanisms yield into the complex behaviour of the lamella and its bounding interfaces.

Each mechanism is now considered in turn.

4.2.-1 Rapid Approach

In the cell, the drop was nearly always released within one to two millimeters of the undeformed bulk interface. One tenth of a second after the release of the drop, the lamella became thin enough (about 3 microns thick) to yield distinct light interference patterns. Often the rapid thinning of the lamella continued to less than 500 A° where rupture then immediately occurred. The time during which a light interference pattern existed was arbitrarily chosen as the drop "rest-time"; for rapid approach to rupture, this rest-time was about 0.1 seconds. If rupture did not occur, the lamella was thick enough to yield longer rest-times, and the rapid approach ceased.

This mechanism of rapid approach is the simplest of all five mechanisms. The drop buoyancy force causes the droplet to accelerate and rapidly approach the bulk interface. Near the interface, a lamella begins to form, and the decreasing thickness of the lamella begins to restrict the flow of liquid from the lamella. This restriction of flow is magnified if the

mobility of the bounding interfaces is reduced by a very viscous oil phase, or if the interfacial concentration of adsorbed surfactant is sufficiently large to permit a significant interfacial tension gradient to be set up. If an interfacial tension gradient may be set up, both the drop buoyancy force and the inertia force which acts on the drop as it decelerates do work on the bulk interface to set up this gradient. By doing work, the drop's kinetic energy may be dissipated and replaced by surface energy. The drop buoyancy force is opposed by the lamella pressure which is set up by the restriction of the flow of water from the lamella because of both the lamella thinness and of the partial or complete immobility of the bulk interface.

The transfer of kinetic energy into the potential surface energy of an interfacial tension gradient is very rapid and, if complete, the period of rapid approach ceases. The radius of the light interference pattern produced by the lamella fluctuated as the drop bounced. This is caused by the partial over-expansion of the bulk interface. The over-expansion results because of the larger average lamella pressure necessary to balance both the drop buoyancy and the initial drop inertia force, compared to the average lamella pressure necessary to balance just the drop buoyancy force. If the transfer of drop kinetic energy to the interfacial tension gradient can not be complete because of insufficient surfactant adsorbed at the interface, then partial mobility of the bulk interface results, and lamella thinning continues until rupture.

4.2-2 Dimple Formation

After rapid approach, the drop and bulk interfaces are very close together. Lamella thicknesses then often yield a black interference pattern. This is about 500 A° thickness. A dimple then begins to form, as shown by the photographs and accompanying relative lamella thickness profiles of Figure (3). Normally, the dimple formed evenly, but sometimes the inflow of water to form the dimple occurred unevenly as shown in Figure (3). This point is discussed further in section 4.3-1.

The explanation for dimpling is straightforward. A large interfacial tension gradient, or gradient in the concentration of adsorbed surfactant, exists as shown in Figures (6) and (7). As discussed in the previous section, the large interfacial tension gradient is caused by both the drop buoyancy and the inertia forces acting on the bulk interface during the rapid approach mechanism. Once the drop is effectively at rest (it may still move slowly upward or downward during lamella thinning) a large force imbalance exists. The surface shear stress now acting on the bulk interface may be represented by equation (9), but the interfacial tension gradient must exceed the surface shear stress because the drop inertia force that was partially responsible for setting up this gradient has been dissipated. There is, therefore, a large force imbalance which causes the bulk interface to contract. The contraction of the bulk interface carries adsorbed surfactant inward, from the region of the

interface near Γ_{max}. This reduces the interfacial tension gradient. If the inward bulk interface velocity U is large, there is a net inflow of water into the lamella. The lamella thickness increases, especially at the center. Further addition of water to the lamella gradually ceases as the interfacial tension gradient in the bulk interface approaches a balance with the surface shear stress.

4.2-3 Slow, Even Thinning

Once dimple formation begins, the minimum lamella thickness at the barrier ring usually increases if the rate of dimple formation is rapid. During slow, even thinning, the dimple center may or may not move down. There is a slow contraction of the bulk interface because there is a decrease in the surface shear stress with a decrease in the over-all lamella thickness. Gradual slow, even thinning occurred at the barrier ring until rupture occurred.

To summarize the lamella behaviour for 10^{-6} gm/l. of S.L.S., the sequence of events is first, the appearance of the rapid approach mechanism. There is approximately the same lamella thickness at all radial locations within the barrier ring. Rapid approach continues until the minumum lamella thickness is 1000 - 2000 A°. The dimple formation mechanism then increases the center lamella thickness, often to 30,000 A°, and the minimum lamella thickness at the barrier ring increases to about 4000 - 6000 A°. Slow even thinning begins and the minimum

lamella thickness decreases to less than 500 A°. There is little change in the center lamella thickness. The slow even thinning mechanism is shown in the last two photographs of Figure (3). Figure (5) shows the slow even thinning mechanism for the case when the rapid approach mechanism ceases at very large lamella thicknesses. This behaviour is observed for 10^{-4} gm/l. of S.L.S.

Hodgson and Woods (17) have derived a simple model to interpret the slow even thinning at the barrier ring. This model assumes that lamella drainage only occurs outside the barrier ring. Since this model accurately describes lamella drainage at the barrier ring, the slow even thinning mechanism is apparently a drainage period during which water is easily lost from the lamella region outside the barrier ring.

Calculations of the volume of water inside the lamella have been done for experimental lamella profiles. These calculations show that there often is no loss of water from the region inside the barrier ring. This may be the result of the slow contraction of the bulk interface.

4.2-4 Uneven Drainage

The contents of the dimpled region of the lamella often flowed preferentially out of one side of the barrier ring. The overall lamella thickness decreased rapidly to give almost a constant lamella thickness with radius, and lamella thinning became very slow. This mode of uneven drainage continued until

rupture occurred. The last photograph of Figure (5) shows the beginning of uneven drainage, primarily at one region of the barrier ring and also the wrinkling of the barrier ring at several other locations. Rupture occurred immediately after this photograph was made. The photographs in Figure (4) illustrate the more usually observed case of uneven drainage during slow, even thinning.

Uneven drainage is the most common mode of drainage behaviour for the range of variables studied in this work, but yet is the least understood. A postulate on the causes of uneven drainage will be formulated here, based on the concepts introduced in Section (3). Since the behaviour of the lamella outside the barrier ring cannot be observed because the large lamella thicknesses do not produce a light interference pattern, the ideas on which this postulate is based can only be judged by how well the postulate can explain the lamella interference pattern data within the barrier ring.

When a drop approaches the bulk interface, surfactant is rapidly swept out of the central region of the interface. An interfacial tension gradient is set up to balance the surface shear stress exerted on the bulk interface. Figure (9) shows that the calculated interfacial concentrations of surfactant, beyond the barrier ring, may exceed the interfacial concentration of surfactant, Γ_t, adsorbed in the quiescent region of the bulk interface, outside the lamella. By setting

Γ_o equal to zero in equation (10), Γ_{max} at r = R may be calculated for specified system physical properties and center lamella pressure p_o, as in Table (2).

Dilation of the quiescent region A of the bulk interface, shown in Figure (7), should occur to reduce the surplus of surfactant in the region of Γ_{max}. There should also be an increase in desorption and in surface diffusion of the adsorbed surfactant molecules from the surplus surfactant region.

However, once the lamella has formed, the calculation of the surface shear stress from curves fitted to the experimental relative lamella thickness profiles has shown that the quantity of surfactant required in the stressed region of the bulk interface rapidly decreases as slow even thinning proceeds. The results of such a calculation are given in Figure (10), for the case when slow even thinning and dimple formation are taking place simultaneously. Therefore, the stressed region of the bulk interface loses surfactant, but this region also requires less surfactant as slow even thinning proceeds.

At some region during this process, probably at r = R, the local value of the surface shear stress exceeds the interfacial tension gradient set up in the bulk interface. This is because the bulk interface has lost surfactant from the stressed region, and now has fewer surfactant molecules than are necessary to balance the surface shear stress everywhere. The bulk interface then becomes mobile in this region. The water in the

lamella in this region now flows outward with less restriction than for an immobile interface. The outward rate of flow increases along the radial line on which mobility first occurred. More surfactant is swept outward along the bulk interface because the surface shear stress is increased. A large quantity of water then rapidly flows through one small region at the barrier ring. This is uneven drainage, and it continues until the equality between the surface shear stress and the interfacial tension gradient is again approached. Slow even drainage begins again, only now the lamella thickness and pressure gradient are much reduced.

The data in Figures (8) and (9) may be used to illustrate further the uneven drainage concept. Curve A of Figure (29) shows the minimum quantity of surfactant that is necessary in the stressed region of the bulk interface to balance the lamella surface shear stress for the lamella profiles of Figure (8). Curve B is a hypothetical curve, postulated to describe the actual quantity of surfactant in the stressed region of the bulk interface. At the point of intersection C of these two curves, the bulk interface contains the minimum quantity of surfactant necessary to balance the surface shear stress, and at an elapsed time of $\theta > \theta_c$, uneven drainage begins.

Two further points should be noted. Uneven drainage is a local phenomenon. It occurs usually at only one location in the bulk interface, but was sometimes observed to occur at

two locations, simultaneously. The second point is that uneven drainage is postulated to begin at $r \doteq R$. The sudden flow of water through the barrier ring is a consequence of the mobility of the bulk interface in the $c \lesssim r \lesssim R$ region. Uneven drainage may also occur if the $r = c$ region of the bulk interface becomes mobile. However, there is no reason to suggest that this region does, in fact, become mobile before any other region of the bulk interface.

4.2-5 Rupture

Nearly all the light interference patterns observed in this work developed a black region before rupture occurred. If rupture occurred and no black region was evident, the reason for premature rupture was often seen to be a piece of dust. This was usually observed for a newly formed interface. Another instance when premature rupture occurred is discussed in section 6.6.

Several explanations have been suggested for the cause of rupture. These explanations require dirt, vibrations, interfacial tension gradients caused by macroscopic thermal fluctuations, van der Waals force, the growth of statistical fluctuations in the temperature at an interface, and Brownian motion. The cleaning probe employed in this work ensured that no dirt was in the interface. The drop-forming technique eliminated macroscopic temperature differences between the drop and bulk interfaces because the oil for the drop was removed from the

location of the bulk oil phase where the lamella was formed. Lang (39) has found that vibrations have little effect on the drop rest-times. De Vries (31) has calculated that the scale of statistical thermal fluctuations is too small to cause rupture. Both MacKay and Mason (21) and Hodgson and Woods (17) have incorporated van der Waals force into lamella drainage models. The latter authors have been able to predict rest-times within a factor of two of the observed rest-times. The use of van der Waals force to cause rupture has also been employed by Vrij, and by Vrij and Overbeek (32, 33) to predict the lamella thickness at which rupture occurs. Their theoretical results compare favourably with experimental measurements made on the lamella thickness at rupture for soap films and for lamellae in oil/water systems. Their calculations also assumed that no double layer repulsion was present to offset the increase in van der Waals force as the lamella thickness decreased.

Light intensity measurements on the thickness of the lamella at rupture were made on the four systems studied in this work, and were also made by Platikanov and Manev (23). Figure (30) shows the results of measurements made in the present work. The measured value of the thickness at rupture of 200 to 400 A° agrees with the measurements made by Platikanov and Manev for their liquid/liquid systems.

Van der Waals force increases gradually as the lamella thickness is decreased. However, rupture occurred very rapidly

in the systems studied. This suggests that van der Waals force may not be the only cause of rupture. This is apparently confirmed by the data in Figure (31) where a typical curve of the lamella thickness as a function of time has been obtained from a light intensity measurement. The theoretical type of lamella thickness behaviour as a function of time is also shown in Figure (31), as predicted from the Hodgson/Woods model. If van der Waals force causes rupture, there should be a rapid, but noticeable decrease in the lamella thickness near rupture.

This argument against the involvement of van der Waals force in rupture is contradicted by the observation that very black soap films 50 A° thick can exist for long periods if van der Waals force is balanced by double layer repulsion.

One solution to this anomaly is that the experimental curve in Figure (31) was taken from a smoothed curve drawn through slightly fluctuating light intensity data. An inflection point in the fluctuating data would not be apparent. If a slight increase in van der Waals force causes additional lamella drainage, the bulk interface may become mobile. Drainage would no longer be viscous, but rather the drainage rate would be limited only by the inertia of the water in the lamella. The curve in Figure (31) that typified the results of the Hodgson/Woods model shows the lamella thickness as a function of time for viscous flow only. Inertial flow would be much more rapid. Lamella drainage to zero thickness could then occur in a very short period.

Although an exact description of the local lamella behaviour when rupture occurs would be complicated because of the influence of the local interfacial surfactant concentration and the electrolyte concentration, Vrij and Overbeek (33) have formulated a simple model which used van der Waals force to cause rupture in a pure fluid/fluid system. Rupture occurs rapidly once a critical local lamella thickness of 200 to 400 A° is reached.

4.3. Application of the Drainage Mechanisms and Light Interference Observations to an Interpretation of the Drop Rest-time Data

The mechanisms describing lamella behaviour have been discussed without reference to a specific oil/water system. In this section, the influence of the system physical properties and of the drop radius on these mechanisms will be discussed through an analysis of the drop rest-time data. Each oil/water system will be discussed individually. In section 6.1, the effect of the physical properties on the drop rest-time will be discussed further.

4.3-1 Toluene/Water

Figures (11) to (15) show the rest-time behaviour for the toluene/water system for increasing quantities of S.L.S. in the aqueous bulk phase.

The mobility of the drop and bulk interfaces accounts for the very small initial drop rest-times for the data in

Figure (11). However, even for the "pure" system, some interfacial contamination is present. This is further illustrated by the data in Table (7). When the drop's kinetic energy can be dissipated by setting up an interfacial tension gradient in the bulk interface, rest-times then become comparatively long. This suggests that surfactant impurities are present, although their source and composition are in doubt. Since the critical interface age, t_c, was also observed to be about four to five minutes for 0.005 ml. toluene drops in a completely pure system (no sodium lauryl sulfate or KCl electrolyte) the addition of 0.01 N. KCl. does not seem to be responsible for the surfactant impurities. Hickman (34) has given an excellent discussion of this problem for his study of boules. Additional discussion of this problem will also be given in section 5.1.

Long rest-times in a supposedly pure oil/water system also suggest that very little surface active impurity is required in the bulk interface to arrest the rapid lamella thinning mechanism. The characterization of this impurity by sodium lauryl sulfate shows that the aqueous phase concentration of impurity should be less than 10^{-9} molar. This is because the rest-time data in Figure (11) have a larger t_c than do the data of Figure (12a). A large t_c is indicative of a small interfacial surfactant concentration.

If there is a minimum quantity of surfactant in the interface when the rapid thinning mechanism is arrested, then

the interfacial concentration of surfactant at the lamella center should be approximately zero. Since the quiescent interfacial concentration, Γ_t, should be very small, the driving force ($\Gamma_{max} - \Gamma_t$) should be large and surfactant will be rapidly lost from the stressed region of the bulk interface.

The observed light interference patterns of the lamellae showed that once rapid lamella thinning ceased, slow, even dimpling followed, but uneven drainage also began almost immediately.

The "pure" system, containing only electrolyte, may be more complex than the explanation suggests. If surfactant impurity is local only to the region where the drop will reach the bulk interface, then the rapid approach of the drop to the interface may be arrested, but the resultant ($\Gamma_{max} - \Gamma_t$) will be large because Γ_t is effectively zero. Therefore, surfactant may be very rapidly lost from the stressed bulk interface region by both surface diffusion and by interface expansion. The discussion given in Section 5.1. supports this supposition.

When 10^{-6} gm/l. of S.L.S. was deliberately added to the water, a shorter period of instantaneous rest-times was observed, as shown in Figure (12a). This decrease in the value of t_c is due to a rapid adsorption of surfactant. Rest-times then became long, with dimple formation and slow even thinning until rupture as the sequence of the mechanisms. Even drainage persisted for this surfactant concentration because surfactant is

rapidly adsorbed at the freshly cleaned interface. Enough surfactant is adsorbed at the bulk interface so that rupture occurs before the minimum quantity of surfactant necessary to support the lamella shear stress is reached. Since the maximum in rest-times at small interface ages may be eliminated by subtracting the time required to form the dimple from the drop rest-time, dimple formation appears to retard the start of slow thinning. The initial barrier ring height at which slow, even thinning begins is not important since lamella thinning is relatively rapid down to thicknesses less than 1500 A°. Most of the time that the drop is at the interface elapses with the minimum lamella thickness at less than 1500 A°. This explains why the time for slow thinning given in Figure (12b) is constant.

Uneven drainage occurred at long interface ages. As the interface ages, the drop is presumably arrested at larger and larger lamella thicknesses since more surfactant is in the interface to allow a larger interfacial tension gradient to be set up sooner during the rapid approach of the drop to the interface. Since the surface shear stress is larger at a larger lamella thickness, as suggested by equation (9) and assuming $\frac{\partial p}{\partial r}$ is relatively constant, the interfacial tension gradient set up must be larger than for smaller interface ages. Slow even lamella thinning occurs rapidly at large lamella thicknesses, so a large imbalance between the surface shear stress

and the interfacial tension gradient in the bulk interface quickly develops. Dimpling takes place rapidly and since the driving force for dimpling is very large, dimples are larger than for small interface ages. According to the postulate on uneven drainage, the loss of surfactant from the stressed region of the bulk interface must exceed the amount that can be lost by the lamella as thinning proceeds. If this imbalance occurs before lamella rupture, uneven drainage occurs. The postulate is too qualitative, however, to allow even a rough quantitative check on this reasoning.

One additional observation for the 10^{-6} gm/l. S.L.S. case is that sometimes the dimple formation was uneven. This is shown by the photographs in Figure (3) for anisole/water. For this case, the dimple contents seemed to follow an exactly reverse path to that for uneven drainage. Liquid appeared to flow through a very small region of the barrier ring and was immediately distributed throughout the lamella. This formed the dimple. The observation partially confirms the uneven drainage postulate. If the rapid drainage mechanism occurs unevenly, an interfacial tension gradient would be developed in only one region of the bulk interface. When the drop is arrested, this uneven interfacial tension gradient causes liquid inflow, exactly the reverse of uneven drainage. Around the rest of the lamella periphery, smaller interfacial tension gradients have been set up because of the preferential flow

out of one region during the rapid approach of the drop to the interface. Therefore, when the pressure gradient in the lamella begins to increase as a result of dimple formation, liquid is initally easily lost through the majority of the lamella periphery, while an interfacial tension gradient in this region is being set up by the expansion of the bulk interface. Liquid flowing into the lamella is therefore rapidly and evenly distributed throughout the lamella. Uneven dimple formation ceases when the surface shear stress balances the existing interfacial tension in this region which caused the uneven formation.

The data in Figure (13) , for 10^{-5} gm/l. of S.L.S., show that the inital period of bulk interface mobility is lost because of the more rapid adsorption of surfactant. Uneven drainage occurred sooner than for the data in Figure (12a).

Figure (14), for an additional ten-fold increase in the aqueous phase surfactant concentration shows only one drop that drained evenly. The remainder of the drops drained unevenly as the interface aged. A decrease in rest-times with very large interface ages, as shown in Figure (14), could be the result of uneven drainage that was observed to occur at large lamella thicknesses. The result of this uneven drainage would be a more rapid slow uneven drainage to rupture than with even drainage.

For the data in Figure (14), the lamella initally seemed to be draining evenly at a large lamella thickness without going

through the dimple formation mechanism. This is a consequence of the drop being arrested at a very large lamella thickness, and the bulk interface contracting as the shear stress on it decreases. Lamella drainage tends to reduce the lamella thickness, but this is balanced by fluid inflow caused by the bulk interface contraction. Thus, the mechanism of dimple formation is occurring simultaneously with the mechanism of slow even drainage. This also occurred for the data in Figure (12a), but slow drainage for the thin lamella was so much slower than dimple formation that the dimple thickness increased. Photographs of the simultaneous occurrence of dimpling and slow even drainage are given in Figure (5) for the anisole/water system.

For a further increase in the aqueous phase surfactant concentration, the data given in Figure (15) show that an equilibrium interfacial concentration of surfactant is rapidly reached and rest-times show little tendency to change after an interface age of 10 minutes. Drainage was completely uneven.

A further ten-fold increase in the aqueous phase surfactant concentration showed that the rest-times behaviour differed litdefrom the behaviour of the rest-time data given in Figure (15).

In this study, sufficient electrolyte was added to the aqueous phase to limit double layer repulsion to lamella thicknesses less than 100 A°. When rupture occurs, the two oil/water interfaces making up the lamella must have come within molecular

dimensions of one another and joined at some point. Double layer repulsion should prevent this if the drop interface also contains ionic surfactant. However, if the two oil/water interfaces become mobile at thicknesses of 200 to 400 A° because of rapid local lamella drainage caused by the rapidly increasing van der Waals force, then little surfactant will be present at the potential rupture site and double layer repulsion will not be present. If insufficient electrolyte is added to the water phase, double layer repulsion may equal the van der Waals force before the oil/water interfaces can become mobile. This leads to a gradual stop in lamella thinning with no rupture.

4.3-2 Anisole/Water System

Figures (16) to (18) show the rest-time behaviour observed for a concentration of 10^{-6} gm/l. of S.L.S. + 0.01 N. KCl for three different sizes of drops. The 0.020 ml. volume anisole drop produced a lamella with approximately the same barrier ring radius as did a 0.005 ml. volume toluene drop. The lamella mechanisms were: rapid approach to a thin lamella, dimple formation, slow even drainage, followed by uneven drainage, and then rupture. At large interface ages, the dimple formation and slow even drainage mechanisms occurred simultaneously as shown in Figure (5). Figure (32) shows typical lamella behaviour for both clean and aged interfaces for the anisole/water system.

Figures (16) to (18) may be interpreted to show that the bulk interface mobility is a function of drop size. A longer

period of bulk interface mobility is observed for small drops than for large drops. This is not confirmed by the calculations of Γ_t given in Table (2) because the calculations are sensitive to the lamella shape, for large drops. Also, the effect of drop inertia on the initial interfacial tension gradient set up in the bulk interface has not been included in the Table (2) calculations. A simple calculation can show that if the drop potential energy at the drop syringe is stored as surface energy in the interfacial tension gradient of the bulk interface, a 0.005 ml. anisole drop must do 1.5 times more work per unit area of bulk interface than a 0.020 ml. anisole drop. This suggests that since the interfacial tension gradient will be steeper than that used in calculating the values of Γ_t in Table (2), small drops may require a larger Γ_t than do large drops.

While Hodgson and Lee (37) have devised a simple model to account for bulk interface mobility as a function of drop size, their analysis was based on a parallel disc lamella and no consideration was given to an accurate description of the interfacial distribution of adsorbed surfactant. The drop inertia should also be considered in the discussion of the effect of drop size on the mobility of the bulk interface.

The data in Figure (18) for 0.020 ml. anisole drops show that a period of rest-times is observed for which even drainage occurred. This is also observed for the CA/water system. The occurrence of even-uneven modes of drainage

behaviour as the bulk interface ages must be a function of the interfacial concentration of surfactant. No quantitative analysis can be done to account for this behaviour.

Figures (16) to (18) also show that the average drop rest-time increases with an increase in drop size. A larger radius of the lamella for larger drops would cause an increase in the flow path of the lamella water, and also would make the lamella thinner at larger radii, outside the barrier, because of the smaller curvature of the larger drops.

The rest-times in Figures (19) to (21) for 10^{-4} gm/l. of S.L.S. show a change in lamella behaviour from uneven to even drainage as the interface aged. Rapid approach seemed to cease at a large lamella thickness, the lamella center thickness decreased very slowly, and the barrier ring thickness decreased very rapidly, with some expansion of the barrier ring radius. Figure (8) shows the relative lamella thickness profiles for this behaviour. This same lamella behaviour was also observed for the toluene/water system at the same S.L.S. concentration, but uneven drainage always occurred before rupture.

The transformation from uneven to even drainage at small interface ages is not completely understood. As was previously discussed in section 4.2 and will be discussed later in sections 4.2-3 and 4.5, the lamella drainage may be rapid enough to allow the stressed region of the bulk interface to lose surfactant more rapidly than it can be lost at the Γ_{max} region. This would

allow even drainage to continue until rupture. The solution to this transformation problem is probably dependent on the interaction of the rapidity of drainage, the interfacial concentration of adsorbed surfactant, the lamella shape, drop size, and how these variables determine the rate of loss of surfactant.

4.3-3 Cyclohexane-Anisole/Water System

(The CA/water system is 0.16 mole fraction cyclohexane plus 0.84 mole fraction anisole/water.)

Figures (24) to (27) show the rest-time data observed for two drop sizes for the CA/water system. No period of very short rest-times was observed. This may be due to insufficient interface cleaning or it may be dependent on the physical properties of the CA/water system. For the data in Figures (24) and (25) for 10^{-6} gm/l. S.L.S. + 0.01 N. KCl., the period of even drainage is shorter than for the toluene/water system. As was discussed in section 4.3-1 for toluene, the appearance of uneven drainage must depend on the interaction of several variables. Not enough is known about these interactions to be able to state why one oil/water system drains unevenly while another oil/water system drains evenly, for the same interfacial concentration of adsorbed surfactant.

The lamella behaviour for this system for both even and uneven drainage was the same as for the toluene/water and anisole/water systems, as is shown in Figure (32a) for 10^{-6} gm/l.

of S.L.S. The rest-time data in Figures (26) and (27) for 10^{-4} gm/l. of S.L.S. show the same change from uneven to even drainage as the interface aged as did the anisole/water system and the data also show the same persistence of uneven drainage at small interface ages for an increase in the drop size as did the anisole/water system.

The observation that rest-times initially decrease very rapidly and eventually become so small as the interface ages that the rest-times are almost independent of drop size for even drainage supports the uneven drainage hypothesis. The rest-times are about 1.5 sec., 2.0 sec., and 2.5 sec. for 0.005 ml., 0.010 ml., and 0.020 ml. volume anisole drops, respectively. If lamella drainage to the rupture thickness is possible before the two curves in Figure (29) intersect, then drainage will be even.

4.3-4 Cyclohexanol/Water System

Figures (22) and (23) show the rest-time data observed for the cyclohexanol/water system. The lamella behaviour for this oil/water system is extremely complex, but is the same for both aqueous surfactant concentrations. For the 10^{-4} gm/l. S.L.S. case, the initial lamella behaviour changed more rapidly than for the 10^{-6} gm/l. case, but the lamella drained evenly longer. The sequence of lamella profiles is shown in Figure (33). The lamella drainage is first even for lamella profile number (1), and the lamella center thins rapidly at (2). The

dimple center springs up, as in (3), very rapidly and even drainage immediately becomes uneven at (4). The lamella drainage then becomes even in profile (5), and uneven in profile (6), opposite the first site of uneven drainage. Uneven drainage ceases a second time, as in profile (7), and drainage is then slow and even until rupture occurs at profile (8). For the 10^{-4} gm/l. case, the dimple deflates more completely than for the 10^{-6} gm/l. case.

The initial period of rapid dimple formation is probably a result of the large oil viscosity of this system. When the oil drop first approaches the bulk interface, a very large surface shear stress is exerted on the bulk interface because the large cyclohexanol viscosity resists complete bulk interface mobility. However, if the bulk interface does expand slightly, an interfacial tension gradient is set up. When the surface shear stress acting on the bulk interface decreases as the lamella thickness decreases, the bulk interface contracts rapidly for a short time because a large imbalance exists between the surface shear stress and the interfacial tension gradient. This rapid bulk interface contraction causes dimpling.

The immediate occurrence of uneven drainage after dimple formation cannot be caused by surfactant loss from the bulk interface because the viscosity of the oil phase is large. Hartland (38,43) has implied that uneven drainage is caused by

circulation of oil inside the drop, for viscous liquid/liquid systems.

When uneven drainage occurs in sequence (4), lamella drainage is primarily from the site of uneven drainage. The bulk interface gradually sets up an interfacial tension gradient to balance the surface shear stress at the site of uneven drainage. Outward flow from the lamella, therefore, must increase at all other points around the lamella periphery since the water flowing at the site of uneven drainage experiences a larger resistance to flow because the mobility of the bulk interface decreases.

Since the region of the lamella periphery diametrically opposite to the first site of uneven drainage has had little flow through it, any interfacial tension gradient set up there is small. The lamella thickness rapidly decreases at the initial region of uneven drainage, since water flows more freely in the region of the lamella where the bulk interface is partially mobile. Uneven drainage now begins on the opposite side of the lamella.

The same lamella behaviour for the cessation of uneven drainage is again repeated at the second site of uneven drainage, but since lamella thicknesses are now small all around the periphery, about 5000 A°, interfacial tension gradients that have been set up now are sufficiently large to prevent the occurrence of uneven drainage a third time. The lamella liquid

thus oscillates from one side of the lamella to the other for one or two seconds since the surface shear stress is not large enough to overcome the existing interfacial tension gradients, the latter aided by large oil viscosity. Drainage is even and remains even.

At small interface ages, uneven drainage persisted for longer periods than for aged interfaces. This is presumably because of the difficulty in setting up an interfacial tension gradient to balance surface shear stress at the site of uneven drainage, since little surfactant had adsorbed at the bulk interface.

The criterion of the bulk interface mobility determining the onset of uneven drainage seems towork well in the interpretation of the lamella behaviour for this system. However, the cause of the initial uneven drainage is unknown.

For this system, the effect of the interfacial surfactant concentration on drop rest-times is not clear. With 10^{-6} gm/l. S.L.S., rest-times became smaller as the interface aged, but rest-times appeared to remain constant for 10^{-4} gm/l., regardless of the interface age, and are larger than for 10^{-6} gm/l.

4.4. Interpretation of the Hodgson-Woods Drainage Types

Hodgson and Woods (17) have given a summary of the lamella light interference patterns observed for the toluene/water and anisole/water systems. The present work has extended

both the aqueous phase concentration of S.L.S. and the number of systems studied and has found no new drainage "types". The drainage types of Hodgson and Woods will now be decomposed into the five mechanisms of lamella behaviour already discussed in this chapter.

4.4-1 Type I

Type I is simply the rapid approach mechanism, which is caused by the mobility of the bulk interface. Rapid approach continues until the lamella ruptures.

4.4-2 Type II

Type II occurs for 10^{-6} gm/l. S.L.S. + 0.01 N. KCl. Rapid approach, dimple formation, and slow even or uneven drainage, followed by lamella rupture are the mechanisms which occur for Type II.

4.4-3 Type III

Type III occurs for a large surfactant concentration. The rapid approach mechanism ceases at a large lamella thickness, and drainage becomes uneven. Uneven drainage continues until the lamella ruptures. The 10^{-4} gm/l. S.L.S. + 0.10 N. KCl. toluene/water combination characterizes this behaviour.

4.4-4 Type IV

Type IV also occurs at a large surfactant concentration, but rapid approach ceases and simultaneous dimple formation and

slow even drainage occur at large lamella thicknesses.

5. Discussion of Hodgson's Experimental Techniques

The rest-time data which have been presented in this chapter show the large influence that the drop size and the interface age have on the rest-time distributions. Hodgson's drop-forming and interface cleaning techniques will therefore be discussed to determine their influence on the rest-time data.

5.1 The Interface Cleaning Technique

Once the aqueous surfactant solution was placed in the reservoir and the coalescence cell was filled, the bulk interface was cleaned approximately twenty times before the reservoir was refilled. Since the cleaning of the interface is similar to foam fractionation, the aqueous phase concentration of surfactant should decrease as cleaning re-adsorption, and cleaning, etc., proceed.

A simple mathematical model may be formulated to investigate the effect of interface cleaning on the aqueous phase concentration of surfactant.

A mass balance on the surfactant in the cell yields:

$$\frac{d}{dN} (c\bar{V}) = - n A - c q$$

where c = aqueous phase surfactant concentration, molecules/cm^3

N = number of times the interface is cleaned

n = number of molecules/cm^2 adsorbed at the interface before each cleaning

q = volume of water removed during each cleaning, cm^3

A = interfacial area, cm^2

V_o = solution volume in cell plus reservoir

$V = V_o - Nq$, the volume of aqueous surfactant solution in the cell plus reservoir after N cleanings

If $n = Kc$ for a small change in c and if equilibrium adsorption is assumed, the above equation is integrated to yield:

$$\frac{c}{c_o} = \left(\frac{V}{V_o}\right)^{\frac{KA}{q}}$$

If the exponent, $\frac{KA}{q}$, is small, interface cleaning will have little effect on c. For 10^{-6} gm/l. S.L.S. + 0.01 N. KCl., n is calculated from Davies and Rideal (36) to give $K = 1.55 \times 10^{-3}$ cm. Since q is about 2.5 ml. and A is 12.5 cm^2., $\frac{KA}{q} = 0.00775$. The small value of the exponent shows that interface cleaning has little influence on the aqueous phase concentration even up to a maximum of 20 cleanings.

The extent to which surface active impurities appear to be removed by this interface cleaning technique is illustrated by the data in Table (7). These data show that the oil or aqueous phase concentration of the unknown impurity is greatly

reduced because the critical interface age, t_c, is doubled for ten interface cleanings. This rapid reduction in the apparent bulk phase concentration of surface active impurity is contrary to the results of the calculation just done for S.L.S.

For each determination of the value of t_c given in Table (7), several drops were used. The drop syringe therefore penetrated the oil/water interface several times between each interface cleaning. If an impurity of some unknown composition was adsorbed on the side of the syringe, the interface may be contaminated each time the syringe touched the interface. As the number of drops formed during the t_c determinations increased, the amount of impurity on the syringe should decrease. This should decrease the interface contamination and should result in larger t_c values. This explanation shows that the impurity is adsorbed at the bulk interface where it will have the most influence: precisely in the region where the drop will reach the bulk surface.

5.2. The Drop-Forming Technique

The plunging and withdrawing of the capillary tip through the bulk interface disturbs the already adsorbed surfactant. This may be the cause of the saw-tooth effect observed for some rest-time data, especially evident in the data of Figure (12a). There is seemingly an optimum time between forming drops for this technique. Repeatedly forming and releasing a drop immediately after the previous drop coalesces may not allow

sufficient time for the adsorbed surfactant in the bulk interface to be evenly distributed for each successive drop. If there is too long a time between drops, especially at concentrations of 10^{-4} and 10^{-3} gm/l. of S.L.S., the trend in rest-times with interface age is measured only coarsely, and any vagaries in rest-times will further obscure this trend. For the data presented in this work, at least one minute elapsed between the arrival of each drop at the interface.

The interface was therefore allowed to remain quiescent for 30 - 45 seconds, depending on the magnitude of the rest-times.

Drops were quickly formed on the syringe. Too long a formation time would allow surfactant to adsorb at the drop interface, especially with the higher concentrations of surfactant used. Since the formation of the drop is rapid, the oil in the drop may circulate. The rest-time data in this work are all subject to the influence of this expected circulation, although its exact influence is unknown. By increasing the drop formation times at small surfactant concentrations, no apparent effect on rest-times was observed. Thus, drop circulation would seem to have only a very small influence on lamella drainage.

Once the drop was formed, it was slowly forced off of the syringe and allowed to rise the short distance of one to two mm. to the bulk interface. However, increasing the distance of rise of the drop to three or four cm. had no apparent effect on rest-times, and this is equivalent to "shooting" the drop at

the interface.

Finally, the use of the drop-forming technique obviates the need for close temperature control of the cell and reservoir contents. Coalescence studies require that no temperature difference exists between the drop oil phase and the bulk oil phase because temperature differences will cause both interfacial tension gradients and thermal convection currents. When the drop oil reservoir is external to the cell, close temperature contol is necessary. However, for Hodgson's drop forming technique, the drop oil is taken from the region of the bulk interface where the eventual coalescence will take place. No temperature control was used on the cell in this study. Room temperature was 17 - 27°C. and was recorded for most of the rest-time data taken.

5.3. Validity of Data Obtained by Using the Interface Cleaning and Drop-Forming Techniques

The validity of the rest-time data obtained by using the interface cleaning and drop-forming techniques in a coalescence study may be questioned. For example, the variability of the rest-time data among investigators is unknown. The rest-time versus interface age distributions may be different if the syringe does not puncture the interface continually. The drop-forming technique may affect the interfacial adsorption of surfactant. The extent to which the interface cleaning probe cleans the interface is unknown.

Three sets of data are given in Figure (34) to observe the reproducibility of data among investigators. The data of Hodgson and Lee (14) were taken for 0.0042 ml. toluene drops in a toluene/water system with 4×10^{-6} gm/l. S.L.S. + 0.01 N. KCl. The data of Hodgson and Woods (17) and the data of the present work were taken on the same apparatus for 0.005 ml. toluene drops for 3×10^{-6} gm/l. S.L.S. + 0.01 N. KCl. There is a significant difference between the two rest-time distributions obtained by different investigators for the same oil/water system for the same apparatus.

Both the data from the present work and the data of Hodgson and Lee (14) show the observation of a $\tau_{max.}$ of about 11 to 12 seconds, and show a t_c of one to two minutes. The slightly more rapid decrease in rest-times as the interface aged for the Hodgson and Lee data may be accounted for by more rapid adsorption of surfactant from the slightly more concentrated aqueous solution of S.L.S.

The data of Hodgson and Woods are radically different from the data obtained in the present work. The Hodgson and Woods data have a t_c of four minutes, the data do not have the characteristic maximum in rest-times at a small interface age, and the rest-times do not decrease significantly as the interface ages. The data of Hodgson and Woods are similar to the data given in Figure (11) for the "pure" toluene/water system, although the latter data show uneven drainage as the mode of lamella behaviour.

Reproducibility of data for the same investigator is good for the two experimental techniques used, as is shown by Hodgson and Lee (14). The long t_c of four minutes for the Hodgson and Woods data suggests that the aqueous phase concentration of S.L.S. may be less than 10^{-6} gm/l.. Eagland and Franks (35) have shown that the solute in aqueous solutions of sodium lauryl sulfate undergoes slow hydrolysis to lauryl alcohol at a solution/air surface. Lauryl alcohol is more surface active than S.L.S. and this may account for the behaviour of the Hodgson and Woods data if the surfactant solution was stored for a long period before use. The data from the present study were for aqueous S.L.S. solutions less than one week old and stored in stoppered glass volumetric flasks. Eagland and Franks do not mention the rate or extent of conversion of the hydrolysis reaction.

In summary, there are significant differences between data obtained from the same apparatus. There is no conclusive evidence to account for the differences.

Two effects of the repeated puncturing of the bulk interface have previously been mentioned. The drop-forming technique may be responsible for the saw-tooth behaviour of the data in Figure (12a), and may also be the source of interfacial contamination suspected in Figure (11) data. The effect of interface puncturing on the rest-time distributions cannot be isolated since no additional studies have been done where

the interface cleaning technique was used, but where drops were formed by a non-puncturing method. However, the small scatter in rest-time data measured for larger concentrations of S.L.S., ($>10^{-5}$ gm/l.), indicates that rapid adsorption and surface diffusion of surfactant may erase any variations in the interfacial concentration of surfactant caused by interface puncture. This erasure of variations in the interfacial concentration of surfactant also applies to the effect that the drop syringe movement has on the interfacial adsorption of S.L.S. from the aqueous phase. Any variation in the gradient of the aqueous phase concentration of surfactant which exists at the bulk interface may be quickly erased because of the large aqueous phase concentration of surfactant.

There is an effect of interface cleaning on rest-time reproducibility. This is attributed to the removal of dirt and dust particles from the bulk interface. The motion of these interfacial particles toward the cleaning probe is easily seen for a freshly formed interface when the interface is observed through the microscope while cleaning is in progress. The entire interface must move toward the cleaning probe at different rates, and because of the large size of the four cm. diameter interface and of surface adsorption, the interfacial surfactant concentration will vary with distance from the probe. Therefore, the interfacial surfactant concentration will be near zero only close to the probe. The exact interfacial

surfactant concentration at the interface center where the drop rises cannot be calculated accurately, but is presumed to be small. This is confirmed by the observation of very small rest-times, which suggest small interfacial surfactant concentrations, for 10^{-6} gm/l. S.L.S. at small interface ages.

Interface cleaning, therefore, is effective in removing interfacial impurities and does reduce interfacial surfactant concentrations to small values. Rest-time data obtained by using the interface cleaning probe and by using the drop forming technique are affected by these techniques, but the data are free from the influence of macroscopic interfacial impurities and are therefore more representative of the interfacial surfactant concentration that must exist for the particular set of variables studied.

6. Discussion of Additional Observations

The interpretation of the drop rest-times as a function of interface age was the primary purpose of this study. However, several additional observations should be discussed.

6.1. Physical Property Dependence of the Rest-time Data

In the coalescence literature, rest-time correlations do not consider the mode of drainage, even or uneven, or interface age, and the correlations use mean rest-times to simplify the often-wide distribution of rest-times. The observation of the lamella light interference pattern and the measurement of

the interface age allow a more meaningful comparison of rest-time data to be made among oil/water systems. For example, rest-times for different oil/water systems can be more realistically compared for those drops that have the same patterns of lamella drainage and have the same interfacial concentration of adsorbed surfactant.

The physical property dependence of the Hodgson/Woods model (17) may be used to correlate selected rest-time data. This model predicts that drainage rates, hence rest-times, should be independent of the oil/water system density difference. Equation (13a) has been derived from the Hodgson/Woods model by assuming that if a standard rest-time, τ_s, is known, then the rest-time for any other oil/water system for the same conditions of lamella drainage and interfacial surfactant concentration can be calculated. The equation is:

$$\tau_p = \tau_s \cdot \frac{d_p^2}{d_s^2} \cdot \frac{\gamma_s}{\gamma_p} \cdot m \qquad \text{.....(13a)}$$

This equation shows that rest-times vary directly with the square of the drop radius, and inversely with the interfacial tension. These variables make the flow path narrower if d_p increases and if γ_p decreases. Larger rest-times therefore result. The factor m measures the interface mobility, and is used to take oil viscosity into account. If the drop viscosity is small, then m is approximately equal to one. If the oil drop viscosity is about 30 cp., then m may approach two.

Table (8a) shows a comparison between the even drainage rest-time data and the equation (13a) rest-times predicted from equation (13a) for toluene/water as a standard. The rest-time data for cyclohexanol/water are for a combination of both even and uneven drainage; the particular mode of drainage observed for that system. Agreement is reasonable, to within an almost constant value of + 30% for two of the oil/water systems. Too large a standard rest-time can account for the large percentage difference.

Uneven drainage rest-time data could not be correlated well with this approach. There may be an unaccounted factor such as the degree of interface mobility during uneven drainage which must be considered.

To evaluate the dependence of rest-times on drop diameter, the values in Table (8b) of the index n' used in the equation $\mathcal{T} = K_n d^{n'}$ are given. These values of n' were obtained by varying the drop volume and measuring the drop rest-time at a given interface age of usually 6 - 12 hours. For both even and uneven drainage, n' has values between one and three. This is in agreement with the Hodgson/Woods model, which uses a value of n' of two, but disagrees with the parallel disc model which uses n' equal to 5.

An additional comparison may be made. Equation (13b) was derived from the parallel disc model property dependence.

This equation is:

$$\tau_p = \tau_s \cdot \left(\frac{d_p}{d_s}\right)^5 \cdot \left(\frac{\gamma_s}{\gamma_p}\right)^2 \cdot \frac{\Delta\rho_p}{\Delta\rho_s} \cdot m \quad \ldots\ldots(13b)$$

The values of rest-times calculated from this equation are given in Table (8c). A comparison with the observed average rest-time data shows a large, variable, under-estimation of rest-times. However , the parallel disc model predicts the rest-time variation with a change in drop size and with a change in the oil/water system physical property dependence.

The Hodgson/Woods model and the parallel disc model bracket the observed rest-time results. The former model results are too large, and the latter model results are too small.

6.2. Drop Sliding and the Location of Uneven Drainage

The bulk interface was kept raised at its center to prevent the lateral motion of the drop, However, the drop often arrived at the interface off-center, and slid about 0.05 cm. for one or two seconds, until it reached the bulk interface zenith.

For the 10^{-6} gm/l. S.L.S. case, and especially for toluene drops, an apparent consequence of sliding was the occurrence of uneven drainage at the former downstream side of the lamella. Uneven drainage, however, only occurred when the mode of drainage for non-sliding drops was also uneven; the sliding of the drop, therefore, seemed to uniquely locate the site of uneven drainage.

The expected interfacial tension gradient in the bulk interface, generated by sliding, is shown in Figure (35). If dimpling and slow even drainage are occurring, the former downstream side of the bulk interface should contain less surfactant than does the upstream side. Therefore, the interfacial tension gradients set up to balance the surface shear stress will be unequal in magnitude. Less surfactant must be lost from the downstream region of the lamella periphery if uneven drainage is to occur.

For larger aqueous phase concentrations of S.L.S., the effect of drop sliding on the location of uneven drainage was not apparent.

During slow, even drainage for small surfactant concentrations and for a partially aged interface, uneven drainage sometimes occurred simultaneously at approximately opposite sides of the lamella. This was often followed by a reversion to even drainage at very small lamella thicknesses. This behaviour appears to be simply a coincidental occurrence, although why it never occurred at larger interface ages is not known.

6.3. Rupture

Lamella rupture occurred very rapidly. Therefore, an attempt to use high speed photography to photograph the light interference pattern at rupture through the microscope was unsuccessful. Low film velocities were used in the camera because the level of light intensity provided by the small 100 watt,

quartz iodide, tungsten light source was very low.

At a large aqueous phase concentration of S.L.S. and a small concentration of electrolyte, an all-gray light interference pattern for uneven drainage often was observed to scallop along the pattern edge. This is illustrated by the drawing in Figure (36). Within one second after scalloping was observed, the lamella ruptured. The rapid formation of the very black light interference colour produced in the scalloped region is similar to the description of the occurrence of black spots in lamellae examined by Frankel and Mysels (20), and interpreted by Princen and Mason (40). Scalloping appears to result when the lamella falls into a free energy minimum. Therefore, some double layer repulsion must be present at lamella thicknesses of less than 1000 A°. The occurrence of double layer repulsion at less than 1000 A° thickness is assumed responsible also for the very slow lamella drainage observed in the gray region of the lamella light interference pattern.

6.4. Surfactant Adsorption Rate

Hickman (34) has also found boule stability to be dependent upon interfacial impurities. In the present work, an aqueous phase surfactant concentration as low as 10^{-9} molar is capable of affecting drop rest-times. Since the drop rest-time is sensitive to the interfacial surfactant concentration, then the value of the interface age for rest-times which show little further change with an increase in interface age can

indicate when an almost-equilibrium quantity of surfactant has been adsorbed.

The interface age when this occurs is compared with an adsorption time calculated from the Ward/Tordai equation (36) for equilibrium adsorption. The Ward/Tordai equation is valid for inital adsorption only, but may be used to calculate an approximate adsorption time. The results of the calculations are given in Table (5). The agreement is poor at small aqueous phase concentrations. This is expected since the time taken for equilibrium adsorption to occur for a small aqueous phase S.L.S. concentration should be large. Despite their large sensitivity to the interfacial concentration of adsorbed surfactant, drop rest-times are insensitive to the small increments in interfacial surfactant concentration that occur over long periods near equilibrium adsorption.

6.5. The Light Interference Pattern Radius

For even drainage, the barrier ring is very close to the edge of the light interference pattern. Outside the barrier ring, the lamella thickness increases very rapidly. Close observation is necessary to detect three or four additional interference rings, since the rings are faint, and close together.

The observed radius of the light interference pattern may be compared with the radius of the barrier ring calculated from two models. These models, the parallel disc model and the equilibrium model, predict the lamella radius at which the

dynamic pressure in the lamella equals zero. The radii predicted by these models have been purported to predict the barrier ring radius, since these models assume that the dynamic lamella pressure falls to zero at the barrier ring. It has been shown both semi-empirically (27) and theoretically in Chapter 4 that the dynamic lamella pressure is not equal to zero at the barrier ring. However, these simple models may be useful in a coincidental prediction of the barrier ring radius, even though these models are based on faulty assumptions. The barrier ring radius is assumed equivalent to the light interference pattern radius.

Table (4) gives the comparison. The parallel disc model predicts barrier ring radii that are too small, since it assumes an average lamella pressure of $\frac{2\gamma}{d}$. The better agreement of the equilibrium model with the data is due to the assumption of an average lamella pressure of $\frac{\gamma}{d}$ for this model.

The light interference pattern radius was observed to be independent of the type of lamella drainage. Radii were measured for both even and uneven drainage, and were used in obtaining the observed radii given in Table (4).

6.6. Local Depressions in the Lamella

Local depressions in the lamella thickness seemed to appear infrequently, but more often for an aged or freshly formed bulk interface. These depressions moved about in the lamella

as if caught in the flow of water from the lamella, and this proved useful in the interpretion of the lamella drainage patterns. Figure (37) shows a drawing of a light interference pattern for the uneven drainage of a toluene drop at an aged interface, for 10^{-6} gm/l. of S.L.S. + 0.01 N. KCl. This drawing shows that the radius of the depression is large when compared with the radius of the light interference pattern. The depression was observed to be about 1000 - 2000 A° deep (0.1 - 0.2 μ.), and had a radius of about 20 μ..

The depressions seemed to occur spontaneously, were often in groups of two or three, and were usually observed along the edge of the interference pattern. Sometimes, the depressions appeared in the center of the lamella. The depressions often slowly disappeared over a time of two or three seconds. Their appearance in amber, white, or gray coloured light interference patterns often resulted in immediate rupture.

A local increase in the bulk interfacial tension of the bulk interface could increase the radius of curvature of the interface. This would account for the depression in lamella thickness. Surface diffusion and bulk interface contraction could account for the disappearance of the depression. However, why the phenomenon initially appears is unknown.

6.7. The Effect of a Non-ionic Surfactant and of Electrolyte Concentration on Drop Rest-times

An ionic surfactant is soluble in polar liquids such

as water, but essentially insoluble in non-polar oils. A non-ionic surfactant may be both partially oil and water soluble. The presence of surfactant in the oil phase can radically alter the lamella behaviour because adsorption of surfactant may now occur from the underlying oil phase during lamella drainage (42). For a water soluble surfactant, adsorption of surfactant from the water lamella is small because the volume of solution in the lamella is small.

In this work, a water soluble non-ionic surfactant, 2 - (2-ethoxy-ethoxy) ethanol, was also used in concentrations of 0.05 and 0.50 ml. of surfactant per litre of water, plus 0.01 N. KCl. Lamella behaviour was analogous to the 10^{-5} and 10^{-4} cases for S.L.S. for toluene/water for both concentrations, respectively. The electrolyte concentration is important when an ionic surfactant is used. Double layer repulsion was evident when 0.01 N. KCl. was used with 10^{-4} gm/l. S.L.S., but not when the electrolyte concentration was 0.05 to 0.10 N. KCl. While rupture often occurred when double layer repulsion was evident, drainage for black coloured lamellae was very slow, and rest-times were large. The addition of a more concentrated KCl solution resulted in more rapid drainage to rupture.

7. Summary and Conclusions

This chapter presents part of the results of an extensive investigation into the rest-time and lamella behaviour for oil drops for four oil/water systems. Single oil drops of

various controllable sizes were released at the bulk oil/water interface and their rest-times were measured as a function of the age of the bulk interface, measured from the time of cleaning. The simultaneous observation of the light interference pattern, produced by illumination of the lamella formed between the drop and bulk interfaces with white light, resulted in the formulation of five distinct mechanisms for lamella behaviour. These mechanisms were used to explain the observed lamella behaviour. Some of the experimentally obtained profiles of the relative lamella thickness were fitted by a semi-empirical polynomial. The interfacial distribution of surfactant could then be calculated for each profile. An hypothesis was formulated, based on these calculations, to explain the occurrence of uneven drainage.

The light interference patterns and the five lamella behaviour mechanisms were then used to discuss the observed rest-times which were measured as a function of interface age.

Many conclusions may be reached as a result of this work. These conclusions are presented for three separate areas; the conclusions reached from a consideration of the drop rest-time results, the conclusion reached from a consideration of the light interference patterns, and the conclusion reached from a consideration of the experimental techniques used in this work. The conclusions from each area are presented in turn.

A. For Rest-times

(1) Instantaneous drop rest-times were only observed for 0 to 10^{-6} gm/l. of S.L.S. at small interface ages, for the toluene/water and anisole/water systems. The other two systems studied did not exhibit instantaneous rest-times. These instantaneous rest-times are attributed to mobility of both the drop and bulk interfaces, for small interfacial concentrations of adsorbed surfactant.

(2) The length of time, t_c, that the rest-times are instantaneous as the bulk interface ages, is a function of the drop size. The value of t_c was about 3 minutes for a 0.005 ml. anisole drop, and zero minutes for a 0.010 ml. anisole drop, for surfactant adsorption from a 10^{-6} gm/l. aqueous solution of S.L.S.

(3) A distinct maximum in drop rest-times was observed for the toluene/water and anisole/water systems. This maximum occurred soon after drop rest-times ceased being instantaneous. This maximum was not observed for the other two oil/water systems. For the toluene/water system, for 10^{-6} gm/l. of S.L.S., the maximum in drop rest-times was removed by subtracting the time taken to form the dimple, τ', from the total drop rest-time, τ. The resulting value of $\Delta\tau$, where $\Delta\tau = \tau - \tau'$, was constant for all interface ages. This was interpreted to mean that slow even drainage begins at roughly a constant lamella thickness each time.

(4) Drop rest-times usually decreased as the interface aged.

(5) The distance of rise of the drop to the interface and the expected circulation of liquid inside the drop had no effect on the drop rest-times for the low viscosity oils. The effect of these variables on drop rest-times was not studied for the viscous cyclohexanol/water system.

(6) Drop rest-times are reproducible from apparatus to apparatus, but are sensitive to small changes in drop size and are sensitive to the aqueous phase concentration of S.L.S.

(7) Composite figures were drawn to summarize the rest-times as a function of the interface age. There is a very complex dependence of the drop rest-time and of lamella behaviour on the interfacial concentration of surfactant.

(8) Changes in the oil/water system physical properties had an effect on the drop rest-times, but the effect of each individual physical property on the rest-time could not be isolated for the four oil/water systems studied. The effect of the drop radius on the drop rest-time was easily measured. The exponent n' in the equation $\tau = K_n \, d^{n'}$ was found to have a value between 1 and 3. This is in agreement with the Hodgson/Woods model which has an n' of 2.

(9) Correlations of the rest-time data as a function of the oil/water system physical properties could be made by employing simple equations derived from the Hodgson/Woods and parallel disc models. The Hodgson/Woods model predicts drop

rest-times to within +30%, and the parallel disc model to within -70% of the observed data. These correlations are for only even lamella drainage, and are compared with the drop rest-times which were measured for as close as possible to the same interfacial concentration of adsorbed surfactant.

B. For the Lamella Behaviour Interpreted From Light Interference Patterns

(1) Despite the wide range of oil/water system physical properties and the wide range of S.L.S. concentration used in the toluene/water study, no new lamella drainage patterns could be added to those already observed by Hodgson and Woods, for low viscosity oils.

(2) The interfacial concentration of adsorbed surfactant has an effect on the type of lamella drainage observed for individual drops. For the three low oil viscosity systems, the lamellae either drained evenly (E) or unevenly (UE). For the cyclohexanol/water system, the lamella behaviour observed for each drop was independent of the interfacial concentration of adsorbed surfactant. The lamella drainage behaviour for this latter system was observed to be E→UE→E.

(3) The interfacial concentration of adsorbed surfactant has an effect on the lamella behaviour. Over the range of the aqueous phase concentrations studied, the following lamella behaviour was observed as the interfacial concentration of adsorbed surfactant increased.

For toluene/water:

E, UE for 0.005 ml. drops.

For anisole/water:

UE, E, UE for 0.005 ml. and 0.010 ml. drops.

For CA/water:

E, UE, E, UE for 0.0025 ml. and 0.005 ml. drops.

(4) The observed light interference patterns were decomposed to yield five distinct mechanisms for the lamella behaviour. Each of these mechanisms was interpreted in terms of the flow of water from the lamella and of the interfacial movement of the bulk interface. These mechanisms are useful models on which any theoretical description of the lamella behaviour can be based. These mechanisms were employed to interpret the rest-time behaviour.

(5) When the observed profiles of relative lamella thickness for one particular drop were fitted by the polynomial described in Chapter 2, the radial distribution of the interfacial concentration of adsorbed surfactant could be calculated. The calculations showed that the interfacial concentration of adsorbed surfactant near the outside edge of the stressed region of the bulk interface, Γ_{max}, exceeded the average interfacial concentration of adsorbed surfactant at the bulk interface, Γ_t, for some of the profiles.

(6) If Γ_{max} is greater than Γ_t, an hypothesis for the cause of uneven drainage may be postulated. This hypothesis

was used to interpret the complex lamella behaviour observed for the cyclohexanol/water system, and also was successfully used to interpret the uneven formation of a dimpled lamella.

(7) The use of the light interference technique allowed several unique observations to be made on the lamella. Lamella drainage was observed to be always uneven at an aged interface. Local depressions in lamella thickness were observed, particularly for a freshly formed interface, or for an interface one or two hours old. The thickness of the lamella at rupture was estimated to be 200 - 400 A°, based on light intersity measurements taken from coloured ciné photographs.

However, the light interference technique, was found unsuitable to measure the thickness of the lamella outside the barrier ring because the lamella thickness changed very rapidly as the radial distance from the barrier ring increased.

(8) The barrier ring radius estimated by the equilibrium model predicted the radius of the light interference pattern reasonably well.

(9) A non-ionic surfactant, 2 - (2-ethoxy-ethoxy) ethanol was used in place of S.L.S. and was found to give the same lamella behaviour for the toluene/water system as did 10^{-6} and 10^{-4} gm/l. of S.L.S.

C. <u>For the Experimental Techniques</u>

(1) The drop-forming technique may have an influence on the rest-time data. This technique may have contaminated

the bulk interface when rest-time data were taken for the "pure" toluene/water system.

(2) The use of the interface cleaning probe has no effect on the aqueous concentration of surfactant when the interface is cleaned repeatedly.

Nomenclature

A - area of coalescence cell oil/water interface, cm^2.

I - light intensity of black region of light interference pattern

I_o - light intensity of white region of light interference pattern

K - a constant relating interfacial and bulk surfactant concentrations at equilibrium adsorption, cm.

K_n - a constant used in $\Gamma = K_n d^{n'}$

N - number of times the oil/water interface is cleaned

N. - normality of KCl. electrolyte

R - radius of lamella at which lamella pressure is zero, cm.

R_e - radius at which lamella pressure is zero, calculated from equilibrium model, cm.

S - lamella shear stress, $dyne/cm^2$.

SM - minimum number of surfactant nolecules needed to balance surface shear stress in the bulk interface, $0 \leq r \leq R$.

U - radial velocity of bulk interface at any radius, cm./sec.

V - volume of aqueous surfactant solution in the coalescence cell, ml.

---

a_i - the coefficients in equation (5). See Appendix A2 for values

c - the aqueous surfactant concentration, $molecules/cm^3$.

c_i - the coefficients defined in equation (10). See Appendix A2

d - drop radius, cm.

g - gravitational constant, 981 cm./sec^2.

k' - constant defined in equation (8). Value used is 1.7×10^{-14} dyne-cm.

m - number of immobile interfaces

n - equilibrium interfacial concentration of surfactant, molecules/cm^2.

n' - exponent in equation for dependence of rest-time on drop diameter, $\hat{\tau} = K_d^{n'}$

n_i - number of light quarter wave-lengths

p - lamella pressure at any radial distance, dyne/cm^2.

p_o - center lamella pressure

q - volume of water withdrawn from the coalescence cell for each interface cleaning, ml.

r - any radial distance, cm.

r - inside radius of capillary of drop syringe, cm.

t - interface age, min.

t_c - critical interface age at which rest-times > 0.1 sec., min.

t_m - interface age at which drainage mode changes, min.

u - radial velocity of water in the lamella, cm./sec.

$\bar{v}$ - velocity vector at any point in the water lamella, (unless labelled otherwise), cm./sec.

y - lamella thickness at any radial distance, cm.

y_o - center lamella thickness

z - any vertical height, cm.

Greek Symbols

γ_o - interfacial tension of the pure oil/water system, dyne/cm.

γ - interfacial tension at any radial distance

θ - elapsed time of drop at the interface, sec.

λ_o - wave-length of light in a vacuum, A°.

μ' - refractive index

θ' - actual thickness of lamella, cm.

$\mu'\theta'$ - optical path thickness of light in lamella, cm.

$\Delta\rho$ - oil/water system density difference, gram/ml.

μ - liquid viscosty, poise

μ. - symbol for micron unit

τ - drop rest-time at any interface age, sec.

τ' - time taken to form a dimple

$\Delta\tau$ - equals $\tau - \tau'$, the time for slow drainage

τ_∞ - drop rest-time at an interface aged several hours

τ_p - predicted drop rest-time

τ_s - a standard drop rest-time

Γ - interfacial surfactant concentration in the bulk interface at any radial distance, molecules/cm^2.

Γ_o - interfacial surfactant concentration at r = 0, in the bulk interface

Γ_t - interfacial surfactant concentration at the quiescent bulk interface, t minutes after cleaning the interface

$\Gamma_{max.}$ - maximum interfacial surfactant concentration in the bulk interface, at r = R

Bibliography

1. Cockbain, E. G. and T. S. McRoberts, J. Colloid Sci. 8 440-451 (1953).
2. Biswas, B. and D. A. Haydon, 3rd Int'l Congress on Surface Active Substances Vol. IV 580-584.
3. ibid., Kolloid Zeitschrift 185 31-38 (1962).
4. Hodgson, T. D. and J. C. Lee, J. Colloid and Int. Sci. 30 (1) 94-108 (1969).
5. Hawksley, J. L. and G. V. Jeffreys, A.I.Ch.E.J. 11 (3) 413-424 (1965).
6. Lawson, G. B. and G. V. Jeffreys, Trans. Inst. Chem. Engrs 43 T294-T298 (1965).
7. Mahajan, L. D., Kolloid Zeitscrift 69 (1) 16-21 (1934).
8. Charles, G. E. and S. G. Mason, J. Colloid Sci. 15 (3) 235-267 (1960).
9. Neilsen, L. E., R. Wall, and G. Adams, J. Colloid Sci. 13 441-458 (1958).
10. Gillespie, T. and E. K. Rideal, Trans. Fara. Soc. 52 173-183 (1956).
11. Miura, M. and C. Uno, J. Sci. Hiroshima Univ. 20A (3) 171-176 (1957).
12. Weatherford, W. D. Jr., Private Communication (1968).
13. Elton, G. A. H. and R. G. Picknett, 2nd Int'l Congress on Surface Active Substances (London) Vol. I 287 (1957).
14. Watanabe, T., Bull. Chem. Soc. Japan 31 (2) 236-243 (1958).
15. Derjaguin, B. V. et.al. J. Colloid Sci. 19 113-135 (1964).

16. Derjaguin, B. V., and A. S. Titievskaya, 2nd Int'l Congress on Surface Activity (London) Vol.II 211-19 (1957).

17. Hodgson, T. D. and D. R. Woods, J. Colloid and Int. Sci. 30 (4) 429-446 (1969).

18. Lindblad, N. R., J. Colloid Sci. 19 729-743 (1964).

19. MacKay, G. D. M. and S. G. Mason, J. Colloid Sci. 18 674-683 (1963).

20. Charles, G. E., R. S. Allan, and S. G. Mason, J. Colloid Sci. 16 (2) 150-165 (1961).

21. MacKay, G. D. M. and S. G. Mason, Can. J. Chem. Eng. 41 203-212 (1963).

22. Platikanov, D., J. Phys. Chem. 68 (12) 3619-3624 (1964).

23. Platikanov, D. and E. Manev, Proc. IV Int'l Congress on Surface Active Substances: Physics and Chemistry of Surface Active Agents: Vol.II 1189-1197 (1964).

24. Scheludko, A., Kolloid Zeit. 155 39 (1957).

25. Van den Temple, M., J. Colloid Sci. 13 125-133 (1958).

26. Hartland, S., Trans. Inst. Chem. Engrs 45 T97-T114 (1967).

27. Burrill, K. A. and D. R. Woods, J. Colloid and Int. Sci. 30 (4) 511-524 (1969).

28. Lawrence, A. C. S. "Soap Films" Bell, London (1929).

29. Frankel, K. J. et.al. "Soap Films--A Study of Their Thinning" Pergamon Press, London (1959).

30. Bird, R. B., W. E. Steward, and E. N. Lightfoot, "Transport Phenomena", Wiley (1960).

31. De Vries, A. J., Recueil des Travaux 77 81-91, 209-223, 283-296, 383-399, 441-461 (1958).

32. Vrij, A., Disc. Fara. Soc. (No. 42) 23-33 (1966).

33. Vrij, A. and J. Th. G. Overbeek, J. A. C. S. 90 (12) 3074-3078 (1968).

34. Hickman, K. et.al. I.E.C. 59 (10) 18-41 (1967).

35. Eagland, D. and F. Franks, Third International Congress on Surface Active Substances 539-544 (1960).

36. Davies, J. T. and E. K. Rideal, "Interfacial Phenomena" Academic, New York (1963).

37. Lee, J. C. and T. D. Hodgson, Chem. Eng. Sci. 23 1375-1397 (1968).

38. Hartland, S., Trans. Inst. Chem. Engrs. 46 T275-T282 (1968).

39. Lang, S., Ph.D. Thesis , U.C., Berkeley (1962).

40. Ross, S. and E. S. Chen, "Chemistry and Physics of Interfaces", A.C.S., Washington 44-56 (1965).

41. Princen, H. M. and S. G. Mason, J. Coll. Sci. 29 156-172 (1965).

42. Hodgson, T. D., Ph.D. Thesis Swansea (1966).

43. Hartland, S., Chem. Eng. Sci. 24 (3) 611-3 (1969).

44. Chappelear, D. C., J. Colloid Sci. 16 186-190 (1961).

Table 1. Physical Properties

Oil/Water System	γ dynes/cm.	μ_{oil} cp.	$\Delta\rho$ grams/ml.	oil refractive index	gm/l. S.L.S.* + normality of KCl
Toluene/Water	35.0	0.59_L	0.133	1.497_L	10^{-6}+0.01N. 10^{-5}+0.01N. 10^{-4}+0.10N. 10^{-3}+0.10N.
Anisole/Water	20.5	1.32_L	0.0097	1.518_L	10^{-6}+0.01N. 10^{-4}+0.05N.
CA/Water (0.16 m.f. cyclohexane+0.84 m.f. anisole/Water)	28.9	0.85	0.053	1.494	10^{-6}+0.01N. 10^{-4}+0.05N.
Cyclohexanol/Water	3.93	32.8	0.051	1.46_L	10^{-6}+0.01N. 10^{-4}+0.05N.

* sodium lauryl sulfate

See next page for notes on Table 1.

Table 1. Notes

1. L. indicates literature value from Handbook of Physics and Chemistry, at 20°C.
2. All other values are experimentally determined from this work, at 25°C.
3. The oil and water were mutually saturated before measurements were made.
4. Water viscosity is assumed to be that of pure water for all systems except the cyclohexanol/water system. For this system, the water viscosity was measured to be 0.98 cp. . The viscosity of pure water at 25°C. is 0.89 cp. . Viscosity measurements wre made with an Ostwald viscometer.

Table 2. Effect of Oil/Water System Variables on Interfacial Properties

					(1)	(2)	(3)	(4)	(5)	(6)	(7)
Oil/ Water System	Drop Volume (ml.)	Drop Radius d (cm.)	γ dynes/ cm.	$\Delta\rho$ grams/ ml.	P_o dynes/ cm^2.	R radius at which r=0 (cm.)	Average Surface Shear Stress dyne/ cm^2.	Minimum Quantity of S.L.S. SM molecules	Γ_{max} molecules/ cm^2.	Γ_t	$\Gamma_{max}-\Gamma_t$
Toluene /Water	0.005*	0.1061	35.0	0.133	330.0	5.02×10^{-2}	1.31	7.94×10^{10}	1.77×10^{13}	1.00×10^{13}	7.7×10^{12}
Anisole /Water	0.005	0.1061	20.5	0.0097	190.0	1.78×10^{-2}	2.14	2.23×10^{9}	3.29×10^{12}	2.23×10^{12}	1.07×10^{12}
					200.0	1.74×10^{-2}	2.30	2.11×10^{9}	3.25×10^{12}	2.21×10^{12}	1.04×10^{12}
	0.020*	0.1682			120.0	4.50×10^{-2}	0.535	1.55×10^{10}	4.10×10^{12}	2.44×10^{12}	1.66×10^{12}
					130.0	4.32×10^{-2}	0.600	1.24×10^{10}	3.54×10^{12}	2.11×10^{12}	1.43×10^{12}
CA/ Water	0.005*	0.1061	28.9	0.053	270.0	3.50×10^{-2}	1.54	2.05×10^{10}	8.85×10^{12}	5.36×10^{12}	3.49×10^{12}

* These drop volumes produce the same radius of the light interference pattern.

Table 2. Notes

The quantities in columns (1) to (7) were calculated as follows:

Column (1) $p_o = \frac{\gamma}{d}$ (or $\frac{\gamma}{d} + 10.$ dynes/cm.^{2})

Column (2) $R = \frac{4Wg}{\pi p_o}$ (from polynomial pressure model of equation (7))

Column (3) Approximate average shear stress $= \frac{p_o}{R} \times 2 \times 10^{-4}$

Column (4) $SM = \sum_{r=0}^{R} \Gamma_r \, 2\pi r \, \Delta_r$ (from equation (12) with $\Gamma_o = 0$)

Column (5) Γ_{max} is found from equation (12) with $r = R$

Column (6) $\Gamma_t = \frac{SM}{\pi R^2}$ (This equation expresses an arbitrary value for Γ_t)

Column (7) This column is obtained by subtracting the values in column (6) from the values in column (5).

Table 3a. Summary of Rest-time Data for all Systems, for 10^{-6} gm/l. S.L.S. +0.01 N. KCl

(1)	(2)	(3)	(4)		(5)	(6)	(7)	(8)
Oil/ Water System	Drop Volume (ml.)	Range of Interface Age $\tau<1$ sec. $c-t_c$ min.	τ_{max} (sec.) and Interface Age (min.)		Mode of Drain-age at t_c	Mode of Drainage Changes at t_m to:	Mode of Drainage at t_∞ and $\bar{\tau}_\infty$	Average Rest-time for Range of Inter-face Age Studied
			t	τ_{max}				
Toluene/ Water	0.005*	0-1	2	12	Even	-	Uneven $\bar{\tau}_\infty = 8$	10
Anisole/ Water	0.005	0-2	4	15	Uneven	-	Uneven $\bar{\tau}_\infty = 1$	10
	0.010	0	2	27	Uneven	-	Uneven $\bar{\tau}_\infty = 2$	15
	0.020*	0	6	34	Even	Uneven $t_m = 3$	Uneven $\bar{\tau}_\infty = 5$	20
Cyclo-hexanol/ Water	0.001*	0	3	110	Composite of Even and Uneven	-	Composite $\bar{\tau}_\infty = 40$	70
CA/ Water	0.0025	0	0	6	Even	Uneven $t_m = 2$	Uneven $\bar{\tau}_\infty = 3$	7
	0.005*	0	0	16	Even	Uneven $t_m = 4$	Uneven $\bar{\tau}_\infty = 4$	10

* These drop volumes produce the same radius of the light interference pattern.

Table 3b. Summary of Rest-time Data for all Systems, for 10^{-4} gm/l. S.L.S. +0.05 N. KCl

(1)	(2)	(3)	(4)		(5)	(6)	(7)	(8)
Oil/ Water System	Drop Volume (ml.)	Range of Interface Age 1 sec. $0-t_c$ min.	τ_{max} (sec) and Interface Age (min.) t	τ_{max}	Mode of Drainage at t_c	Mode of Drainage Changes at t_m to:	Mode of Drainage at t_∞ and $\bar{\tau}_\infty$	Average Rest-time for Range of Interface Age Studied
Toluene/ Water	0.005	0	1	7	Even	Uneven $t_m = 1$	Uneven $\bar{\tau}_\infty = 2$	5
Anisole/ Water	0.005	0	1	8	Uneven	Even $t_m = 2$	Uneven $\bar{\tau}_\infty = 3$	2
	0.010	0	0	28	Uneven	Even $t_m = 4$	Uneven $\bar{\tau}_\infty = 8$	3
	0.020	0	0	31	Uneven	Even $t_m = 12$	Uneven $\bar{\tau}_\infty = 10$	5
Cyclo-hexanol/ Water	0.001	0	-	240 (no max.)	Composite of Even and Uneven Drainage	-	Composite $\bar{\tau}_\infty = 195$	240
CA/ Water	0.0025	0	0	4	Uneven	Even $t_m = 2$	Uneven $\bar{\tau}_\infty = 1$	1
	0.005	0	0	6	Uneven	Even $t_m = 11$	Uneven $\bar{\tau}_\infty = 2$	2

Table 4. Comparison of Simple Mathematical Models for Barrier Ring Radius and Observed Light Interference Pattern Radii

Oil/ Water System	$\Delta\rho$ gm/ml.	γ dyne/ cm.	d cm.	$c_{obs.}$ cm.	$R_{P.D.}$ cm.	$R_{E.M.}$ cm.
Toluene/ Water	0.133	35.0	0.1061	0.021-0.026	0.017	0.024
			0.0842	0.018	0.011	0.015
Anisole/ Water	0.0097	20.5	0.1682	0.022-0.026	0.016	0.022
			0.1340	0.011-0.020	0.010	0.014
CA/ Water	0.053	28.9	0.1061	0.020	0.012	0.017
			0.0842	0.012	0.008	0.011
Cyclo-hexanol/ Water	0.051	3.93	0.0682	0.014	0.014	0.019

$$R_{P.D.} = \sqrt{2}\, d^2 \sqrt{\frac{\Delta\rho g}{3\gamma}} \quad \text{Parallel Disc Model}$$

$$R_{E.M.} = 2\, d^2 \sqrt{\frac{\Delta\rho g}{3\gamma}} \quad \text{Equilibrium Model}$$

These radii are derived in Chapter 4.

Table 5. Calculated and Estimated Times for Equilibrium Adsorption

S.L.S. concentration (gm/l.) + electrolyte	Time from the Ward-Tordai Eqn (min.)	Time estimated from rest-time data(min.)	Γ_t Equilibrium Interfacial Concentration (molecules/cm^2.)
10^{-6}+0.01N.	5000	60	3.24×10^{12}
10^{-5}+0.01N.	430	20	9.31×10^{12}
10^{-4}+0.05N.	80	10	3.3×10^{13} (approx.)
10^{-3}+0.10N.	5	5	1.01×10^{14}

Table 6. Calculated Time to Reach Specified Interfacial Concentrations of S.L.S.

S.L.S. (gm/ml.) + KCl Normality	Γ_e molecules/cm.^{2}	t minutes
10^{-6} + 0.01 N.	3.24×10^{12}	0.005
10^{-5} + 0.01 N.	9.31×10^{12}	0.05
10^{-4} + 0.10 N.	3.3×10^{13}	0.50
10^{-3} + 0.10 N.	1.0×10^{14}	5.0

Equilibrium Adsorption

$$\Gamma = 2\sqrt{\frac{D}{\pi}}\, c\sqrt{t}\, \frac{N}{1000}$$ (Ward-Tordai Equation)

Notes on Table 6.

The terms used in the Ward-Tordai equation are defined as follows:

Γ = interfacial concentration of S.L.S., molecules/cm.^{2}

D = diffusion coefficient of S.L.S. in water; value is assumed to be 6×10^{-6} cm.^{2}/sec.

c = aqueous phase concentration of S.L.S., gram-moles/l.

t = time, sec.

N = Avogadro's Number, 6.02×10^{23} molecules/gram-mole.

The equation may then be written:

$$\Gamma = 1.66 \times 10^{18} c\sqrt{t}$$

Table 7. Effect of Interface Cleaning on the Value of t_c

Pure Toluene/Water System

0.005 ml. toluene drop

Total No. of Times the Interface was Cleaned	t_c minutes	No. of Drops used in Determination of t_c	
1	2	-	
2	2½	-	
3	2¾	-	
4	2½	-	
5	2½	-	
6	3	4	
7	3	3	
8	4½	4	
9	4	1	
10	4½	2	
11	9	6	0.0025 ml. drops

For the eleventh cleaning, 0.0025 ml. drops were used.

Table 8. Comparison of Predicted and Observed Rest-times

(a) Prediction based on the Hodgson/Woods model.

Oil/Water System	d cm.	γ dyne/cm.	m	$\tau_{obs.}$ sec.	$\tau_{pred.}$ sec.	% diff.
Toluene/ Water	0.1061	35.0	1	8	-	-
Anisole/ Water	0.1682	20.5	1	28	34	+22%
CA/ Water	0.0842	28.9	1	5	6.4	+28%
Cyclohex-anol/Water	0.0620	3.93	2	90	97	+8%

The rest-times were chosen, first, for even drainage, and then for t= 5 min., if possible. The S.L.S. concentration was 10^{-6}gm/l.

Table 8.

(b) Dependence of rest-time on drop radius, $\tau = K_n d^{n'}$

Oil/Water System	Diameter Range cm.	n'	
		Even Drainage	Uneven Drainage
Anisole/ Water	0.1061-0.1682	1.1-2.4	1.6-2.5
CA/ Water	0.0842-0.1340	-	0.6
Cyclohexanol/Water	0.0457-0.0620	1.9 — 2.9	

Table 8.

(c) Prediction based on the Parallel Disc model.

Oil/Water System	d cm.	γ dyne/cm.	$\Delta\rho$ gram/ml.	m	$\tau_{obs.}$	$\tau_{pred.}$	% diff.
Toluene/ Water	0.1061	35.0	0.133	1	8	-	-
Anisole/ Water	0.1682	20.5	0.0097	1	28	17	-39%
CA/ Water	0.0842	28.9	0.053	1	5	1.5	-70%
Cyclohex-anol/ Water	0.0620	3.93	0.051	2	90	33	-64%

Figure 1a. Photograph of the Apparatus

Figure 1b. Coalescence Apparatus

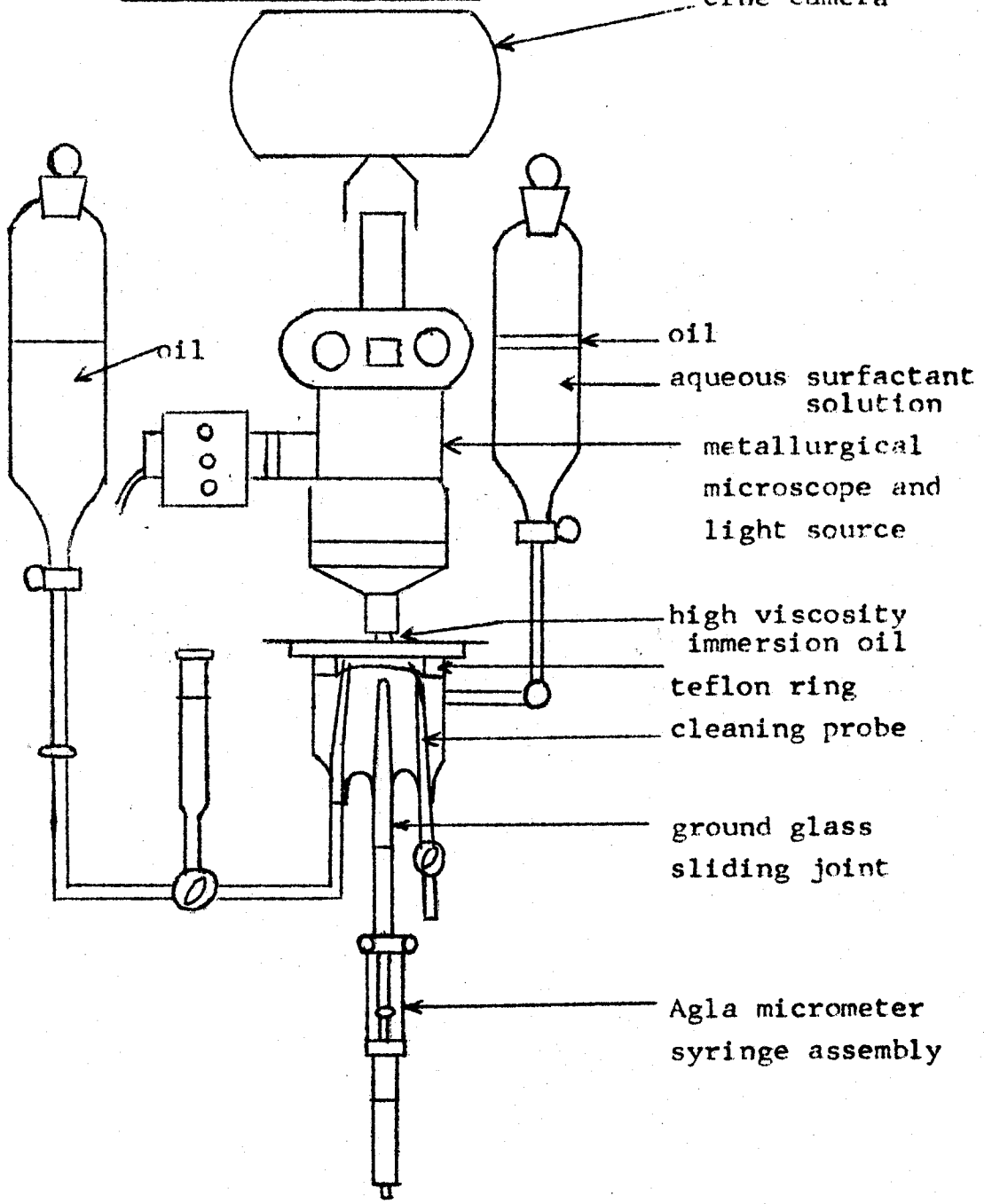

Figure 1c. Detailed Drawing of the Coalescence Cell

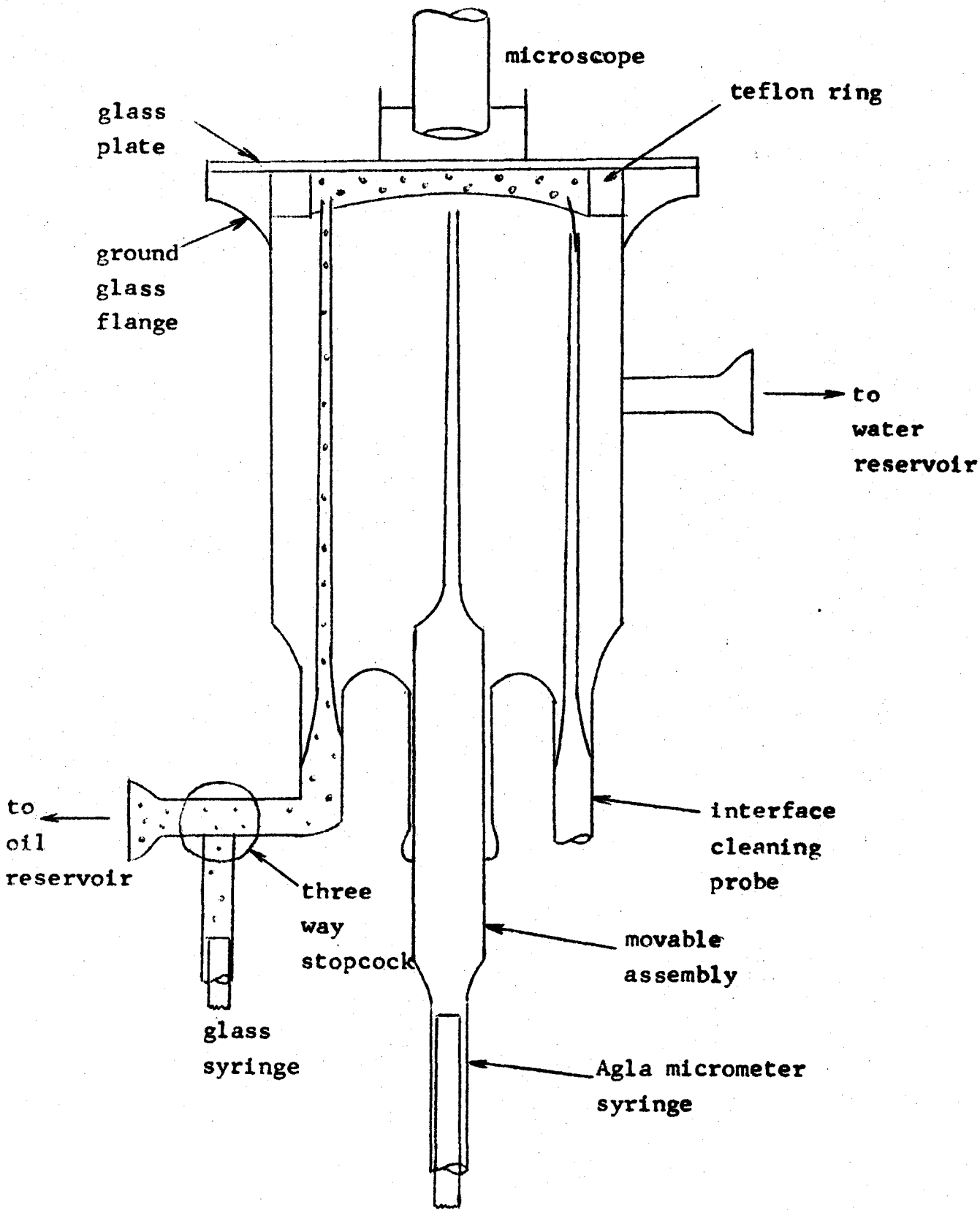

Figure 2. Problem Geometry

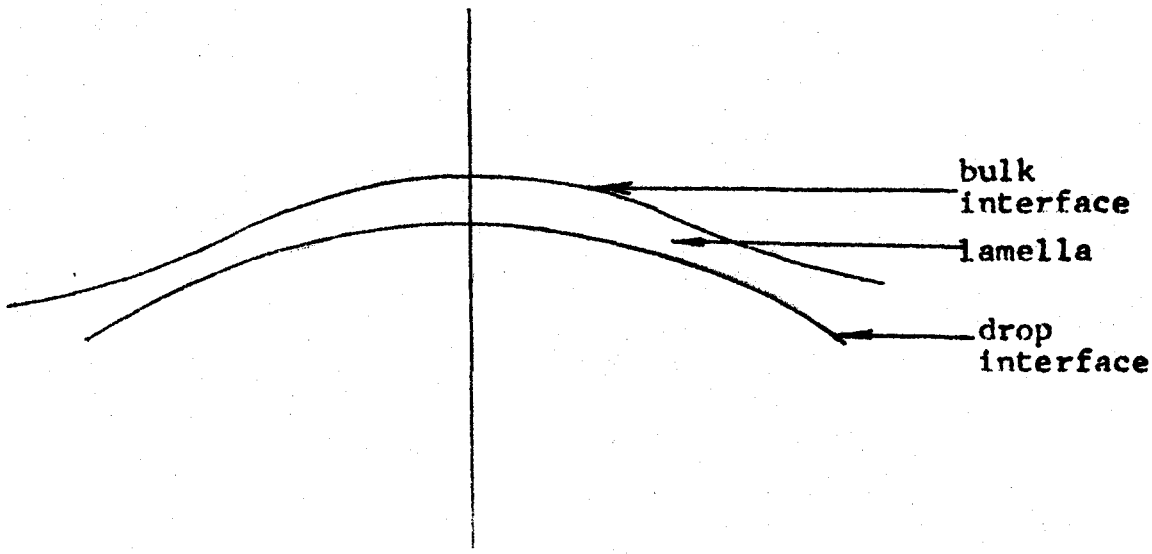

(a) Actual Shape

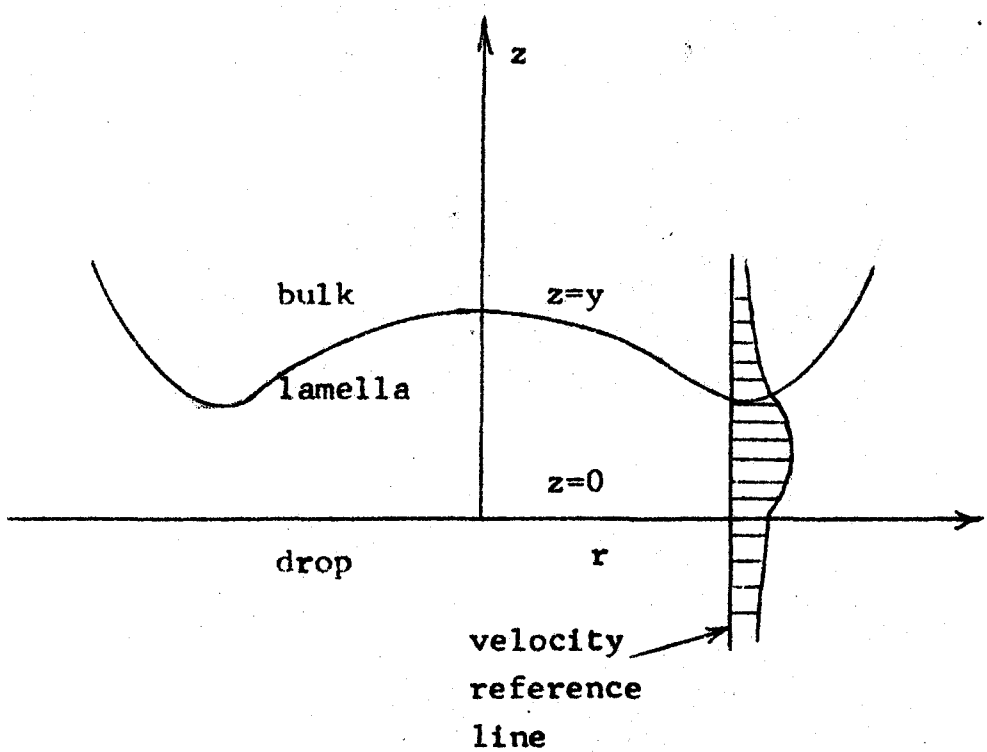

(b) Relative Shape and Expected Velocity Distribution in the Phases

Figure 2.

(c) Idealized Velocity Distribution for Surfactant in the Bulk Interface

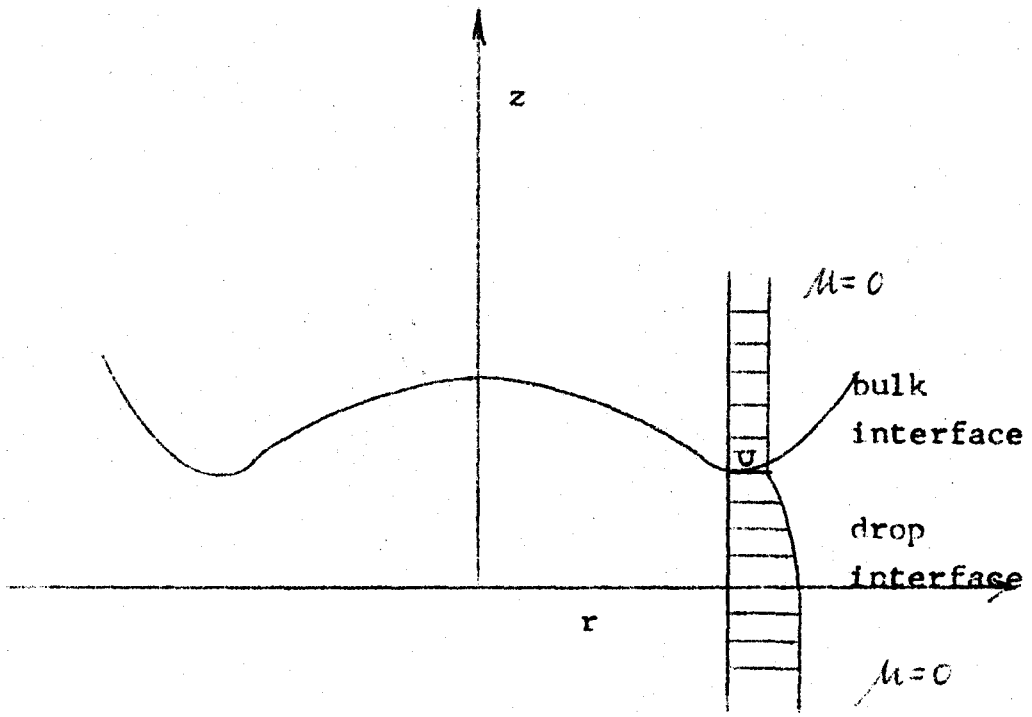

Figure 3. Dimple Formation and Slow Thinning

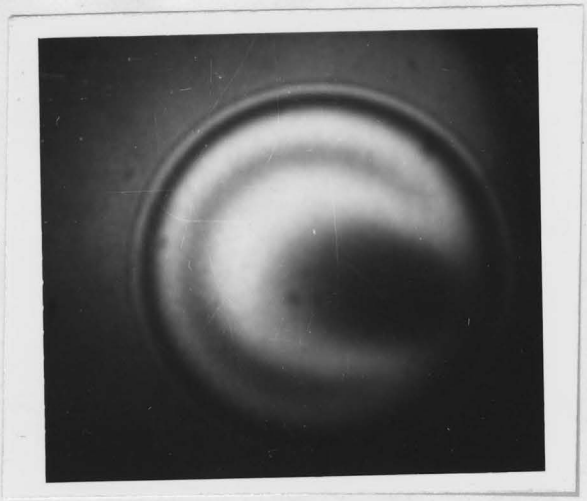

Anisole/Water (1)
0.020 ml. anisole drop
10^{-6} gm/l. S.L.S.+ 0.01 N. KCl
Interface age 0.3 min.

Photograph magnification is approximately 150x.

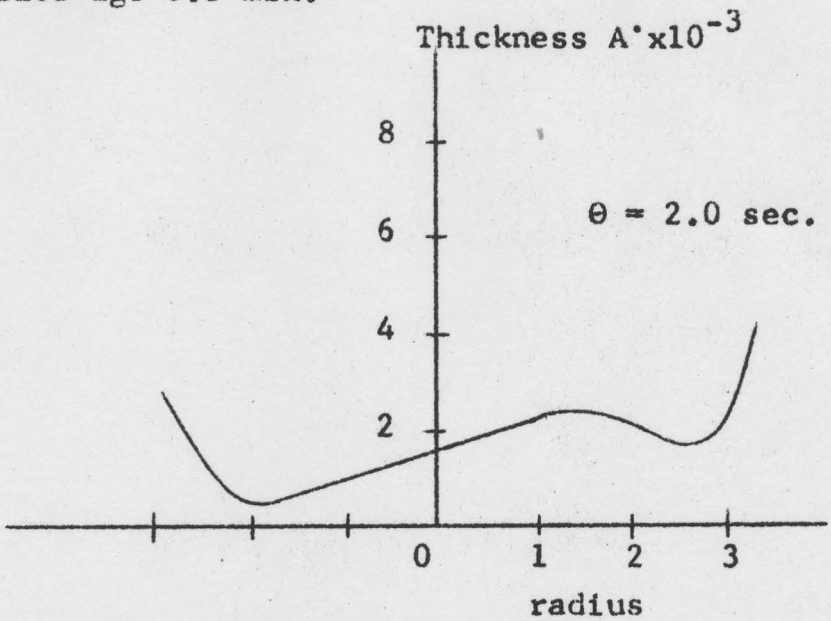

(Radial distance units are arbitrary.)

Figure 3.

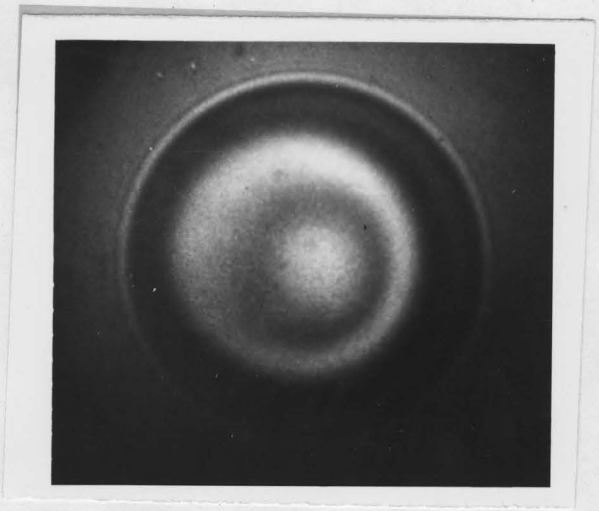

(2)

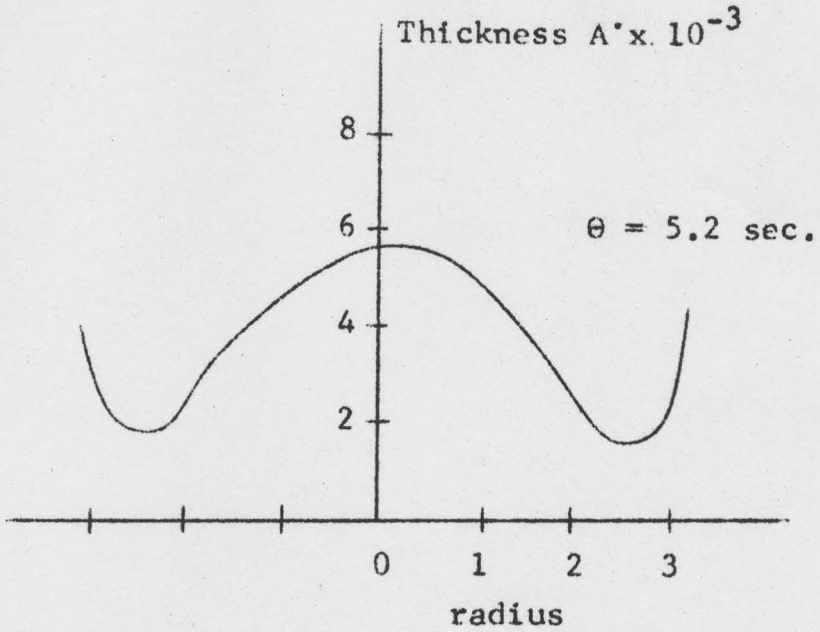

Figure 3.

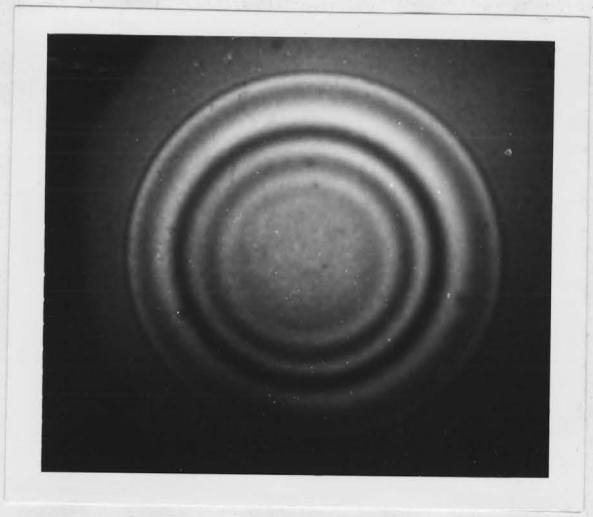

(3)

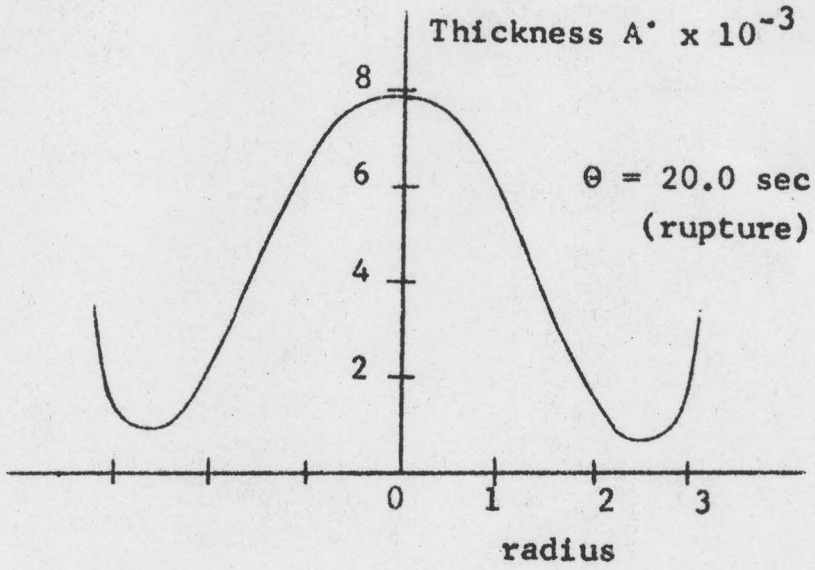

Figure 4. Uneven Drainage

Anisole/Water
0.020 ml. anisole drop
10^{-6} gm/l. S.L.S.+ 0.01 N. KCl
Interface age 5 min.
Magnification 125x

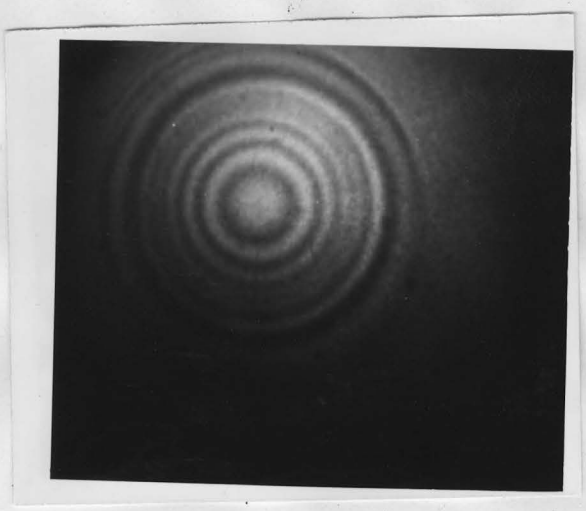

(1)
θ = 4.5 sec.

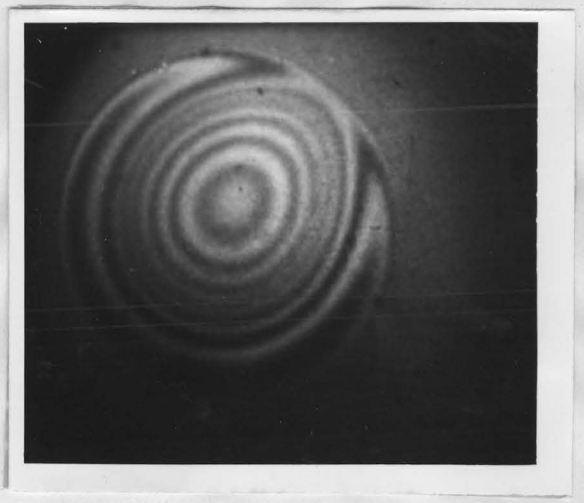

(2)
θ = 5.5 sec.

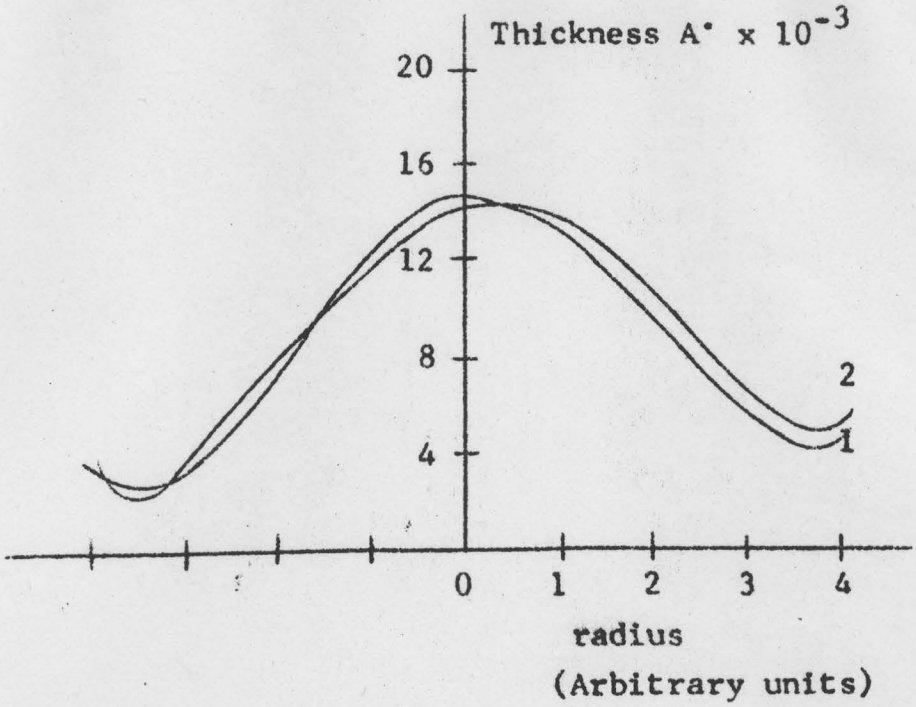

Figure 4.

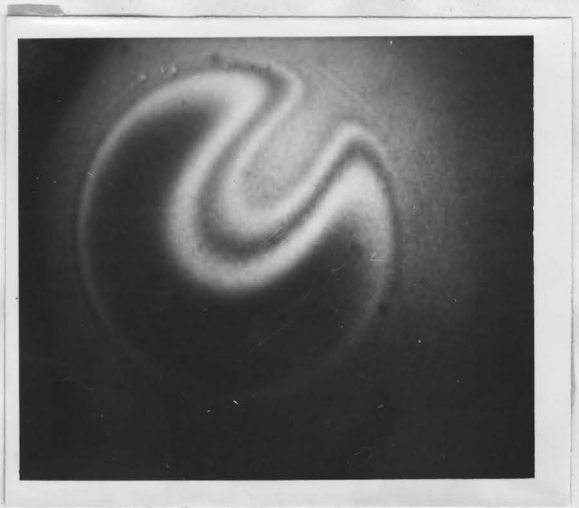

(3)
θ = 6.8 sec.

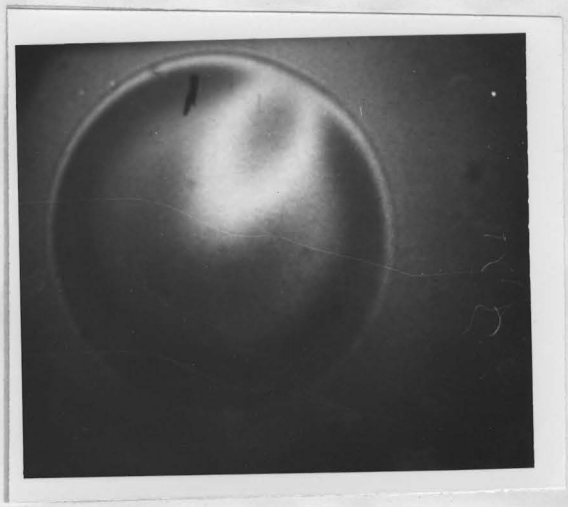

(4)
θ = 9.0 sec.

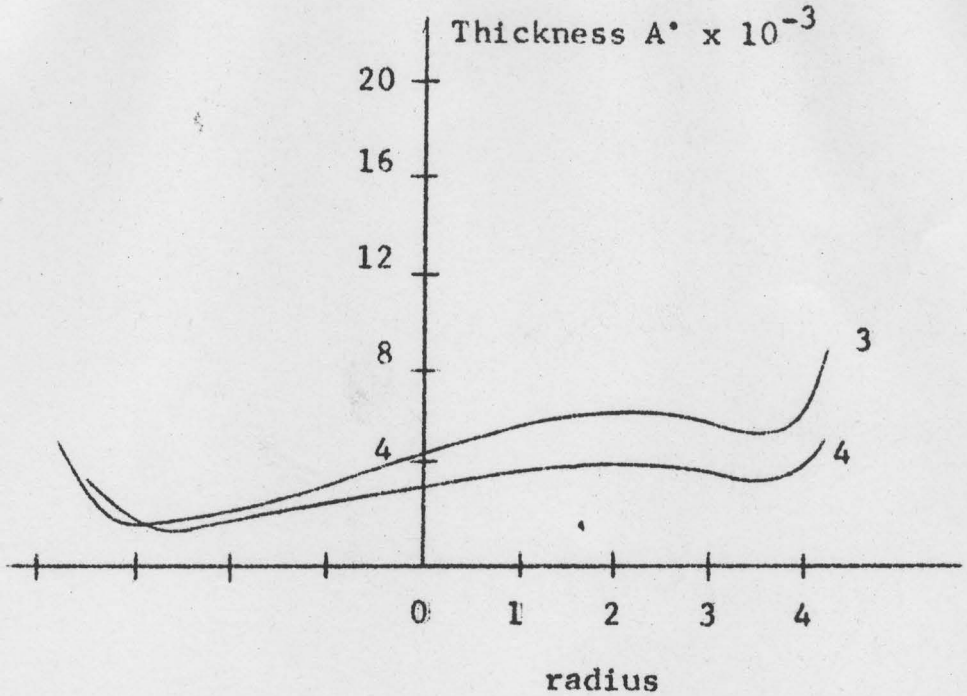

Figure 4.

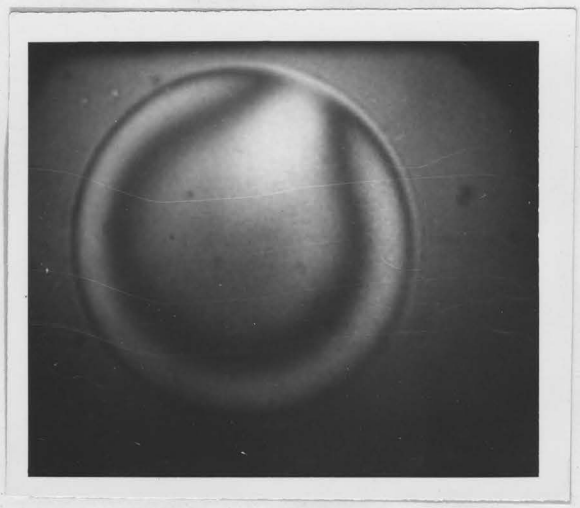

(5)
0 = 10.9 sec.

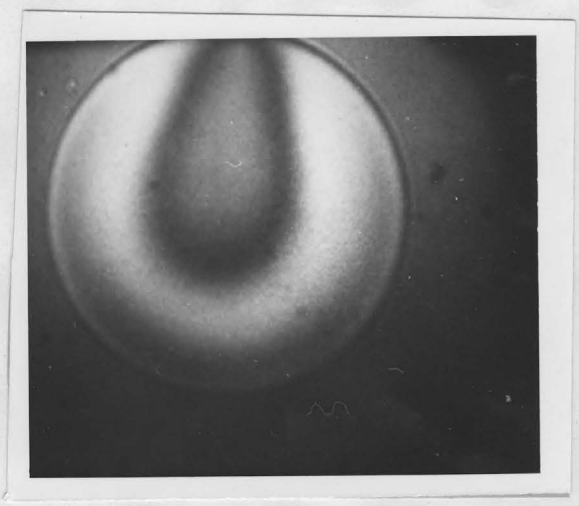

(6)
0 = 21.8 sec.
(rupture)

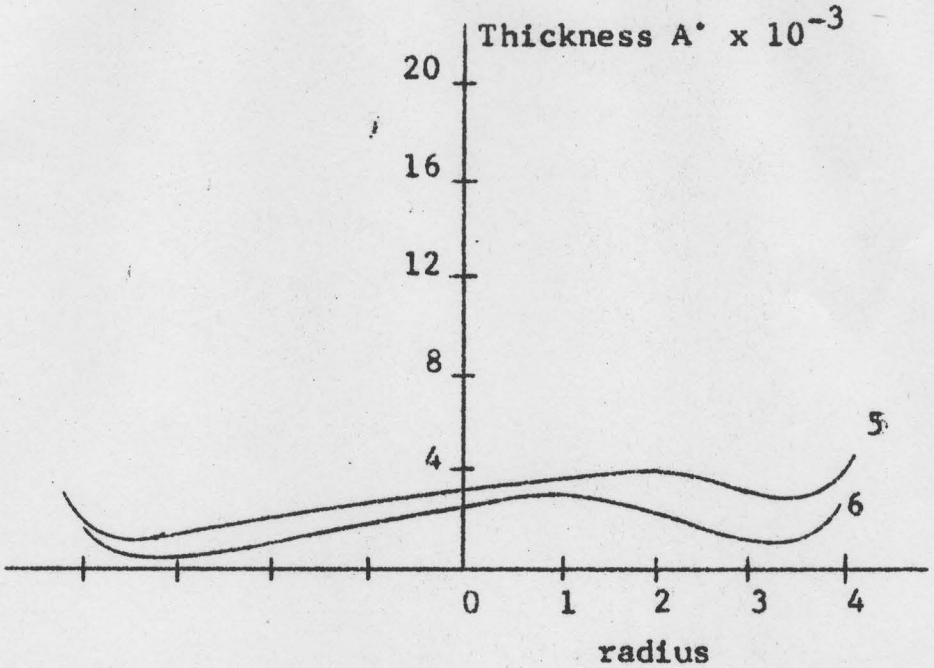

Figure 5. Slow Even Thinning

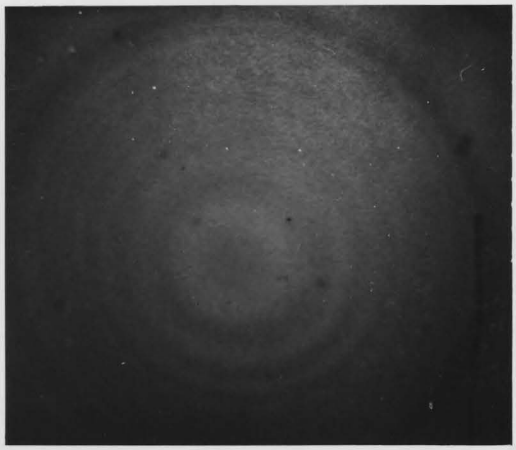

This photograph is for a different time than the given profile.

Anisole/Water (1) Magnification 150x
0.020 ml. anisole drop
10^{-4}gm/l. S.L.S.+ 0.05 N. KCl
Interface age 38 min.

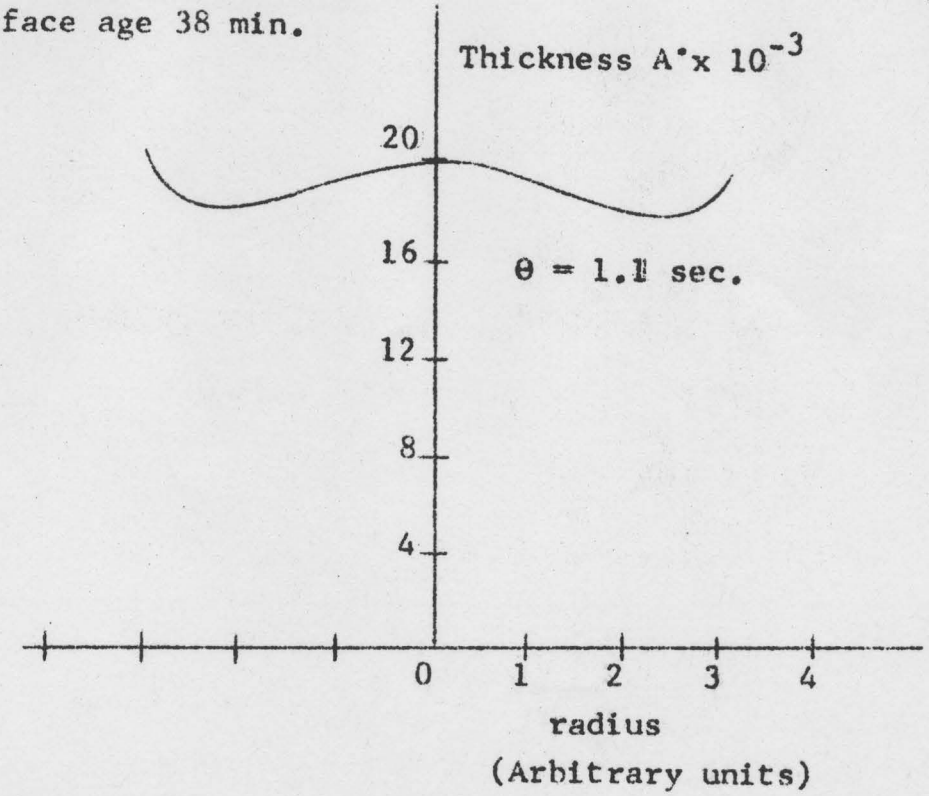

Figure 5.

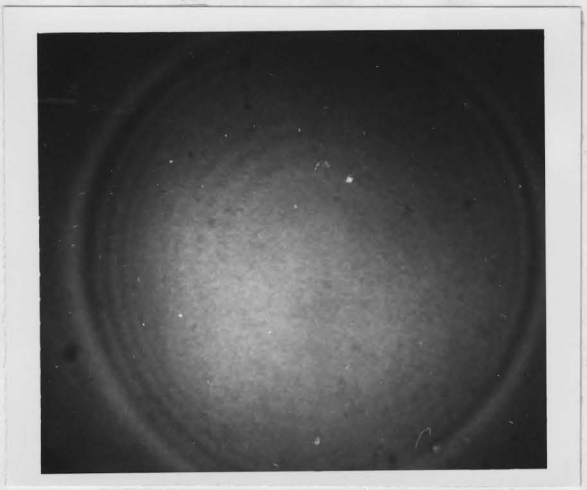

(2)

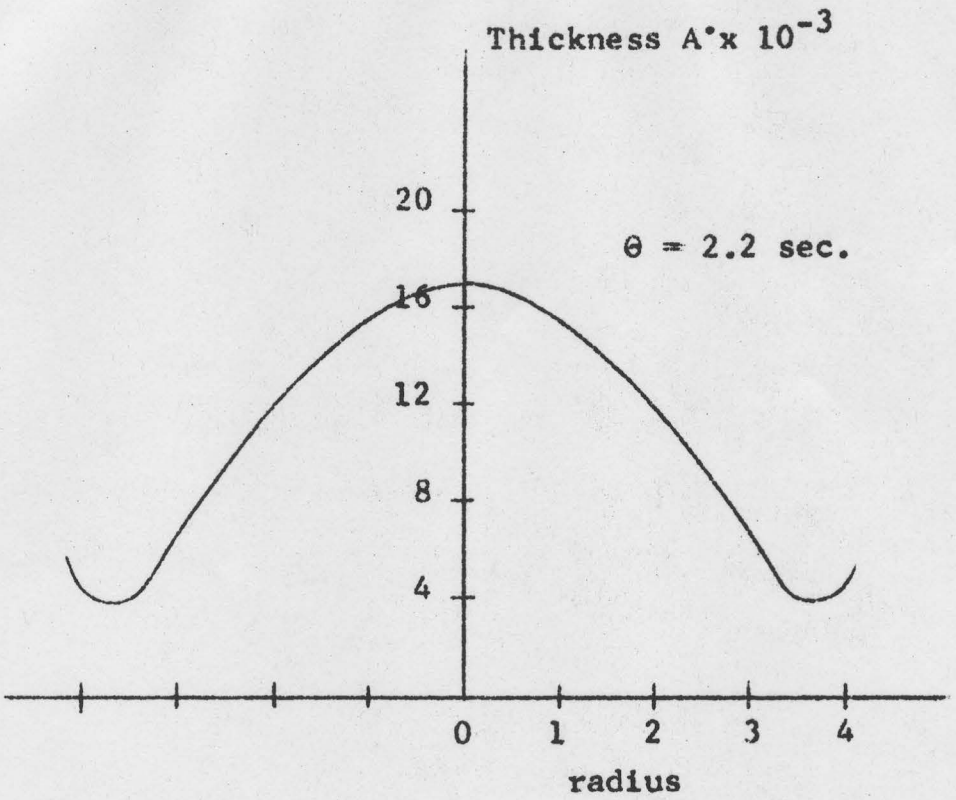

Figure 5.

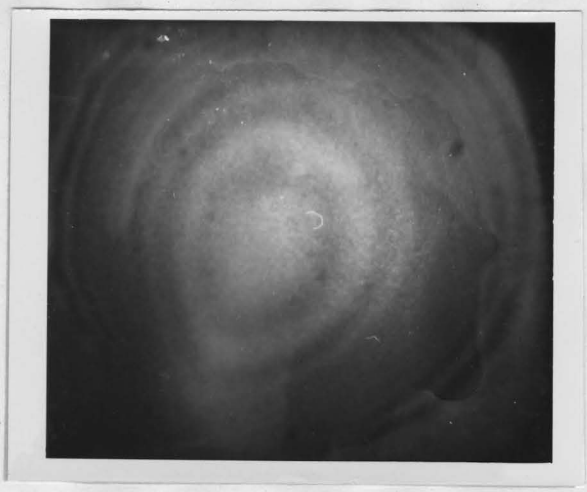

(3)

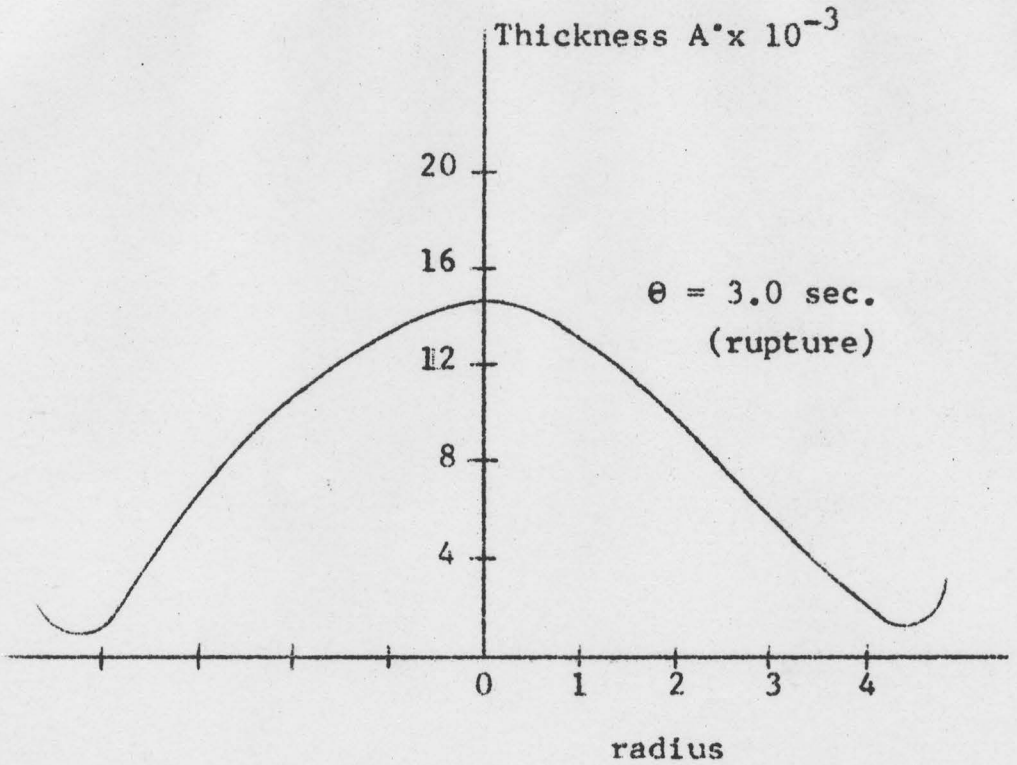

Figure 6. Interfacial Tension in the Bulk Interface as a Function of Radius

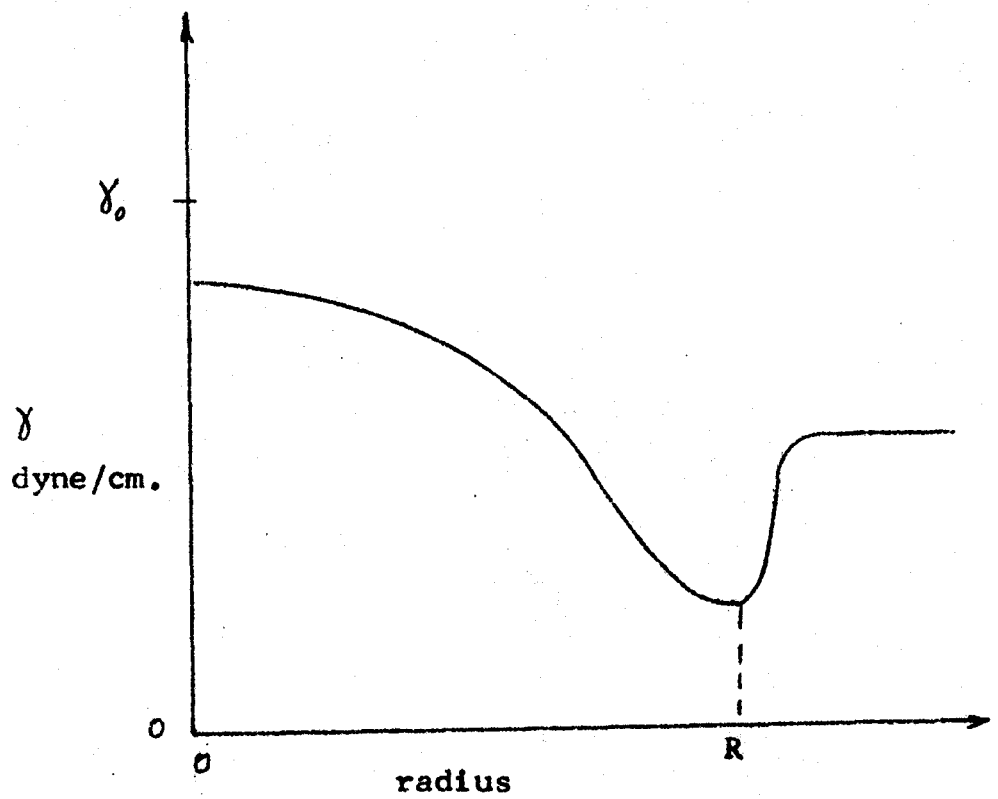

Figure 7. Postulated Dependence of the Interfacial Concentration of Surfactant as a Function of Radius

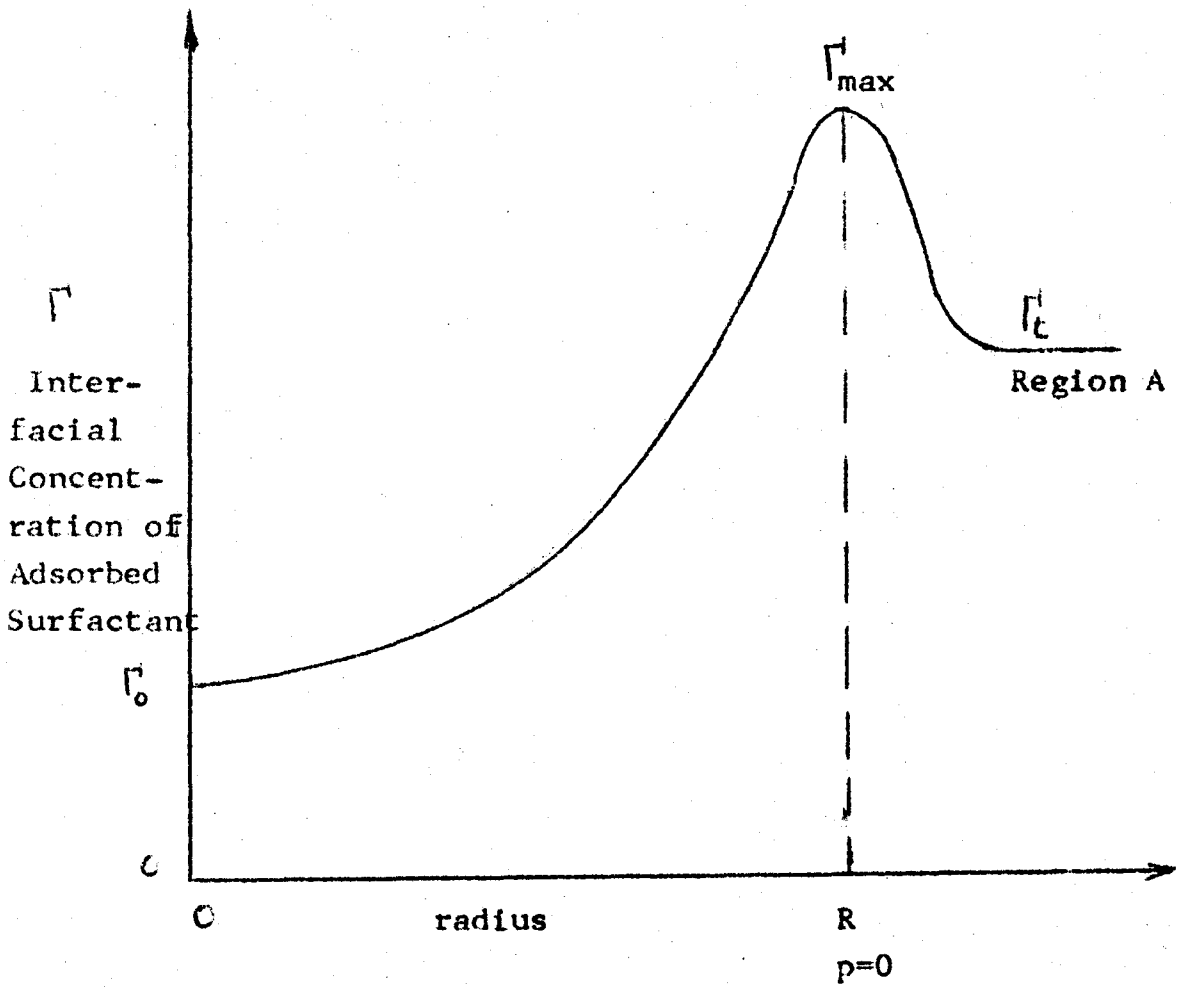

Figure 8. Lamella Thickness Profiles

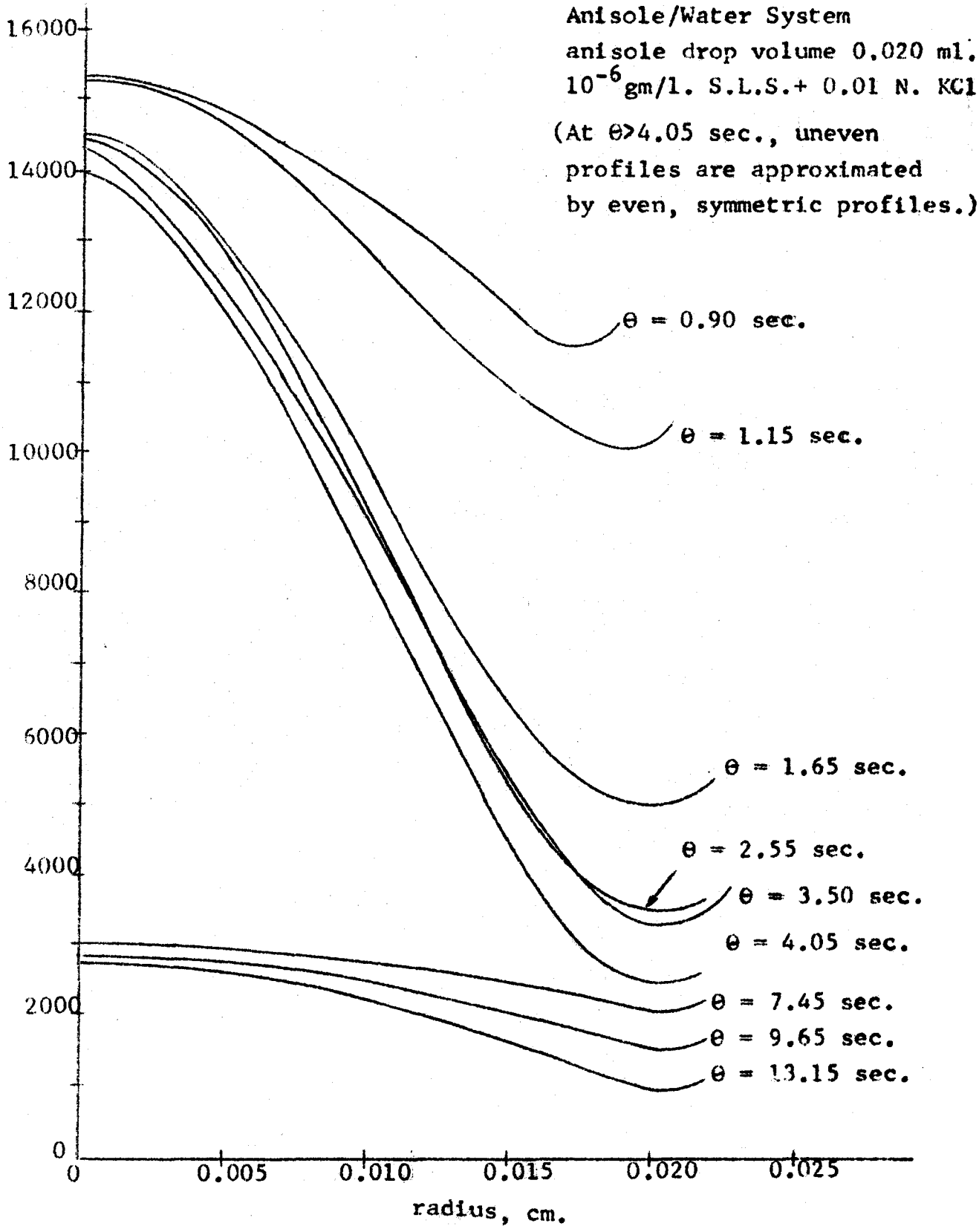

Figure 9. Calculated Γ as a Function of Radius for the Lamella Profiles in Figure 8.

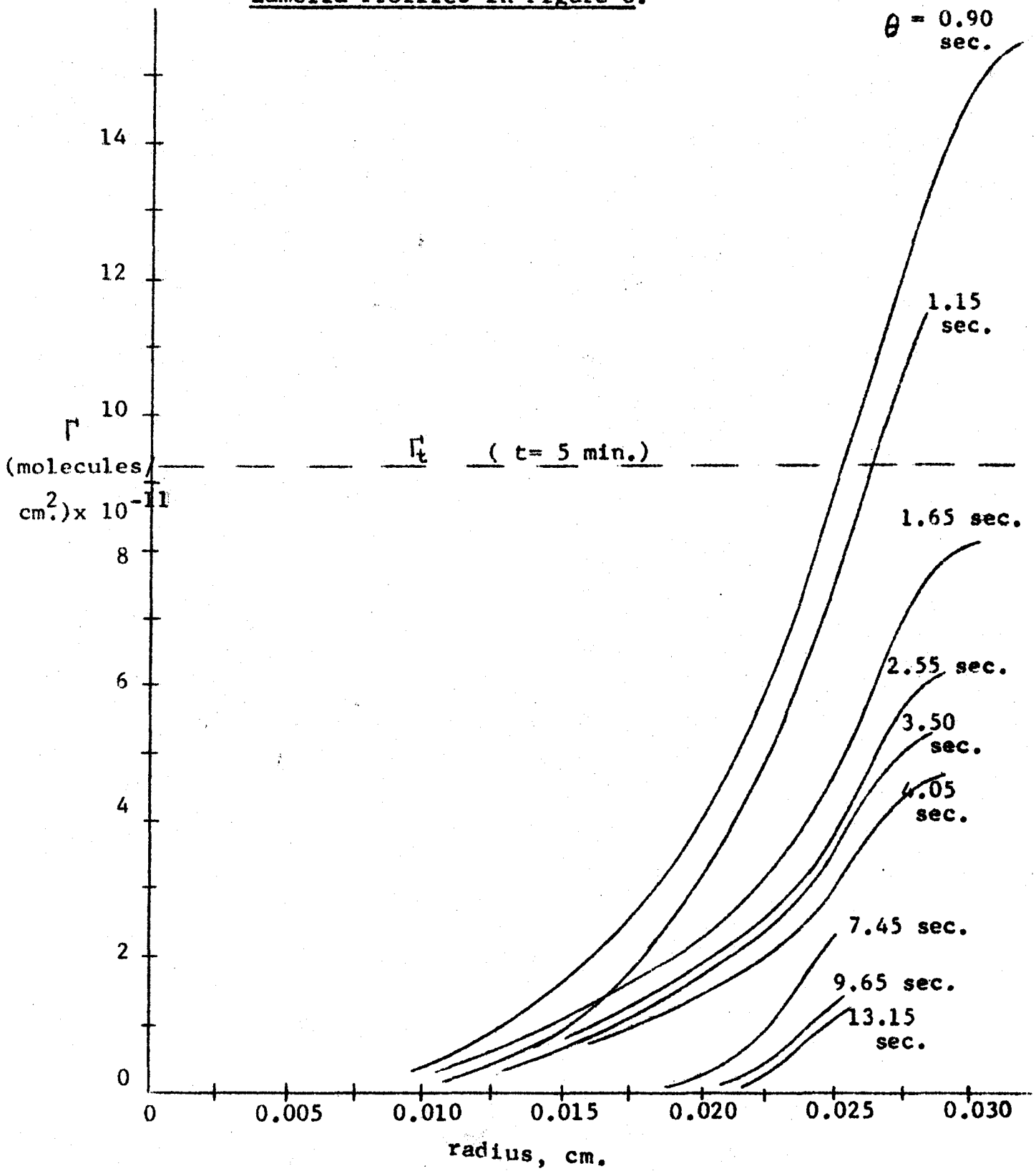

Figure 10. Minimum Quantity of Surfactant (SM) as a Function of Time, for the Profiles in Figure 8.

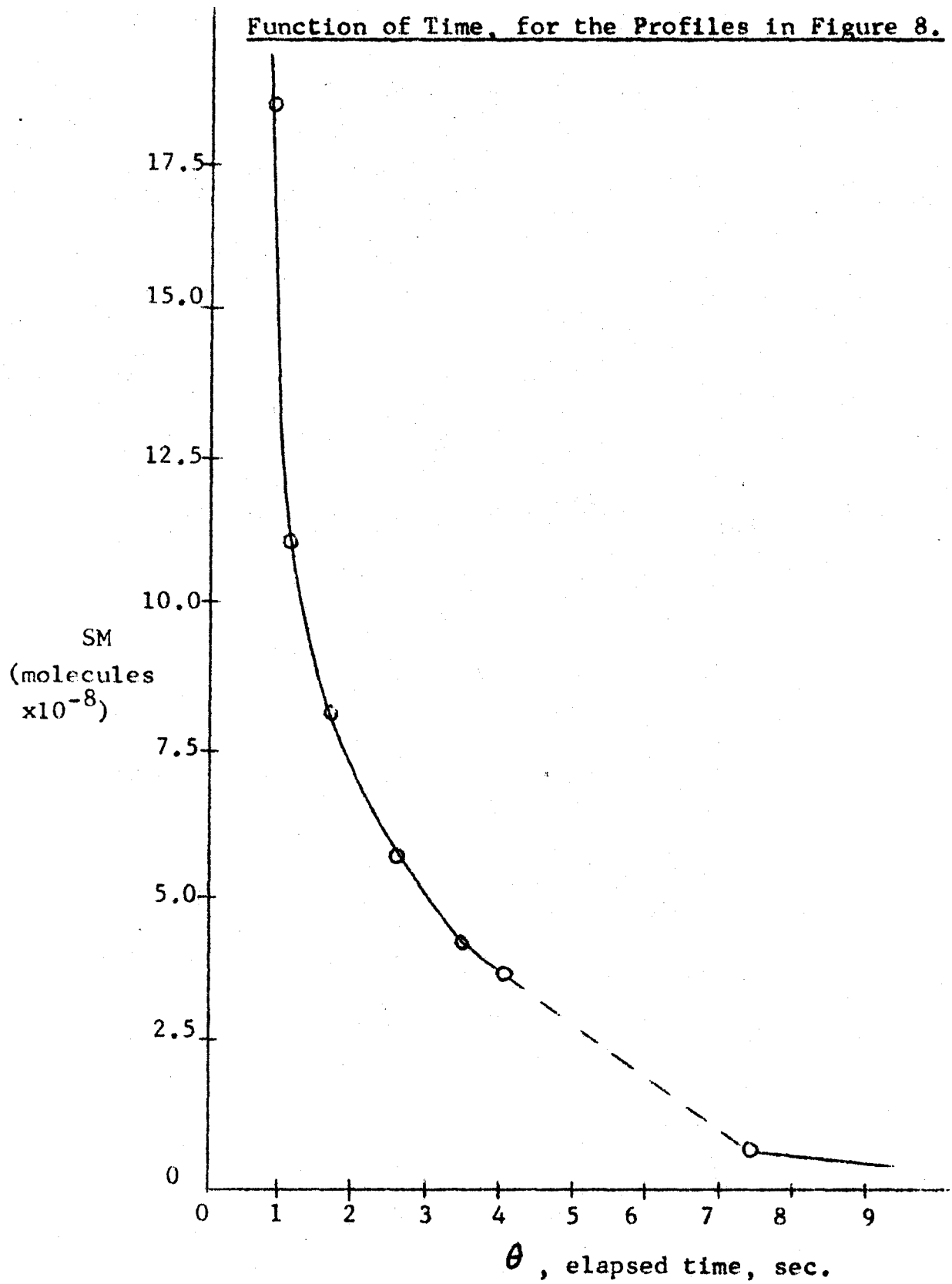

Figure 11. Drop Rest-time versus Interface Age for Pure System + 0.01 N. KCl

Toluene/Water

Drop Volume 0.005 ml.

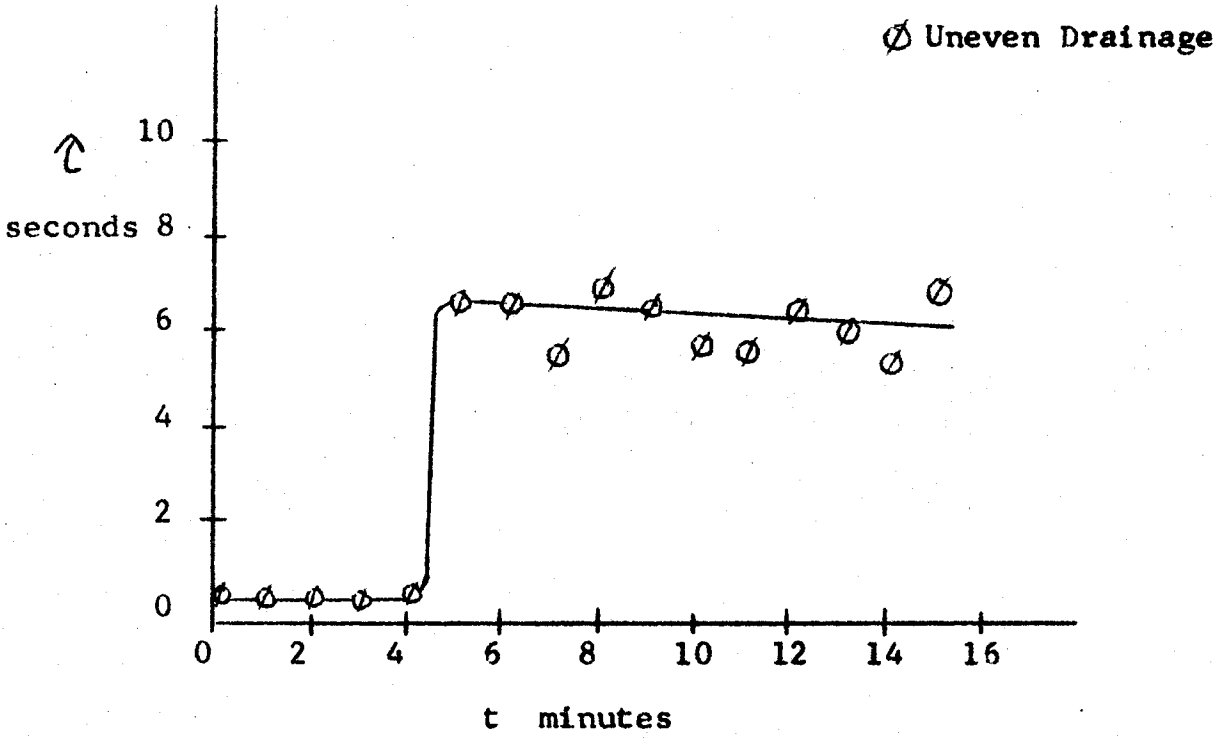

The interface age, t, was measured from the instant that cleaning was stopped.

Figure 12(a) Drop Rest-time versus Interface Age

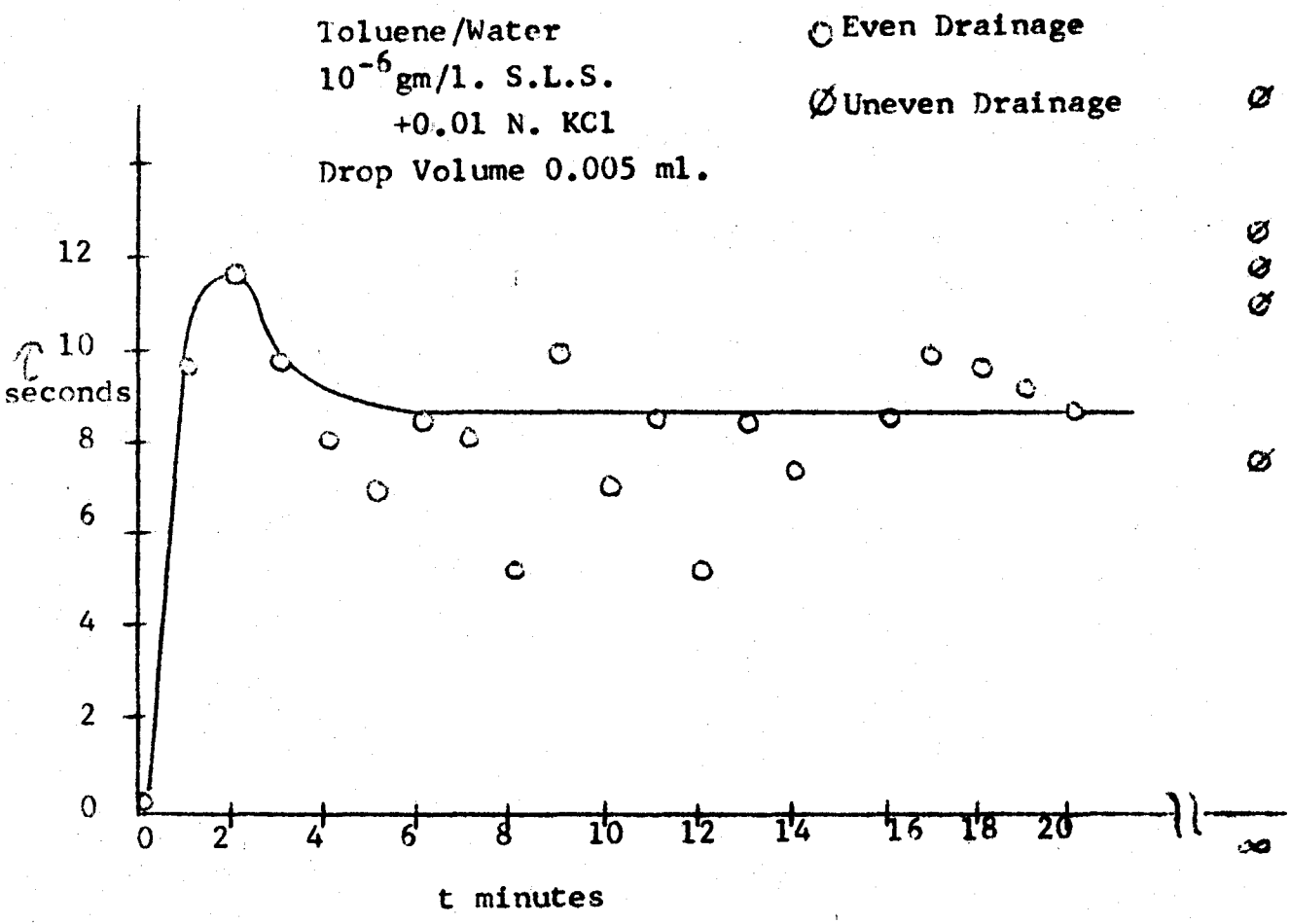

Figure 12(b) $\Delta\tau$ versus Interface Age for the Data in Figure 12a

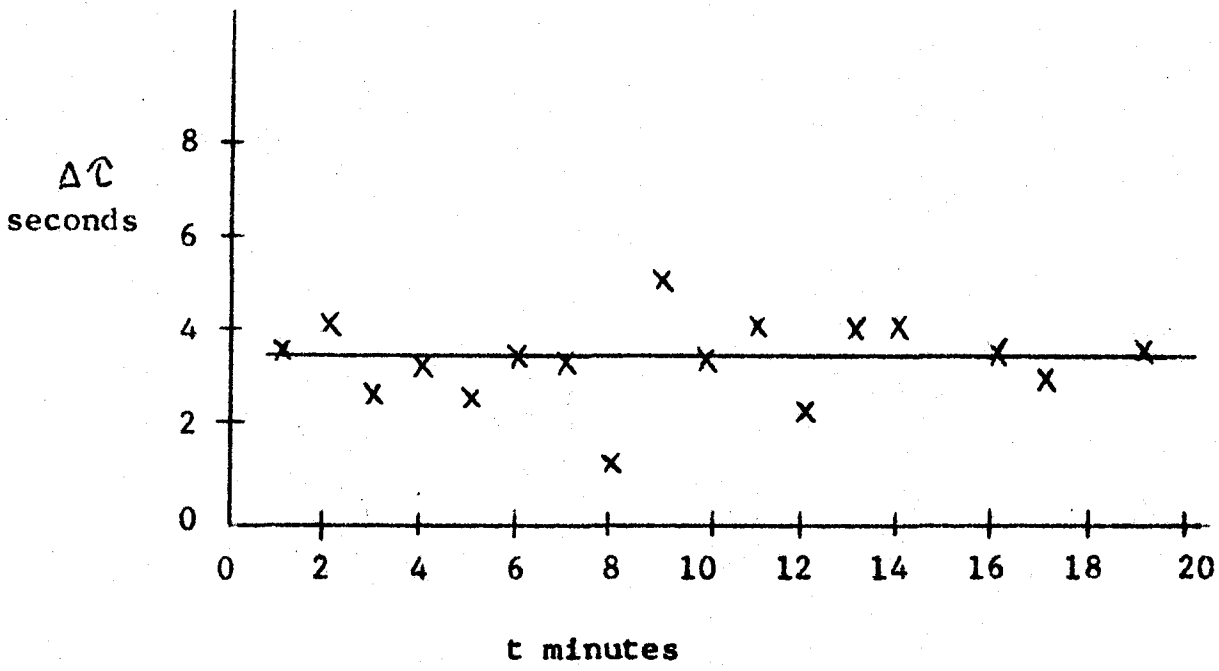

$\Delta\tau$ is defined as $\tau - \tau'$, where τ' is the time required to form the dimple.

Figure 13. Drop Rest-time versus Interface Age

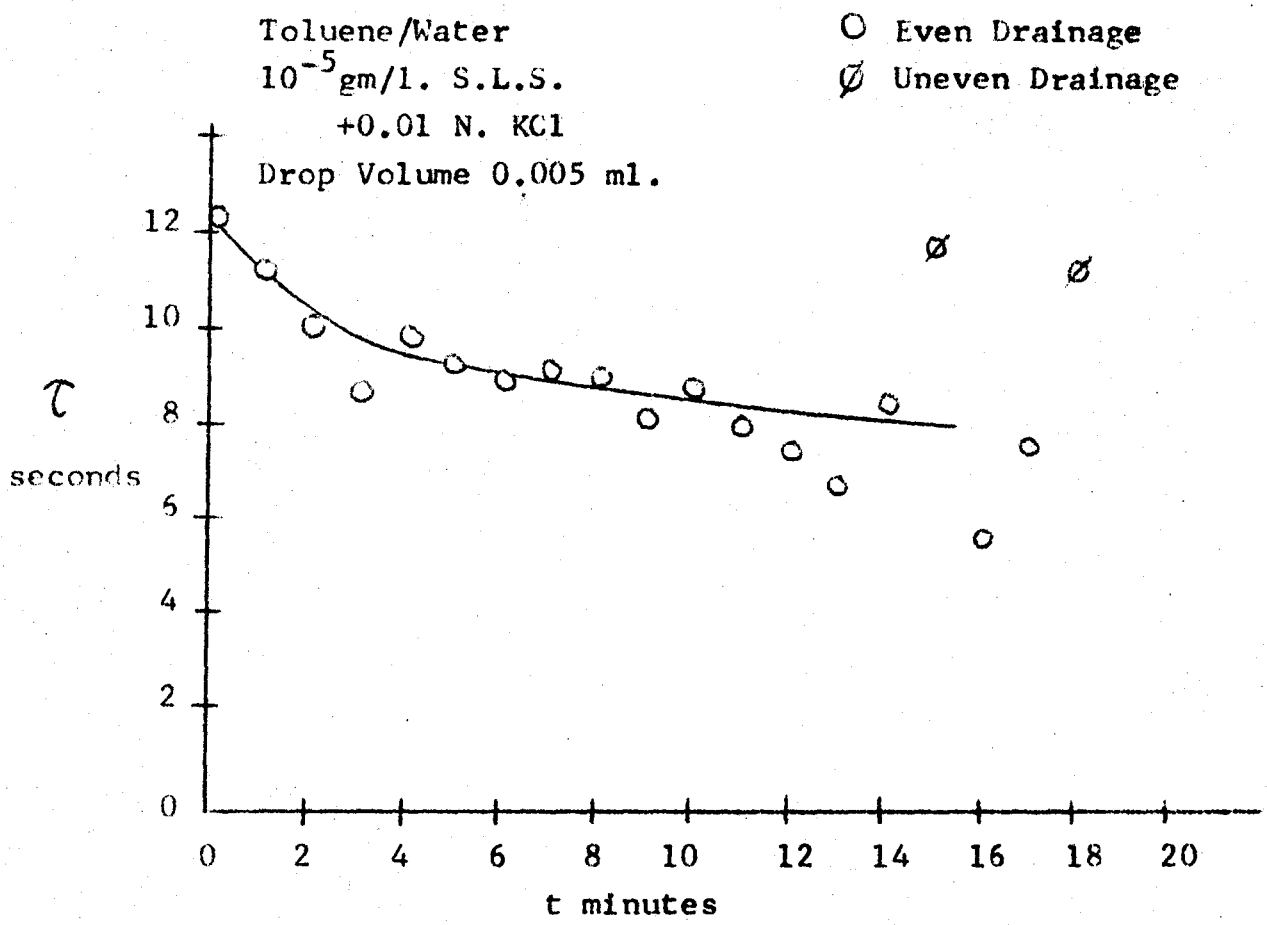

Figure 14. Drop Rest-time versus Interface Age

Toluene/Water
10^{-4}gm/l. S.L.S.
+0.10 N. KCl
Drop Volume 0.005 ml.

O Even Drainage

Ø Uneven Drainage

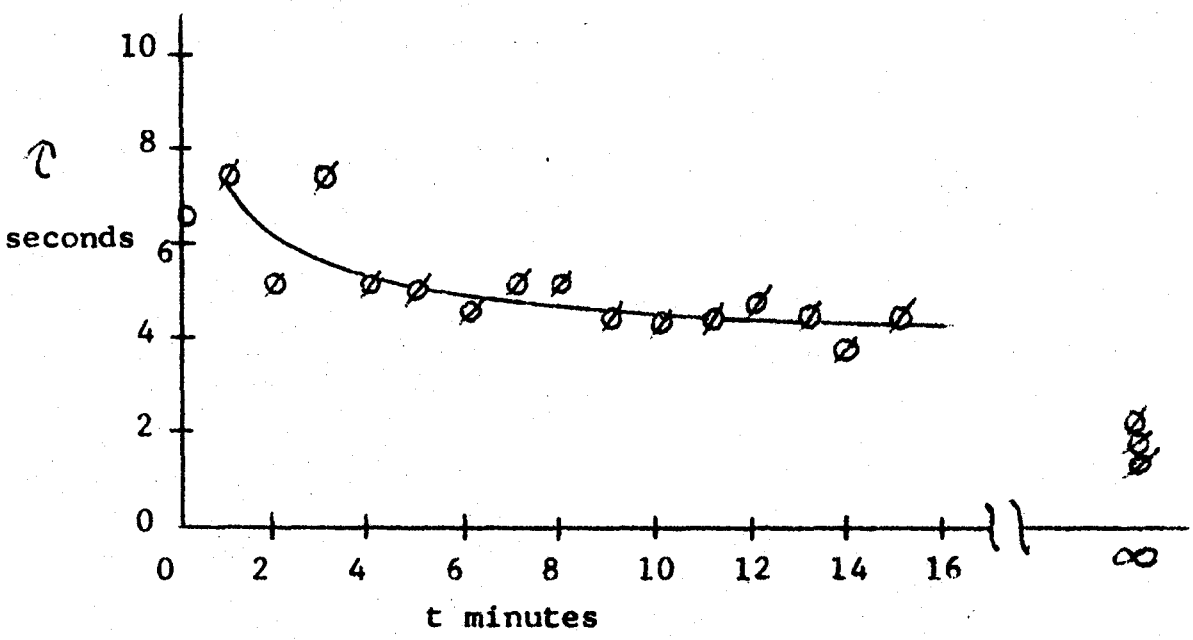

Figure 15. Drop Rest-time versus Interface Age

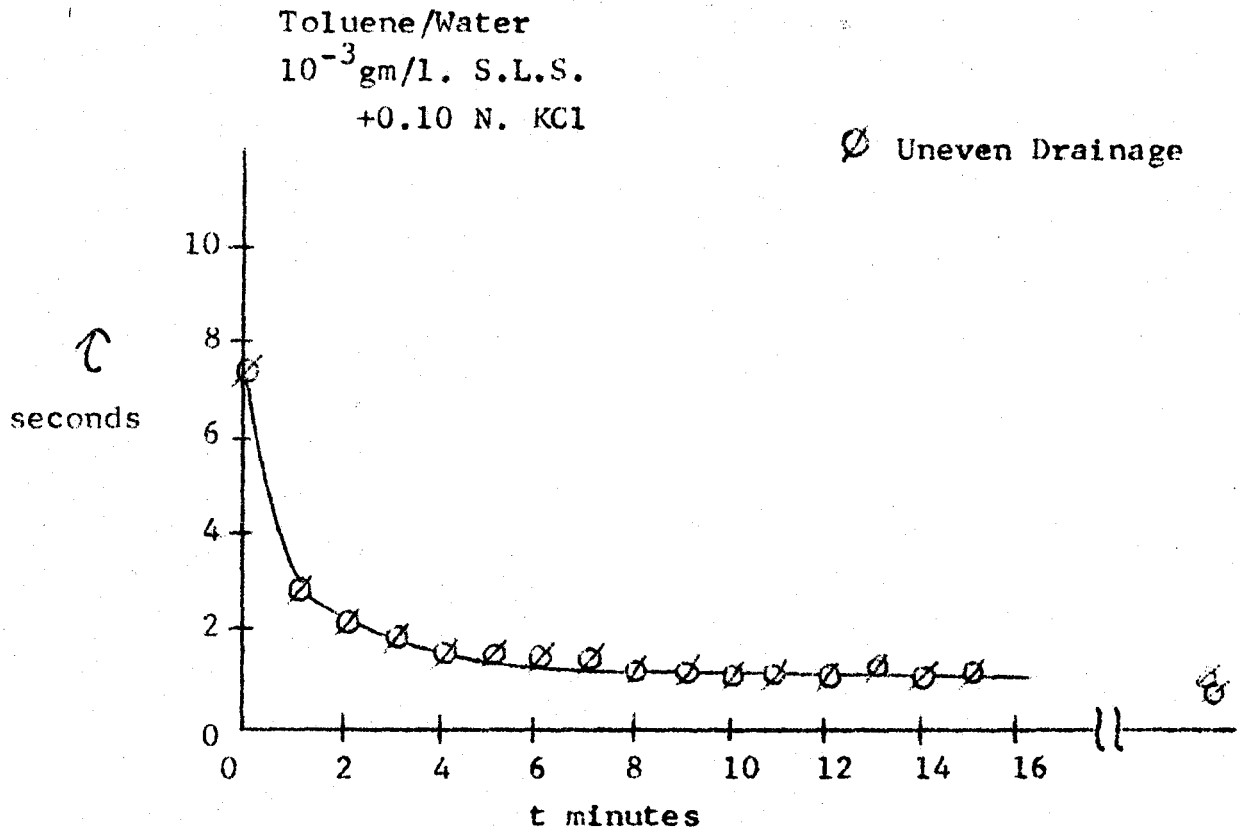

Figure 16. Drop Rest-time versus Interface Age

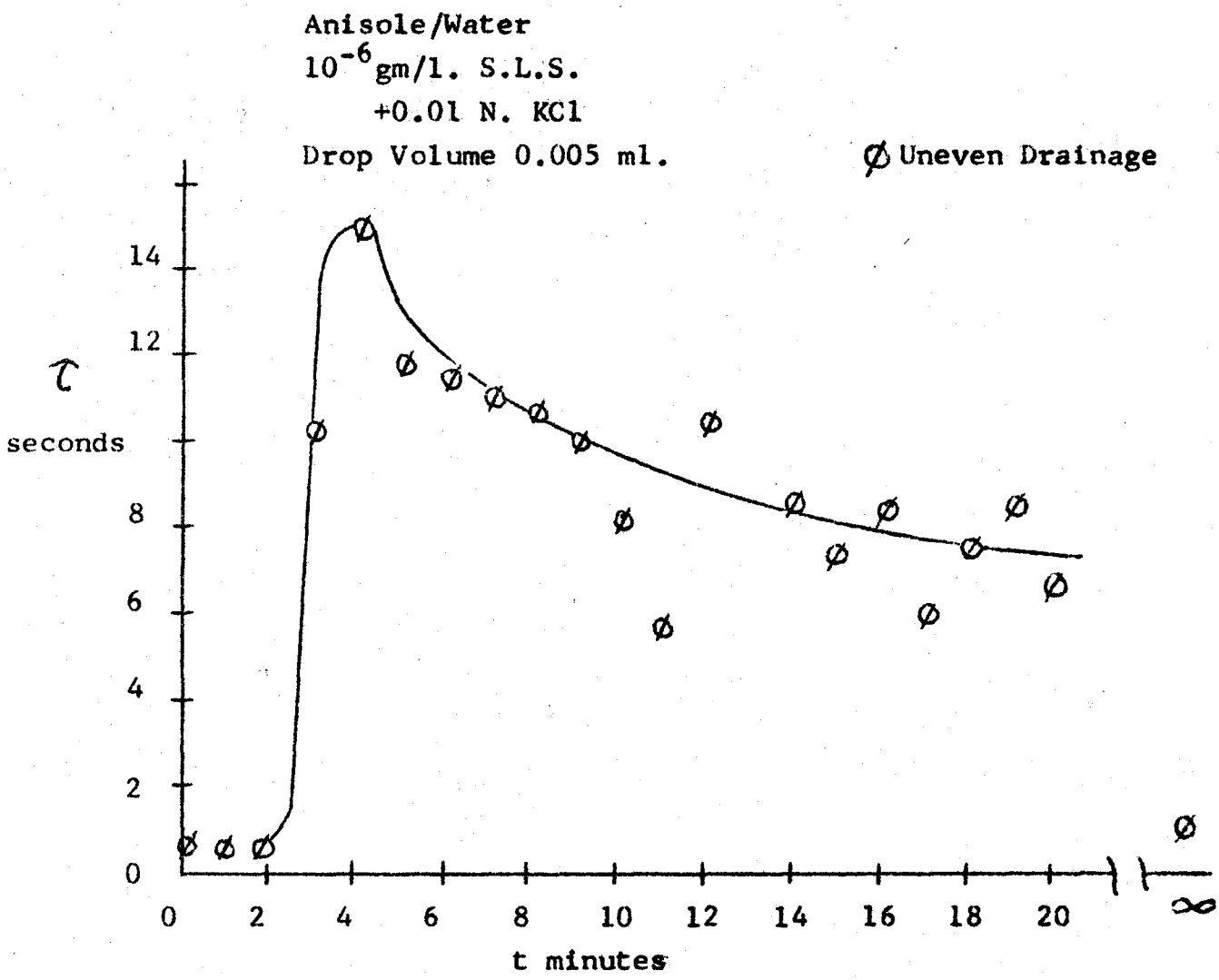

Figure 17. Drop Rest-time versus Interface Age

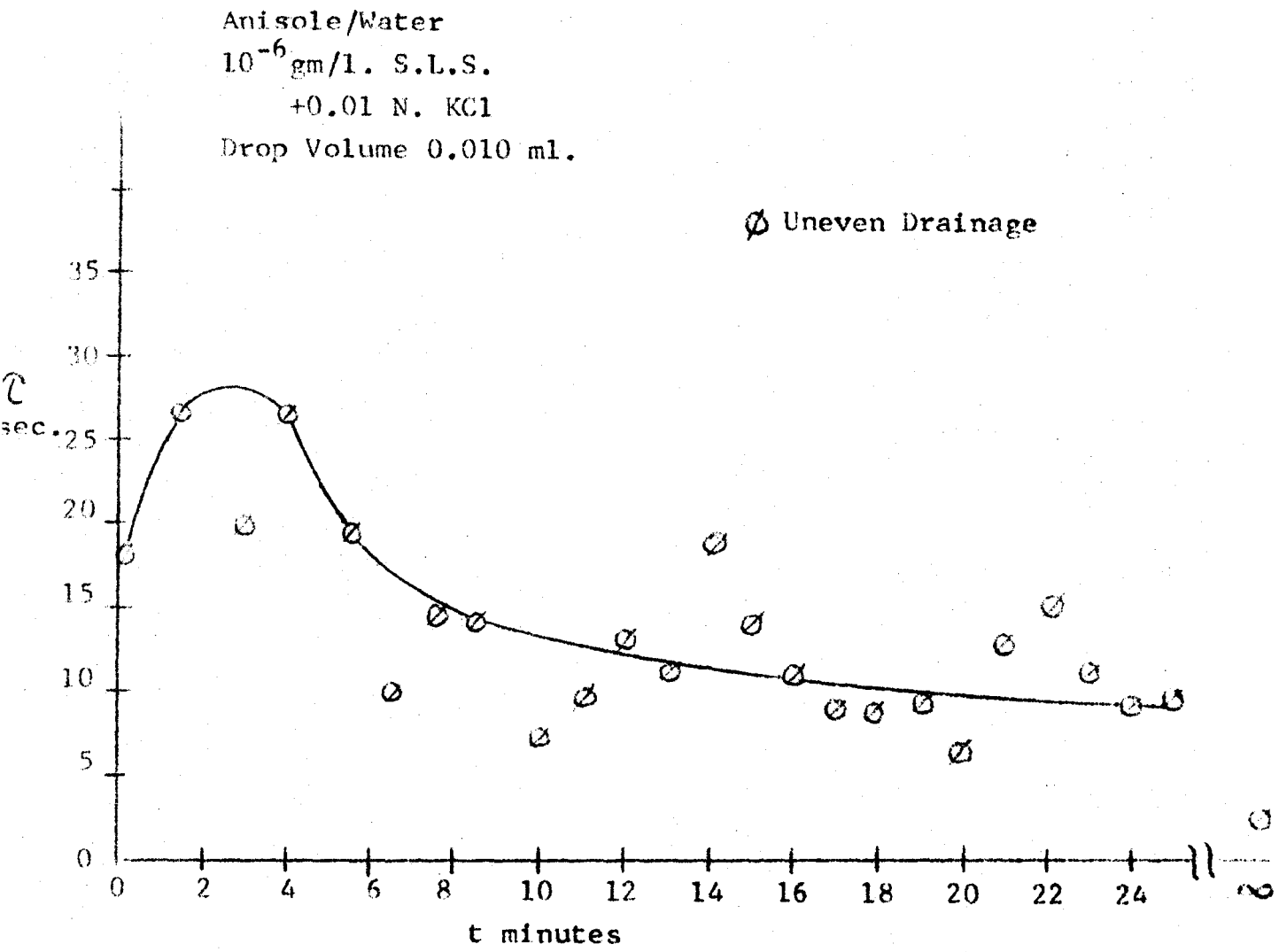

Figure 18. Drop Rest-time versus Interface Age

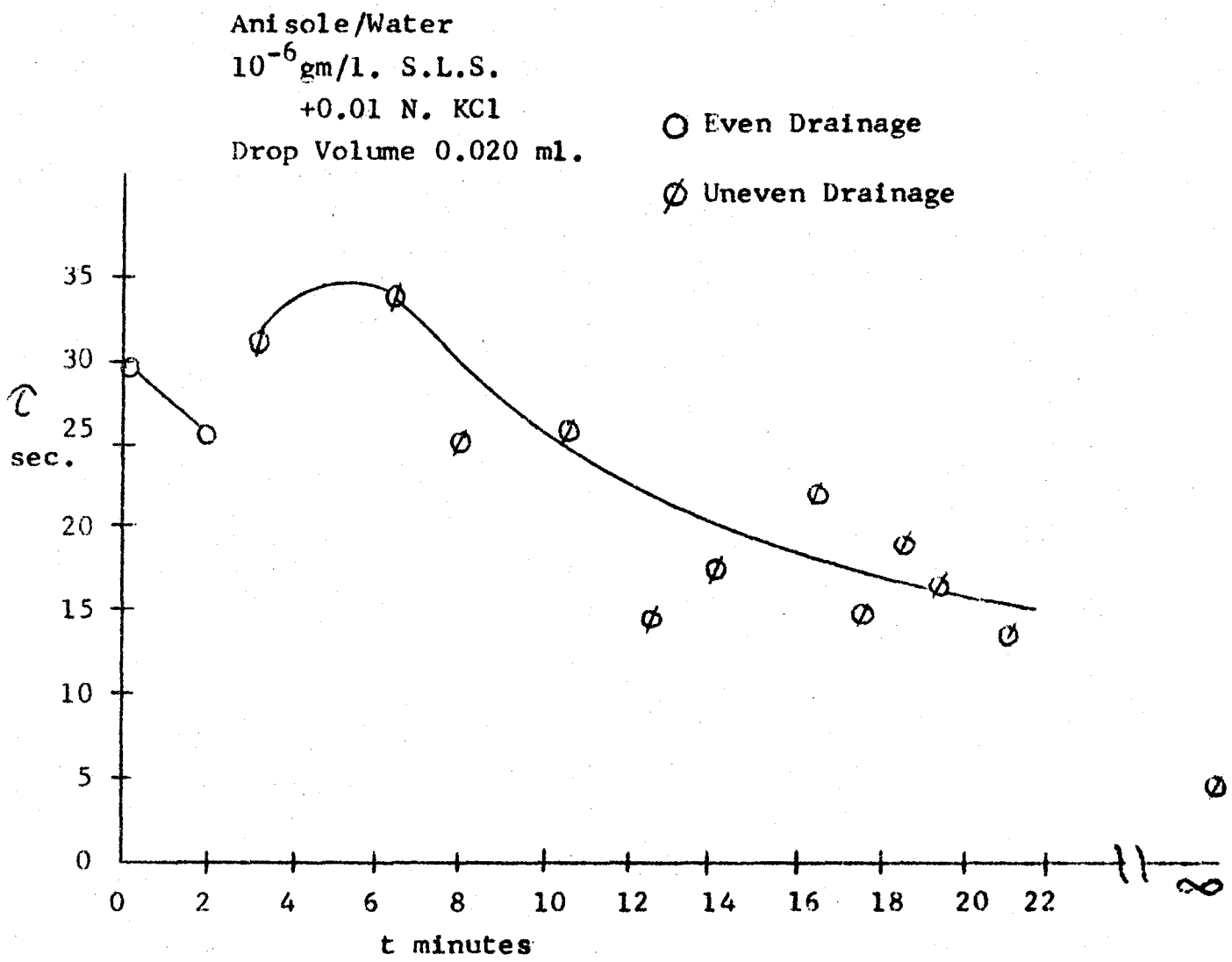

Figure 19. Drop Rest-time versus Interface Age

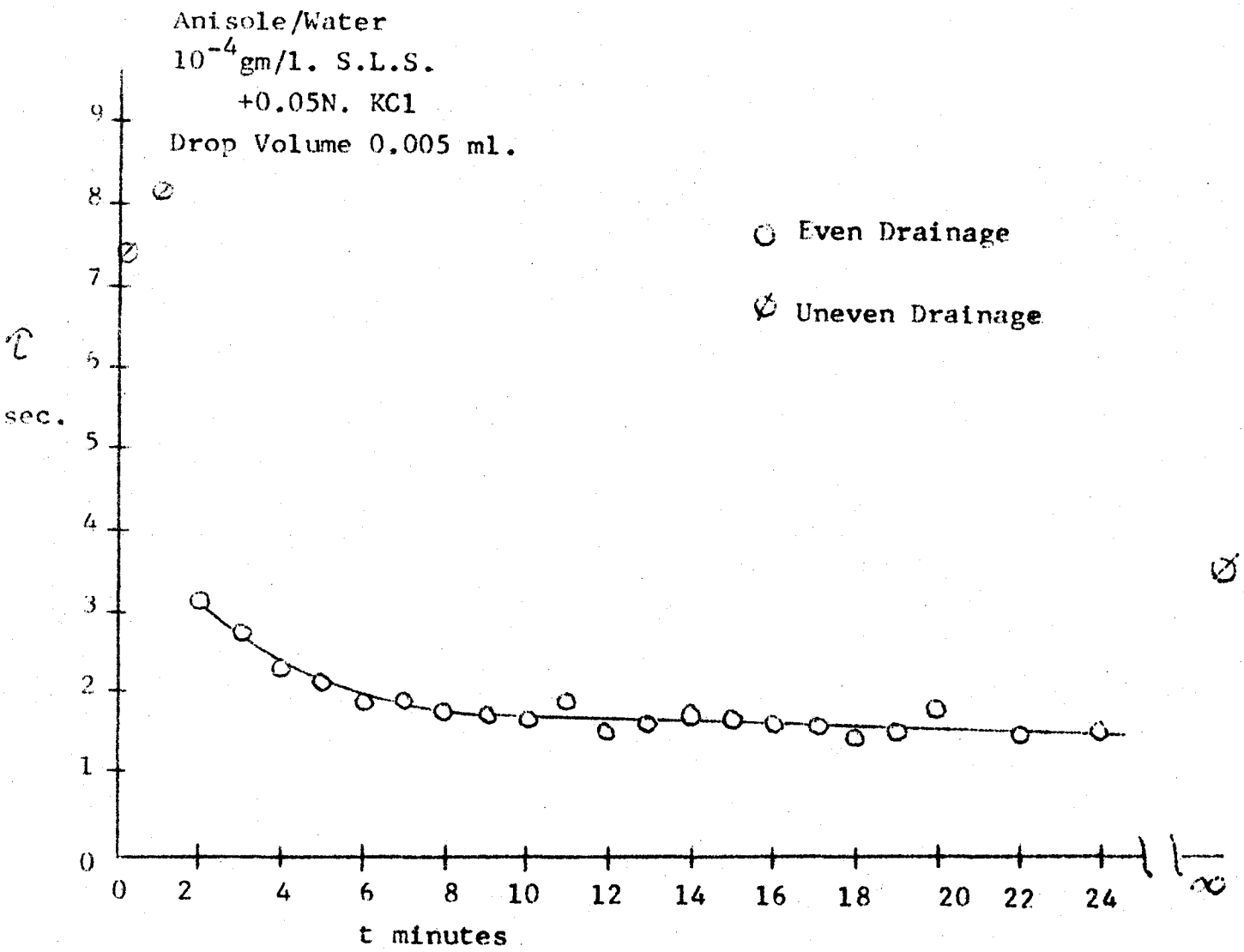

Figure 20. Drop Rest-time versus Interface Age

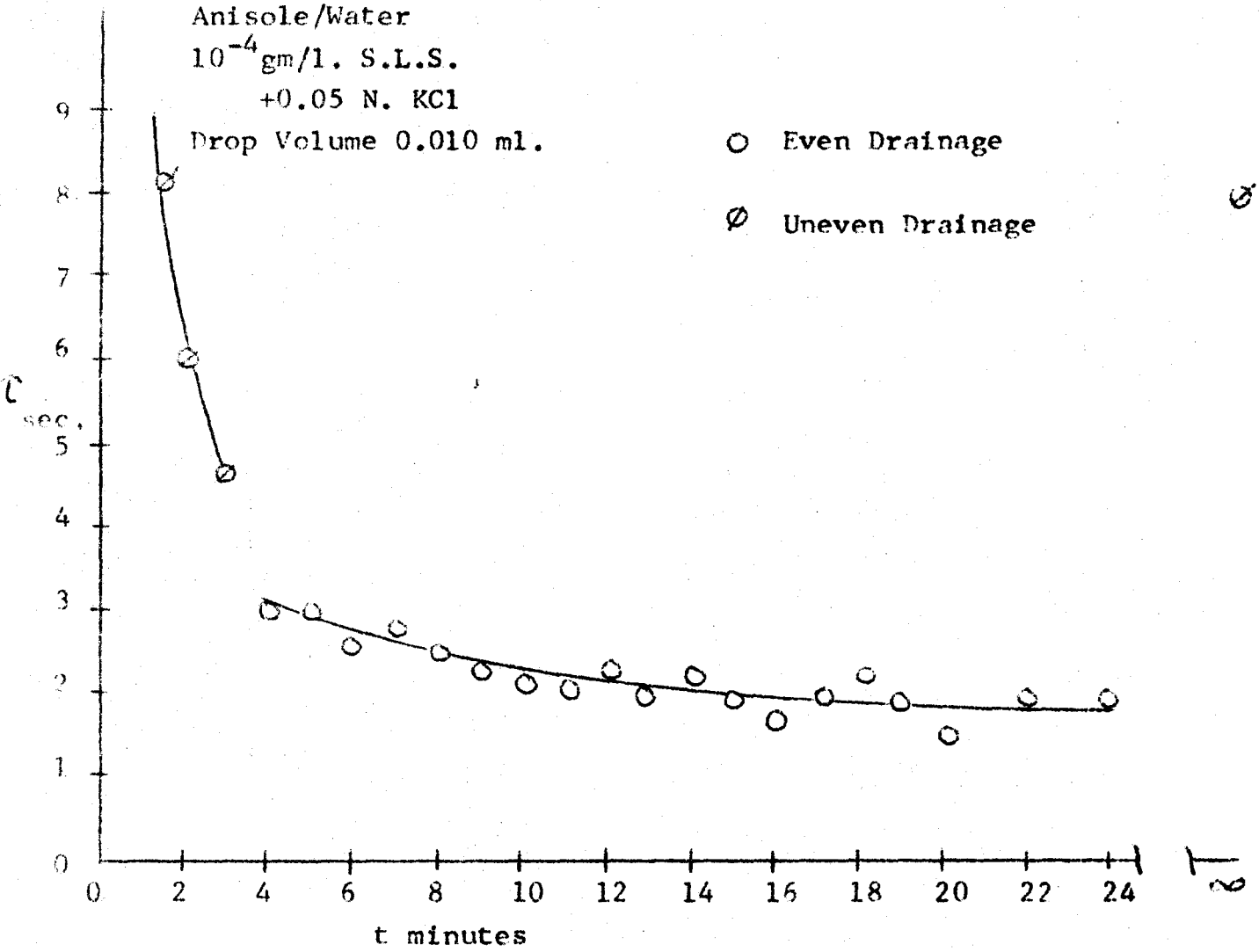

Figure 21. Drop Rest-time versus Interface Age

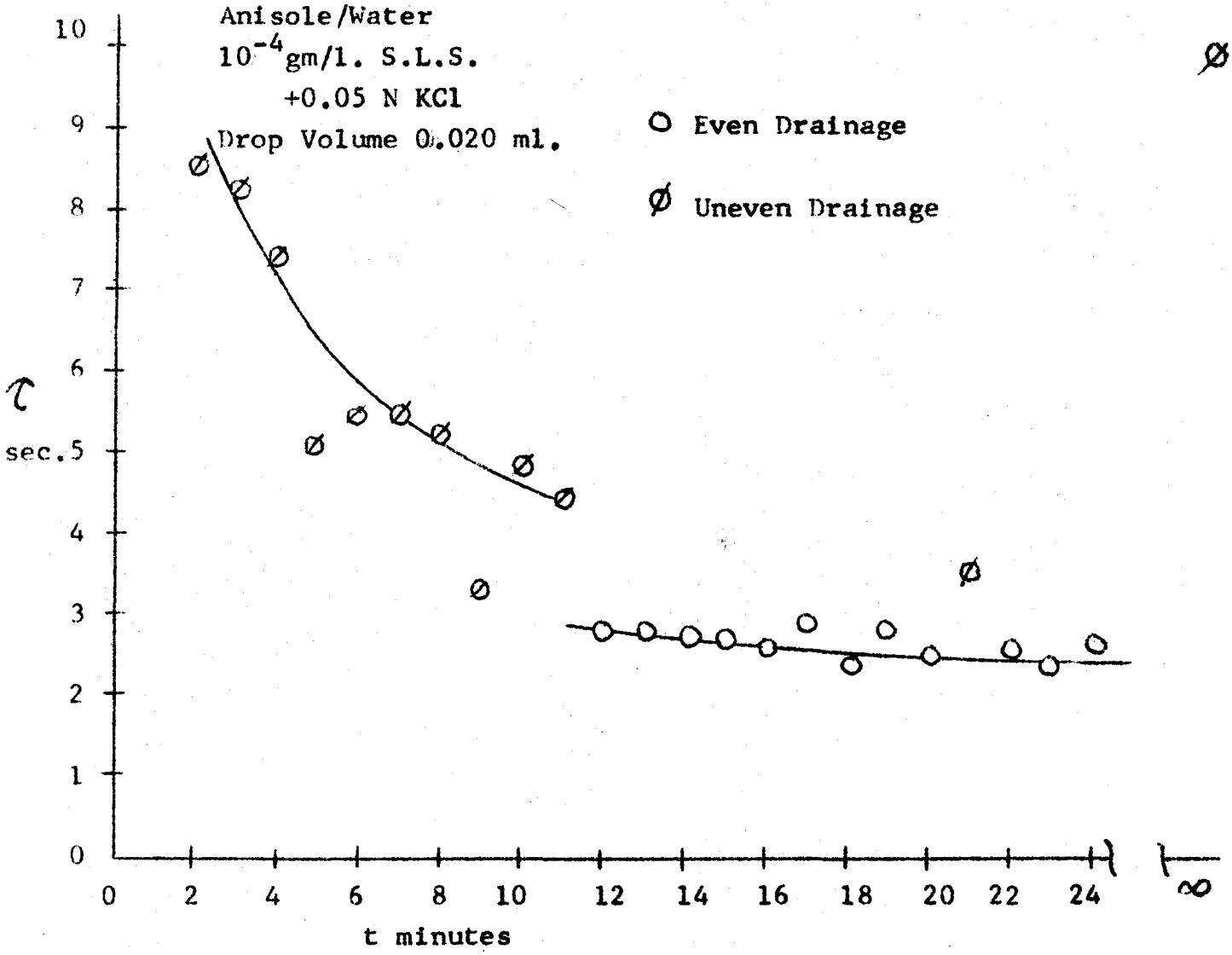

Figure 22. Drop Rest-time versus Interface Age

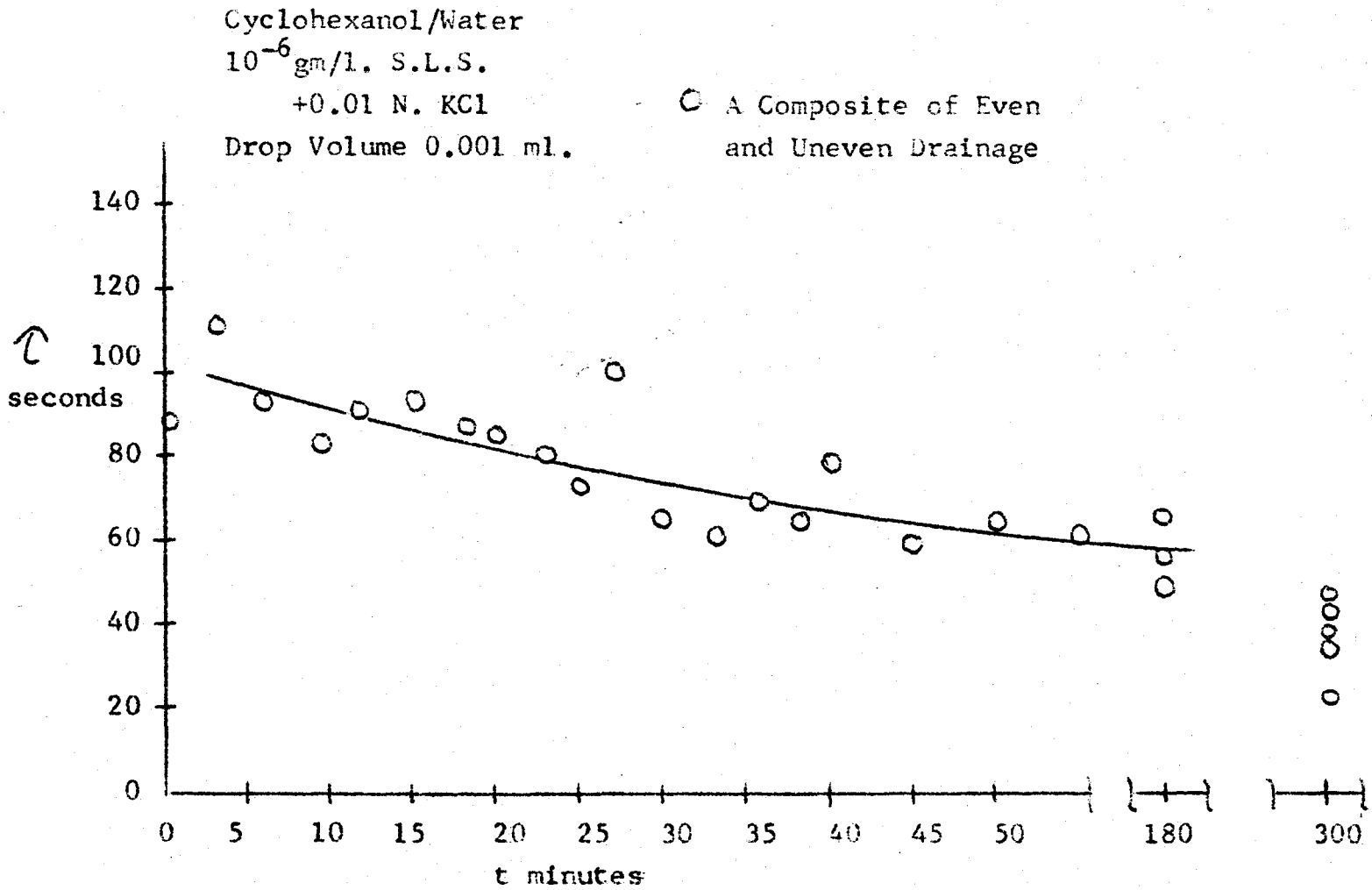

Figure 23. Drop Rest-time versus Interface Age

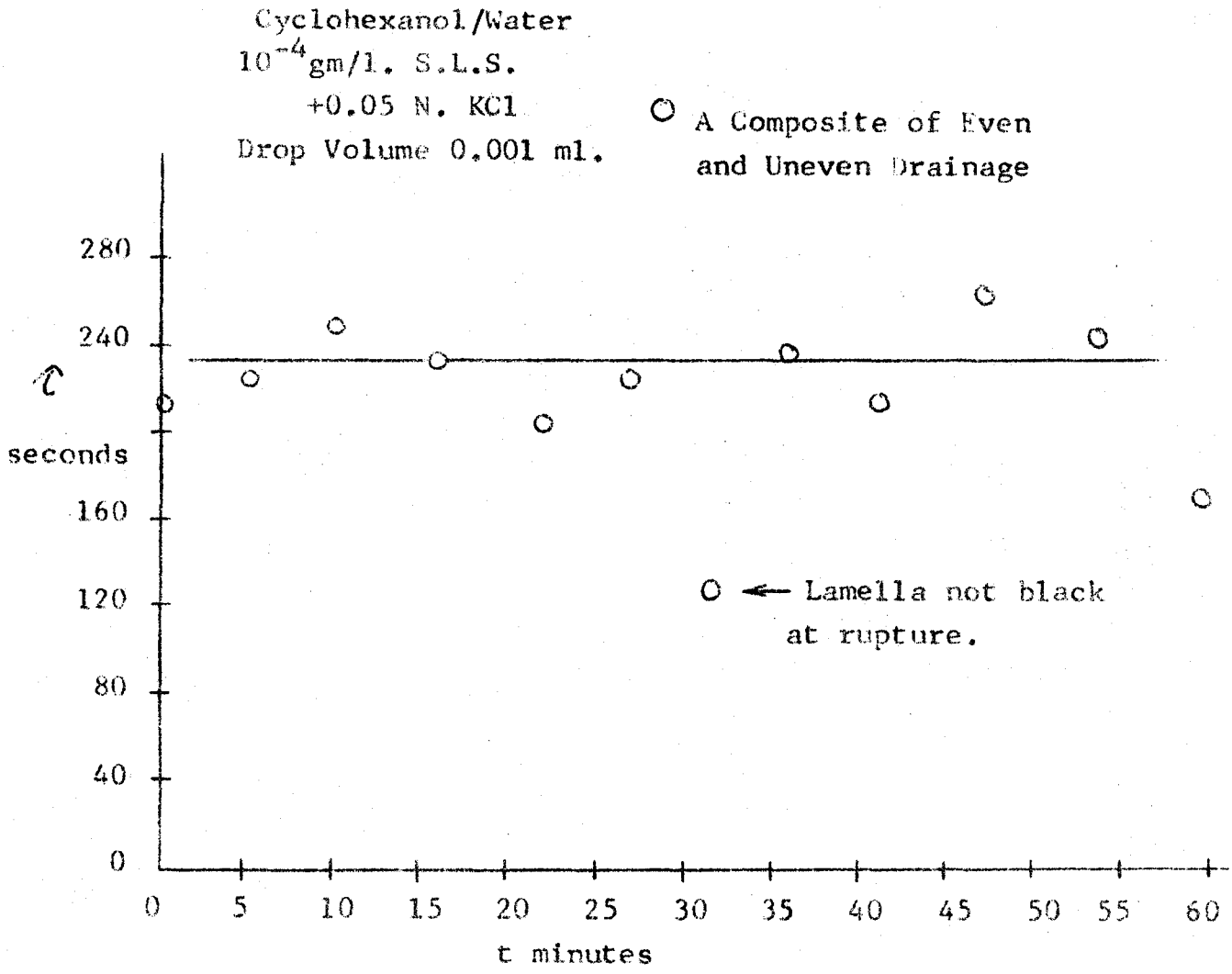

Figure 24. Drop Rest-time versus Interface Age

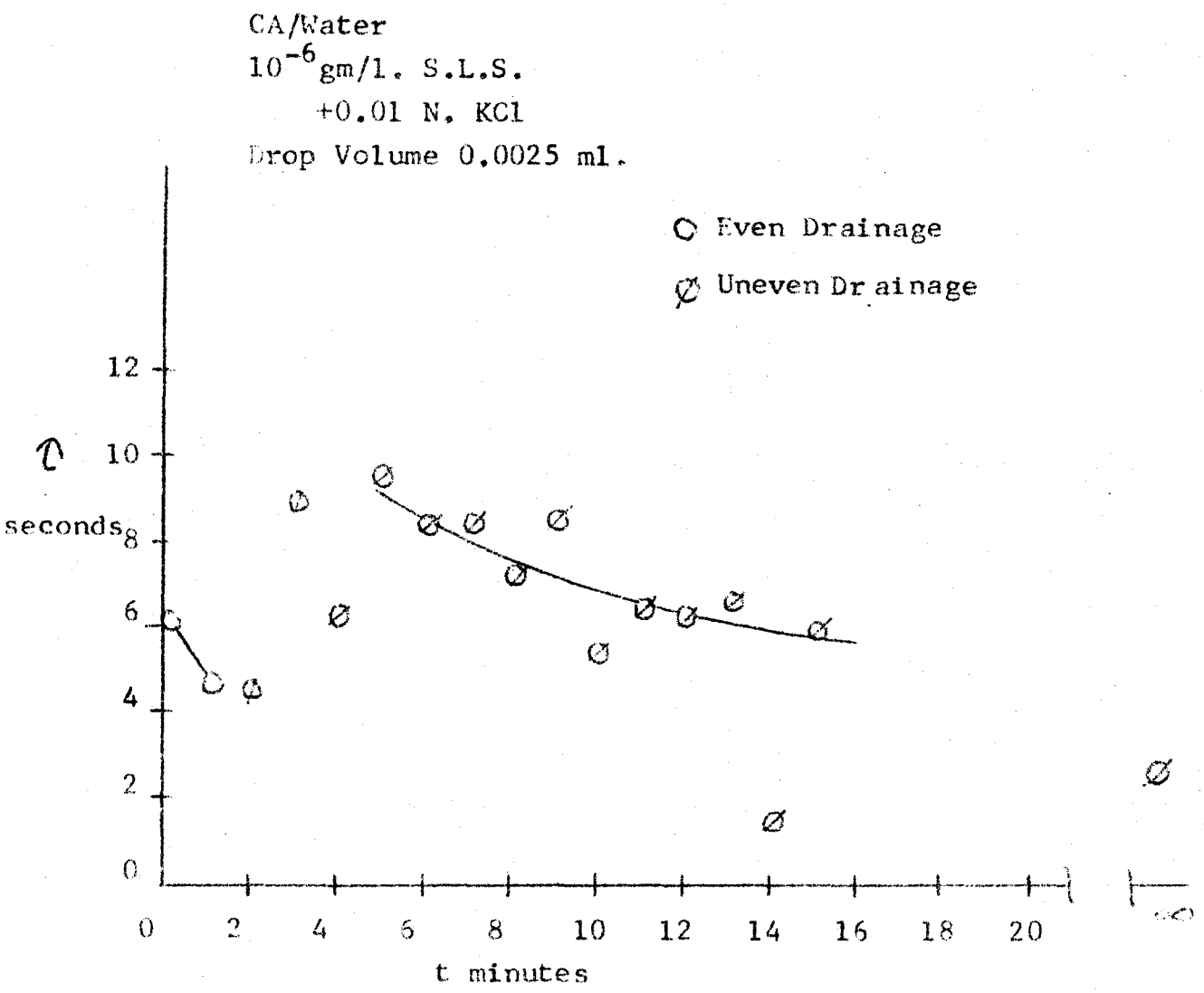

Figure 25. Drop Rest-time versus Interface Age

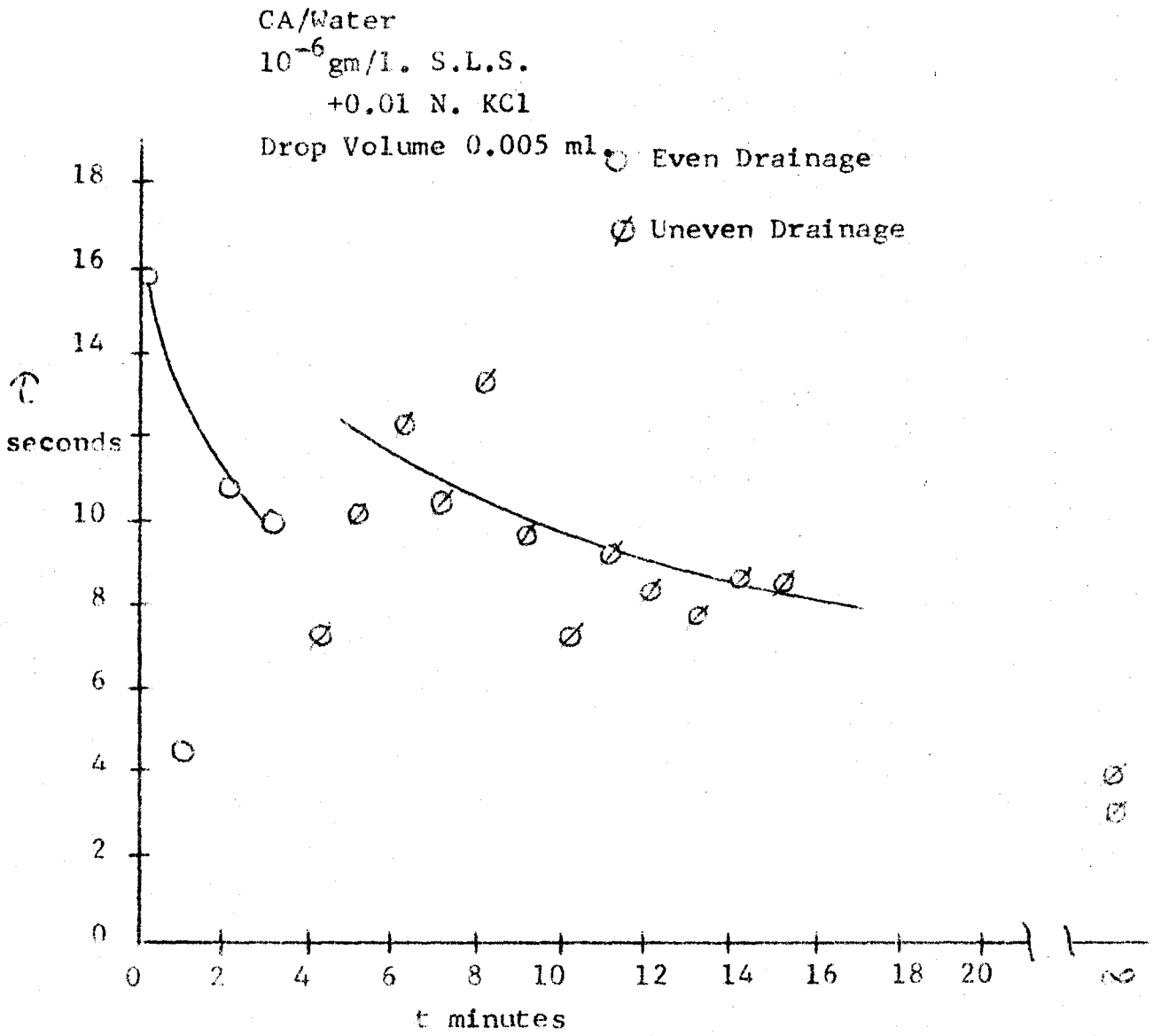

Figure 26. Drop Rest-time versus Interface Age

CA/Water
10^{-4}gm/l. S.L.S.
+0.05 N. KCl
Drop Volume 0.0025 ml.

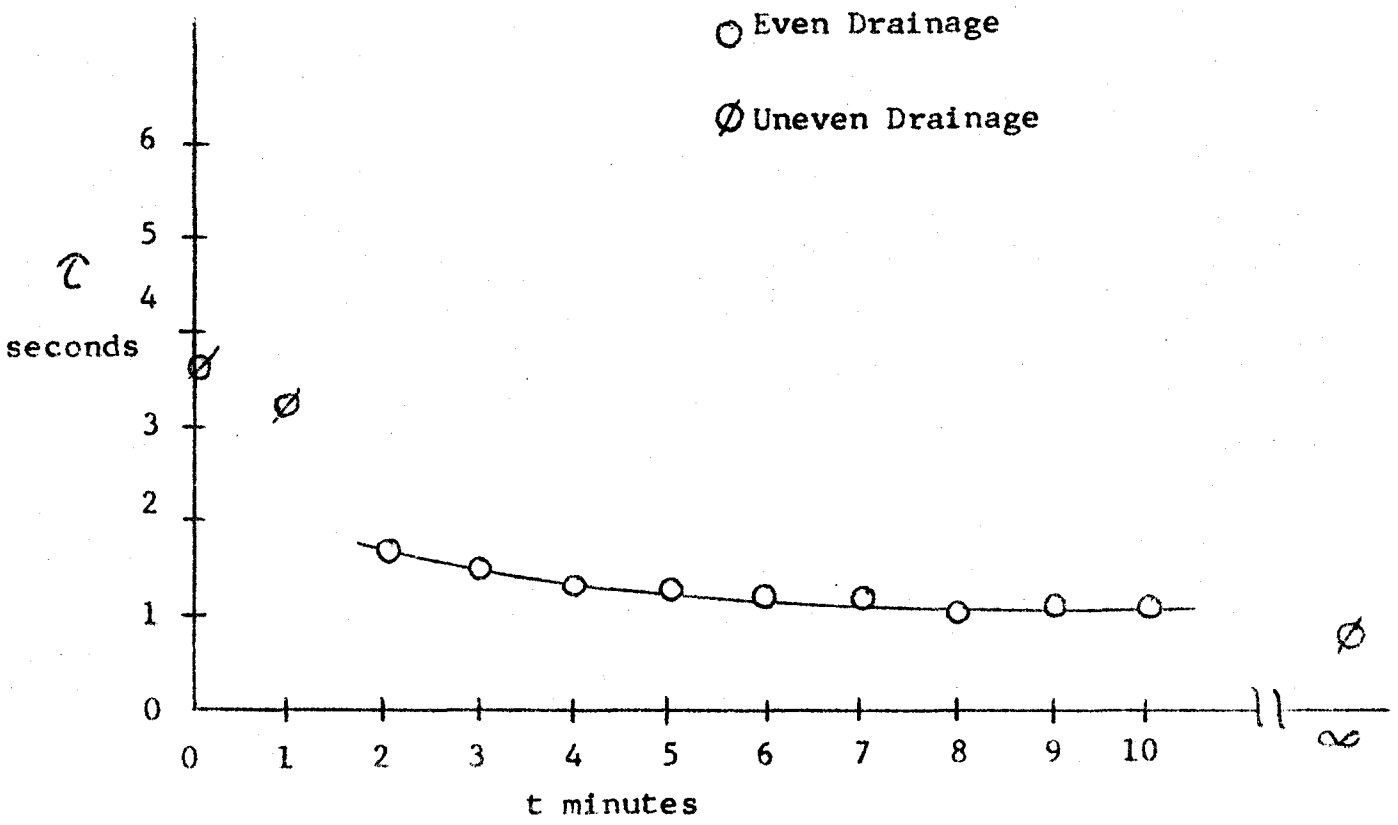

Figure 27. Drop Rest-time versus Interface Age

CA/Water
10^{-4} gm/l. S.L.S.
+0.05 N. KCl
Drop Volume 0.005 ml.

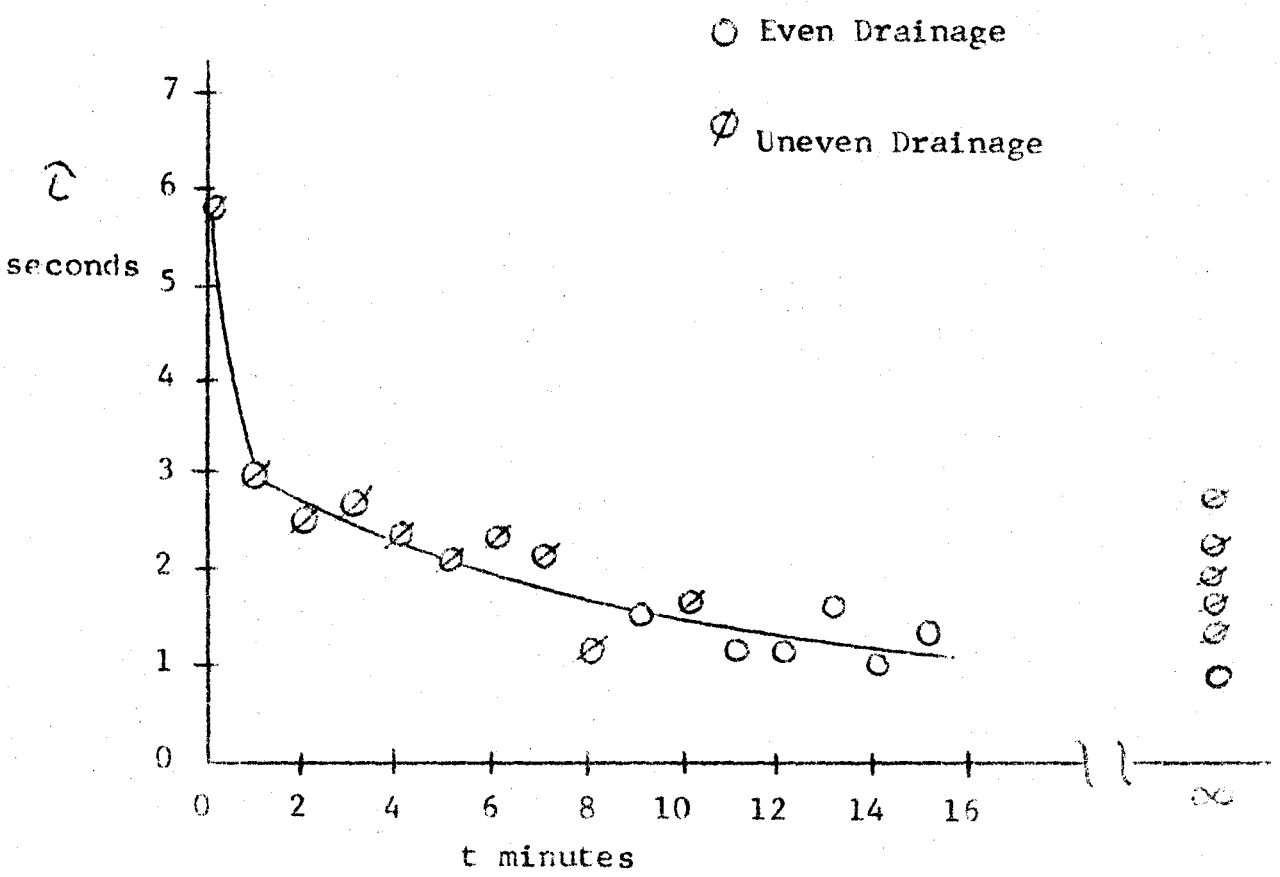

Figure 28a. Composite Figure of Drop Rest-times

Level	S.L.S.(gm/l.)+Electrolyte
A	10^{-6}gm/l. +0.01 N. KCl
B	10^{-5}gm/l. +0.01 N. KCl
C	10^{-4}gm/l. +0.10 N. KCl
D	10^{-3}gm/l. +0.10 N. KCl

● Even Drainage

Uneven Drainage

Toluene/Water

Drop Volume 0.005 ml.

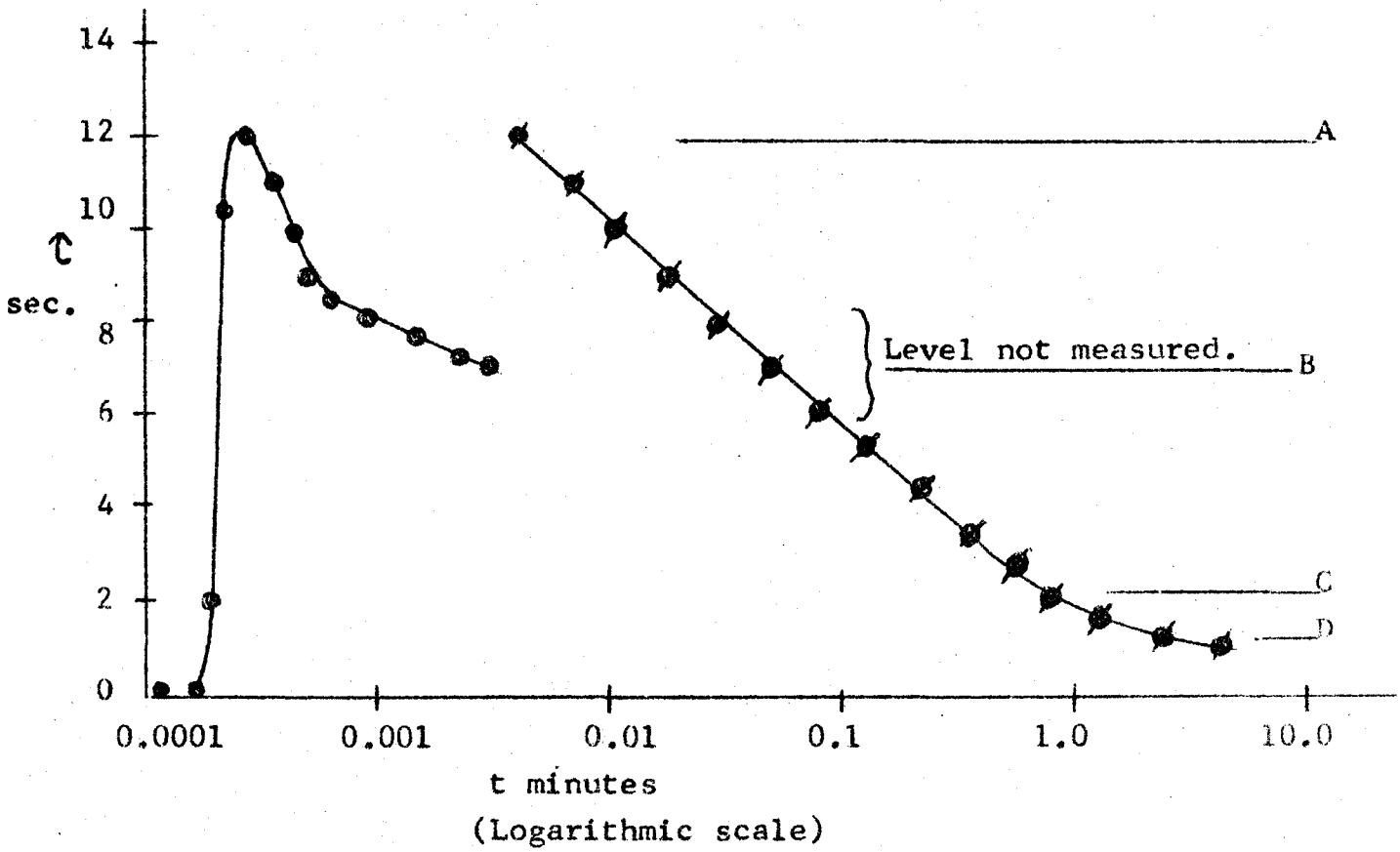

Figure 28b. Composite Figure of Drop Rest-times

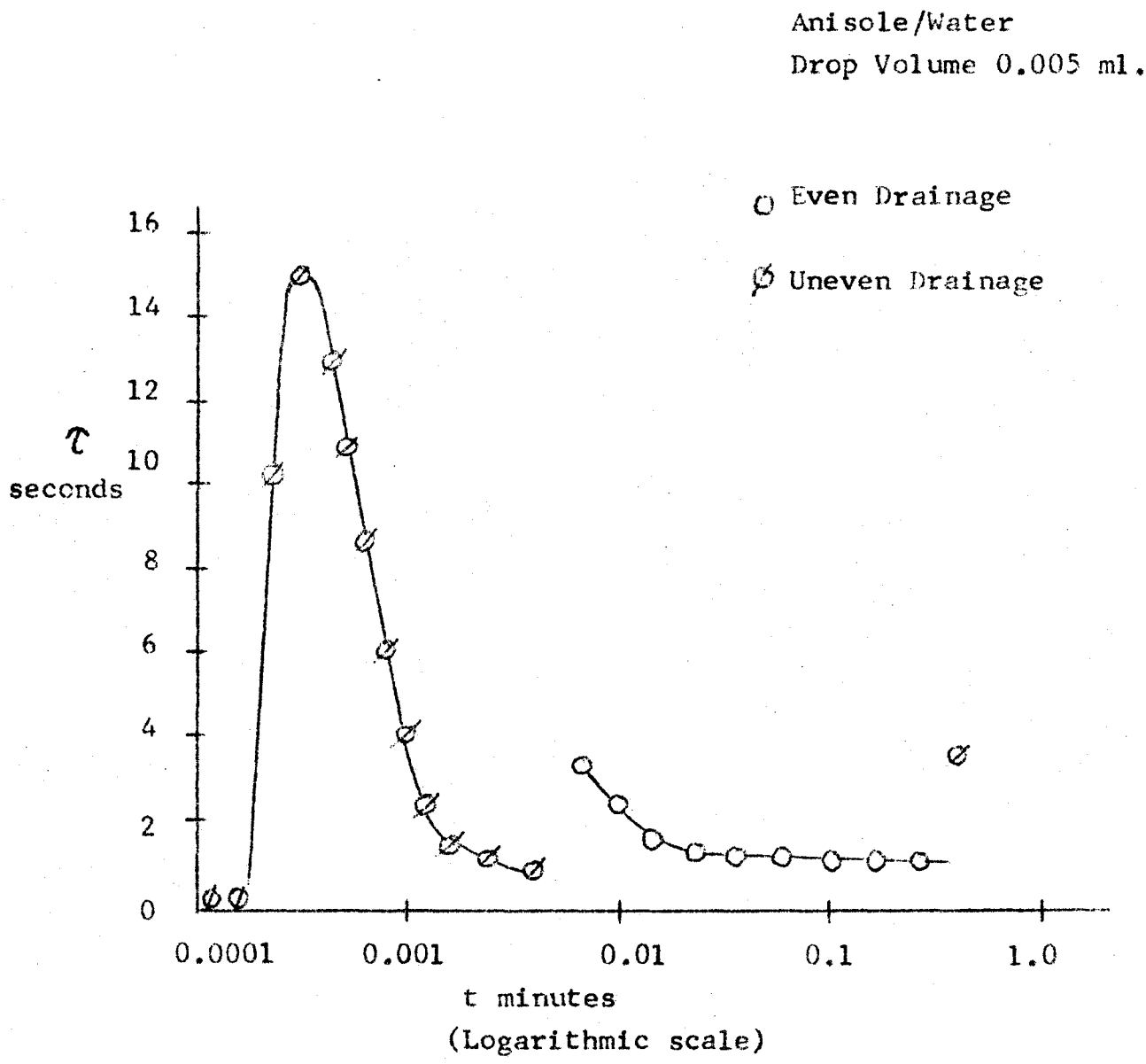

Figure 28c. Composite Figure of Drop Rest-times

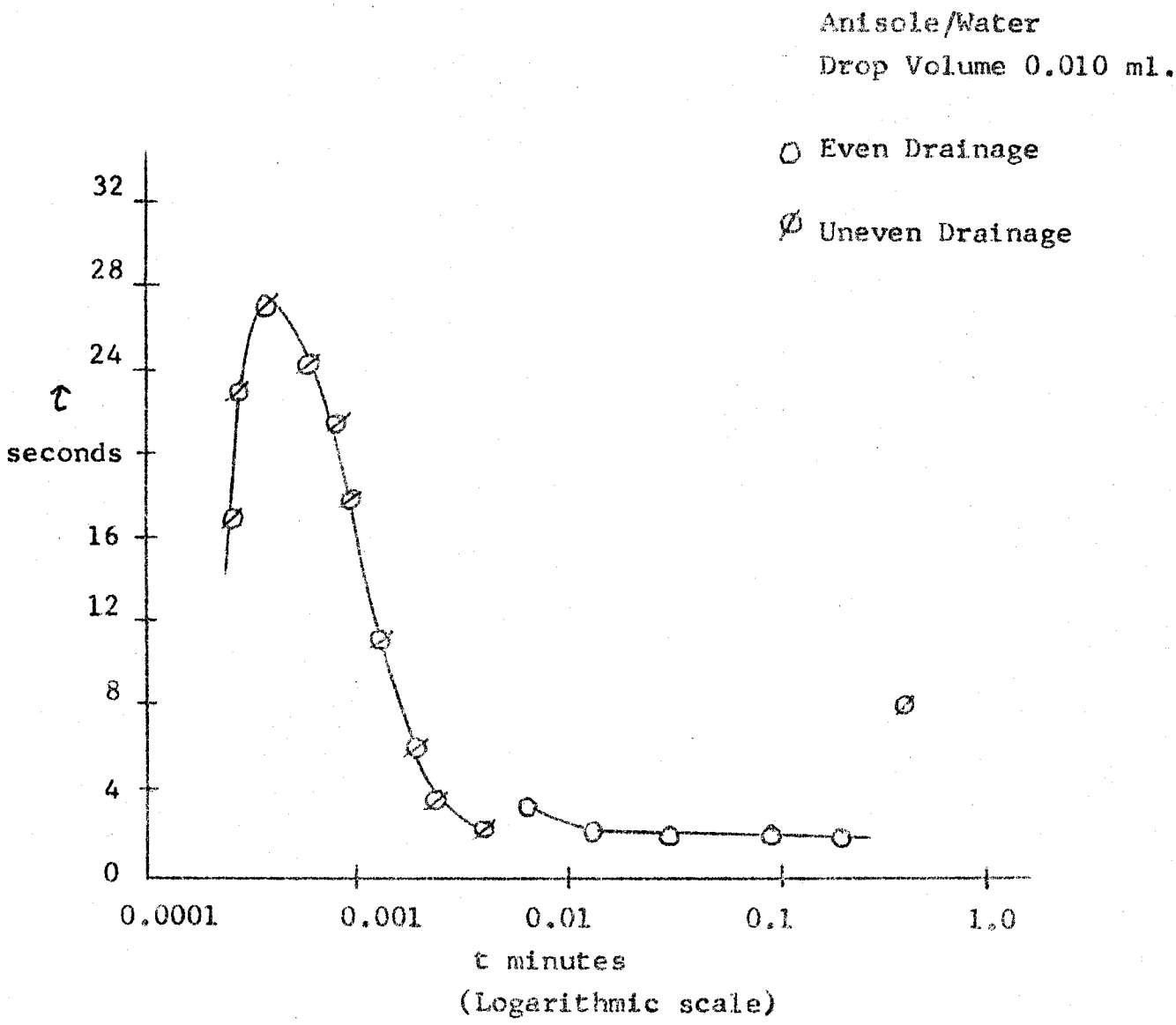

Figure 28d. Composite Figure of Drop Rest-times

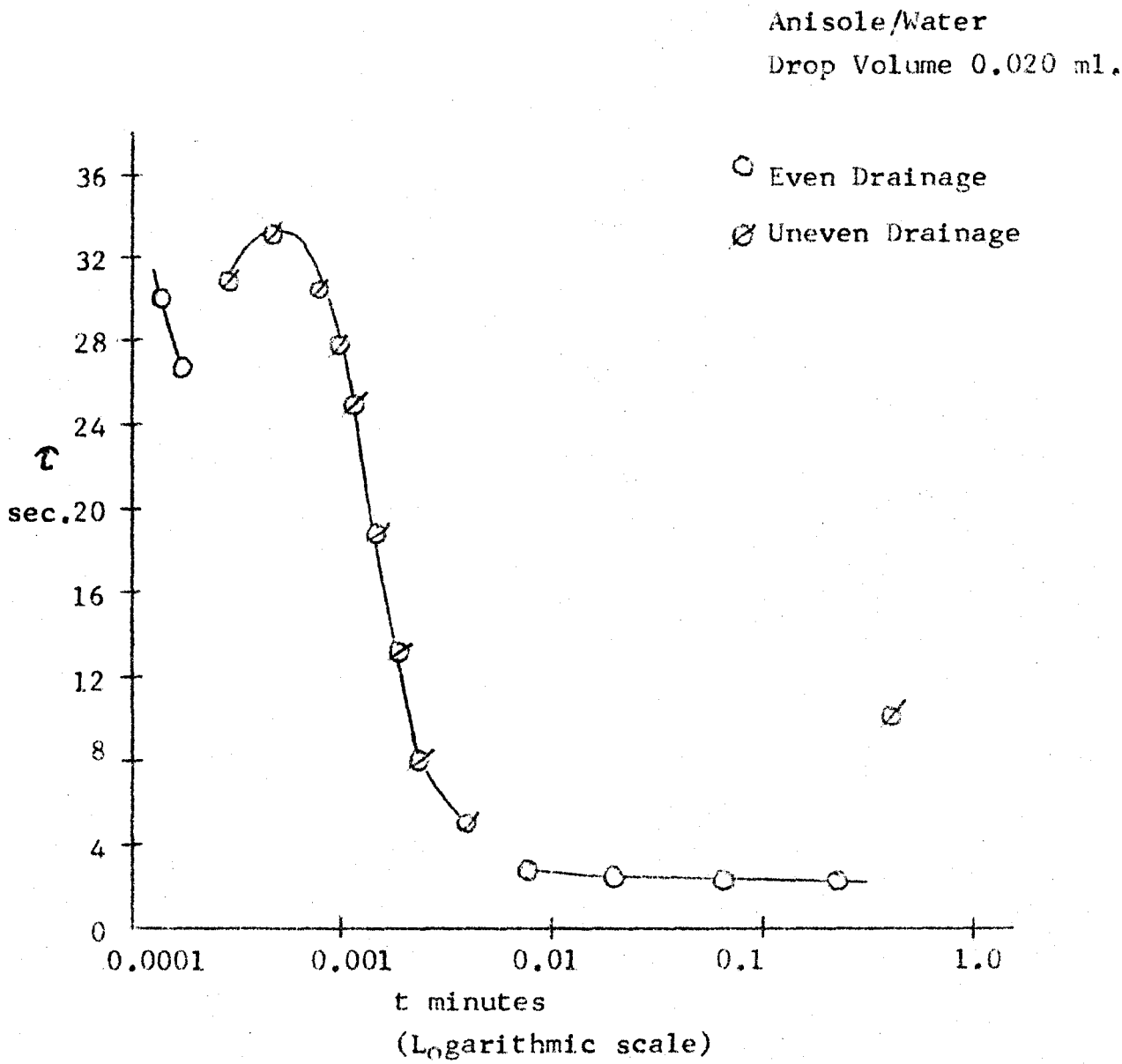

Figure 28e. Composite Figure of Drop Rest-times

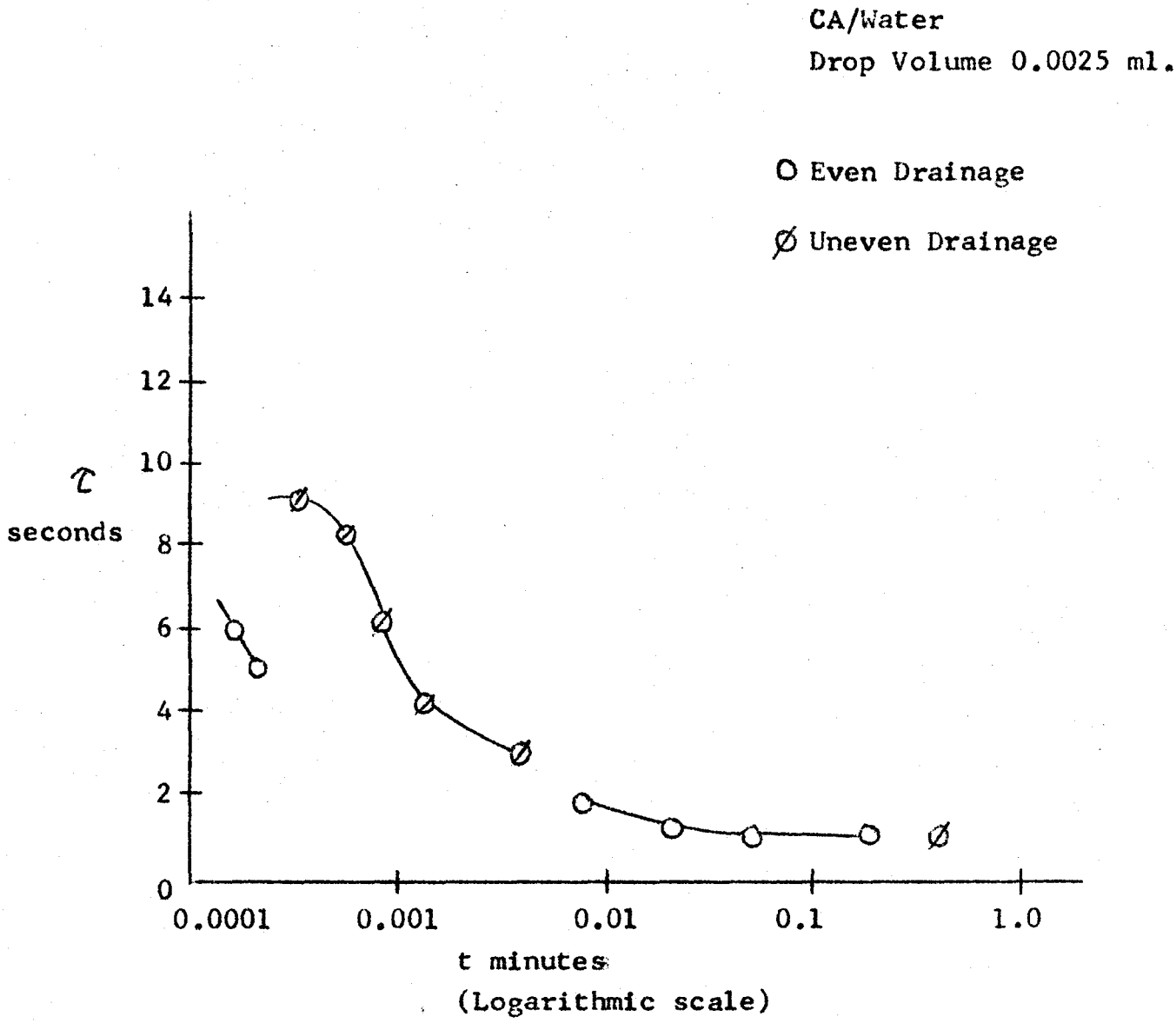

Figure 28f. Composite Figure of Drop-Rest-times

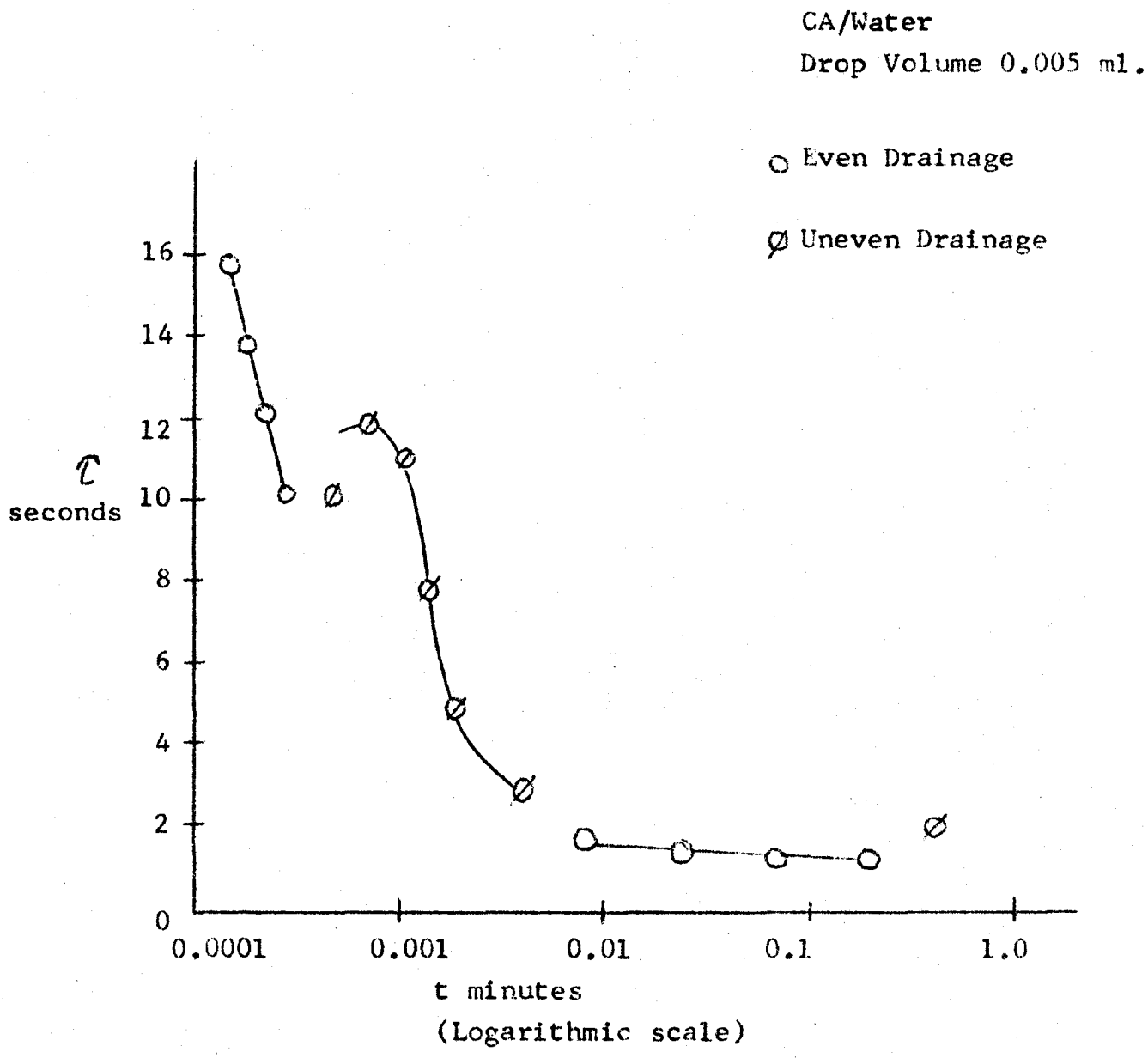

Figure 29. The Uneven Drainage Concept Applied to Typical Data

-Based on Data in Figures (8) and (9).

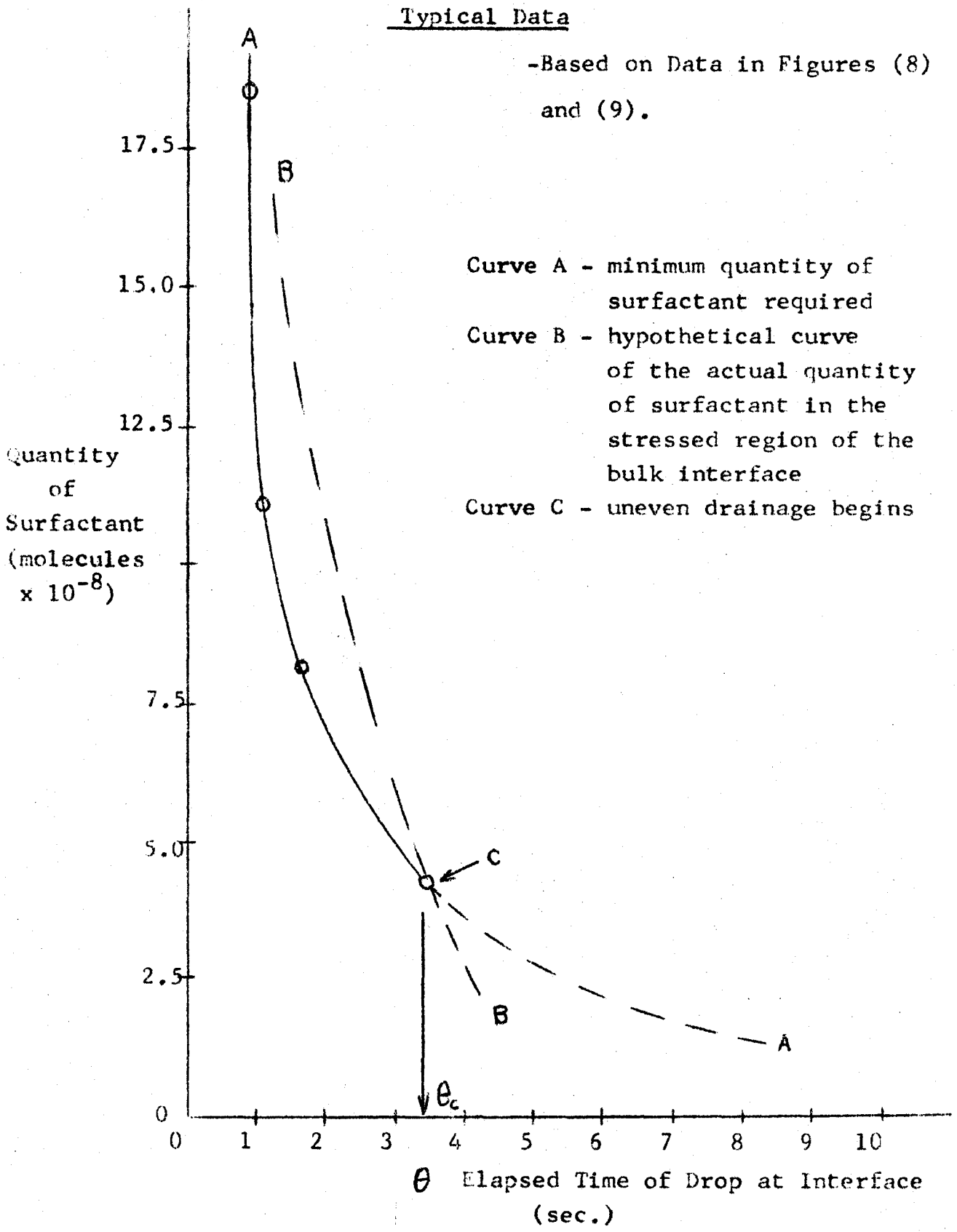

Figure 30. A Histogram of the Lamella Thickness at Rupture as a Function of the Number of Drops Observed- Light Intensity Measurements

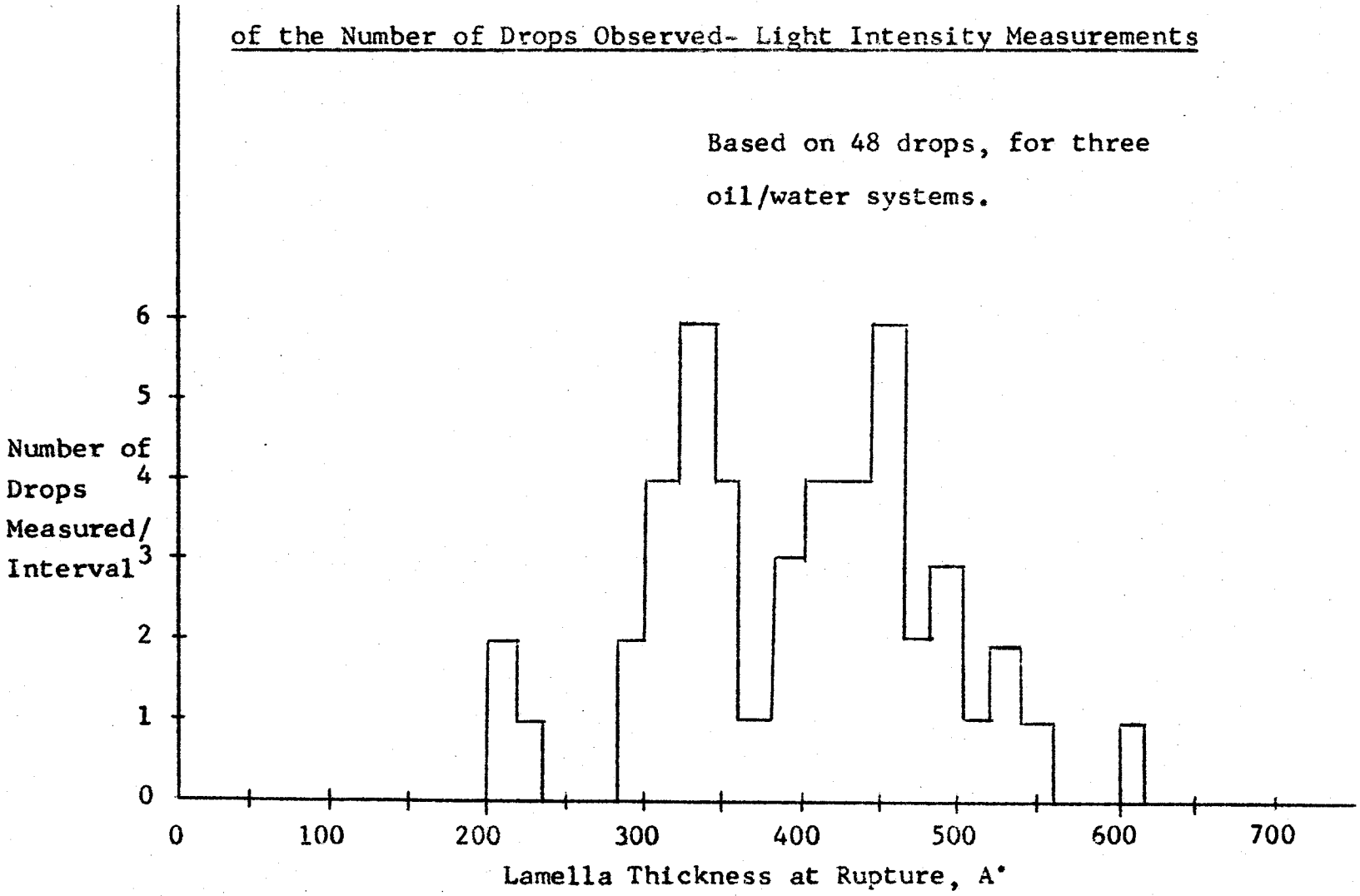

Figure 31. Experimental and Theoretical Behaviour of a Thin Lamella

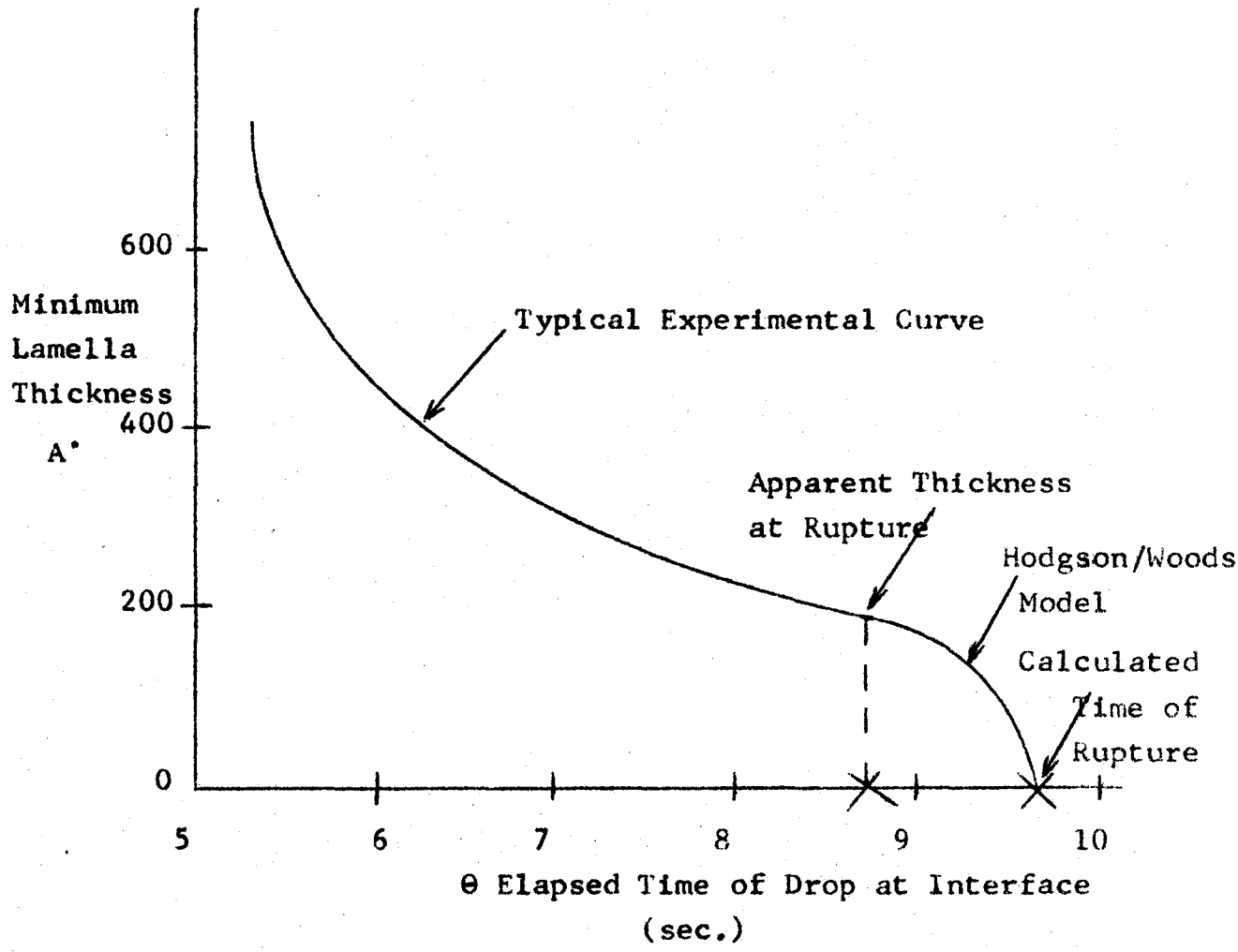

Figure 32a. Lamella Profiles for Sequential Mechanisms

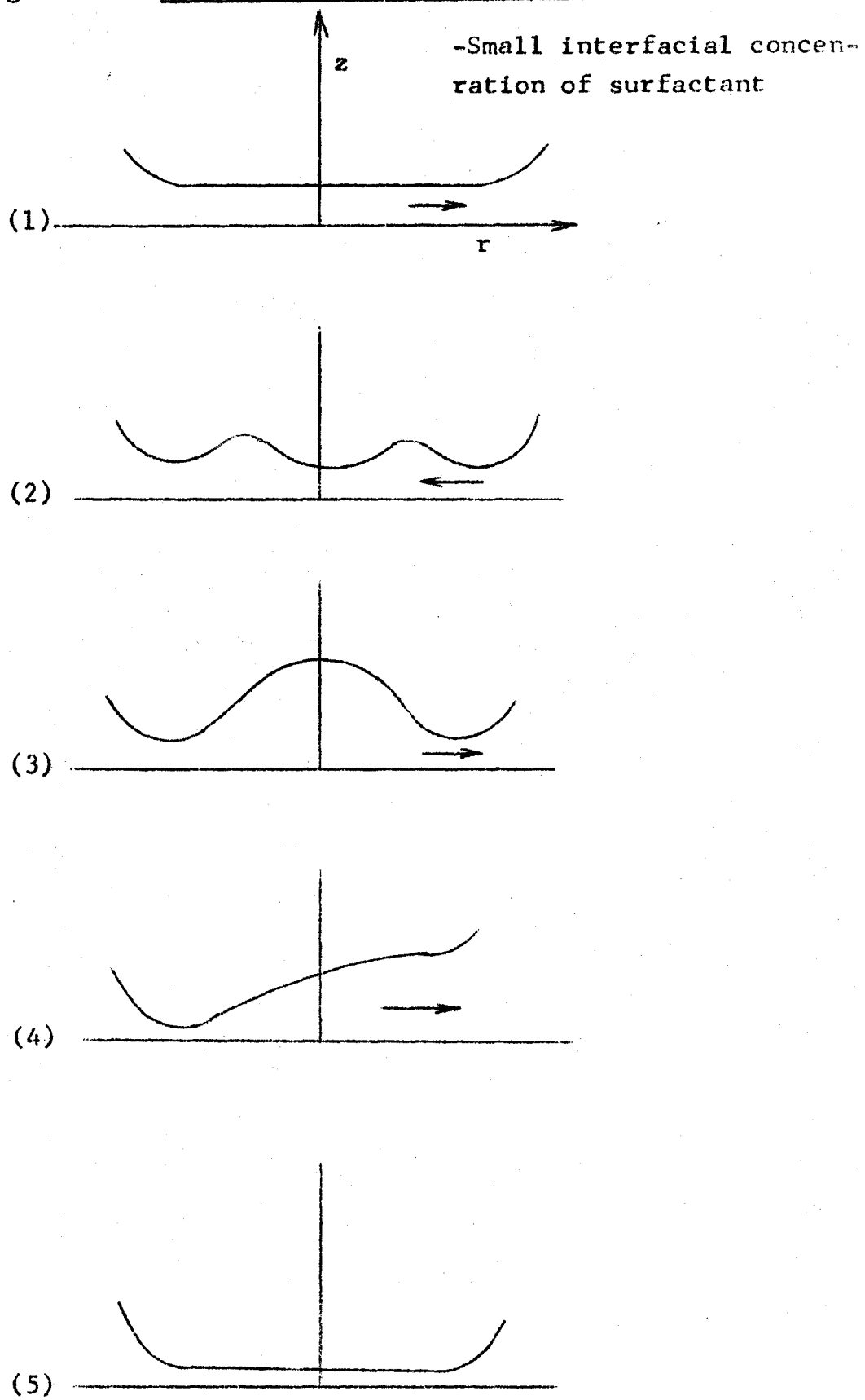

Figure 32b. Lamella Profiles for Simultaneous Mechanisms

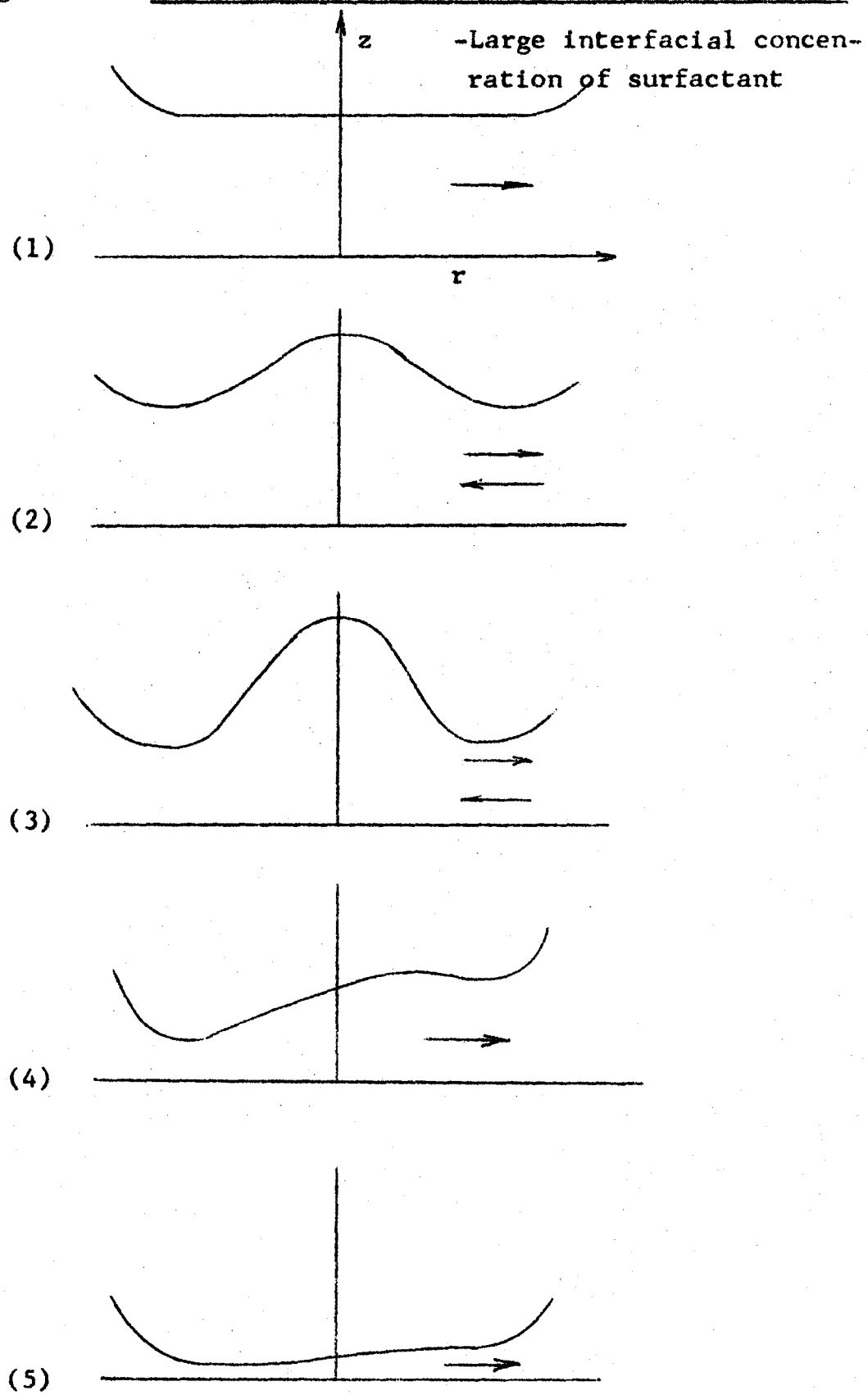

Figure 33. Lamella Behaviour for Cyclohexanol/Water System

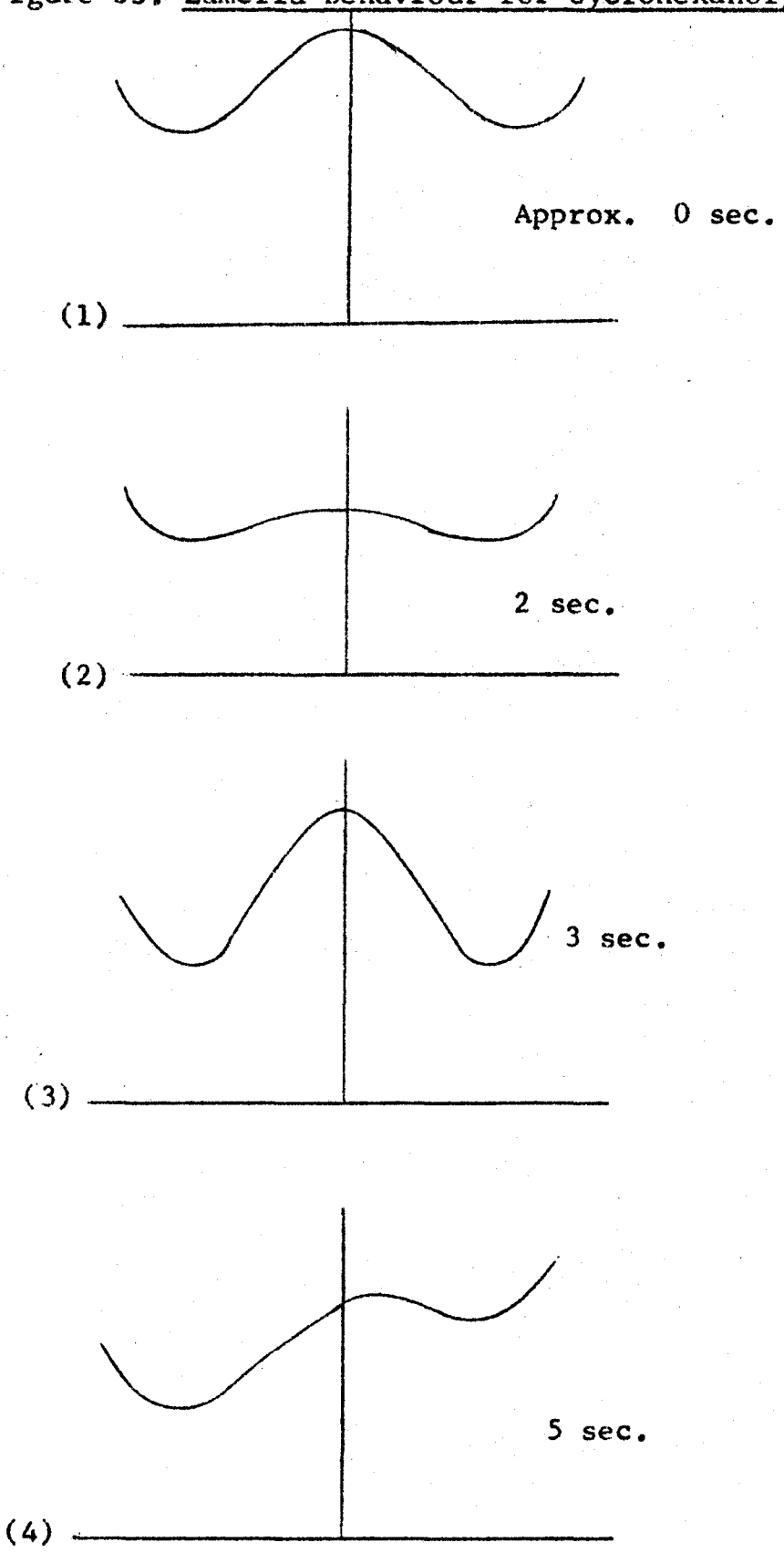

Figure 33.(continued)

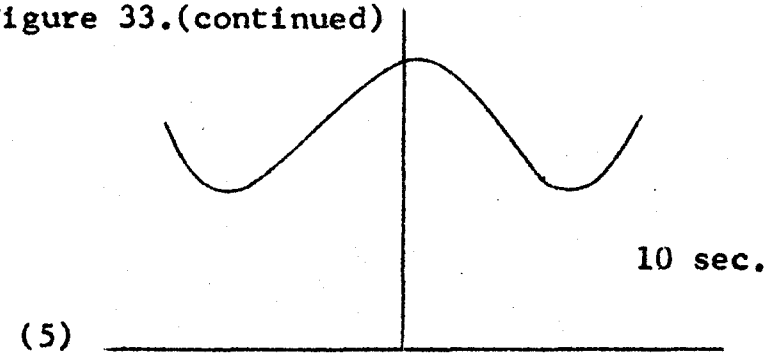

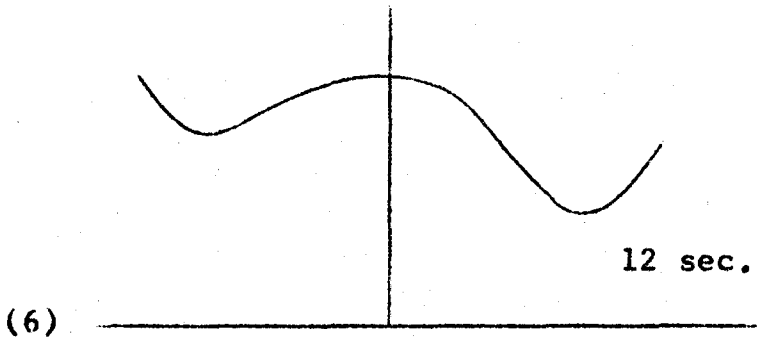

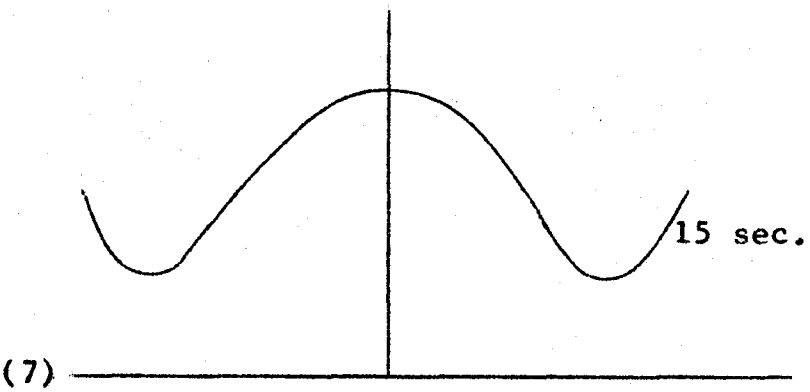

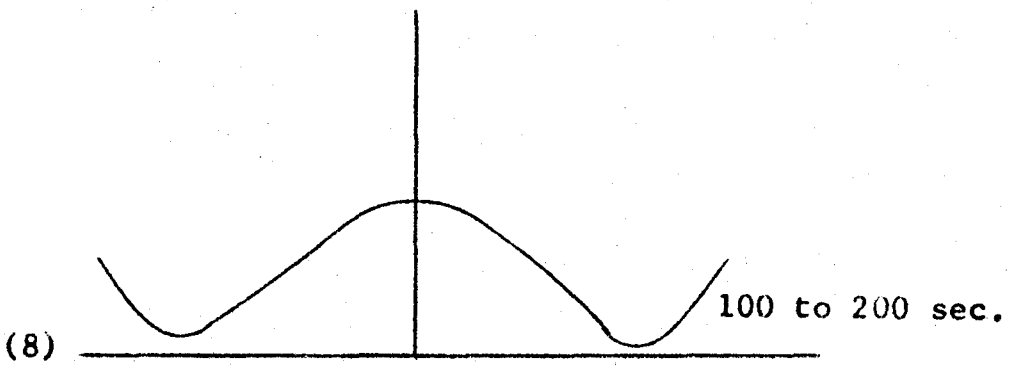

Figure 34. Comparison of Drop Rest-time Data for a 0.005 ml. Toluene Drop

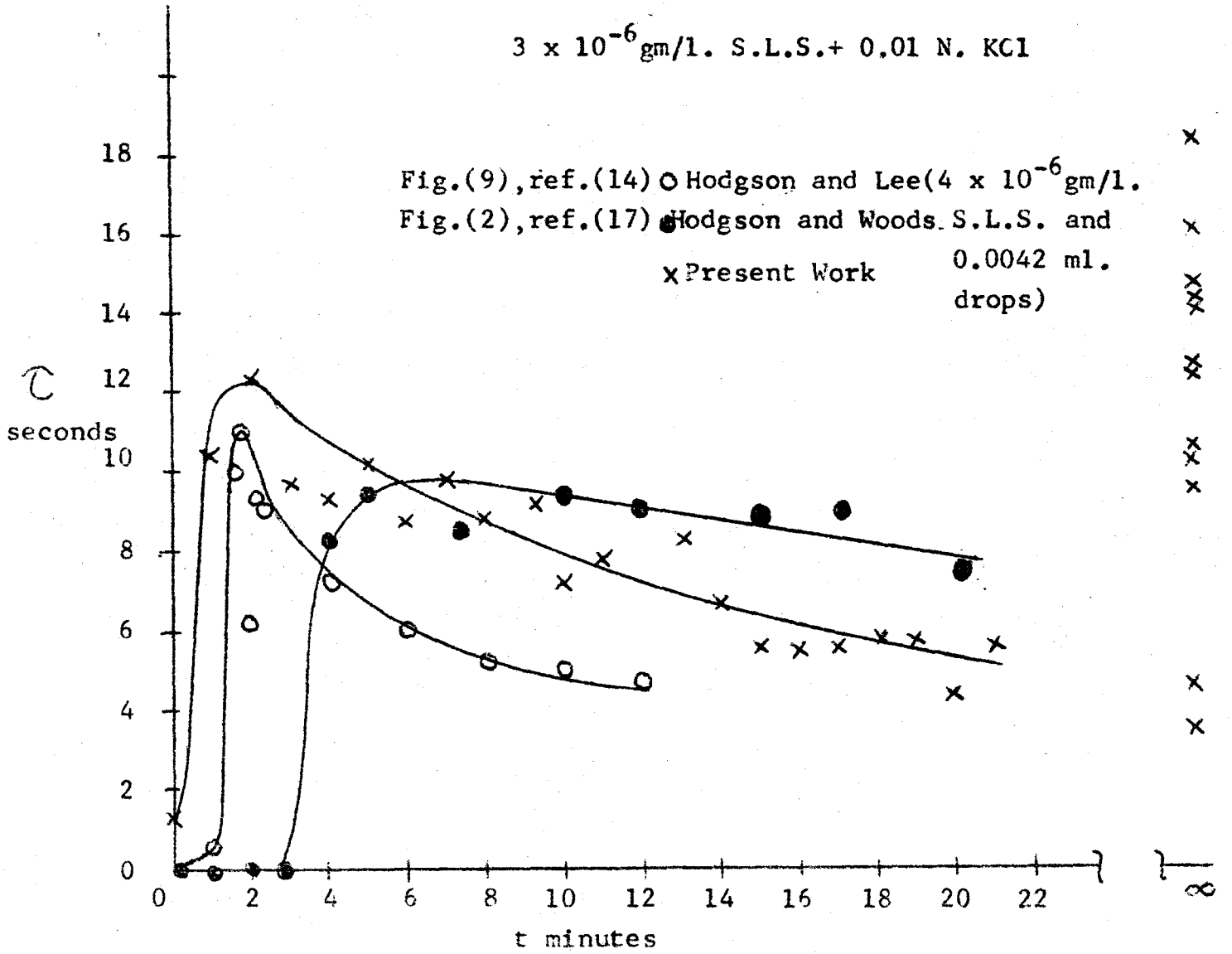

Figure 35. Drop Sliding and the Interfacial Tension Gradient in the Bulk Interface

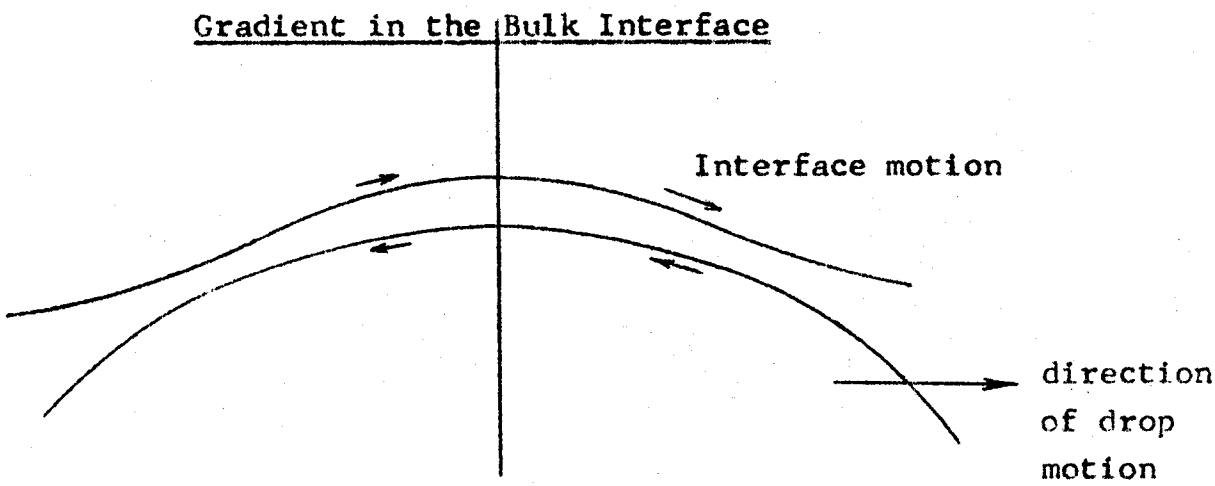

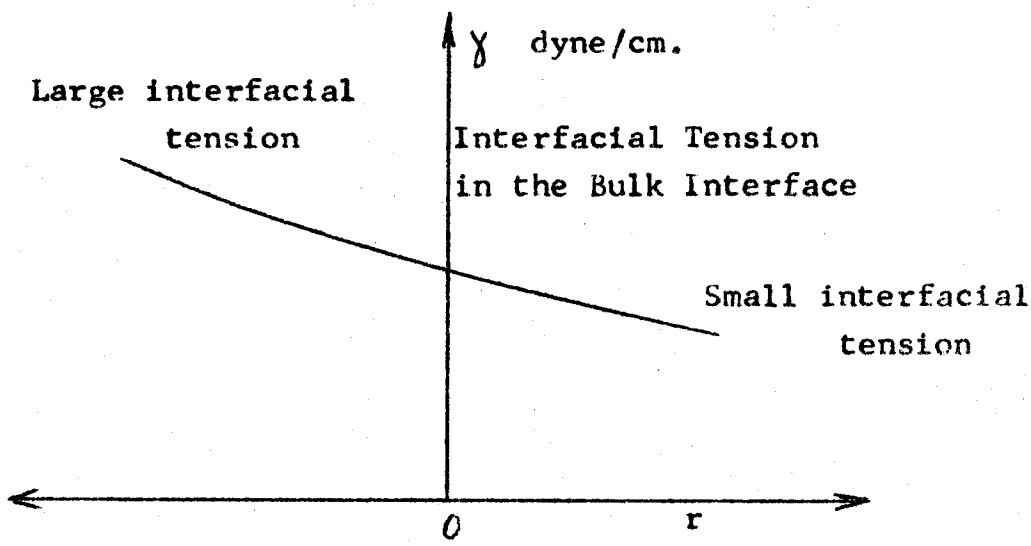

Figure 36. Scalloping at the Lamella Edge

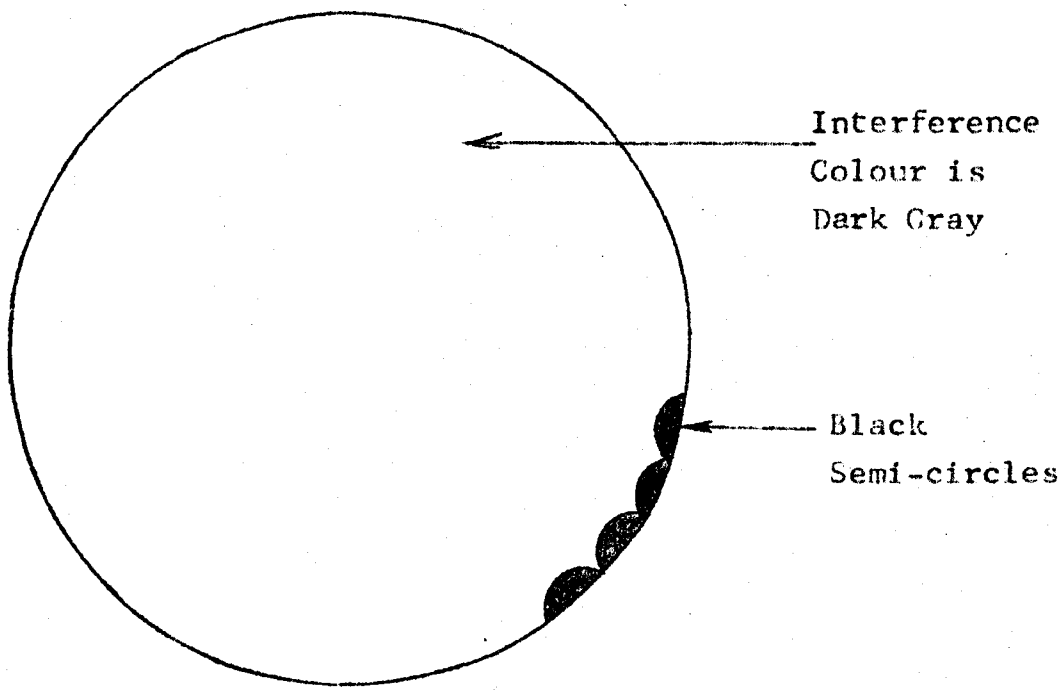

Figure 37. Local Depression in the Lamella

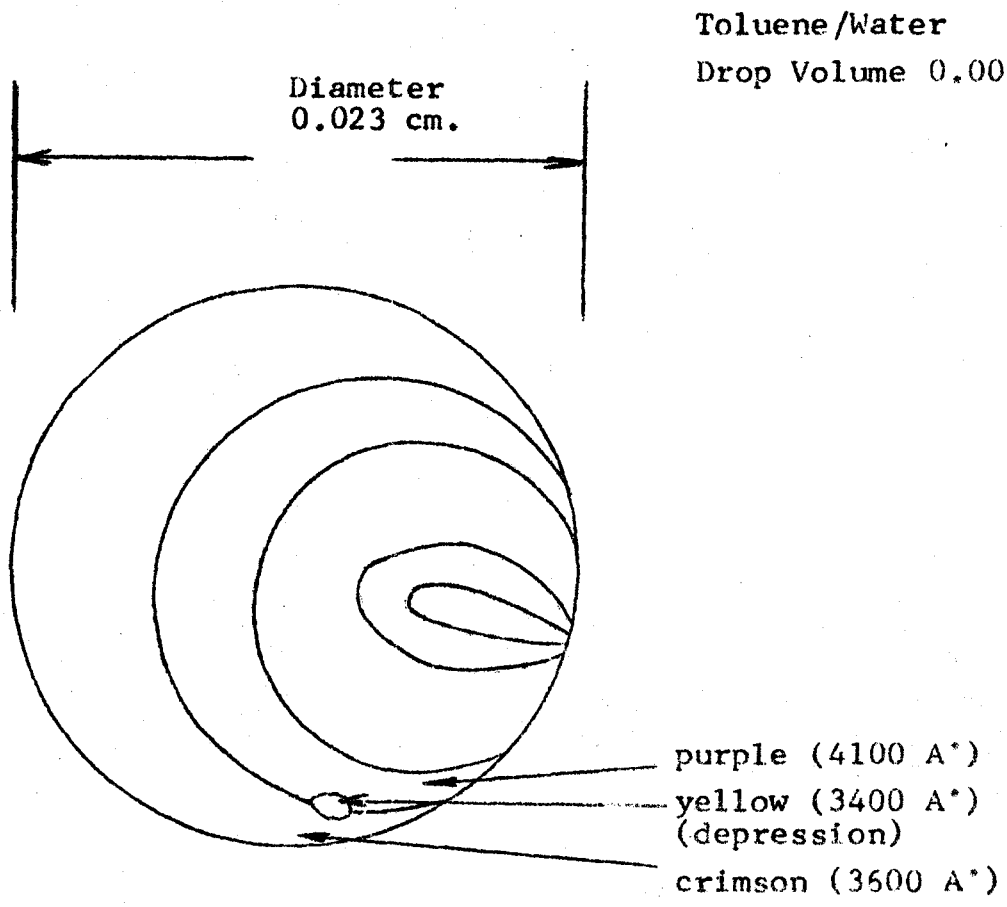

CHAPTER 4

A THEORETICAL PREDICTION OF THE RATE OF DRAINAGE OF THE LAMELLA--THE EXPONENTIAL MODEL OF LAMELLA PRESSURE

Abstract

By assuming an infinite series form for the solution of the simplified equations of motion presented in Part A of this work, general expressions are derived for the lamella dynamic pressure distribution and for lamella drainage. From these expressions, equations for the profiles of the relative lamella thickness and for the bulk interfacial distribution of adsorbed surfactant are also derived.

Solutions of the lamella drainage equation are given, with and without the coupling of the drainage equation with the mass balance equation for the surfactant in the bulk interface.

An exponential model of the dynamic pressure distribution is derived. This model, along with the parallel disc--parabolic type--dynamic pressure distribution, serve as limiting cases to the experimental dynamic pressure distribution. The exponential model also provides equations which are mathematically tractable.

The poor agreement between the solutions of the coupled equations and the experimental profiles of the relative lamella thickness show that the lateral motion of the bulk interface may be more complex than originally suspected. However, the solutions do show the expected qualitative effect of surfactant surface diffusivity on the change with time of the relative

lamella thickness profiles.

In part B of this chapter, a simple solution of the coupled equations is derived. The resulting equation may be used to show the effect of the interfacial concentration of adsorbed surfactant on the change in the lamella thickness at both the lamella center and at the barrier ring.

Part A General Theoretical Analysis of Lamella Drainage

1. Introduction

One aim of coalescence studies is the *a priori* prediction of drop rest-times for any combination of physical properties and of geometric variables. A semi-empirical method of predicting drop rest-times by restricting the lamella behaviour to even drainage has been presented in Chapter (3).

Previous investigators have primarily concentrated on the use of simple mathematical models to interpret rest-time (4) and lamella thinning data (7,13). Normally, the drop interface is considered either mobile or immobile, and the bulk interface is considered laterally rigid, but deformable. Usually the lamella thickness is assumed constant with radius (5). The motion of the bulk interface, as influenced by the balance between the interfacial tension gradient and the surface shear stress is also not considered. These restricted models only describe the lamella thinning data over a very narrow range and so are inadequate for rest-time prediction. However, these models provide insight into the drainage process, and their comparison with lamella thinning data measured by the light interference technique (7, 14, 15) can lead for example to information on the mobility conditions of the interfaces.

Reynolds' drainage model, also called the parallel disc model, is employed frequently. MacKay, Charles and Mason

(6, 7, 10) show that this model is applicable to the description of motion of the minimum lamella thickness, located at the barrier ring, over only a narrow thickness range. Many modifications have been made to the parallel disc model. Chappelear (11) evaluated the decrease in drop buoyancy force caused by bulk interface deformation, as did Princen (12). Hodgson (4) used the parallel disc model, coupled with interface motion caused by drainage, to interpret qualitatively his experimental rest-time results. Overall, the parallel disc model is a concise means of describing the barrier ring thickness variation with time, and may be used to interpret the influence of physical property variables on the change in barrier ring thickness, although over only a narrow range of thickness. From the dependence of the rate of barrier ring thickness on physical properties, the variation in drop rest-time with physical properties may be evaluated.

Another simple model for lamella drainage analyzes the slow approach of a solid sphere to a solid, horizontal, plane interface (8, 9). Drainage rates predicted from this model are generally very rapid, since the bulk interface does not deform. Figure (1) shows a comparison of this model with other models and with barrier ring thickness data for a 0.005 ml. toluene drop in water and for a 0.020 ml. anisole drop in water. This solid sphere model is not useful in rest-time prediction because drainage rates are much more rapid than observed experimentally.

Frankel and Mysels (2) derived a simple model to describe both barrier ring thickness and lamella center thickness changes with time. This model is based on the same restrictive assumptions as the parallel disc model. Platikanov (3) has used this model to describe the time change in lamella thickness at the center and at the barrier ring for thin liquid films trapped between a gas/liquid and solid/liquid interface. Again, this model was found to be useful over only a narrow range. The curves in Figure (1) show that the model coincides with the parallel disc model over the thickness range considered.

The most useful model for rest-time prediction is the Hodgson/Woods model (13). This model neglects lamella drainage from inside the barrier ring, and considers the region outside the barrier ring to be described by an infinitely long cylinder over a horizontal flat plate. Drainage is only from the lamella region outside the barrier ring, and is caused by the approach of the cylinder to the plate. Drop rest-times for the toluene/water system have been predicted to within a factor of two for even drainage, and lamella drainage at the barrier ring is well described, as shown in Figure (1). This model has some theoretical basis, as will be shown in this chapter by analysis of the general drainage equation for liquid/liquid systems.

Hartland (1, 17) has attempted to solve the more complex problem of describing the change in the entire lamella shape with time for a rigid sphere at a deformable liquid/liquid

interface. Several restrictive assumptions are made, however, and Hartland does not treat the more realistic problem of a deformable drop at a deformable liquid/liquid interface. Assumptions such as a constant bulk interface shape outside the barrier ring and zero dynamic pressure at the barrier ring have been shown by Burrill and Woods (15) to be invalid. Hartland's assumption of a spherical cap on the dimple center is an unnecessary approximation, as shown in Appendix A2.

The present work is the first to consider the problem of lamella thinning for the liquid/liquid case. This introduction has stressed rest-time prediction as the criterion to evaluate a mathematical approach, but a fundamental understanding of the fluid mechanics of flow in the lamella must first be gained. Equations which attempt to analyze this flow and the ensuing lamella behaviour will now be considered.

The pressure distribution being studied in this work is for a limiting case. The most realistic representation of the dynamic pressure distribution in the lamella requires that the pressure distribution be presented by a polynomial. Except for the prediction of a few phenomena such as barrier ring radius, this polynomial approach yields equations that are extremely complex mathematically. However, two approximations for the pressure distribution are possible: a parabolic distribution and an exponential distribution. These form the two different limiting cases of the polynomial representation. This

chapter will describe the development and analysis of the exponential form of the pressure distribution. The parabolic form corresponds to the parallel disc approximation of the relative shapes of the interfaces.

2. Basic Equations

A solution of the simplified equations of motion has been assumed. A simple exponential expression results for the lamella dynamic pressure distribution. This expression is then used to determine bulk interface surfactant distribution and relative lamella thickness.

2.1. Equation for Lamella Drainage

A detailed consideration is given to the form of the stream function which satisfies the equations of motion. The form of the stream function suggests the correct form of the pressure distribution. This permits the final form of the stream function to be determined.

2.1-1 The Equations of Motion of the Water in the Lamella

Based on the assumptions of:

(1) Pseudo steady state

(2) Axisymmetry

(3) Incompressible creeping flow

the equations of motion and the continuity equation, as given in cylindrical co-ordinates by Bird, Stewart and Lightfoot (16), become :

$$\frac{1}{\mu}\frac{\partial p}{\partial r} = \frac{\partial^2 u}{\partial r^2} + \frac{1}{r}\frac{\partial u}{\partial r} - \frac{u}{r^2} + \frac{\partial^2 u}{\partial z^2} \qquad \ldots\ldots(1)$$

$$\frac{1}{\mu}\frac{\partial p}{\partial z} = \left[\frac{\partial^2 w}{\partial r^2} + \frac{1}{r}\frac{\partial w}{\partial r}\right] + \frac{\partial^2 w}{\partial z^2} \qquad \ldots\ldots(2)$$

$$\frac{\partial u}{\partial r} + \frac{u}{r} + \frac{\partial w}{\partial z} = 0 \qquad \ldots\ldots(3)$$

By employing the stream function in cylindrical co-ordinates, the velocities may be expressed as:

$$u = \frac{1}{r}\frac{\partial \psi}{\partial z}, \quad w = -\frac{1}{r}\frac{\partial \psi}{\partial r} \qquad \ldots\ldots(4a,b)$$

and assuming: $\frac{\partial^2 w}{\partial r^2} + \frac{1}{r}\frac{\partial w}{\partial r} << \frac{\partial^2 w}{\partial z^2}$

the equations (1 - 3) become:

$$\frac{1}{\mu}\frac{\partial p}{\partial r} = \frac{1}{r}\frac{\partial^3 \psi}{\partial r^2 \partial z} - \frac{1}{r^2}\frac{\partial^2 \psi}{\partial r \partial z} + \frac{1}{r}\frac{\partial^3 \psi}{\partial z^3} \qquad \ldots\ldots(5)$$

$$\frac{1}{\mu}\frac{\partial p}{\partial z} = -\frac{1}{r}\frac{\partial^3 \psi}{\partial r \partial z^2} \qquad \ldots\ldots(6)$$

Taking the derivatives of equations (5) and (6) with respect to z and r, respectively, and subtracting the resulting two equations, yields the final expression as:

$$\frac{\partial^4 \psi}{\partial z^4} + 2\frac{\partial^4 \psi}{\partial r^2 \partial z^2} - \frac{2}{r}\frac{\partial^3 \psi}{\partial r \partial z^2} = 0 \qquad \ldots\ldots(7)$$

Figure (2) shows the geometry of the problem. The vertical scale in this figure is expanded one hundred-fold relative to the horizontal scale.

2.1-2 The Form of the Stream Function

To satisfy all the boundary conditions to be considered later, the velocity in the z-direction, w, must be a function of both r and z. By assuming different forms for w (r, z), such as an infinite series, different forms of the stream function result. A form for Ψ is sought which satisfies all the problem boundary conditions.

Assume:

$$\frac{1}{r}\frac{\partial}{\partial r}\left(r \frac{\partial w}{\partial r}\right) = \sum_{i=0}^{\infty} f_i (z)\, r^i \qquad \ldots\ldots(8)$$

where $i = 0, 2, 4, \ldots$.

The reason for only even values of i being used is discussed in Appendix A2.

2.1-3 An Approximate Form for Ψ

If only the first term in the right hand side of equation (8) is considered, then equation (8) becomes:

$$\frac{1}{r}\frac{\partial}{\partial r}\left(r \frac{\partial w}{\partial r}\right) = f (z)$$

This equation is integrated to yield:

$$w = f\frac{(z)\, r^2}{4} + b$$

where one integration constant has been set equal to zero, since w is finite at r = 0.

By using the stream function relationship, equation (4b),

Ψ is found to be:

$$\Psi(r,z) = -\frac{f(z)\, r^4}{16} - \frac{b(z)\, r^2}{2} + c(z) \qquad \ldots\ldots(9)$$

Equation (9) is substituted into equation (7) to yield:

$$-\frac{r^4}{16} f_{zzzz} - \frac{3}{2} r^2 f_{zz} + \frac{r^2}{2} f_{zz}$$

$$-\frac{r^2}{2} b_{zzzz} - 2 b_{zz} + 2 b_{zz}$$

$$+ c_{zzzz} = 0 \qquad \ldots\ldots(10)$$

The boundary conditions summarized in Table (1) may now be considered. Boundary condition (2b) results from application of L'Hopital's Rule to equation (4a) at $r = 0$.

Equation (9) will only satisfy B.C. (2a) if $c_z = 0$. Therefore c is constant and may arbitrarily be set equal to zero. In equation (10), the coefficients of the like powers in r must be zero if equation (9) is to be a solution. Then:

$$f_{zzzz} = 0 \qquad \ldots\ldots(11a)$$

$$2f_{zz} + b_{zzzz} = 0 \qquad \ldots\ldots(11b)$$

These equations are integrated to yield:

$$f(z) = \frac{a'z^3}{6} + \frac{b'z^2}{2} + c'z + d' \qquad \ldots\ldots(12a)$$

$$b(z) = -\frac{2a'z^5}{120} - \frac{2b'z^4}{24} + \frac{e'z^3}{6} + \frac{g'z^2}{2} + h'z + j' \qquad \ldots\ldots(12b)$$

Substitution of equation (12a,b) into equation (9) and the application of the boundary conditions (1 - 3) indicates:

$$c' = h' = 0 \quad \text{for B.C. (1)}$$

B.C. (2) is satisfied

and $d' = j' = 0$ for B.C. (3). Therefore, the solution for Ψ may be written:

$$\Psi(r,z) = \frac{-r^4}{16}\left(\frac{a'z^3}{6} + \frac{b'z^2}{2}\right) \frac{-r^2}{2}\left(\frac{-2a'z^5}{120} \frac{-2b'z^4}{24} + \frac{e'z^3}{6} + \frac{g'z^2}{2}\right) \qquad \text{.....(13)}$$

If one more term in the infinite series of equation (8) is considered, then equation (8) becomes:

$$\frac{1}{r}\frac{\partial}{\partial r}\left(r\,\frac{\partial w}{\partial r}\right) = f(z) + q(z)\,r^2$$

where $q(z) = f_2(z)$

The resultant form of Ψ is:

$$\Psi(r,z) = \frac{-r^6}{96}\left(\frac{a'z^3}{6} + \frac{b'z^2}{2}\right) \frac{-r^4}{16}\left(\frac{-a'z^5}{15} - \frac{b'z^4}{3} + \frac{e'z^3}{6} + \frac{g'z^2}{2}\right) \frac{-r^2}{2}\left(\frac{-a'z^7}{315} - \frac{b'z^6}{45} - \frac{e'z^5}{60} - \frac{g'z^4}{12} + \frac{m'z^3}{6} + \frac{l'z^2}{2}\right) \qquad \text{.....(14)}$$

where the primed constants of equation (14) are, in general, different in value from the primed constants of equation (13). If more terms in the infinite series of equation (8) are retained, then longer expressions for $\Psi(r,z)$ result.

An examination of the magnitudes of the coefficients in equations (13) and (14), as given in Appendix A2, shows that only terms in z^2 and z^3 predominate, therefore, equation (14) is reduced to:

$$\Psi(r,z) \doteq -\frac{r^6}{96}\left(\frac{a'z^3}{6} + \frac{b'z^2}{2}\right) - \frac{r^4}{16}\left(\frac{e'z^3}{6} + \frac{g'z^2}{2}\right) - \frac{r^2}{2}\left(\frac{m'z^3}{6} + \frac{l'z^2}{2}\right) \qquad \ldots\ldots(15)$$

Since an approximate form for $\Psi(r,z)$ is now known, the lamella pressure distribution can be evaluated.

2.1-4 Lamella Pressure Distribution

Another approximation can be made. Equation (5) can be represented by:

$$\frac{1}{\mu}\frac{\partial p}{\partial r} \doteq \frac{1}{r}\Psi_{zzz} \qquad \ldots\ldots(16)$$

If two more terms in the infinite series for Ψ in equation (8) are taken and equation (16) is evaluated, the result is:

$$\frac{1}{\mu}\frac{\partial p}{\partial r} \doteq -\frac{k'}{2}r - \frac{e'}{16}r^3 - \frac{a'}{96}r^5 - \frac{\varsigma}{288}r^7 - \frac{\eta}{640}r^9 - \ldots \qquad \ldots\ldots(17)$$

If this equation is integrated, and $p = p_o$ when $r = 0$, the

result is:

$$\frac{p}{\mu} = \frac{p_o}{\mu} + \frac{a_1 r^2}{4} + \frac{a_2 r^4}{64} + \frac{a_3 r^6}{576} + \frac{a_4 r^8}{2304} + \frac{a_5 r^{10}}{6400} + \ldots \qquad \ldots\ldots(18)$$

where the individual constants in (17) are represented by the array of constants a_i. This is the form of polynomial pressure distribution described in Appendix A2. The a_i for an infinite series were found to be:

$$a_o = p_o / \mu$$

$$a_1 = -4 \left(\frac{\mu \Pi a_o}{Wg} \right) a_o$$

$$a_2 = 32 \left(\frac{\mu \Pi a_o}{Wg} \right)^2 a_o$$

$$a_3 = -96 \left(\frac{\mu \Pi a_o}{Wg} \right)^3 a_o$$

$$a_4 = 96 \left(\frac{\mu \Pi a_o}{Wg} \right)^4 a_o$$

$$a_5 = \frac{-160}{3} \left(\frac{\mu \Pi a_o}{Wg} \right)^5 a_o$$

$$\vdots$$

The a_i are substituted into equation (18) and if:

$$x = \left(\frac{\mu \Pi a_o}{Wg} \right) r^2 = \lambda r^2,$$

then: $\frac{p}{\mu} = a_o \left(1 - x + \frac{x^2}{2!} - \frac{x^3}{3!} + \frac{x^4}{4!} - \cdots \right)$

This series is simply e^{-x}. Therefore, the lamella pressure distribution is:

$$p = p_o e^{-x} \qquad \text{.....(19)}$$

Figure (3a) shows a typical estimation of p as a function of r for a 0.005 ml. toluene drop in water, with p_o = 350 dynes/cm^2., based on Equation (19). For comparison purposes, the calculated polynomial and parabolic type pressure distributions are also given for the same center lamella pressure.

2.1-5 The Lamella Drainage Equation and the Stream Function

For an infinite series type solution for $\Psi(r,z)$, the form of the stream function can be approximated as:

$$\Psi(r,z) \doteq - \frac{z^3}{6} F(r) - \frac{z^2}{2} G(r) \qquad \text{.....(20)}$$

Since,

$$\frac{1}{\mu} \frac{\partial p}{\partial r} = - \frac{2}{\mu} \lambda p_o r e^{-\lambda r^2}$$

equation (16) is used to find:

$$\frac{-2 \lambda p_o r e^{-\lambda r^2}}{\mu} = \frac{-1}{r} F(r)$$

$$F(r) = \beta r^2 e^{-\lambda r^2} \qquad \text{.....(21)}$$

where $\beta = \frac{2 \lambda p_o}{\mu}$.

The fourth boundary condition may now be applied. If boundary condition (4a) is used in equation (20), the result is:

$$-\frac{y^2}{2} F(r) - y\, G(r) = 0$$

$$G(r) = -\frac{y}{2} F(r)$$

and similarly, if boundary condition (4b) is used:

$$G(r) = -\, y\, F(r)$$

The stream function for both cases is therefore:

$$\psi = -\frac{z^2}{2} F(r) \left(\frac{z}{3} - \frac{y}{m} \right) \qquad \ldots\ldots(22)$$

where m is the number of immobile interfaces. Equation (22) does not satisfy equation (7) because of the two approximations that have been made.

To find the z-direction velocity w of one interface relative to the other, w at z = y is required.

Since $w = \frac{-1}{r} \frac{\partial \psi}{\partial r}$, equation (22) is used to yield:

$$w\Big|_{z=y} = \frac{\partial y}{\partial \theta} = \frac{1}{6m} y^2 \beta e^{-\lambda r^2} \left(-2(3-m)y + 2(3-m) \lambda r^2 y - 3r \frac{\partial y}{\partial r} \right) \qquad \ldots\ldots(23)$$

This equation describes the change in relative lamella shape with time. A much simpler derivation is given in Appendix A2. Before equation (23) can be used, however, an expression must be found for the relative lamella shape, y, as a function of the lamella pressure.

2.1-6 Relative Lamella Shape

The interface geometry is shown in Figure (4). By using the same approximations for the radii of curvature as in a previous paper (15), a force balance may be made at any radial distance r. If p is the dynamic lamella pressure at any radius and if hydrostatic pressure is neglected, then:

$$p = -\gamma\left(\frac{d^2k}{dr^2} + \frac{1}{r}\frac{dk}{dr}\right) \qquad \text{.....(24a)}$$

and

$$p = \frac{2\gamma}{d} + \gamma\left(\frac{d^2h}{dr^2} + \frac{1}{r}\frac{dh}{dr}\right) \qquad \text{.....(24b)}$$

Since $h = k - y$, then:

$$\frac{dh}{dr} = \frac{dk}{dr} - \frac{dy}{dr}$$

and

$$\frac{d^2h}{dr^2} = \frac{d^2k}{dr^2} - \frac{d^2y}{dr^2} .$$

If these expressions for the derivatives of h are substituted into equation (24b) and the result is equated to equation (24a), the result is:

$$\gamma\left(\frac{d^2k}{dr^2} + \frac{1}{r}\frac{dk}{dr}\right) = -\frac{\gamma}{d} + \frac{\gamma}{2}\left(\frac{d^2y}{dr^2} + \frac{1}{r}\frac{dy}{dr}\right) \qquad \text{.....(25)}$$

Since the L.H.S. of equation (25) is equal to -p, then:

$$\frac{d^2y}{dr^2} + \frac{1}{r}\frac{dy}{dr} - \frac{2}{d} = -\frac{2}{\gamma}p \qquad \text{.....(26)}$$

Equation (26) expresses the relative lamella thickness as a function of lamella pressure for a liquid drop at a deformable liquid/liquid interface, subject to the simplifying assumption of $(\frac{dy}{dr})^2$ much less than unity. If equation (19) is substituted into equation (26) and the result is integrated twice, the desired expression results:

$$y = y_o + \left(\frac{1}{2d} - \frac{P_o}{2\gamma} \right) r^2 + \frac{P_o}{2\lambda\gamma} \left(\frac{\lambda^2 r^4}{2.2!} - \frac{\lambda^3 r^6}{3.3!} + \cdots \right) \quad \ldots\ldots(27)$$

The boundary conditions: y is finite at r = 0 and $y = y_o$ at r = 0 were used to evaluate the two integration constants.

2.2. Bulk Interface Mass Balance

Equation (23) was derived by assuming that the bulk interface velocity was zero. However, as discussed in Chapter (3), this cannot be the case for a liquid/liquid interface, even one which contain adsorbed surfactant. As lamella drainage proceeds, the shear stress that the flowing lamella liquid exerts on the bulk interface will change with the change in lamella shape. If it is assumed that the bulk interface has the adsorbed surfactant distributed such that the bulk interface interfacial tension gradient everywhere balances the surface shear stress exerted on the bulk interface, then any change in the surface shear stress must be accompanied by a redistribution of surfactant in the bulk interface. This redistribution of surfactant is caused by surface diffusion, bulk interface

movement, and by adsorption/desorption of surfactant.

Hodgson (4) has previously derived an expression for the surfactant mass balance, but the mass balance is presented here for completeness.

The geometry is given in Figure (5). The interface surfactant concentration at radius r is Γ, U is surface velocity, and $\mathcal{D}_s$ is the surface diffusion coefficient of the surfactant. A surfactant mass balance on the elemental ring of Figure (5) has the following components:

$$\text{Surfactant into the ring} = 2\pi r \left(U\Gamma - \mathcal{D}_s \frac{\partial \Gamma}{\partial r} \right)$$

$$\text{Surfactant out of the ring} = 2\pi (r + \Delta_r) \left(\left(U + \frac{\partial U}{\partial r} \Delta_r \right) \cdot \left(\Gamma + \frac{\partial \Gamma}{\partial r} \Delta_r \right) - \mathcal{D}_s \left(\frac{\partial \Gamma}{\partial r} + \frac{\partial^2 \Gamma}{\partial r^2} \Delta_r \right) \right)$$

$$\text{Surfactant accumulation} = 2\pi r \, \Delta_r \frac{\partial \Gamma}{\partial t}$$

The resultant equation is:

$$U \frac{\partial \Gamma}{\partial r} + \Gamma \frac{\partial U}{\partial r} + \frac{U\Gamma}{r} - \mathcal{D}_s \left(\frac{\partial^2 \Gamma}{\partial r^2} + \frac{1}{r} \frac{\partial \Gamma}{\partial r} \right) = - \frac{\partial \Gamma}{\partial \theta} \quad \ldots\ldots (28)$$

Equation (28) neglects the adsorption/desorption of surfactant during the short time thedrop is at the bulk interface. This will be discussed in a later section.

An expression is now needed to couple equation (28) with the flow of water in the lamella. This coupling equation will result when the bulk interface interfacial tension gradient

is equated to the surface shear stress exerted on the bulk interface by the flowing lamella liquid.

Therefore:

$$\frac{\partial \gamma}{\partial r} = \text{shear stress} = -\mu \left.\frac{\partial u}{\partial z}\right|_{z=0}$$

Since:

$$\left.\frac{\partial u}{\partial z}\right|_{z=0} = \frac{1}{r}\ \Psi_{zz} = \frac{yF(r)}{m}$$

and,

$$\frac{1}{\mu}\ \frac{\partial p}{\partial r} \doteq \frac{-F(r)}{r}$$

then:

$$\frac{\partial \gamma}{\partial r} = \frac{y}{m}\frac{\partial p}{\partial r} \qquad \ldots\ldots(29)$$

For very small interfacial concentrations of surfactant, a linear interfacial concentration--interfacial tension isotherm is assumed. The isotherm is:

$$\gamma = \gamma_o - k'\Gamma \qquad \ldots\ldots(30)$$

where γ_o is the interfacial tension of the pure system and k' is a constant. The final form of the coupling equation results by substituting equation (30) into (29) to yield:

$$\frac{\partial \Gamma}{\partial r} = -\frac{y}{mk'}\frac{\partial p}{\partial r} \qquad \ldots\ldots(31)$$

Since boundary condition (1b) in Table (1) is now $u = U$ at $z = 0$, equation (23) must be modified. The stream function must be of the form:

$$\Psi(r,z) = \frac{-z^3}{6}F(r) - \frac{z^2}{2}G(r) - zH(r)$$

and since $H(r) = -r\bar{U}$ and $G(r) = -y\,F(r)$, the lamella drainage expression for a mobile drop interface becomes:

$$\frac{\partial y}{\partial \theta} = y^2 \beta\, e^{-\lambda r^2}\left(-\frac{2}{3}\, y + \frac{2}{3}\, y\, \lambda\, r^2 - \frac{r}{2}\frac{\partial y}{\partial r}\right) - y\frac{U}{r} - y\frac{\partial U}{\partial r} \qquad \text{.....(32a)}$$

If the drop interface is immobile $H(r) = -r\,U$, but now B.C. (4a) requires:

$$-y\frac{2}{2}\; F(r) - y\, G(r) + r\, U = 0$$

Therefore, the lamella drainage expression for an immobile drop interface becomes:

$$\frac{\partial y}{\partial \theta} = y^2 \beta\, e^{-\lambda r^2}\left(-\frac{y}{6} + \frac{y}{6}\lambda\, r^2 - \frac{r}{4}\frac{\partial y}{\partial r}\right) - \frac{y}{2}\frac{\partial U}{\partial r} - \frac{y}{2}\frac{U}{r} - \frac{U}{2}\frac{\partial y}{\partial r} \qquad \text{.....(32b)}$$

Equations (28), (31) and (32) may now be solved simultaneously to yield the change in lamella shape with time. These equations should describe the behaviour of the lamella for axisymmetric drainage, subject to the assumptions made.

2.3. Bulk Interface Surfactant Distribution

The distribution of surfactant in the bulk interface can be calculated from equation (31). If $\frac{\partial p}{\partial r}$ and y are substituted into equation (31), the result is:

$$\frac{\partial \Gamma}{\partial r} = \frac{\beta \mu\, e^{-\lambda r^2}}{k' m}\left(y_o r + a r^3 + b r^5 + c r^7 + \ldots \right)$$

where $$a = \left(\frac{1}{d} - \frac{P_o}{\gamma}\right)\frac{1}{2}$$

$$b = \frac{P_o}{2\lambda\gamma} \cdot \frac{\lambda^2}{2.2!}$$

$$c = \frac{-P_o}{2\lambda\gamma} \cdot \frac{\lambda^3}{3.3!}$$

The values of a, b, and c were evaluated from equation (27). By integrating over r and letting $\Gamma \rightarrow \Gamma_t$ as $r \rightarrow \infty$, the result is:

$$\Gamma - \Gamma_t = \frac{\beta\mu}{mk'}\left(\frac{-y_o}{2\lambda} - \frac{a}{2\lambda^2} - \frac{ar^2}{2\lambda}\right)e^{-\lambda r^2}$$

$$+ \frac{\beta\mu}{mk'}\left(\frac{-b}{\lambda}\ \frac{-3c}{\lambda^2} - \cdots\right)\frac{e^{-\lambda r^2}}{\lambda^2}$$

$$+ \frac{\beta\mu}{mk'}\left(\frac{-b}{\lambda^2} - \frac{3c}{\lambda^3} - \cdots\right)r^2 e^{-\lambda r^2}$$

$$+ \cdots \qquad \ldots\ldots(33)$$

Equation (33) is an infinite series whose terms are each infinite series. This equation is too awkward to use to find Γ as a function of r but may be used to find Γ at r = 0. The first series in equation (33) may be written as:

$$-\frac{\beta\mu}{mk'}e^{-\lambda r^2}\left(\frac{c_3}{\lambda^3} + \frac{3c_4}{\lambda^4} + \cdots + \frac{c_n(n-1)!}{2\lambda^n} + \cdots\right)$$

where $c_3 = b$

$c_4 = c$

$\cdots$

Since $c_n = \frac{P_o}{2\lambda\gamma} \cdot \frac{\lambda^{n-1}}{(n-1)(n-1)!}$, the series at r = 0 becomes:

$$-\frac{\beta\mu}{mk'} \cdot \frac{P_o}{4\lambda^2\gamma}\left(\frac{1}{2} - \frac{1}{3} + \frac{1}{4} - \ldots \frac{(-1)^{n-1}}{(n-1)} + \ldots\right)$$

which also equals:

$$-\frac{\beta\mu P_o}{mk' 4\lambda^2\gamma} + \frac{\beta\mu P_o}{mk' 4\lambda^2\gamma}\left(1 - \frac{1}{2} + \frac{1}{3} - \ldots\right)$$

The bracketed series is shown in Appendix A2 to converge and equal ln (1+j) with j = 1. If the values of β and λ are expressed in terms of system physical properties, the result is:

$$\Gamma_o = \Gamma_{r=0} = \Gamma_t - \frac{P_o y_o}{mk'} + P_o \frac{0.346Wg}{\pi mk'\gamma} - \frac{Wg}{2\pi mk' d} \qquad \ldots\ldots(34)$$

The probable distribution of interfacial surfactant, as discussed in Chapter (3), is compared with the approach given in this chapter in Figure (6). Equation (34) is expected to underestimate Γ_o because of the difference between the actual distribution of interfacial surfactant and the theoretical distribution.

3. Solution of the Equations

Two cases may be solved. In the first case, the drop may approach a deformable liquid/liquid interface which is laterally rigid. Therefore, the boundary condition on the bulk interface is that U is zero. For the second case, the bulk interface is allowed to move when the surface shear stress

exerted on it changes. For this case, the lamella thinning equation is coupled with the bulk interface mass balance, and the two equations are solved simultaneously. Both cases are considered in turn. Program listings are given in Appendix A2.

3.1. A Laterally Rigid Bulk Interface

Equation (23) was solved numerically on a C.D.C. 6400 digital computer. The starting relative lamella thickness profile was calculated from equation (27) by specifying p_o and y_o for a given set of physical properties. An experimental lamella profile was not used as a starting shape because the pressure distribution used in equation (23) will not describe the experimental lamella pressure distribution, as shown by the comparison given in Figure (3a).

A finite difference formula, using central differences and correct to the second order, was used to estimate $\frac{\partial y}{\partial r}$. The maximum radial distance over which the problem was solved was arbitrarily specified by calculating R for a three term, series type, pressure polynomial. This value of R is an estimate of the radius where the lamella pressure is zero. The formula for R was:

$$R^2 = \frac{3W_g}{\pi p_o}$$

Convergent, stable solutions were obtained by dividing the maximum radial distance, specified by R, into N equal-sized

intervals (N = 200) and by using a time interval of 10^{-4} seconds. If the physical properties in the program were changed to calculate solutions for a new oil/water system, the radial distance increments may become large enough to give an unstable result. This instability is caused by R becoming too large, hence R^2 was often reduced to 50-75% of the value given in the above equation. At the last point in the radial array, point N+1, the slope $\frac{\partial y}{\partial r}$ was estimated by using a Taylor series expansion about the second last point, N. The physical properties of the four oil/water systems studied are given in Table (2).

While only a viscous oil would produce an almost laterally-rigid bulk interface, solutions were found for all four of the oil/water systems studied. This was done because the motion of the bulk interface may be very slight.

Two sets of results are given in Figures (7a,b) for the toluene/water system for m = 1 and m = 2, respectively. One set of results for the anisole/water system is given in Figure (7c) for m = 1, and one set is given in Figure (7d) for m = 2 for the cyclohexanol/water system. All the solutions show a deflation of the dimple in the lamella. If the drop interface is assumed immobile, m = 2, the rate of deflation decreases. This situation of dimple deflation has only been observed experimentally in this work for the cyclohexanol/water system. However, a comparison of Figure (7d) with the observed deflation shown in Figure (11c) shows that deflation is much slower than predicted by the theory presented in this

chapter.

3.2. Liquid Drop Approaching a Mobile Bulk Interface

Equations (28), (31) and (32) were solved numerically when the bulk interface was partially mobile. The method of solution was the same as previous, except that an iterative loop entered the program. Since the initial surface velocity distribution U is not known, it is first assumed everywhere zero. The distribution of the interfacial surfactant concentration is calculated using equations (31) and (34), for the initial lamella shape. The change in lamella shape is calculated over the first time interval $\Delta\theta$, and the change in the interfacial surfactant distribution is calculated, assuming that the interfacial surfactant concentration at the N+1 point remains constant. Equation (28) may then be used to estimate the surface velocity U. These values for U are used in re-evaluating the change in lamella shape in equation (32). This process continued until the successive change in $\frac{\partial y}{\partial \theta}$ at $r = 0$ was less than 1% of the previous value. Convergence was rapid, with less than six iterations being required.

A difficulty was encountered in the selection of a value for $\mathcal{D}_s$, the surface diffusion coefficient of sodium lauryl sulfate. Sakata and Berg (18) measured $\mathcal{D}_s$ for myristic acid monolayers at an air/water interface and found $\mathcal{D}_s$ values of 10^{-4} to 10^{-5} $cm^2/sec.$, dependent on the interfacial

concentration of surfactant. These authors' experimental conditions are different from those in this work; however, $\mathcal{D}_s$ values of 10^{-3} to 10^{-5} $cm^2/sec.$ will be used to characterize the sodium lauryl sulfate.

A difficulty was encountered at the dimple center, $r = 0$. The surfactant mass balance yields $\frac{\partial \Gamma}{\partial \theta}\Big|_{r=0} = 0$ because U and $\frac{\partial U}{\partial r}$ are both zero at $r = 0$. This problem was artifically solved by assuming $\frac{\partial U}{\partial r} \neq 0$ at $r = 0$. Therefore, $\frac{\partial U}{\partial r} = \frac{U_r}{\Delta} = \Delta$. The lamella liquid probably forces the dimple center up as inward flow occurs, and as surfactant flows into the $r = 0$ region by surface diffusion. The lamella light interference pattern for small interface ages often showed the barrier ring and lamella center to have the same thickness; the maximum thickness then occurred approximately half way between them. At larger interface ages, this behaviour was not observed since dimple formation was rapid.

Figures (8a, b, c, d) show typical calculated lamella behaviour for the anisole/water system for various $\mathcal{D}_s$ values and interfacial surfactant concentrations. The interfacial surfactant concentration at $r \longrightarrow \infty$ is denoted by Γ_t, and was chosen so that Γ_o was not negative.

Figures (9) and (10) show the calculated radial distribution of the interfacial surfactant concentration and the bulk interface radial velocity, respectively, for the anisole/water system, for the initial lamella shape given in Figure (8).

There is a maximum in the velocity of contraction of the bulk interface for the curve in Figure (10).

4. Discussion

The assumptions needed to derive the necessary equations will be discussed first. Then the results of the solutions of the equations will be examined.

4.1. Discussion of Assumptions

The assumptions used to simplify the equations of motion, and the assumptions used in deriving the final equations are discussed separately.

4.1-1 Assumptions in the Solution of the Equations of Motion

The pseudo-steady state assumption eliminates the time dependence of the velocities. For example, this assumption is valid if the time acceleration term, $\frac{\partial u}{\partial t}$, has a magnitude much less than the viscous terms in the equation of motion for the r-direction. Since the analytical solution for the lamella velocities does not contain time, the pseudo-steady state assumption can only be checked by doing calculations on the data produced by the problem solution. The results of calculations given in Appendix A2 show that the magnitude of ratio of the time acceleration term to the viscous term, $\frac{\partial^2 u}{\partial z^2}$, is approximately 10^{-6}, and for the z-direction, this ratio is about 10^{-4}. Since these ratios are much less than unity, the

pseudo-steady state assumption is valid.

Imcompressible creeping flow may be assumed when the lamella fluid is incompressible (in this case, water) and when the ratio of the convective acceleration terms to the viscous terms is small. The results of calculations of Appendix A2 show that:

$$N_{RE_r} = \frac{\rho\left(u\frac{\partial u}{\partial r} + w\frac{\partial u}{\partial z}\right)}{\mu\frac{\partial^2 u}{\partial z^2}} = \frac{0(10^{-4})}{0(10^{3})} = 0(10^{-7})$$

and

$$N_{RE_z} = \frac{\rho\left(u\frac{\partial w}{\partial r} + w\frac{\partial w}{\partial z}\right)}{\mu\frac{\partial^2 w}{\partial z^2}} = \frac{0(10^{-6})}{0(10^{1})} = 0(10^{-7})$$

The results of calculations in Appendix A2 also show that:

$$\frac{\partial^2 w}{\partial r^2} + \frac{1}{r}\frac{\partial w}{\partial r} = 0(10^{-1})$$

and

$$\frac{\partial^2 w}{\partial z^2} = 0(10^{3})$$

and also:

$$\frac{\partial^2 u}{\partial r^2} + \frac{1}{r}\frac{\partial u}{\partial r} - \frac{u}{r^2} = 0(10^{1})$$

$$\frac{\partial^2 u}{\partial z^2} = 0(10^{5})$$

therefore,

$$\text{r-direction viscous terms} \doteqdot \mu \frac{\partial^2 u}{\partial z^2}$$

$$\text{z-direction viscous terms} \doteqdot \mu \frac{\partial^2 w}{\partial z^2}$$

A final assumption used in deriving the lamella shape is that $\frac{\partial p}{\partial z}$ is much less than $\frac{\partial p}{\partial r}$. By using the above order of magnitudes, it is found that:

$$\frac{\partial p}{\partial r} = 0(10^3)$$

and

$$\frac{\partial p}{\partial z} = 0(10^1)$$

The inequality of pressure gradients is also valid.

The axisymmetry assumption is not restrictive since flow is only in the r and z directions.

In the formulation of the problem, as depicted by Figure (2), the curvature of the lamella was assumed to have no effect on the lamella drainage. To check this assumption, a more accurate representation of the problem geometry is given in Figure (13).

By making the lamella liquid follow a curved path, the upper bulk interface must have a force exerted on it by the flowing lamella liquid. In Appendix A2, it is shown that the dynamic pressure exerted on the upper bulk interface because of centrifugal force is 0 (10^{-9}) dyne/cm^2. This is insignificant relative to the lamella pressure of the order 10^2 dynes/cm^2.

Therefore, lamella curvature is neglected.

When the equations are solved, an initial lamella shape is calculated from equation (27). This shape is valid if the slopes of the bounding interfaces are approximately less than or equal to 0.1. It is shown in Chapter (2) that this approximation is valid for the bulk interface for a toluene drop in water and is approximately valid for a large part of the radius of the drop interface. This is further confirmed by calculations given in Appendix A2.

4.1-2 Assumptions in the Surfactant Mass Balance Equation and the Remaining Assumptions Used in the Lamella Behaviour Solution

In formulating the problem, the bulk interface was assumed to contract or expand to allow the interfacial tension gradient to balance the shear stress exerted on it by the flowing lamella liquid. However, the bulk interface motion will also be opposed by the viscosity of the discontinuous phase liquid. Therefore, the assumption that the bulk interface moves unencumbered by the underlying liquid is not valid, but is used to simplify the problem, since the equations of motion would have to be solved in both the drop and bulk liquids to allow the bulk interface motion and drop interface motion to be determined. The solutions given in this chapter are for ideal cases only of either zero or infinitely large discontinuous phase viscosities.

No adsorption or desorption of surfactant from the bulk interface is assumed to occur while lamella thinning is occuring. The results of calculations which are summarized in Table (3) show that for a sodium lauryl sulfate concentration less than 10^{-3} gm/l. in the aqueous phase, the initial adsorption time for 10^{12} molecules/cm^2. at a clean interface is greater than one second. If there is a radial variation in the interfacial concentration of adsorbed surfactant of approximately 5×10^{12} molecules/cm^2. and if the problem solution time is less than one second, then the radial gradient in the interfacial concentration of surfactant will be unaltered by adsorption. However, for the 10^{-3} gm/l. case, adsorption of surfactant should be considered.

The final assumption is that a linear relationship exists between the interfacial tension and the interfacial surfactant concentration, Γ. From Davies and Rideal (19), Langmuir's adsorption equation is written as:

$$\Gamma = \frac{\beta' c'}{(1+c'/a)}$$

where β' and a are constants and c' is the aqueous phase surfactant concentration. If c' is small, $\Gamma \doteq \beta' c'$. From the Gibbs adsorption isotherm, the equality is written:

$$\Gamma = \frac{c'}{K'T} \frac{d\gamma}{dc'} = \beta' c'$$

$$\therefore \quad \frac{d\gamma}{dc'} = \beta' RT \qquad \ldots\ldots(35)$$

Since the left hand side of equation (35) equals a constant, the linear adsorption isotherm assumed in this work should be valid for small continuous phase surfactant concentrations of the order of 10^{-9} molar.

4.2. Discussion of Solutions

The results given in Figures (7a-c) for the toluene/water and anisole/water systems show that lamella drainage leads to dimple deflation. Experimentally, these two oil/water systems did not show dimple deflation. Figures (11a,b) show the lamella behaviour observed for the anisole/water system for 10^{-6} and 10^{-4} gm/l. of S.L.S., respectively. In Chapter (3), mechanisms were formulated to account for the observed lamella behaviour. Nearly all of these mechanisms were based on the concept of a bulk interface which moved to balance a change in the surface shear stress. Therefore, the calculated solutions in Figures (7a-c) should not agree with the experimentally observed lamella behaviour.

The time taken to solve equation (23) on a C.D.C. 6400 digital computer was five minutes for a problem solution time of 0.5 seconds. The problem solution time of 0.5 seconds was sufficiently long to show that dimple deflation did occur, but did not require an unreasonably large amount of computer time.

When the motion of the drop interface is restricted by setting m = 2, the deflation of the dimple is reduced because the lamella drainage rate is reduced.

Equation (23) was also solved for the cyclohexanol/water system. The results of the solution are given in Figure (7d). When these results are compared with the experimental results shown in Figure (11c) for this oil/water system, the lamella behaviour is observed to be predicted qualitatively, but the rate of drainage for the predicted lamella behaviour is too large. There is no apparent explanation for this discrepancy. However, a slow contraction of the bulk interface may take place and therefore restrict lamella drainage for the experimental data.

Figures (8a-d) for the anisole/water system show very complex lamella behaviour. For Figures (8a) and (8b) the entire lamella thickness, from the lamella center to radii outside the barrier ring, increased and then the lamella center began to decrease with the barrier ring thickness still increasing. When the surface diffusion coefficient is increased, the interfacial tension gradient is more easily reduced, compared with the case when only bulk interfacial contraction takes place. Therefore, the profiles in Figure (8b) show that the lamella thickness at r = 0 increases less than the profile in Figure (8a), and also decreases more rapidly. The profiles in Figure (8c) show that a further increase in $\mathcal{D}_s$ results in

no increase in the center lamella thickness, and the barrier ring thickness ($r \doteqdot 0.014$ cm.) decreases. The dimple deflates very rapidly.

When the interfacial surfactant concentration is increased, there is little interfacial contraction required to balance continually the surface shear stress. Therefore, the profiles in Figure (8d) show slow, steady dimple deflation.

None of these results agree quantitatively with the experimentally determined lamella profiles, as shown by the various profiles in Chapter (3), and in this chapter in Figures (11a-c). There are obvious differences between the observed and calculated results. There was no barrier ring expansion for the calculated data, rapid thinning of the lamella at the barrier ring was slow for the calculated profiles, and the thinning at the lamella center for the calculated results was very rapid.

These differences may be caused by having to choose a reference point for the interfacial surfactant concentration. The reference point for the interfacial concentration of surfactant was chosen at the N+1 point for the results of the solutions given in Figure (8). A reference point for the interfacial surfactant concentration is necessary to initiate the solution. The algorithm for the solution is given in Figure (14). This algorithm shows that the equations to be solved must be uncoupled to initiate the program. The

distribution of Γ as a function of r is calculated for the initial lamella thickness profile, and must be recalculated for the newly calculated lamella thickness profile, $\Delta\theta$ seconds later. To calculate the new distribution of Γ requires that some value of Γ remain constant. This allows $\frac{\partial\Gamma}{\partial\theta}$ to be calculated as a function of r, and therefore U may be calculated as a function of r. The choice of a reference point at the N+1 point results in the U_i all being negative because the slope of the Γ distribution decreases at nearly all radial locations. Consequently, the U at the barrier ring may be very large and negative. This causes a decrease in the rate of lamella thinning at the barrier ring. Lamella drainage at the barrier ring is slower than would be predicted by the parallel disc model. It was observed experimentally that the lamella thickness may increase at all radial locations inside the barrier ring. This is illustrated by the data in Figure (11a). If the reference point for the interfacial surfactant concentration is chosen at the barrier ring, dimple deflation is very rapid, since, relative to the barrier ring, the radial profile of the interfacial surfactant concentration becomes steeper between the lamella center and the barrier ring radius, located at r = c.

Since the choice of a reference point was arbitrary and since the solutions are strongly dependent on this point, no further solutions were run on the computer. As mentioned

in Chapter (3), there is probably a loss of surfactant from the stressed bulk interface region. This should be considered before the interfacial movement can be accurately described.

Neither the parallel disc - parabolic type - pressure distribution nor the exponential type presented in this chapter describe the lamella pressure distribution accurately. Both expressions are boundaries on the realistic pressure distribution, as represented by the polynomial pressure distribution of Figure (3a). Therefore, any solutions given using the exponential type pressure distribution reflect the lack of accuracy that this pressure distribution has, relative to the realistic pressure distribution.

4.3. Physical Property Dependence of Lamella Drainage

Each term in equation (23) may be analyzed to determine its physical property dependence. Three terms may be defined:

$$T_1 = -\frac{2(3-m)}{6m} \beta y^3 e^{-\lambda r^2}$$

$$T_2 = -\frac{2(3-m)}{6m} \beta \lambda r^2 y^3 e^{-\lambda r^2}$$

$$T_3 = -\frac{3}{6m} \beta r \frac{\partial y}{\partial r} y^2 e^{-\lambda r^2}$$

If the radius is small, then equation (23) depends only on T_1. Since:

$$\beta = \frac{2}{\mu} \frac{\pi P_o^2}{Wg}$$

and if $p_o \doteq \frac{\gamma}{d}$, then:

$$T_1 = -\frac{2(3-m)}{6m} \cdot \frac{2}{\mu} \frac{\pi \gamma^2}{d^2 W g} y^3$$

$$= -\frac{(3-m)}{2m} \frac{\gamma^2}{\mu d^5 \Delta\rho g} y^3$$

This is the same parameter dependence as the parallel disc model.

At the barrier ring, T_1 and T_2 are both significant. An expression for the barrier ring radius, c, may be derived from equation (27) by differentiating this equation with respect to r and by setting $\frac{\partial y}{\partial r} = 0$ for r = c. For the first three terms of equation (27), the result is:

$$c^2 = \frac{2Wg\gamma}{\pi p_o^2}\left(\frac{p_o}{\gamma} - \frac{1}{d}\right) \qquad \ldots\ldots(36)$$

If $\frac{p_o}{\gamma} - \frac{1}{d} = \frac{K}{d}$ and $p_o = \frac{\gamma}{d}$, where K is a constant, this expression may be written:

$$c^2 = 2K \frac{d\, Wg}{\pi \gamma} \qquad \ldots\ldots(37)$$

where $0 \leq K \leq 1$ for all cases of dimpling observed. Therefore,

$$T_2 = \frac{2(3-m)}{6m} \cdot \frac{2}{\mu} \frac{\pi \gamma^2}{d^2 Wg} \cdot \frac{\pi \gamma}{d\, Wg} \cdot \frac{2KdWg}{\pi \gamma} y^3$$

with the exponential dependence neglected. This equation becomes:

$$T_2 = \frac{K(3-m)}{m} \frac{\gamma^2}{\mu d^5 \Delta\rho g} y^3$$

Again, the lamella drainage rate at the barrier ring shows the parallel disc parameter dependence.

The third term, T_3, only becomes important relative to T_1 and T_2 outside the barrier ring. If the slope of the lamella profile is expressed by $\frac{c}{d}$, and if $r \doteq c$, then:

$$T_3 = -\frac{3}{6m} \cdot \frac{2}{\mu} \cdot \frac{\pi \gamma^2}{d^2 Wg} \cdot \frac{c^2}{d} y^2$$

with the exponential dependence neglected, and:

$$T_3 = -\frac{2K}{m} \frac{\gamma}{\mu d^2} y^2$$

Term T_3 has the same parameter dependence as does the Hodgson/Woods model. Term T_3 becomes increasingly important as the radius outside the barrier ring increases, and , as shown by the Hodgson/Woods model, the rate of lamella thinning is rapid. These parameter dependencies provide insight into the reason for barrier ring expansion. At the barrier ring, the drainage rate is controlled by the parallel disc type parameter dependence. An incremental distance outside the barrier ring, the drainage rate is more rapid because of the increased radius and lamella thickness, and also because of the Hodgson/Woods type dependence of term T_3. An equation based on this argument is derived in Section A2.11 to describe barrier ring expansion.

4.4. Radial Distribution of Surfactant Adsorbed in the Bulk Interface

In Chapter (3), the pressure polynomial given in Chapter (2) was used to calculate the radial distribution of surfactant adsorbed at the bulk interface. For example, Figure (9) of Chapter (3) shows the interfacial surfactant concentration distribution for $\theta = 1.15$ seconds for the relative lamella thickness profile given in Figure (8) of Chapter (3). The radial concentration distribution showed Γ_r exceeded Γ_t at large radii. The surfactant distribution has been calculated in this chapter for the profile at $\theta = 1.15$ sec. in Figure (8) of Chapter (3), for the exponential type model. The results are given in Figure (12).

Two curves for the interfacial distribution of surfactant were calculated for the relative lamella thickness profile. The first curve is for $p_o = 131.6$ dyne/cm^2.; the same center lamella pressure as used for the polynomial. However, the exponential type pressure distribution does not give the same lamella profile as does the series type polynomial. This is shown in Figure (3b). A second surfactant distribution was calculated for $p_o = 150.0$ dyne/cm^2. This latter pressure produces a lamella profile approximately the same as that for the profile at $\theta = 1.15$ sec. in Figure (8) of Chapter (3).

The curves in Figure (12) show that the interfacial surfactant concentrations rise more steeply for the exponential

type model than for the polynomial model. This is expected since the pressure gradient, hence the surface shear stress, is larger for the exponential model at small radii. The curves in Figure (12) for the exponential model were calculated by assuming $\Gamma_o = 0$. The values of Γ_t required to yield the $\Gamma_o = 0$ condition were 3 to 4 x 10^{12} molecules/cm^2. These values of Γ_t are much larger than the calculated Γ_t for adsorption at an interface 5 minutes old, for 10^{-6} gm/l. S.L.S. + 0.01N. KCl.

Therefore, these calculations show that the necessary Γ at large radii may exceed the Γ_t adsorbed at the quiescent region of the bulk interface. This imbalance between the required Γ and the actual Γ_t is in agreement with previous calculations based on the polynomial model presented in Chapter (2). The polynomial in Chapter (2) was employed in Chapter (3) to formulate a postulate on the cause of uneven drainage.

5. Conclusions

Lamella drainage has been analyzed completely from fundamentals. Numerical solutions for cases when the bulk interface is laterally rigid show that the lamella thickness decreases most rapidly at the lamella center. This leads to dimple deflation. Drainage is more rapid for a mobile drop interface than if the interface is immobile.

Trial solutions for the case when the bulk interface movement depends on the change in surface shear stress are

given and are shown to be very complex. The effect of increasing the surface diffusion coefficient is to reduce bulk interface contraction and therefore to increase lamella drainage. Similarly, an increase in the interfacial concentration of adsorbed surfactant causes less bulk interface contraction and therefore more rapid lamella drainage.

The theoretical analysis also yields an expression for the dynamic pressure distribution in the lamella. This expression shows an exponential decay of dynamic pressure in the lamella and is seen to be an upper bound on the actual dynamic pressure distribution of the lamella, as described by the pressure polynomial. The usefulness of this exponential expression is limited, however, because of the boundary condition $p \longrightarrow 0$ as $r \longrightarrow \infty$.

The lack of agreement between the observed and predicted lamella behaviour suggests that the bulk interface movement is more complicated than expected. Based on the arguments of Chapter (3), and the results of this chapter, one factor for the complex interface movement could be the loss of surfactant from the stressed region of the bulk interface.

Part B Parallel Disc Analysis

1. Introduction

An analysis, analogous to that done in Part A, may be made for parallel disc geometry. The resulting equations yield a simple model for lamella drainage. This model describes the lateral motion of the bulk interface and can be used to calculate the local rate of drainage at any radius in the lamella.

2. Derivation of Equations

For the parallel disc model, the lamella thickness remains constant with radius. This model approximates a dimpled lamella because the change in lamella thickness with radius is small. Therefore, in an approximate mathematical analysis, the local lamella thickness, y, may be assumed independent of radius, even for a dimpled lamella.

A mass balance may be made over an elemental volume for the water in the lamella. The resultant expression is equation (3) in section (A2.1). This expression may be rewritten with $\frac{\partial y}{\partial r}$ equal to zero and, if the interface is mobile, for m equal to one.

The equation is:

$$\frac{\partial y}{\partial \theta} = \frac{h^3}{3\mu}\left(\frac{\partial^2 p}{\partial r^2} + \frac{1}{r}\frac{\partial p}{\partial r}\right) - h\frac{\partial U}{\partial r} - \frac{hU}{r} \qquad \text{.....(38)}$$

In this expression, the local lamella thickness, y, has been replaced by the lamella thickness at the barrier ring, h, since y is constant and must equal h. In equation (38), the dependence of $\frac{\partial y}{\partial \theta}$ on radius is included implicitly in the pressure terms, and in the interfacial velocity .

A mass balance over an elemental area for the surfactant adsorbed at the bulk interface has been made in Chapter (4). From equation (28) of Chapter (4), with the diffusivity, $\mathcal{D}_s$, equal to zero, the mass balance for the adsorbed surfactant is:

$$-\frac{\partial \Gamma}{\partial \theta} = \frac{U \partial \Gamma}{\partial r} + \frac{\Gamma \partial U}{\partial r} + \frac{\Gamma U}{r} \qquad \text{.....(39)}$$

To couple the bulk and interfacial phases, a linear adsorption isotherm is assumed, and equation (5) of Chapter (3) for the surface shear stress may be employed. These equations are:

$$\gamma = \gamma_o - k'\Gamma \qquad \text{.....(40a)}$$

and

$$S = -h\frac{\partial p}{\partial r} \qquad \text{.....(40b)}$$

where S is the surface shear stress exerted by the lamella liquid on the bulk interface, and y has been replaced by h in equation (40b).

The pressure distribution for the parallel disc model has been derived in section (A2.10). The equation for this

distribution is:

$$p = \frac{2F}{\pi R^4} (R^2 - r^2)$$

Therefore, the radial pressure gradients may be written:

$$\frac{\partial p}{\partial r} = -\epsilon r \qquad \text{.....(41a)}$$

$$\frac{\partial^2 p}{\partial r^2} = -\epsilon \qquad \text{.....(41b)}$$

where $\epsilon = \frac{4F}{\pi R^4}$

F is the drop buoyancy force and R is the radius at which the lamella pressure is zero.

If the interfacial tension gradient in the bulk interface is equated to the surface shear stress, given in equation (40b), the result is:

$$k' \frac{\partial \Gamma}{\partial r} = h \epsilon r \qquad \text{.....(42)}$$

Equation (42) may be integrated with respect to r. The result is:

$$\Gamma = \Gamma_t + \frac{h \epsilon}{2 k'} (r^2 - R^2) \qquad \text{.....(43)}$$

where the boundary condition $\Gamma = \Gamma_t$ at $r = R$ was used. The interfacial concentration ot adsorbed surfactant in the bulk interface t minutes atter the interface was cleaned is Γ_t.

Equations (42) and (43) are approximations, since the gradient $\frac{\partial \Gamma}{\partial r}$ must depend upon y and not h. Since it has

been assumed that y is approximately equalto h, then h is replaced by y in equation (43) and the time derivative is found. The result is:

$$\frac{\partial \Gamma}{\partial \theta} \doteq \frac{\epsilon}{2\,k'} (r^2-R^2) \frac{\partial y}{\partial \theta} \qquad \ldots\ldots(44)$$

These expressions for Γ, $\frac{\partial \Gamma}{\partial r}$, and $\frac{\partial \Gamma}{\partial \theta}$ may be substituted into equation (39) to yield:

$$\overbrace{\frac{2\,k'}{\epsilon\,(R^2-r^2)} \left(\Gamma_t + \frac{h\epsilon}{2\,k'} (r^2-R^2) \right)}^{a(r)} \frac{\partial U}{\partial r}$$

$$+ \overbrace{\frac{2\,k'}{\epsilon\,(R^2-r^2)} \left(\frac{h\epsilon\,r}{k'} + \frac{\Gamma_t}{r} + \frac{h\epsilon}{2k'r} (r^2-R^2) \right)}^{b(r)} U$$

$$= \frac{\partial y}{\partial \theta}$$

This equation may be re-written:

$$a(r) \frac{\partial U}{\partial r} + b(r)\, U = \frac{\partial y}{\partial \theta} \qquad \ldots\ldots(45)$$

where the functions a(r) and b(r) are defined as shown. When the pressure derivatives given in equations (41a,b) are substituted into equation (38), the result is:

$$-h \frac{\partial U}{\partial r} - \frac{h}{r} U \quad \frac{-2\epsilon h^3}{3\mu} = \frac{\partial y}{\partial \theta}$$

or,

$$c(r) \frac{\partial U}{\partial r} + d(r)\, U + g(r) = \frac{\partial y}{\partial \theta} \qquad \ldots\ldots(46)$$

where $c(r) = -h$, (independent of radius)

$$d(r) = -\frac{h}{r}$$

$$g(r) = -\frac{2\epsilon h^3}{3\mu}$$

Equations (45) and (46) are equated to yield a first order linear ordinary differential equation. The result is:

$$\frac{\partial U}{\partial r} + PU = Q \qquad \ldots\ldots(47)$$

where $$P = \frac{b - d}{a - c}$$

$$Q = \frac{g}{a - c}$$

Equation (47) may be solved using an integrating factor. This factor is defined as:

$$F' = \exp\left(\int P \, dr \right)$$

$$= r\, e^{fr^2}$$

where $$f = \frac{h\epsilon}{2k'\Gamma_t}$$

$$P = \frac{h\epsilon r^2 + k'\Gamma_t}{k'\Gamma_t r}$$

$$Q = \frac{\epsilon^2 h^3}{3\mu k'\Gamma_t} \quad (r^2 - R^2)$$

The solution of (47) may be written:

$$r\, e^{fr^2} U = \int r\, e^{fr^2} \, Q \, dr$$

$$= \left(- \frac{\epsilon R^2 h^2}{3\mu} + \frac{\epsilon h^2 r^2}{3\mu} - \frac{2k' \Gamma_t h}{3\mu} \right) e^{fr^2} + C_1$$

To find C_1, let U be zero at the lamella center.

Then:

$$C_1 = \frac{\epsilon R^2 h^2 + 2k' \Gamma_t h}{3\mu}$$

The final solution for U may be written:

$$U = - \frac{(\epsilon R^2 h^2 + 2k' \Gamma_t h)}{3\mu r} (1-e^{-fr^2}) + \frac{\epsilon h^2 r}{3\mu} \qquad \text{.....(48)}$$

The application of L'Hopital's rule to equation (48) will show that U approaches zero as r approaches zero. Since U is known, equation (48) may be substituted into equation (38) to yield:

$$\frac{\partial y}{\partial \theta} = \frac{2\epsilon}{3\mu} h^3 (e^{nh}-2) + \frac{\epsilon^2 R^2 h^4 e^{nh}}{3\mu k' \Gamma_t} \qquad \text{.....(49)}$$

where $$n = - \frac{2F r^2}{\pi R^4 k' \Gamma_t}$$

The solution to equation (49) describes the change in lamella thickness with time. This model will be called the coupled model. While the coupled model has been derived by assuming that the lamella pressure distribution is given by the parabolic pressure distribution predicted from the parallel disc

model, the coupled model and the parallel disc model are entirely different. The coupled model does not require a parallel disc lamella, and it includes the effect of the contraction of the bulk interface.

Equation (49) contains the factor $k' \Gamma_t$. This is the interfacial tension lowering which occurs when the interfacial concentration at the bulk interface is Γ_t.

Two additional equations may be obtained from equation (49). If there is no adsorbed surfactant, then $k' \Gamma_t$ is zero, and at the barrier ring, y is equal to h. Equation (49) then becomes:

$$\frac{dh}{d\theta} = - \frac{4 \epsilon h^3}{3 \mu} \qquad \text{.....(50)}$$

If equation (49) is evaluated at the lamella center, the following equation results:

$$\frac{dy_o}{d\theta} = - \frac{2 \epsilon h^3}{3 \mu} + \frac{\epsilon^2 R^2 h^4}{3 \mu k' \Gamma_t} \qquad \text{.....(51)}$$

where y is equal to y_o when r is equal to zero.

The second term in equation (51) does not become infinitely large as $k' \Gamma_t$ approaches zero, because h also approaches zero. Therefore, if $k' \Gamma_t$ is zero, there is no surfactant at the bulk interface, and only the rapid drainage mechanism will be observed. There will be no slow, even drainage.

Equation (50) expresses the maximum possible rate of lamella thinning at the barrier ring. This maximum rate occurs

if there is no contraction of the bulk interface to reduce lamella drainage. This maximum rate is also twice the drainage rate predicted by the parallel disc model, for a mobile drop interface.

3. Solution of the Equations

Since equations (44), (50) and (51) are strongly dependent on R, several values for R should be used in the solution of these equations. The parabolic pressure distribution predicted by the parallel disc model has been used to derive equations (49), (50) and (51). However, the average lamella pressure may still be specified. Two values for this average pressure may be used. If the center lamella pressure is p_o, the average lamella pressure will be $\frac{p_o}{2}$ for a parabolic pressure distribution. Then, a force balance between the lamella pressure and the drop buoyancy force results in the following equation for R^2:

$$\frac{p_o}{2} \pi R^2 = Wg$$

$$R^2 = \frac{2Wg}{\pi p_o}$$

This result for R^2 will be called the approximate model.

If the equilibrium model (11) is used, the lamella pressure is assumed constant at the value p_o, the center lamella pressure. Therefore, a force balance, done as before, yields:

$$R^2 = \frac{Wg}{\pi p_o}$$

This result for R^2 will be called the equilibrum model. In Chapter (3), the value of R predicted by the equilibrum model

agreed with the observed radius of the barrier ring, measured from light interference patterns. Since the lamella pressure has been shown in Chapter (2) to be not equal to zero at the barrier ring, the equilibrium model may express a lower limit on the value of R. The approximate model is arbitrarily used to express an upper limit on R.

Equation (50) for the maximum rate of thinning at the barrier ring was solved for both values of R. The value of p_o in these models for R was chosen as $\frac{\gamma}{d}$, since this pressure has been shown previously in Chapter (3) to result in a parallel disc lamella.

Equation (49) was solved at the barrier ring, with the values $k' \Gamma_t = 0.001$ and 0.01 dyne/cm., for the value of R predicted by the equilibrium model, for the toluene/water and anisole/water systems. Approximate values of the barrier ring radius were assumed for both systems.

The results for these six solutions for the rate of thinning at the barrier ring are shown in Figure (15a,b). Typical lamella thinning data are also given for both oil/water systems. These thinning data are not strongly dependent on the interface age, as shown by the anisole/water data. The interfacial tension lowering, $k' \Gamma_t$, is 0.01 and 0.1 dyne/cm., approximately, for 10^{-6} and 10^{-4} gm/l. of S.L.S., respectively.

Equation (49) was solved numerically for the entire

lamella. The results are given in Figure (16) for a 0.005 ml. toluene drop in water, for $k' \Gamma_t = 0.001$ dyne/cm. Figures (17) and (18) show the calculated velocity distribution in the bulk interface, and the calculated distribution of surfactant adsorbed at the bulk interface, respectively, for the initial lamella profile in Figure (16). For the results in Figure (18), Γ_t is small, and nearly all the calculated values of Γ are negative. Since this is not valid, the values of Γ have been adjusted to give $\Gamma_0 = 0$. This difficulty is discussed further in the next section.

Equation (51) for the rate of lamella drainage at the lamella center was solved for $k' \Gamma_t = 0.001$ and 0.01 dyne/cm., for various initial lamella thicknesses of 2×10^{-5} to 1×10^{-4} cm. Some of the results are given in Figure (19).

4. Discussion of the Solutions

A comparison of the results of the coupled model with the data in Figure (15) shows that the coupled model predicts drainage rates which are too small. A comparison of the coupled results and the parallel disc model results given in Figure (1) shows that the coupled model of equation (49) predicts a drainage rate slower than does the parallel disc model, if $k' \Gamma_t$ is not zero. The assumption has been made that the motion of surfactant into the central region of the lamella occurs only by contraction of the bulk interface, for the coupled model. However, surface diffusion of surfactant will also occur and

will reduce the interfacial tension gradient of the bulk interface. Consequently, a slight expansion of the bulk interface in the region of the barrier ring may occur if surface diffusion is significant in the redistribution of surfactant. This slight expansion of the bulk interface should allow more rapid thinning at the barrier ring.

Further work has not been done on the refinement of the coupled model, for several reasons. The coupled model is based on the parabolic pressure distribution predicted by the parallel disc model. This pressure distribution inaccurately describes the realistic pressure distribution. Also, the simplicity of the coupled model result,as represented by equation (49), would be removed if terms were included in the derivation of equation (49) to account for surface diffusion. A differential equation results which cannot be solved analytically. Therefore, the attempt to increase the accuracy of the model restricts its simplicity. A simple model to describe barrier ring drainage for all values of the interfacial surfactant concentration is still required.

The results given in Figure (15) show that a change in the value of R strongly influences the lamella drainage. The effect of R on the drainage prediction may be more significant than the effect of surface diffusion. The pressure gradient in the lamella is very steep for a small value of R. Therefore, drainage of the lamella is rapid.

The results of the numerical solution of equation (49) are given in Figure (16). These results show that the dimpling of the lamella also causes the thickness of the lamella to increase at the barrier ring. The results in Figure (16) agree well with the lamella behaviour shown in Figure (11a) for an anisole drop. Figure (17) shows the radial velocity distribution in the bulk interface for the initial lamella profile in Figure (16). This form of the distribution of U with radius agrees with the results of calculations for U from the more complex analysis of Part A. However, the magnitude of the values of U in Figure (17) are a factor of ten smaller than those results in Figure (10). This may be partially due to the thick lamella which was employed in the calculation of the results in Figure (10).

The distribution of Γ as a function of radius is given in Figure (18) for the initial lamella shape in Figure (16). The values of Γ were adjusted to give $\Gamma_o = 0$, since equation (43) yields negative values for Γ when $k'\Gamma_t = 0.001$ dyne/cm. Therefore, the results in Figure (16) are not experimentally valid, but they are still mathematically valid. These results are presented to show that a small interfacial concentration of surfactant can cause lamella dimpling.

The solution of equation (51) for the effect of an increase in the interfacial concentration of surfactant on the motion of the lamella center is shown by the results in Figure

(19). For ten-fold increase in $k'\Gamma_t$ to 0.01 dyne/cm., there is a large decrease in the extent of lamella dimpling. A large interfacial concentration of adsorbed surfactant, Γ_t, permits the bulk interface to contract at a slower rate than with a smaller Γ_t, because less movement is required to transfer surfactant inward in order to maintain the balance between the interfacial tension gradient and the surface shear stress. However, this reasoning does not account for the less rapid thinning predicted at the barrier ring, for this large $k'\Gamma_t$ value. The initial starting heights of the lamella center and of the barrier ring height also have an effect on the extent of dimpling. A small increase in the starting heights from 2000 A° to 4000 A° results in more rapid dimpling. The contraction of the bulk interface will be more rapid for an increase in the starting heights because the drainage of the lamella will be rapid. Therefore, the surface shear stress exerted on the bulk interface will change rapidly. The bulk interface must also contract rapidly to maintain the balance between the surface shear stress and the interfacial tension gradient. Since the contraction of the bulk interface has been shown to cause dimpling, a rapid contraction of the bulk interface should cause rapid dimpling.

One final calculation may be made from this model. If viscous flow in the lamella only occurs when the bulk interface contains sufficient surfactant to balance the surface shear stress, then equation (14) may be used to calculate the center lamella thickness, y_o, when slow even drainage begins.

If Γ_o equals zero, the result is:

$$y_o = \frac{2k' \Gamma_t}{\epsilon R^2} \qquad \ldots\ldots(52)$$

The value of Γ_t may be calculated from the Ward/Tordai equation used in Chapter (3). For 10^{-6} gm/l. of S.L.S., for a 0.005 ml. toluene drop in water, equation (52) was used to calculate y_o. The results are given in Table (A2.3).

These results show that the height, y_o, increases as the interface is aged ~~because the bulk interface is aged~~ because the bulk interface contains more adsorbed surfactant and, therefore, can balance a larger surface shear stress. A larger surface shear stress will occur for an increase in the lamella thickness. Experimental observations of the light interference patterns have shown that rapid drainage of the lamella apparently ceased at lamella thicknesses of zero to 2000 A°, for 10^{-6} gm/l. of S.L.S. This lamella thickness at the cessation of rapid drainage increased slowly as the interface aged. A large effect of the interface age on the lamella thickness at which rapid drainage ceased was only observed at interface ages less than five minutes, for 10^{-6} gm/l. of S.L.S.

5. Conclusions

A simple model has been derived which accounts for the contraction of the bulk interface during lamella drainage. The contraction of the bulk interface causes dimpling of the lamella and decreases the rate of lamella drainage at the barrier ring.

An increase in the interfacial concentration of surfactant causes a decrease in the rate of lamella dimpling, because of a decrease in the rate of contraction of the bulk interface near the lamella center. An increase in the initial height at which dimpling begins, results in more rapid dimpling because the bulk interface contracts more rapidly.

This model was derived by using the concepts of lamella and bulk interface behaviour which were given in Chapter (3) and expressed mathematically in Part A of Chapter (4). From the reasonable agreement of the results of the coupled model with experimental observation, the concepts used in its derivation are substantiated.

Nomenclature

K = constant defined by equation (37)

N = number of radial increments used in finite difference solution

R = radius at which $p = 0$, cm.

R' = gas constant

T = absolute temperature

U = bulk interface radial velocity, cm./sec.

W = drop weight, grams.

---

a_o = p_o/μ

c = barrier ring radius, cm.

c' = aqueous bulk phase concentration of surfactant

d = drop radius, cm.

g = gravitational constant, cm./sec.^{2}

h = height of drop interface above an arbitrary horizontal reference line

k = height of bulk interface above an arbitrary horizontal reference line

k' = constant defined in equation (30). Value is approx. 1.4×10^{-14} dyne-cm. for S.L.S.

m = number of immobile interfaces

p = dynamic lamella pressure at any radial location, dyne/cm.^{2}

p_o = p at $r = 0$

r = any radial location, cm.

t = time, sec.

u = radial velocity, cm./sec.

w = vertical velocity, cm./sec.

x = dimensionless distance, r^2

y = height of drop interface relative to the bulk interface, cm.

y_o = y at $r = 0$

z = any vertical location, cm.

Ψ = stream function

Γ = interfacial concentration of surfactant at any radial location, molecules/cm.^{2}

Γ_o = Γ at $r = 0$

Γ_t = Γ at $r \longrightarrow \infty$ for time t

$\mathcal{D}_s$ = surface diffusion coefficient of surfactant, cm.^{2}/sec.

$\beta = \frac{2 \lambda P_o}{\mu}$

β' = a constant

π = 3.1416

$\lambda = \frac{\mu \pi P_o}{Wg}$

γ = interfacial tension, dyne/cm.

γ_o = interfacial tension for the pure oil/water system

ρ = density, gram/ml.

$\Delta\rho$ = oil/water system density difference

μ = absolute viscosity, gram/cm.^{2}-sec.

θ = time, sec.

Bibliography

1. Hartland, S., Chem. Eng. Sci. 24 987-995 (1969).
2. Frankel, S. P. and K. J. Mysels, J. Phys. Chem. 66 (1) 190-1 (1962).
3. Platikanov, D., J. Phys. Chem. 68 (12) 3619-24 (1964).
4. Hodgson, T. D., Ph.D. Thesis, Swansea (1966).
5. Charles, G. E. and S. G. Mason, J. Colloid Sci. 15 (3) 235-267 (1960).
6. Charles, G. E., R. S. Allan and S. G. Mason, J. Colloid Sci. 16 (2) 150-165 (1961).
7. MacKay, G. D. M. and S. G. Mason, Can. J. Chem. Eng. 41 203-212 (1963).
8. MacKay, G. D. M. and S. G. Mason, J. Colloid Sci. 16 (6) 632-635 (1961).
9. ibid. and M. Suzuki, J. Colloid Sci. 18 (1) 103-4 (1963).
10. MacKay, G. D. M. and S. G. Mason, J. Colloid Sci. 18 674-683 (1963).
11. Chappelear, D. C., J. Colloid Sci. 16 186-190 (1961).
12. Princen, H. M., J. Colloid Sci. 18 178-195 (1963).
13. Hodgson, T. D. and D. R. Woods, J. Colloid and Interface Sci. 30 (4) 429-446 (1969).
14. Burrill, K. A. and D. R. Woods, to be published (Chapter 3).
15. Burrill, K. A. and D. R. Woods, J. Colloid and Interface Sci. 30 (4) 511-524 (1969).
16. Bird, R. B., W. E. Steward, and E. N. Lightfoot, "Transport Phenomena" Wiley, New York (1965).

17. Hartland, S, "The Profile of the Draining Film Beneath a Liquid Drop Approaching a Plane Interface". Paper presented at C.I.C. Conference, Montreal (1968).

18. Sakata, E. K. and J. C. Berg, I.E.C. Fund 8 (3) 570-575 (1969).

19. Davies, J. T. and E. K. Rideal, "Interfacial Phenomena" Academic Press, New York (1961) pg. 183-4.

Table 1. Problem Boundary Conditions

Velocity	Independent Variable	Stream Function	Boundary Condition Number
$u = 0$	$z = 0$	$\psi_z = 0$	1a
$u = U$	$z = 0$	-	1b
$u = 0$	$r = 0$	$\psi_z = 0$	2a
		$\psi_{rz} = 0$	2b
$w = 0$	$z = 0$	$\psi_r = 0$	3
$u = 0$	$z = y$	$\psi_z \Big\vert_{z=y} = 0$	4a
OR			
$\frac{\partial u}{\partial z} = 0$	$z = y$	$\psi_{zz} \Big\vert_{z=y} = 0$	4b

$z = y$ locates the drop interface

$z = 0$ locates the bulk interface

Table 2. System Physical Properties

Parameters	Oil/Water System			
	Toluene/ Water	Anisole/ Water	Cyclohex-anol/Water	CA/ Water
$\Delta\rho$	0.133	0.0097	0.051	0.053
γ	35.0	20.5	3.93	28.9
μ_d(cp.)	0.59_L	1.32_L	32.8	0.850
Drop Volume	0.005	0.020	0.001	0.005
d	0.1061	0.1682	0.062	0.1061
P_o	360.0	150.0	75.0	300.0
y_o	1.5×10^{-4}	1.5×10^{-4}	1.5×10^{-4}	1.5×10^{-4}
m	1	1	2	1

See notes on Table 2.

Notes on Table 2.

1. All dimensions are in c.g.s. units.
2. μ_d is oil viscosity.
3. The water viscosity is 0.894 cp. .
4. Mixture CA is 0.84 mole fraction anisole and 0.16 mole fraction cyclohexane.
5. L signifies a literature value from the Handbook of Physics and Chemistry, at 20°C .
6. All other values in the table were measured experimentally in this work, at 25°C .
7. The oil and water were mutually saturated before physical properties were measured.

Table 3. Calculation of the Time Required to Adsorb 10^{12} Molecules/cm^2 of S.L.S.

gram/litre of S.L.S.	x	time (minutes)
10^{-6}	9	500
10^{-5}	10	5
10^{-4}	11	$5x\ 10^{-2}$
10^{-3}	12	$5x\ 10^{-4}$

The Ward/Tordai equation employed for this calculation is written:

$$t = \frac{1}{60}\left(\frac{10^{12}}{5.78x\ 10^{x}}\right)^2$$

Table 4. Calculation of the Center Lamella Thickness at the Beginning of Slow, Even Drainage

10^{-6} gm/l. S.L.S.+0.01 N.KCl

0.005 ml. toluene drop

t minutes	$k'\Gamma_t$ dynes/cm.	Calculated y_o, A°	Observed y_o, A°
0	0	0	0
5	0.0017	13,900	1000
10	0.0024	19,600	1000
15	0.0029	23,700	1600
20	0.0034	27,800	1600
25	0.0038	31,100	1600

Sample Calculation of $k'\Gamma_t$ (Ward/Tordai equation)

$$\Gamma_t = 5.78 \times 10^9 \sqrt{t \times 60}$$

t = 5 min.

$\therefore \quad \Gamma_t = 1.0 \times 10^{11}$ molecules/cm^2

$k = 1.7 \times 10^{-14}$ dyne-cm./molecule

$\therefore \quad k'\Gamma_t = 1.7 \times 10^{-3}$ dyne/cm.

Figure 1a. Comparison of the Lamella Thinning Models with Typical Data for Barrier Ring Thinning - Toluene/Water

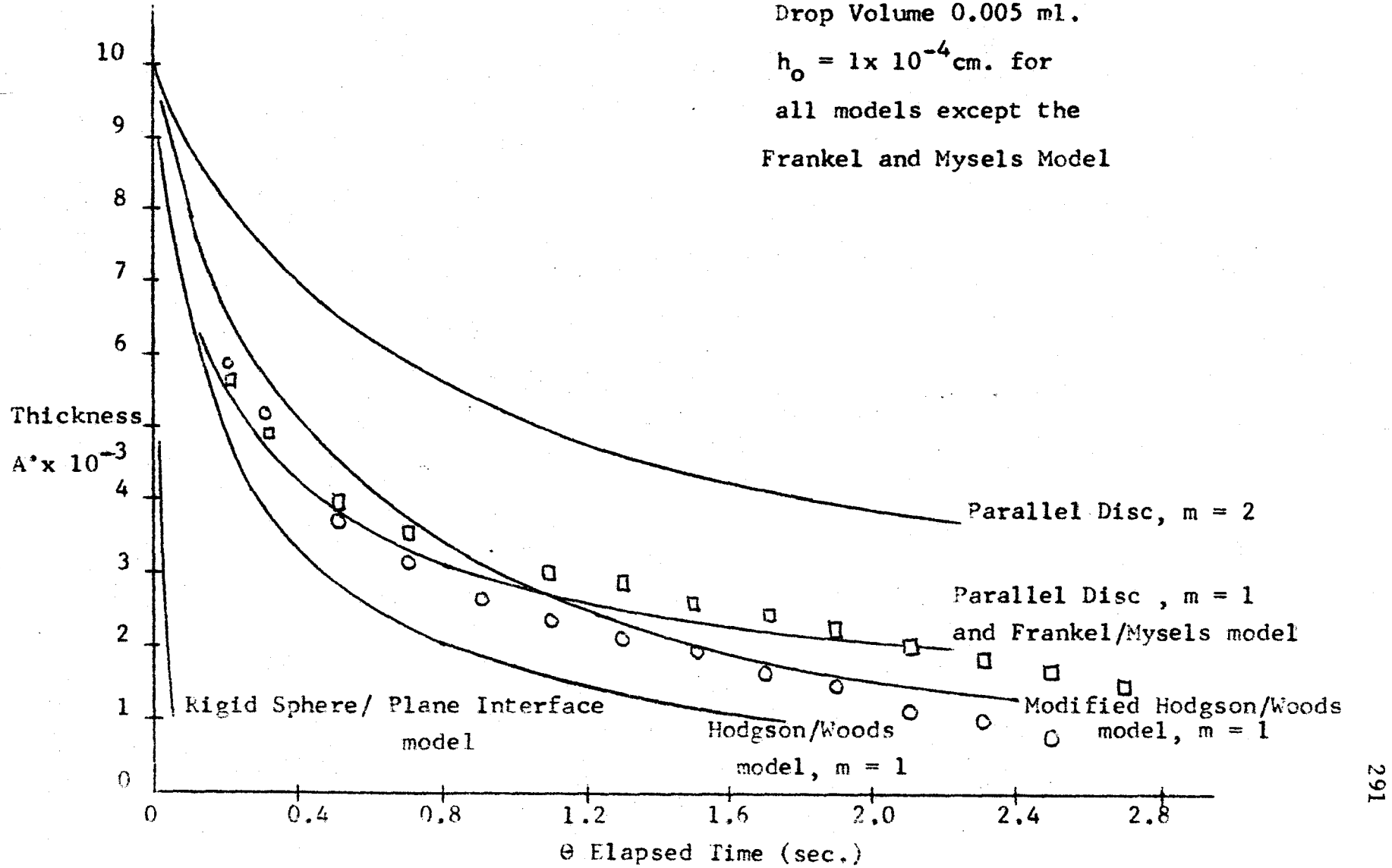

Figure 1b. Comparison of the Lamella Thinning Models with Typical Data for Barrier Ring Thinning - Anisole/Water

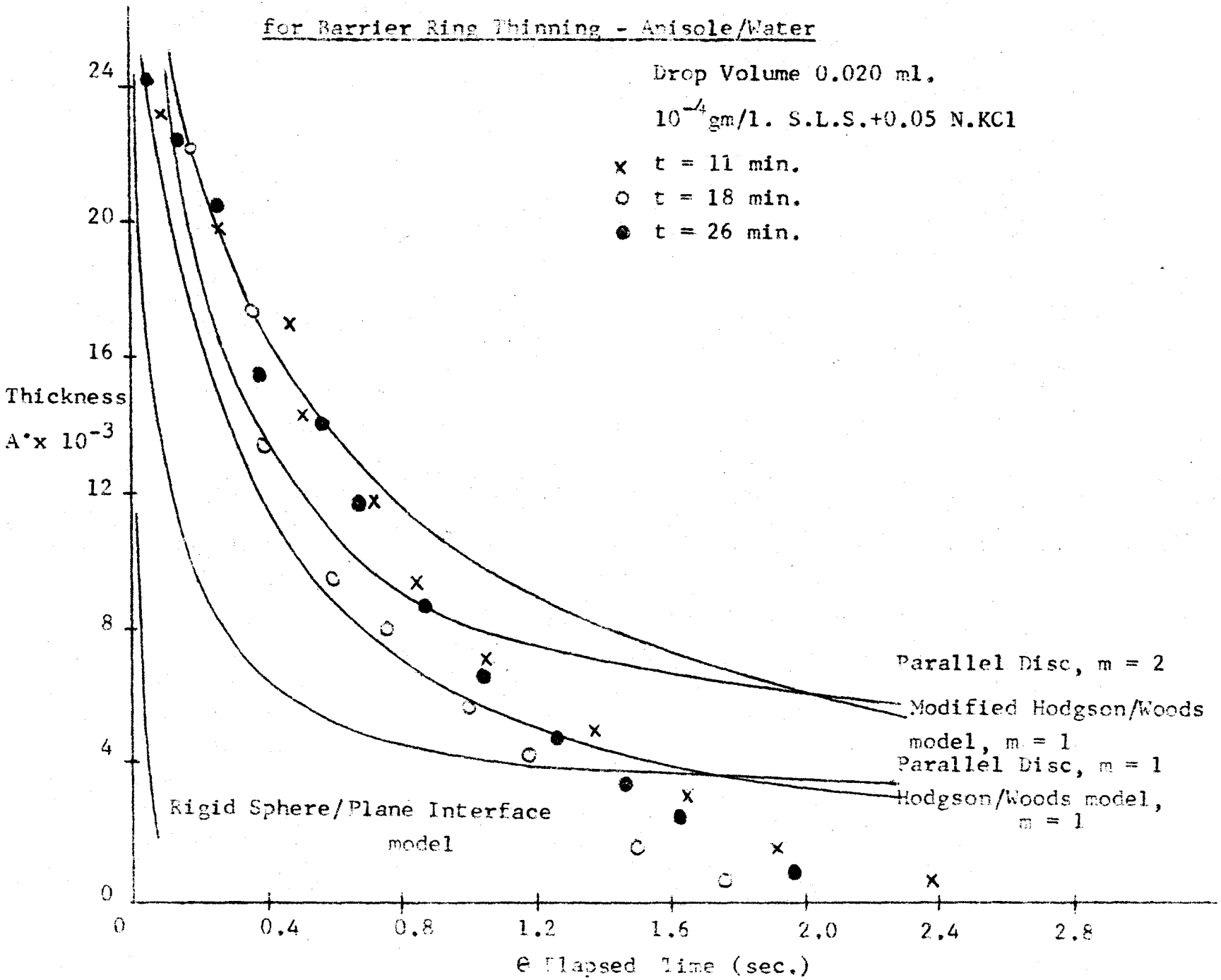

Equations Used to Calculate the Curves in Figure (1)

$h = h_o$

$\theta = \theta_o$

and

$$R = d^2 \sqrt{\frac{2\Delta\rho g}{3\gamma}} \qquad \text{(Based on the parallel disc model)}$$

1. Parallel Disc Model

$$\left(\frac{1}{h_o^2} - \frac{1}{h^2} \right) = \frac{-16\gamma^2 (\theta - \theta_o)}{d^5 \Delta\rho g \mu m^2}$$

m = 1, one immobile interface

m = 2, two immobile interfaces

2. Rigid Sphere/ Plane Interface Model

$$\ln \left(\frac{h_o}{h} \right) = \frac{2 d \Delta\rho g (\theta - \theta_o)}{9\mu}$$

3. Frankel/Mysels Model

$$h = \left(\frac{0.060\ m^2\ d^5 \Delta\rho g \mu}{\gamma^2 \theta} \right)^{\frac{1}{2}}$$

4. Hodgson/Woods Model

$$\left(\frac{1}{h_o} - \frac{1}{h} \right) = \frac{-\gamma (\theta - \theta_o)}{6\mu d^2}$$

This model contains the following assumptions:

1. One immobile interface.
2. Radius of cylinder is d .
3. Lamella pressure at the barrier ring is $\frac{\gamma}{d}$.

5. Modified Hodgson/Woods Model

$$\left(\frac{1}{h_o} - \frac{1}{h} \right) = \frac{-\gamma (\theta - \theta_o)}{12 \mu d^2}$$

This modification of the model contains:

1. One interface is immobile.
2. Radius of cylinder is d.
3. Lamella pressure at the barrier ring is $\frac{\gamma}{2\ d}$.

Calculation Details for Figure 1b.

1. Parallel Disc Model:

$h_o = \infty$

$\theta = 0$

2. Rigid Sphere/Plane Interface Model:

$h_o = 3 \times 10^{-4}$cm.

$\theta_o = 0$

3. Hodgson/Woods (and Modified) Model:

$h_o = 3 \times 10^{-4}$cm.

$\theta_o = 0$

Figure 2. Problem Geometry

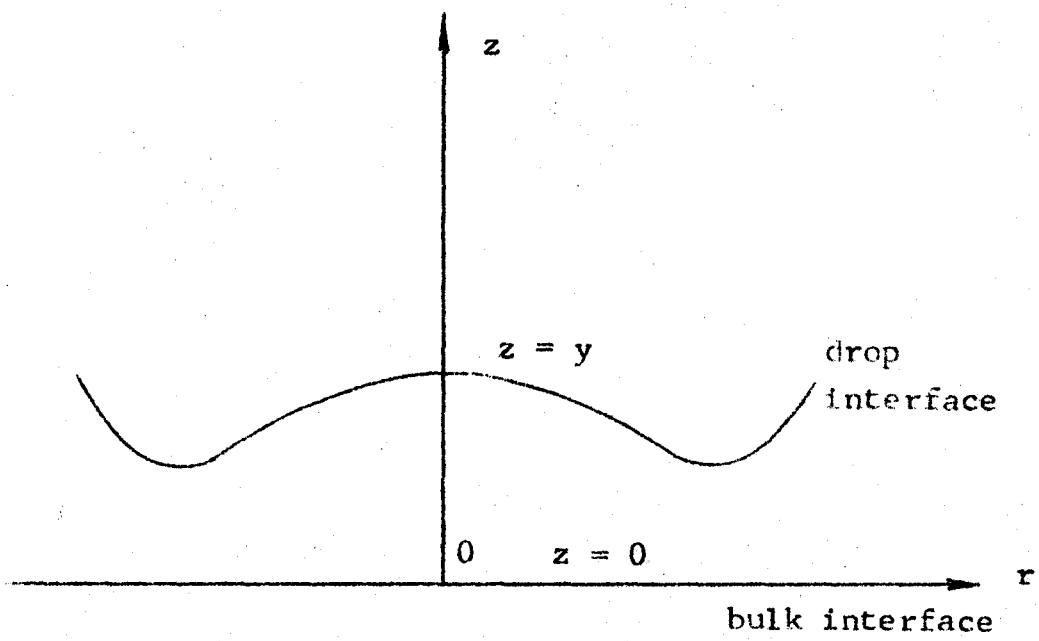

Figure 3a. Calculated Lamella Pressure Distributions for Three Models

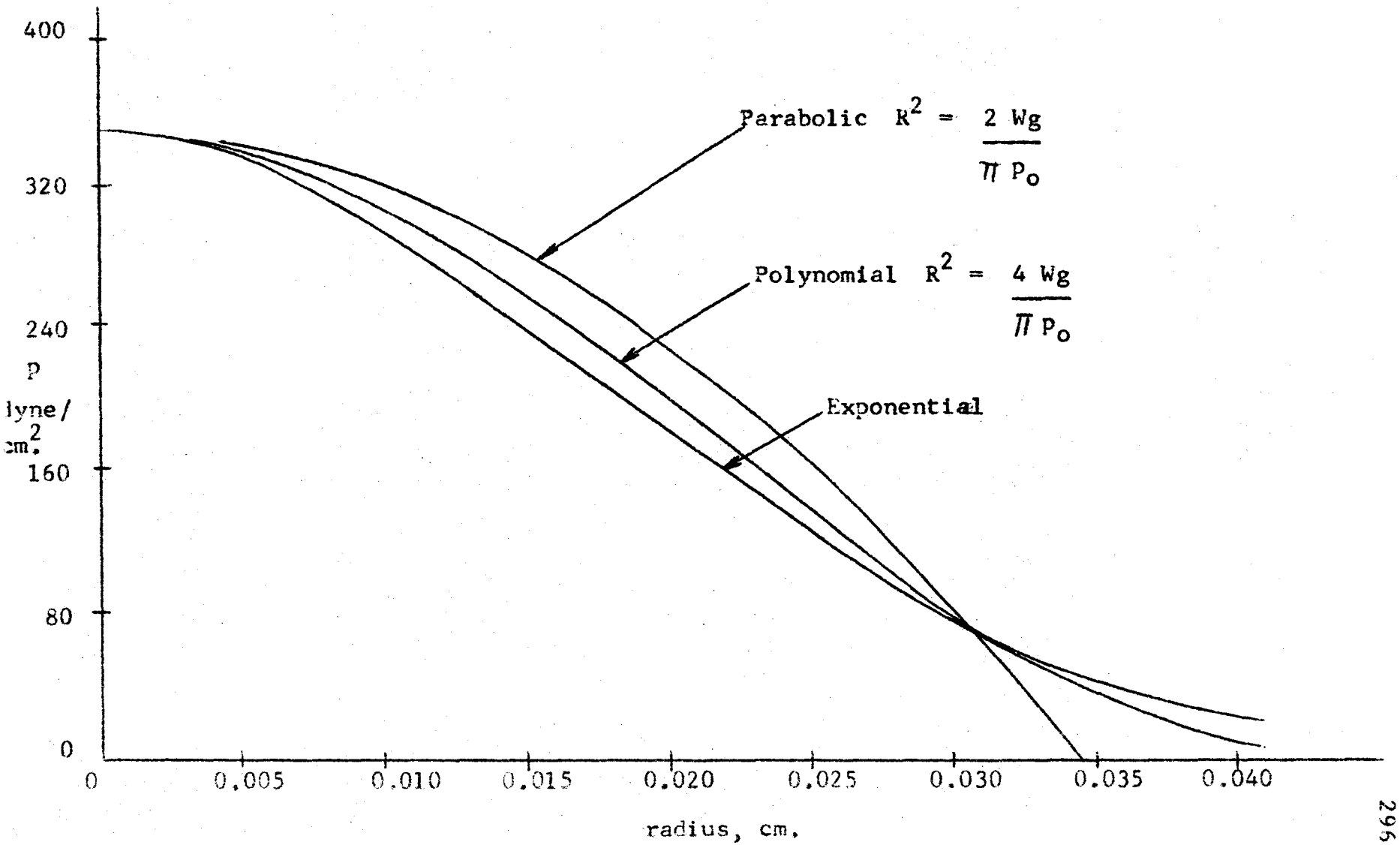

Figure 3a. Pressure Models

1. Parabolic (Parallel Disc Model)

$$p = p_o\left(1 - \left(\frac{r}{R}\right)^2\right)$$

$$\text{where} \quad R^2 = \frac{2\,Wg}{\pi\, p_o}$$

2. Polynomial (Series Type, in Appendix A2)

$$p = p_o - 3\,p_o\left(\frac{r}{R}\right)^2 + 3\,p_o\left(\frac{r}{R}\right)^4 - p_o\left(\frac{r}{R}\right)^6$$

$$\text{where} \quad R^2 = \frac{4\,Wg}{\pi\, p_o}$$

3. Exponential

$$p = p_o\, e^{-\lambda r^2}$$

$$\text{where} \quad \lambda = \frac{\pi\, p_o}{Wg}$$

Figure 3b. Calculated Relative Lamella Shapes for the Three Pressure Models in Figure (3a)

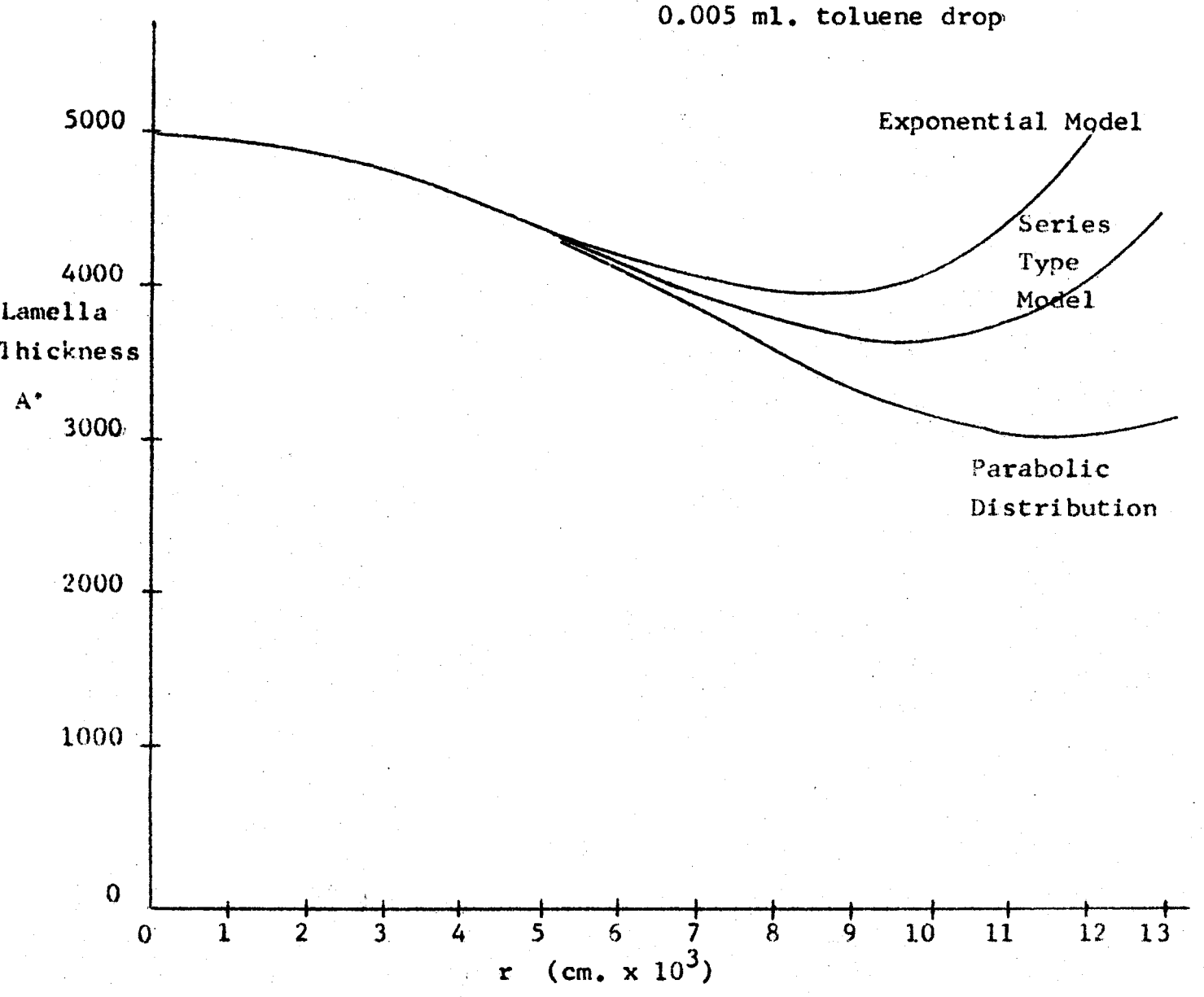

Figure 4. Interface Geometry

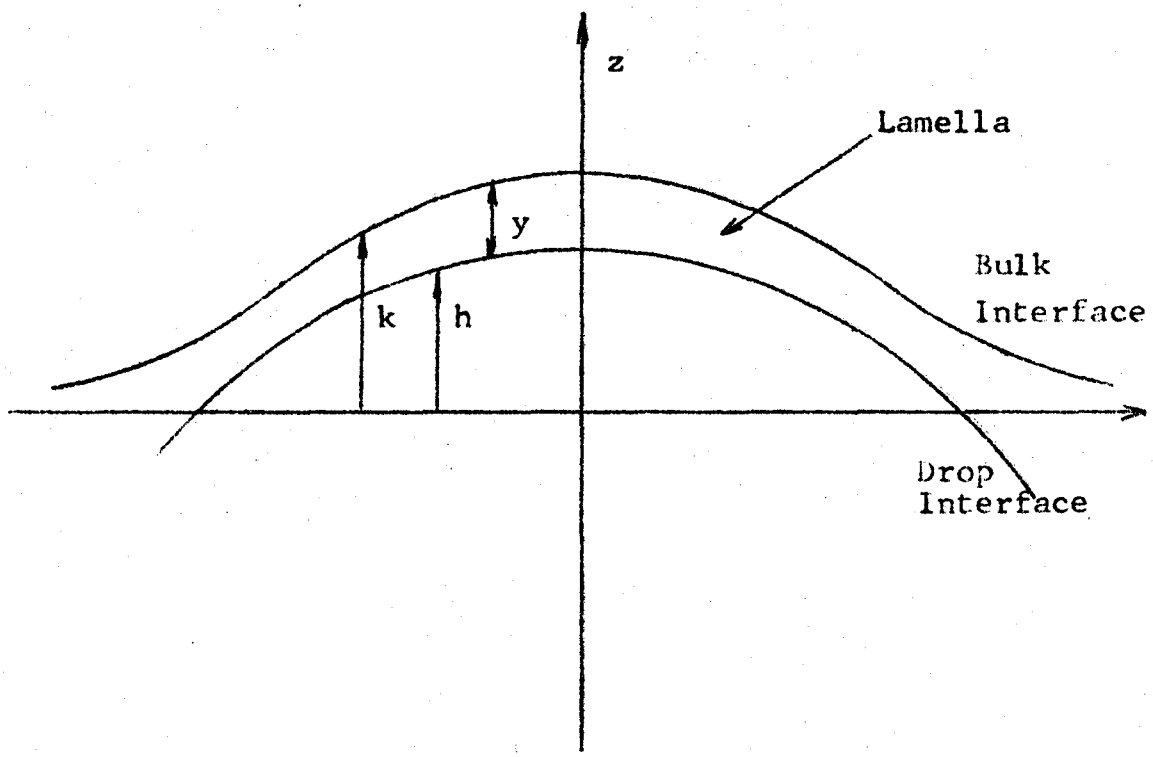

Figure 5. Bulk Interface Geometry

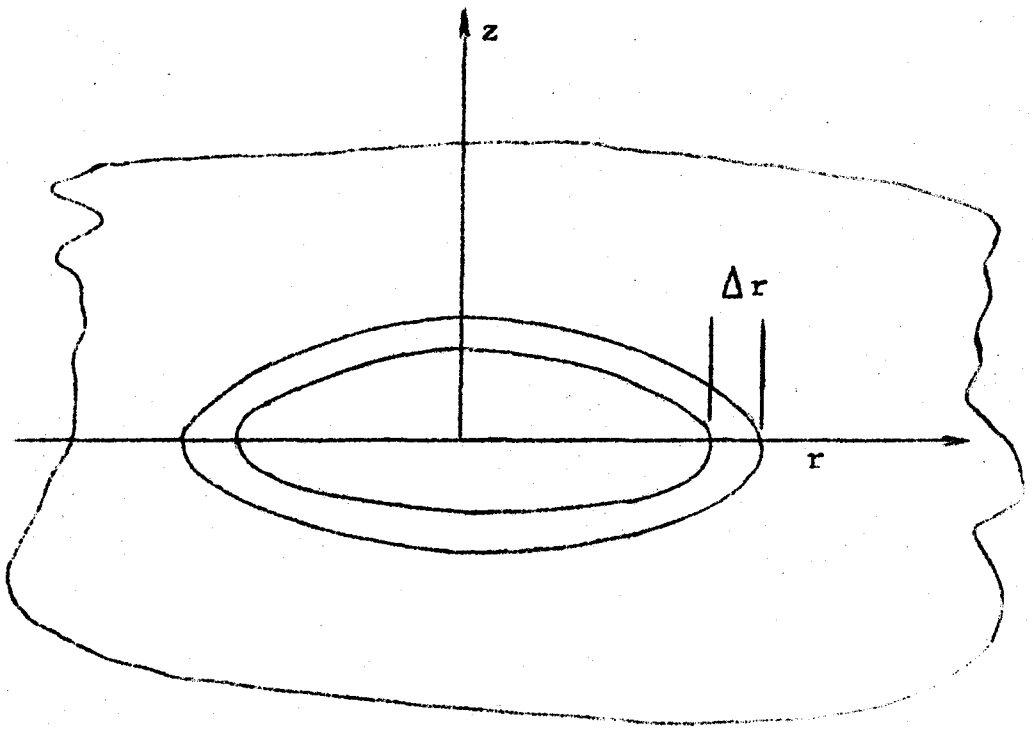

Figure 6. Comparison Between the Expected Interfacial Distribution of Surfactant and the Distribution Predicted by Equation (33)

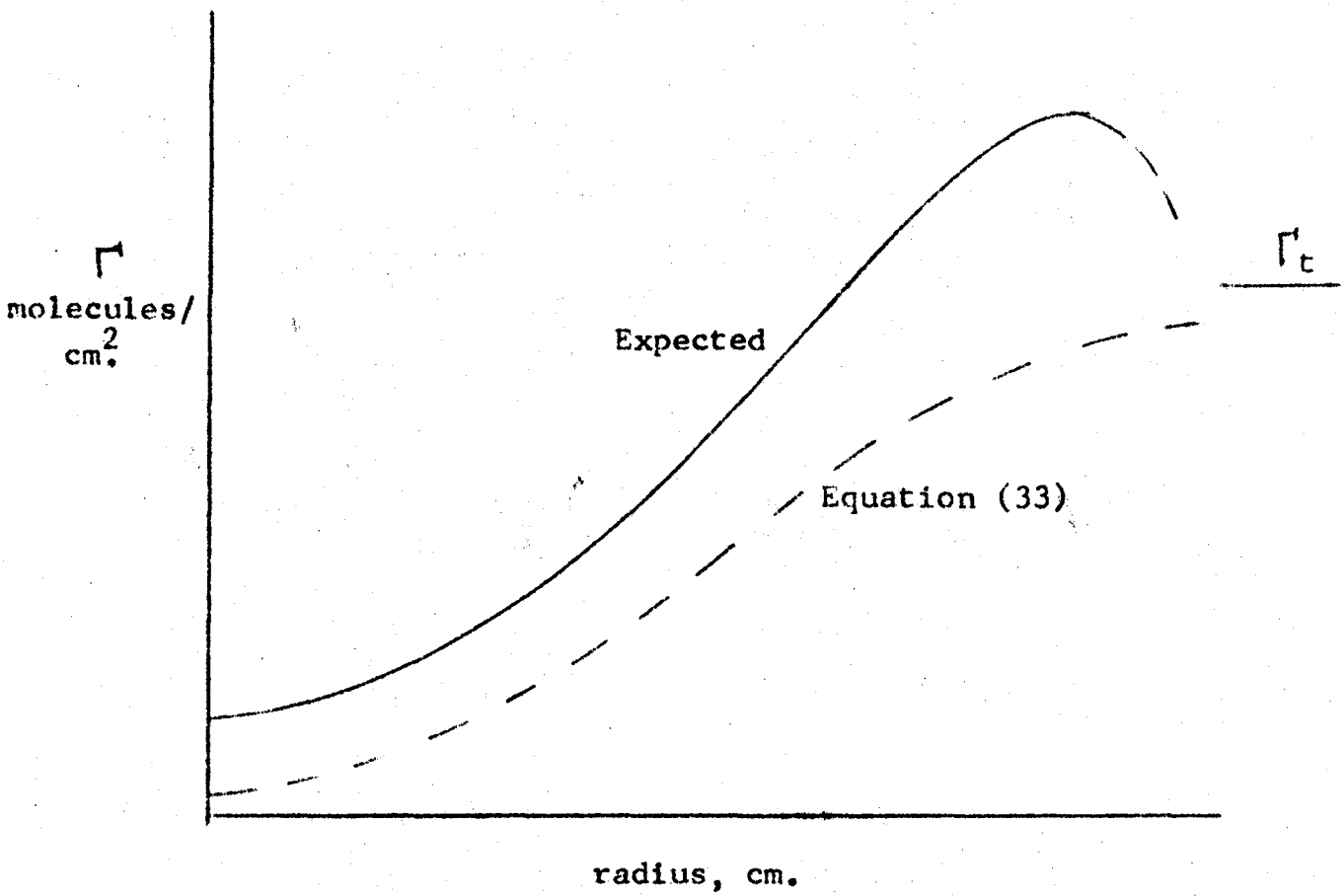

Figure 7a. Lamella Thinning for the Bulk Interface Laterally Rigid

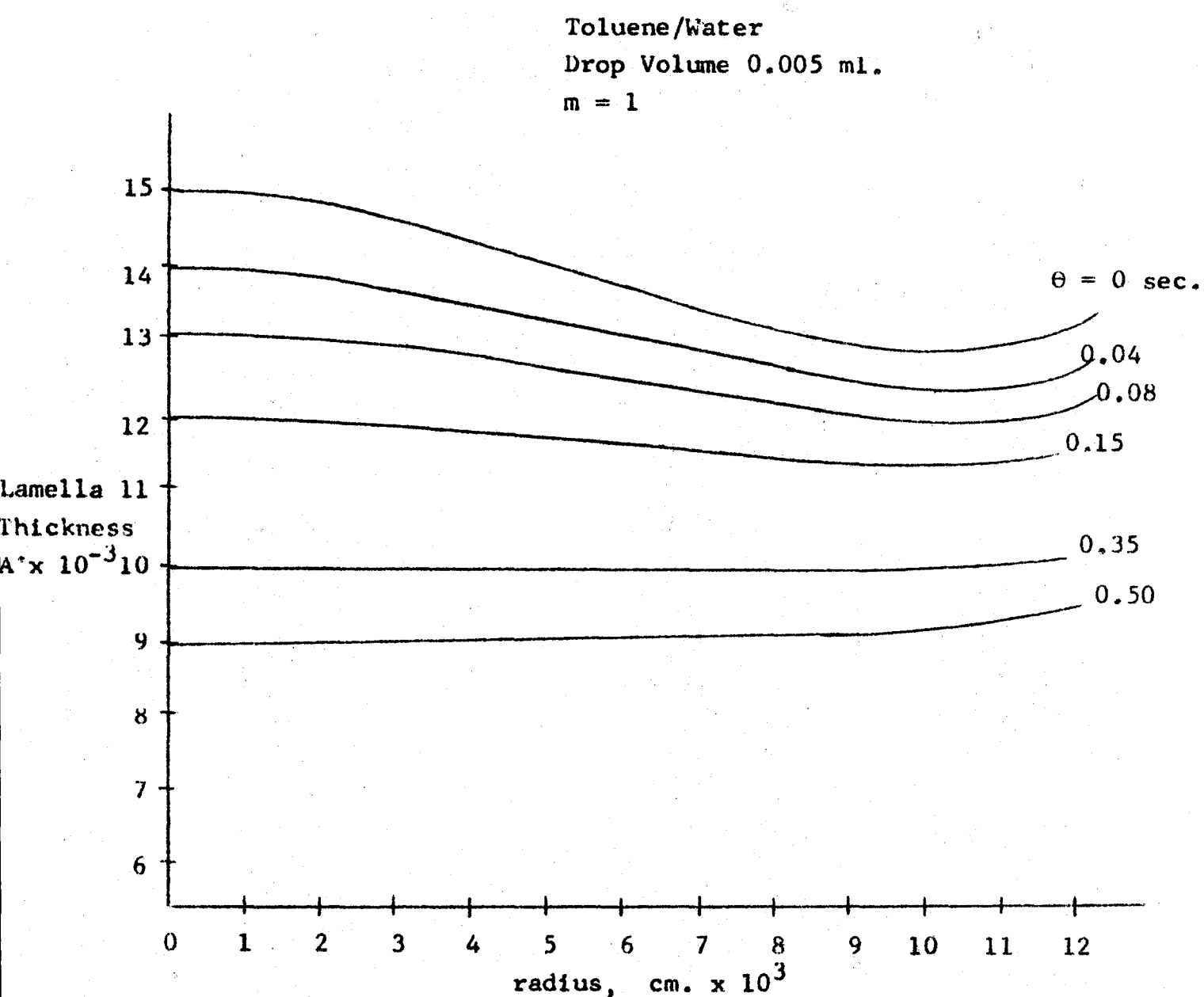

Figure 7b. Lamella Thinning for the Bulk Interface Laterally Rigid

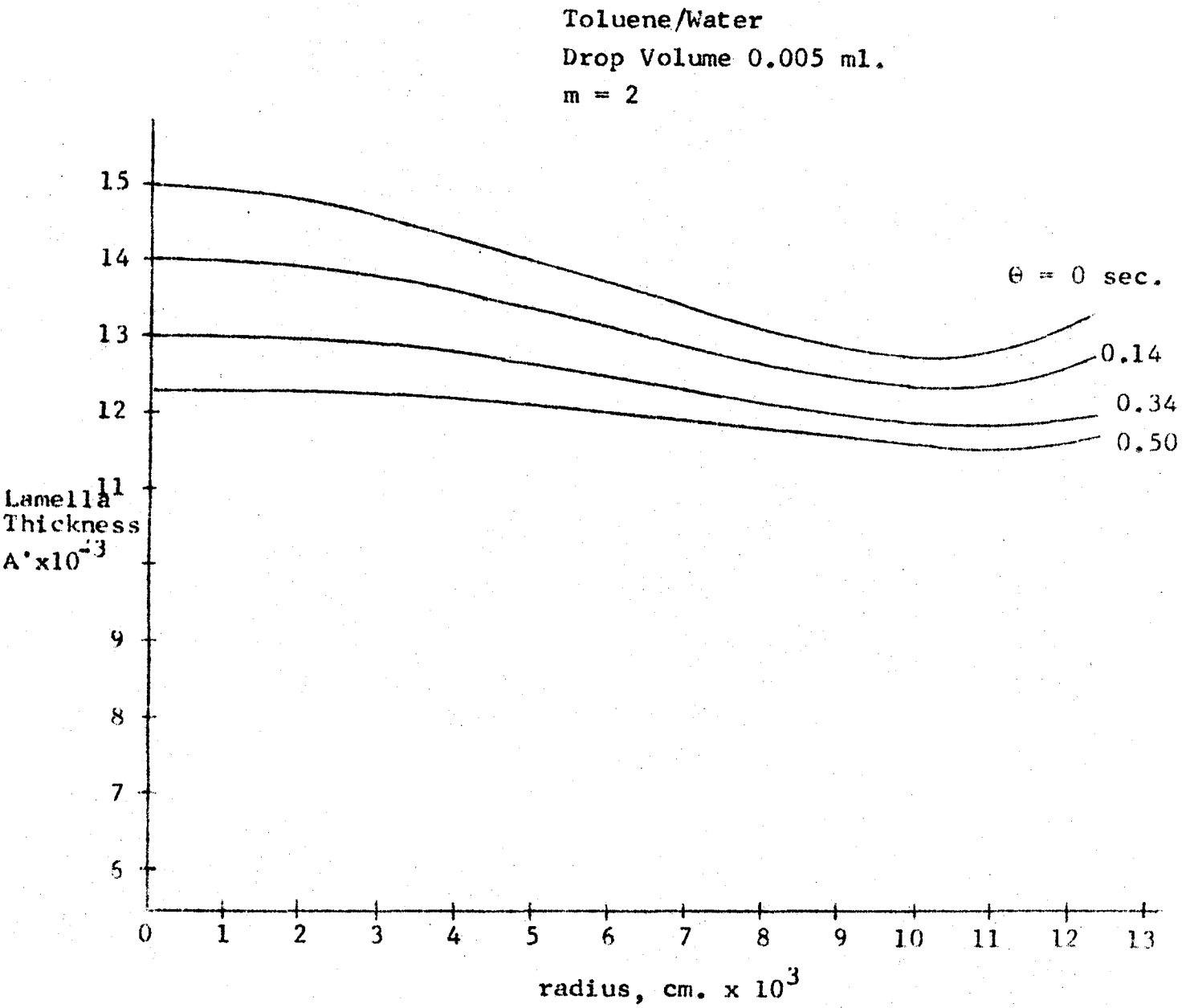

Figure 7c. Lamella Thinning for the Bulk Interface Laterally Rigid

Anisole/Water
Drop Volume 0.020 ml,
m = 1

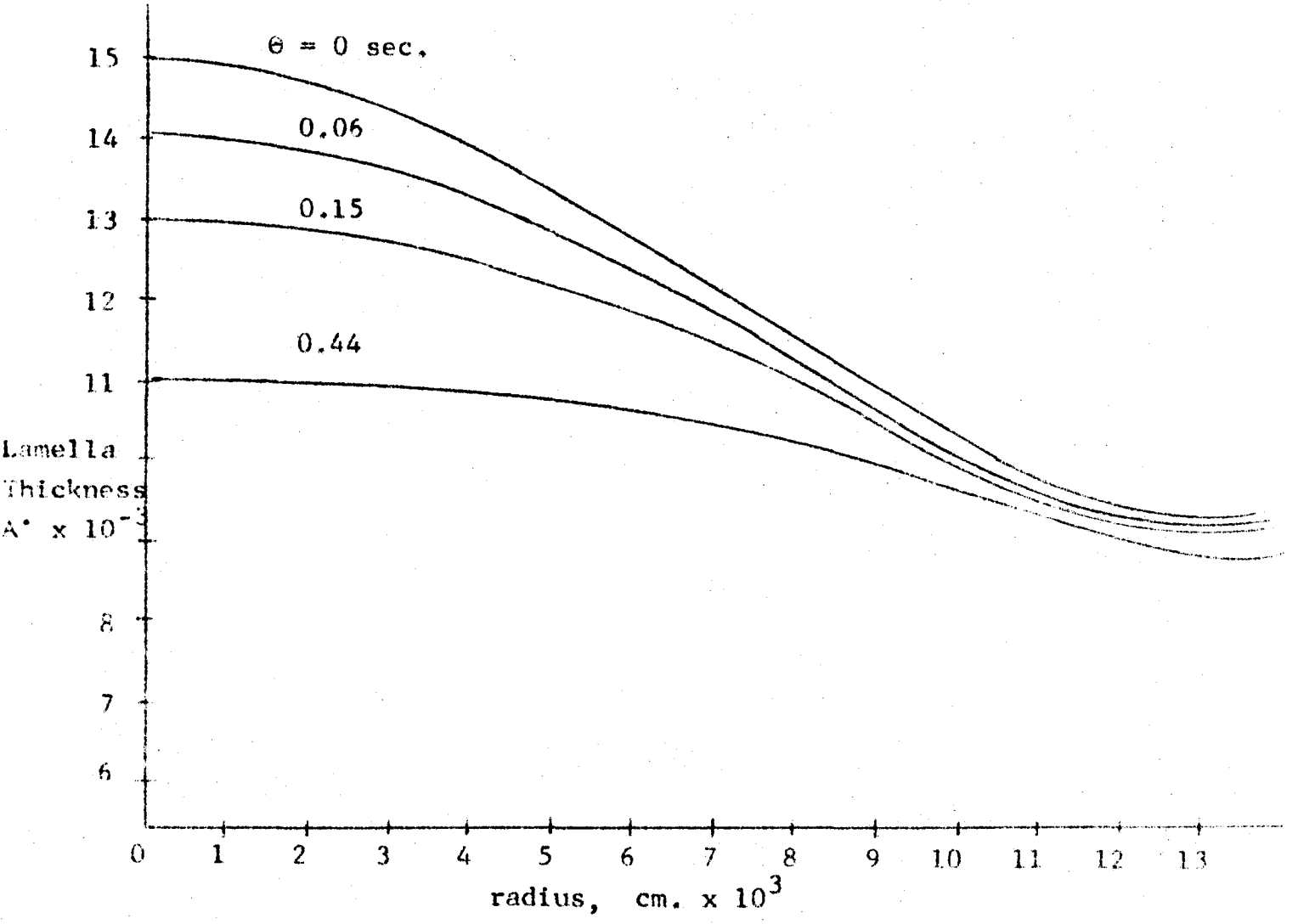

Figure 7d. Lamella Thinning for the Bulk Interface Laterally Rigid

Cyclohexanol/Water
Drop Volume 0.001 ml.
m = 2

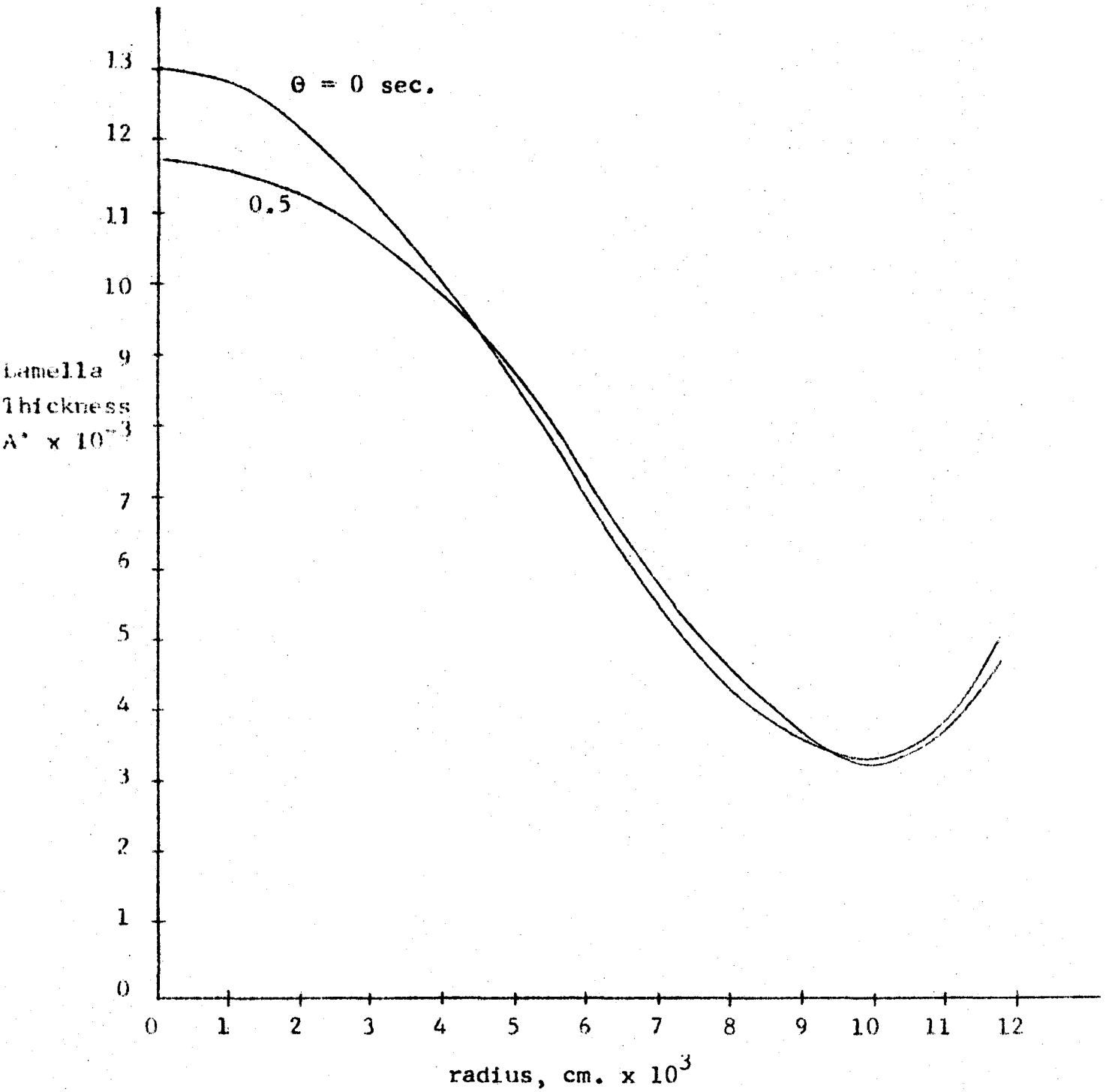

Figure 8a. Calculated Lamella Thinning

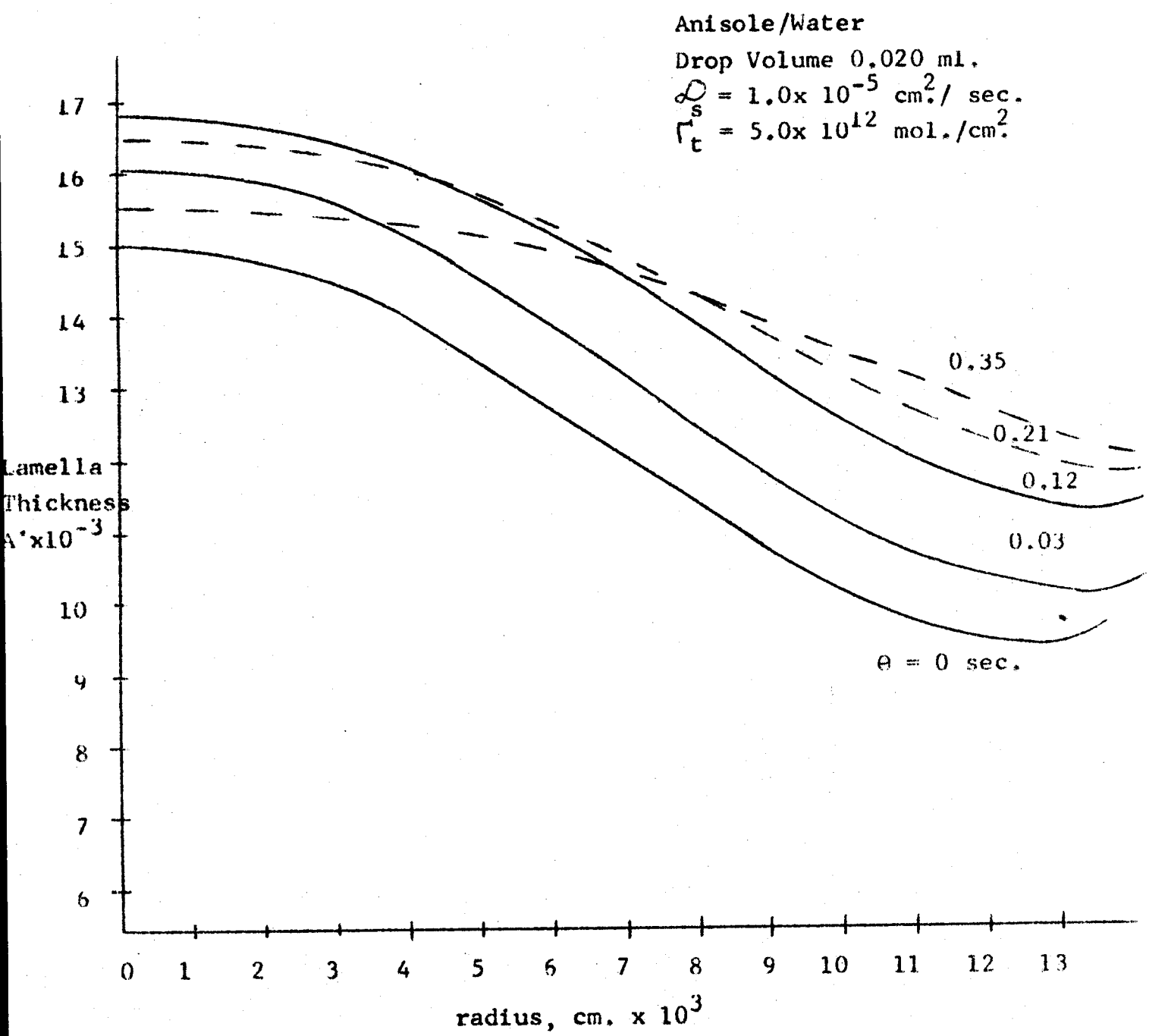

Figure 8b. Calculated Lamella Thinning

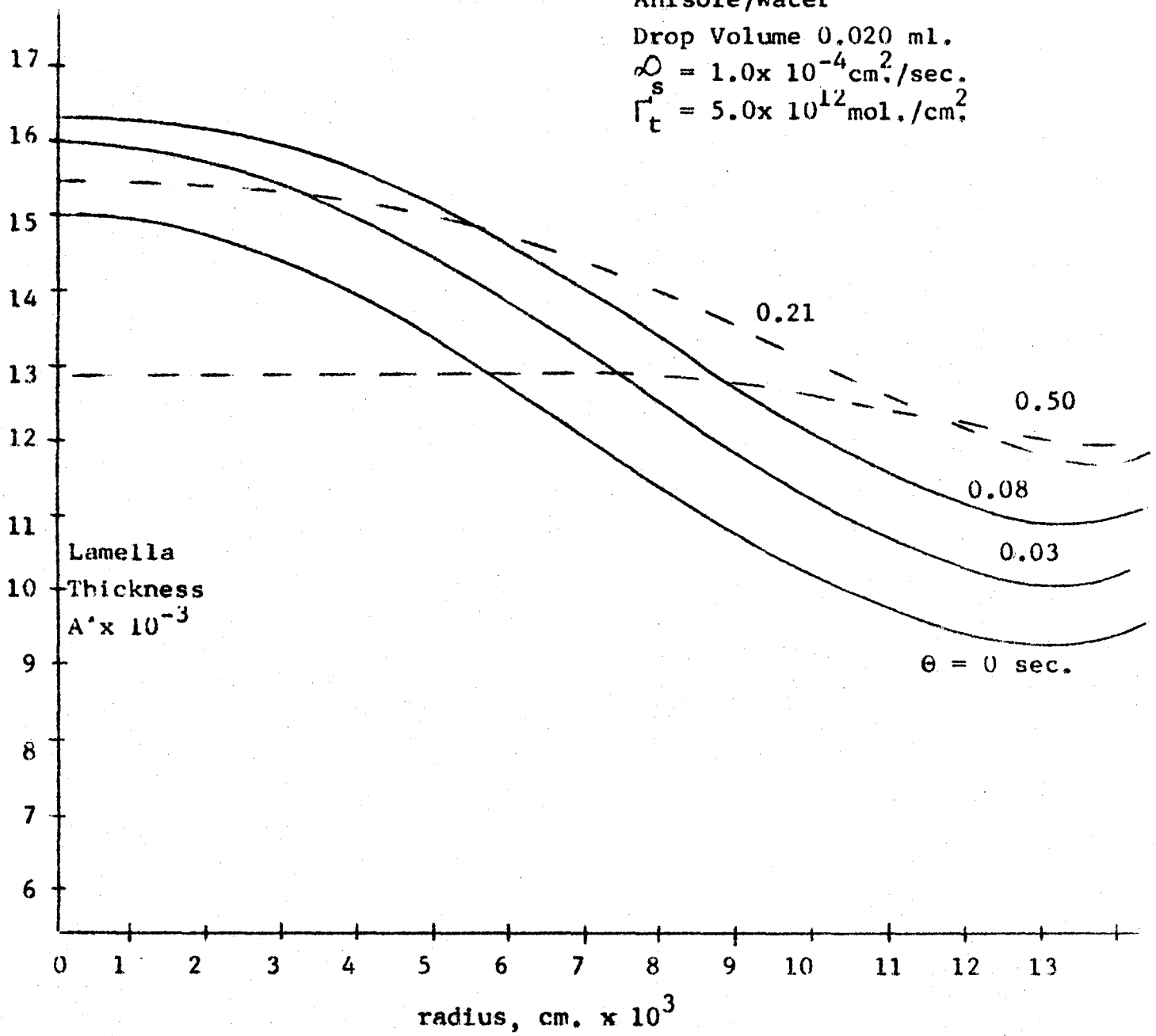

Figure 8c. Calculated Lamella Thinning

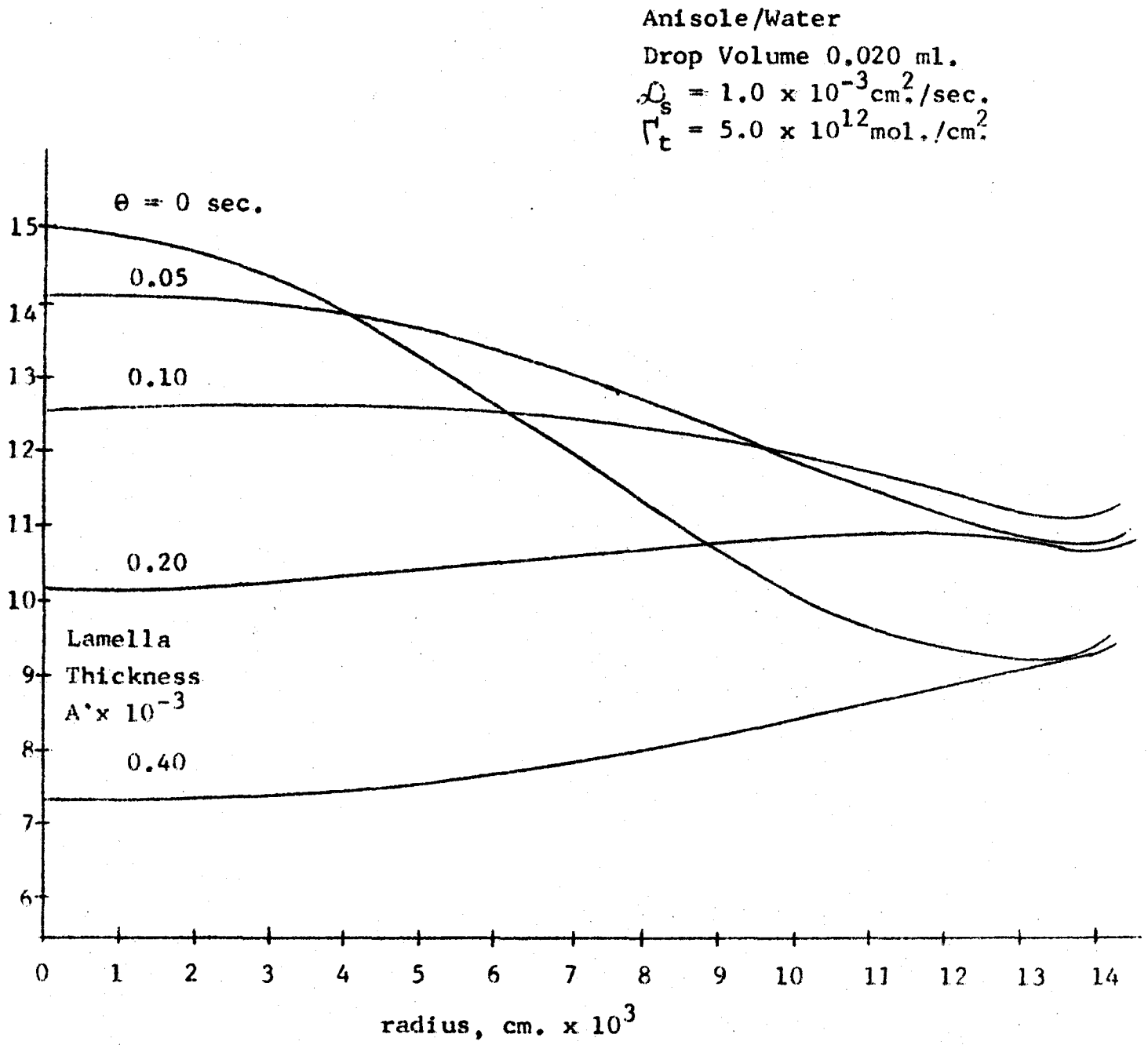

Figure 8d. Calculated Lamella Thinning

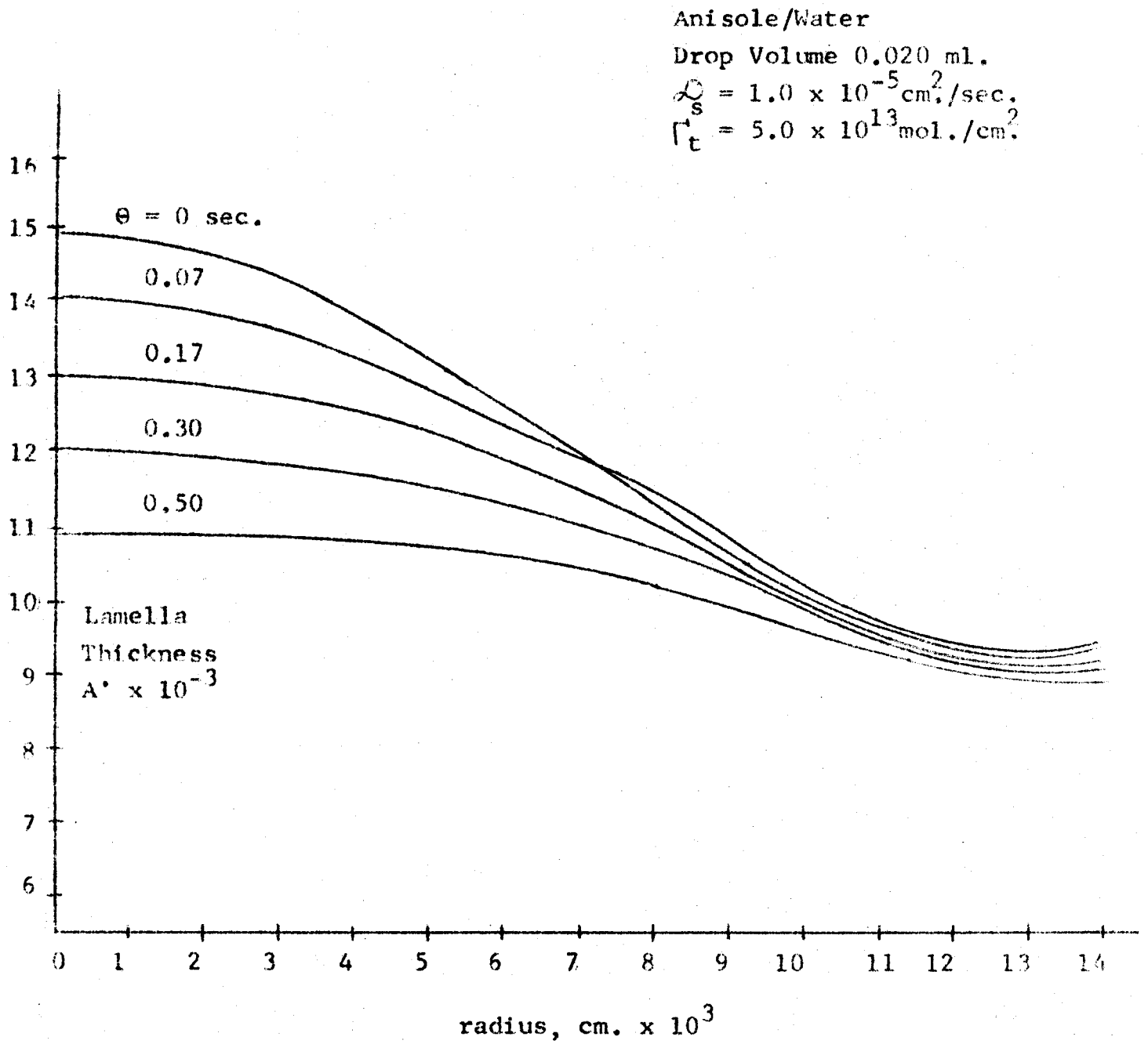

Figure 9. Radial Distribution of Surfactant in the Bulk Interface

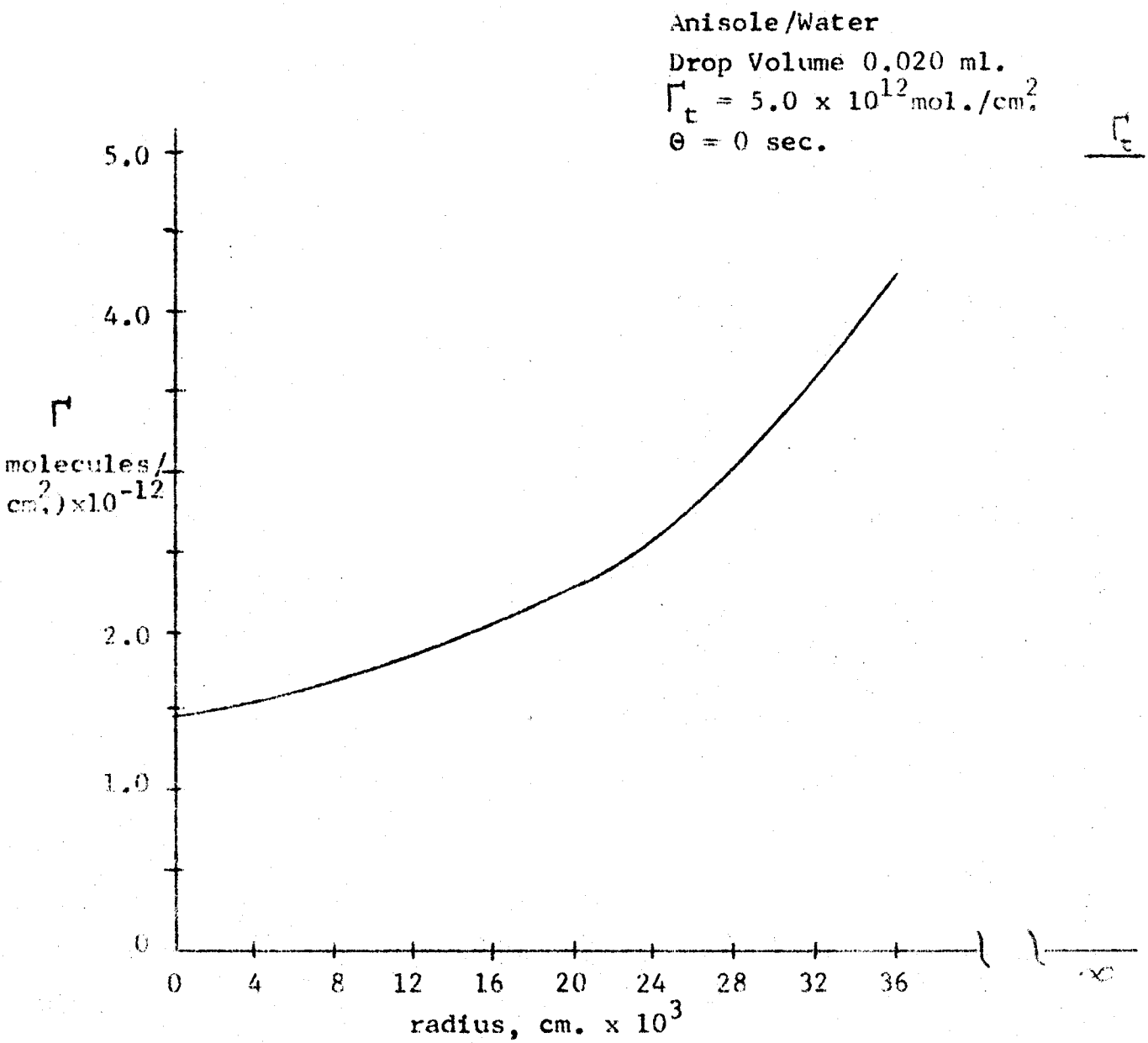

Figure 10. Radial Velocity of the Bulk Interface During Lamella Thinning

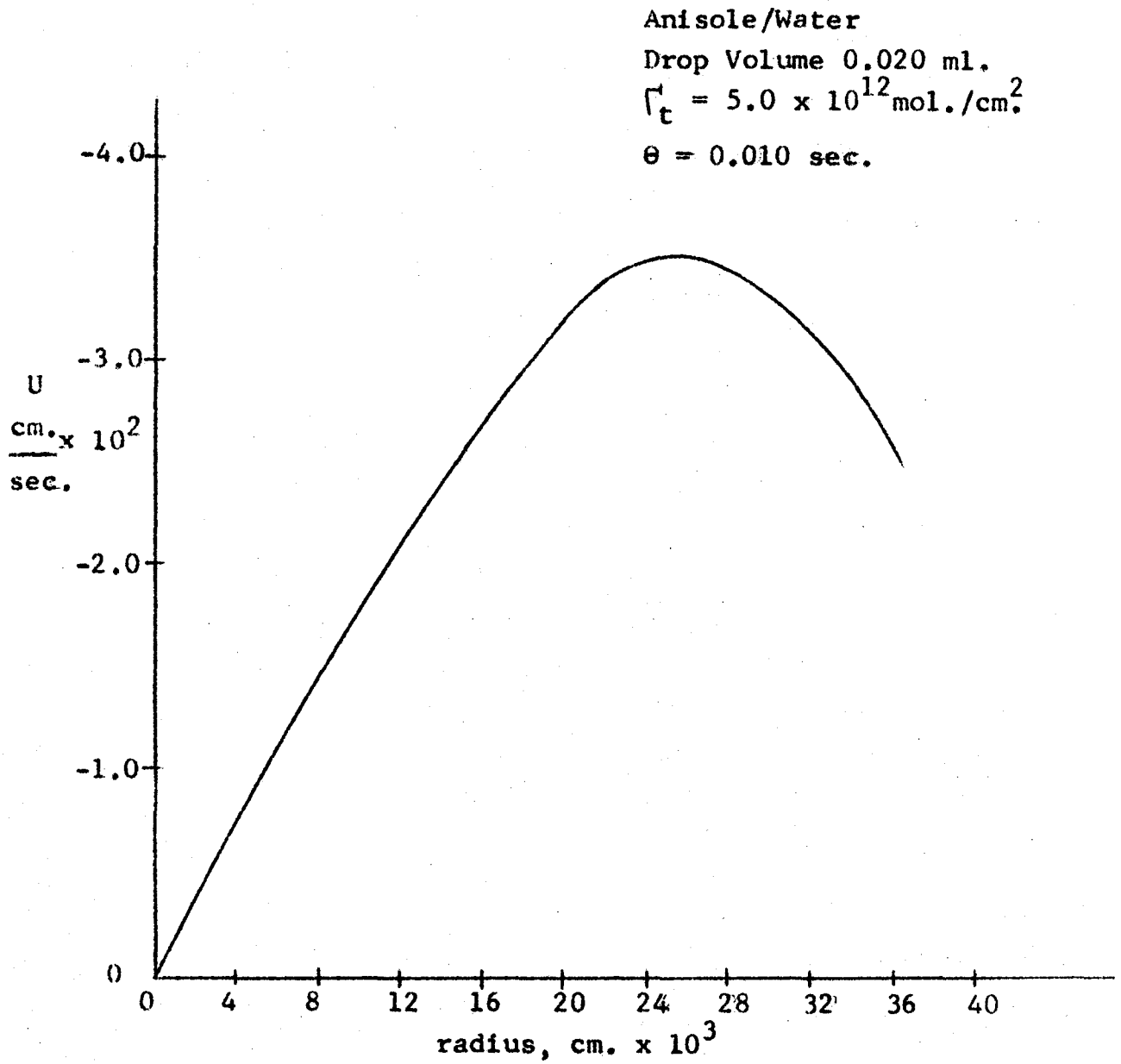

Figure 11a. Observed Dimpling and Slow, Even Thinning

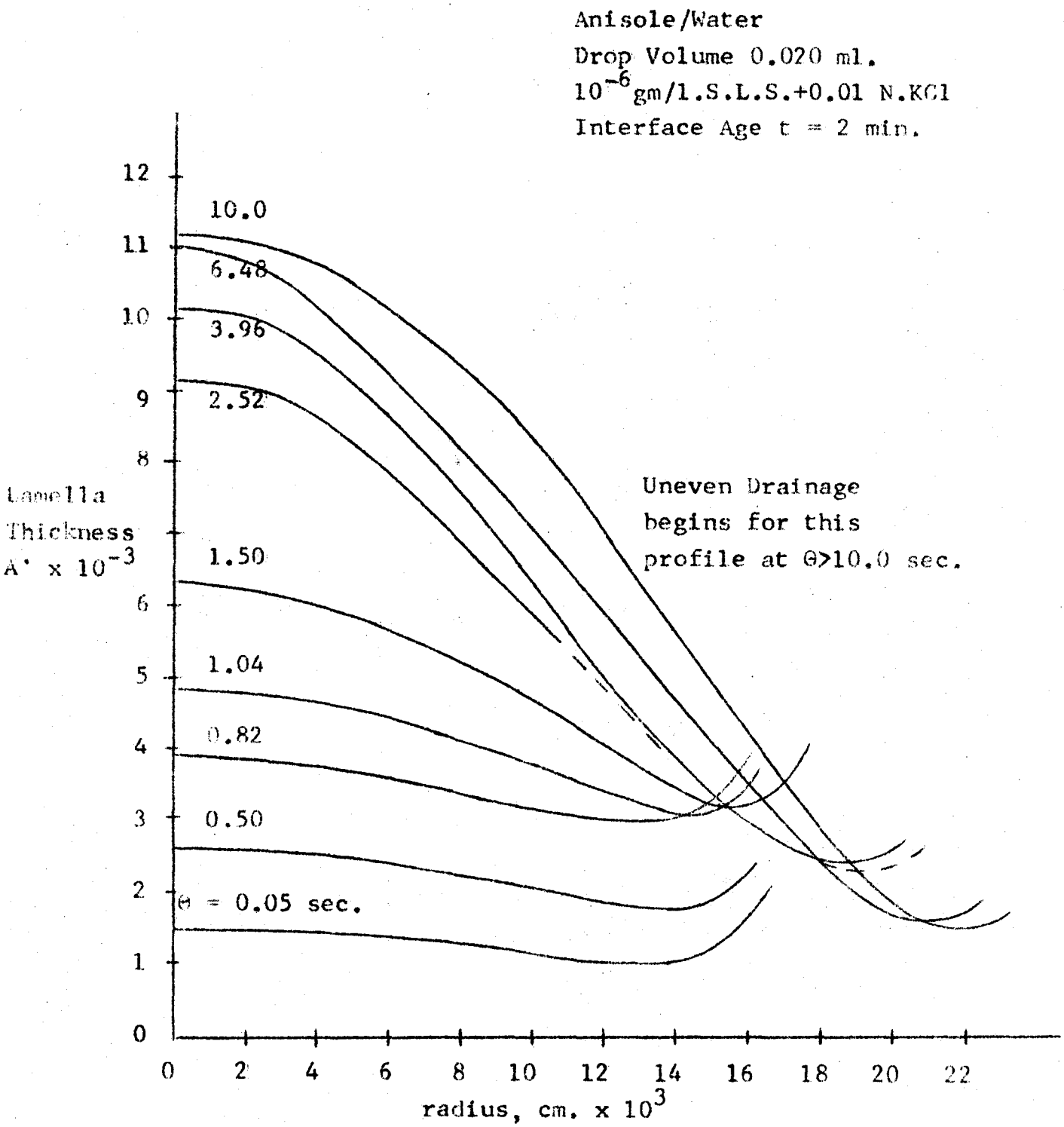

Figure 11b. Observed Dimpling and Simultaneous Slow, Even Thinning

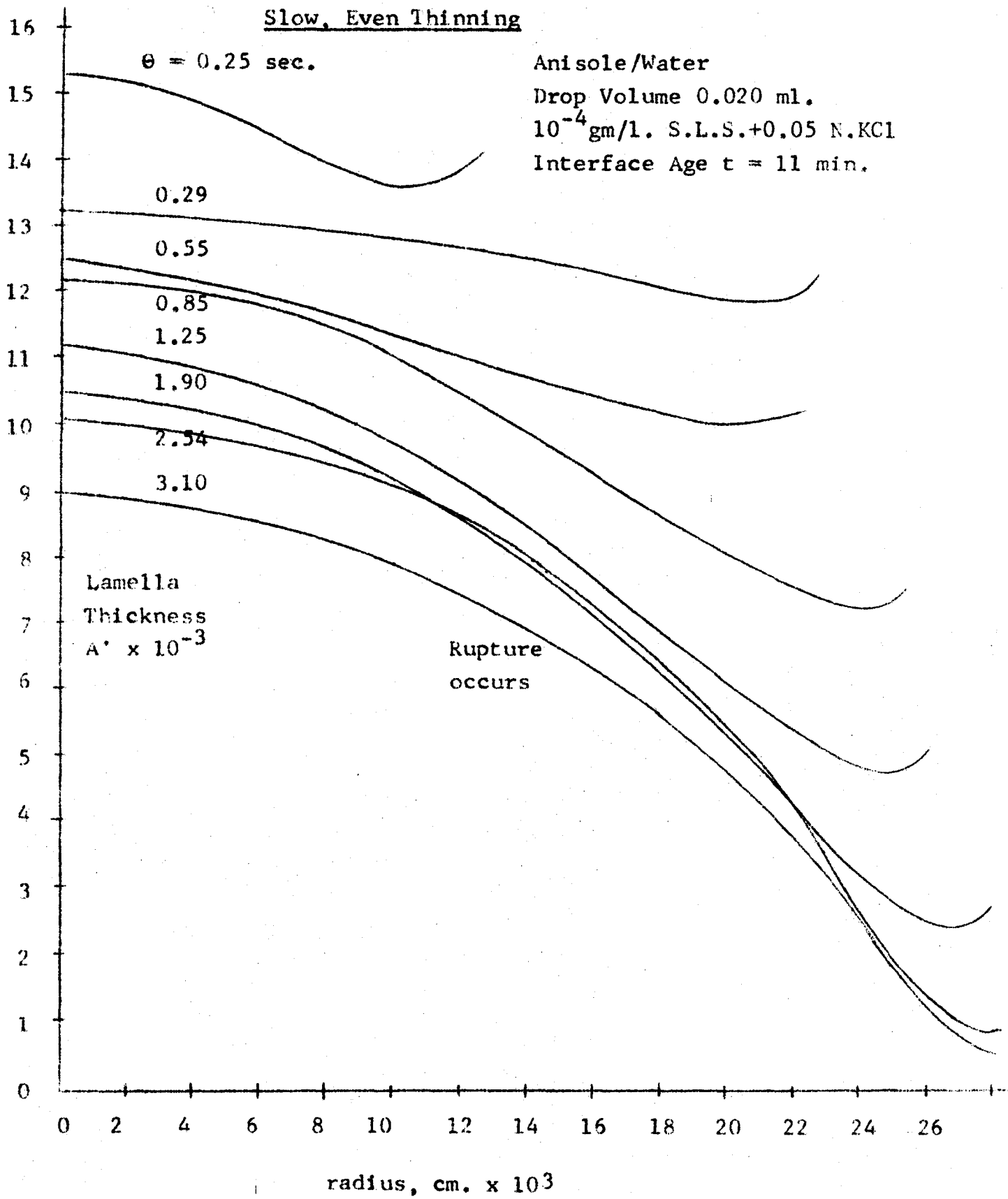

Figure 11c. Observed Slow, Even Thinning

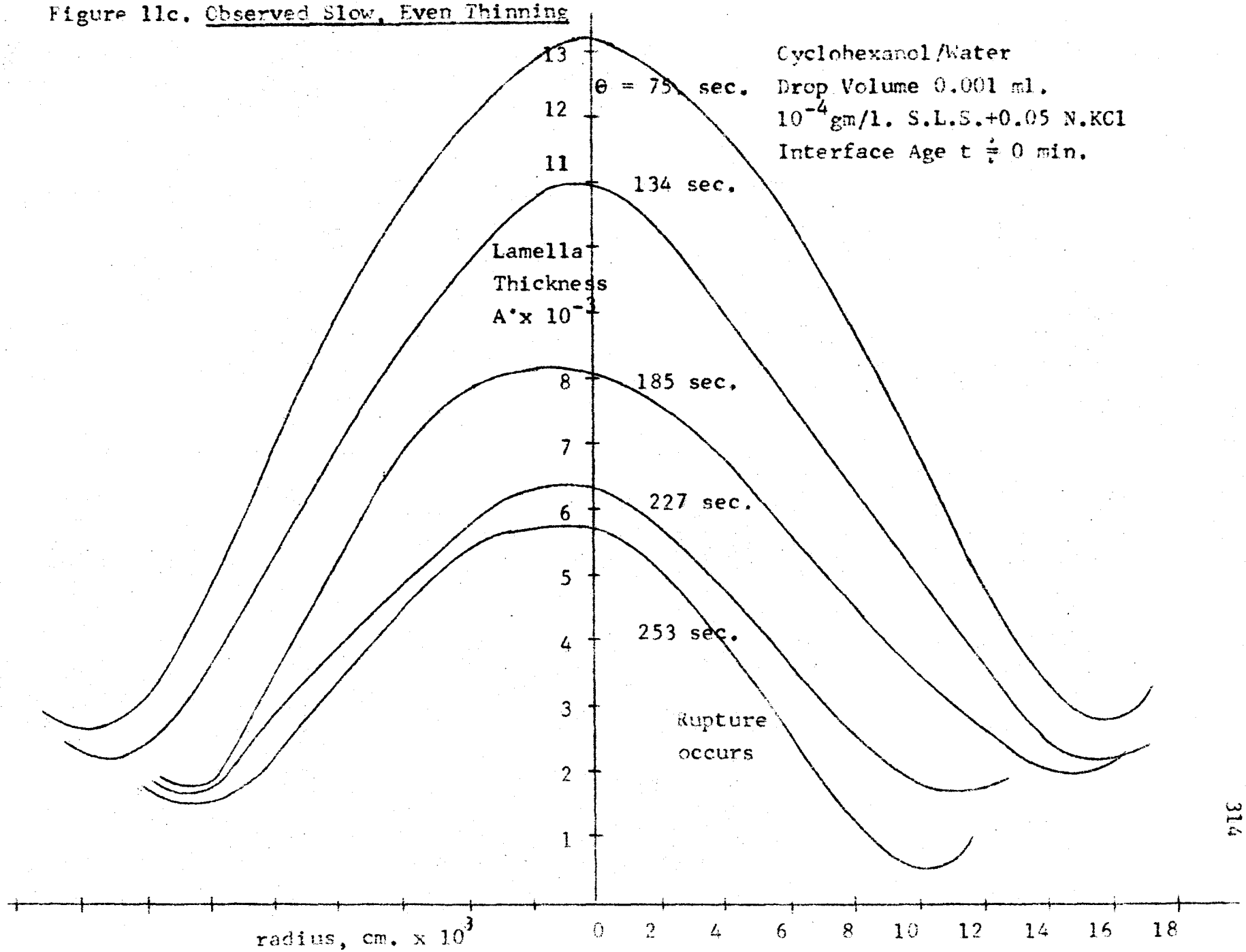

Figure 12. Comparison of Surfactant Concentration in the Bulk Interface, for Two Models

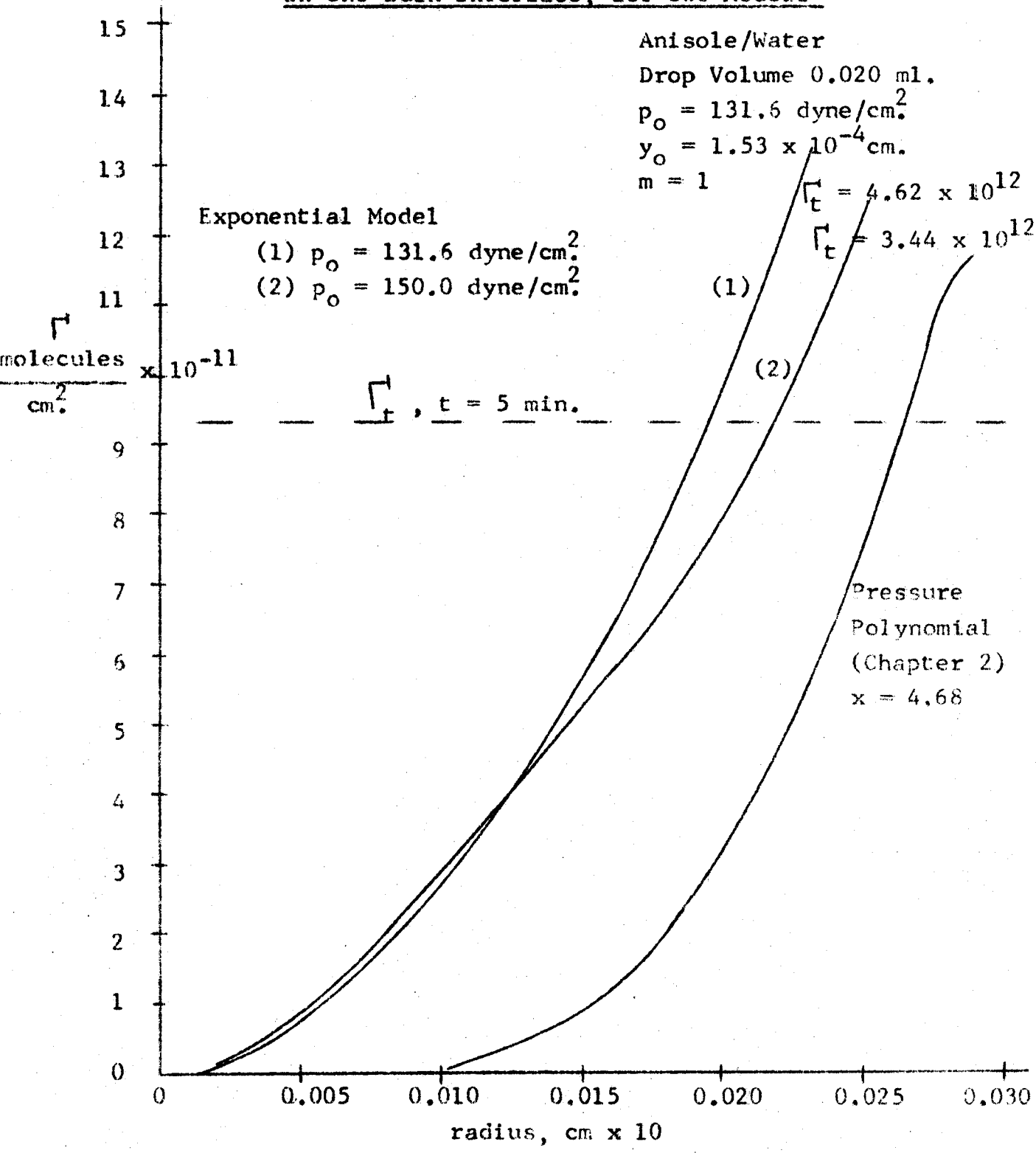

Figure 13. Re-description of Problem Geometry

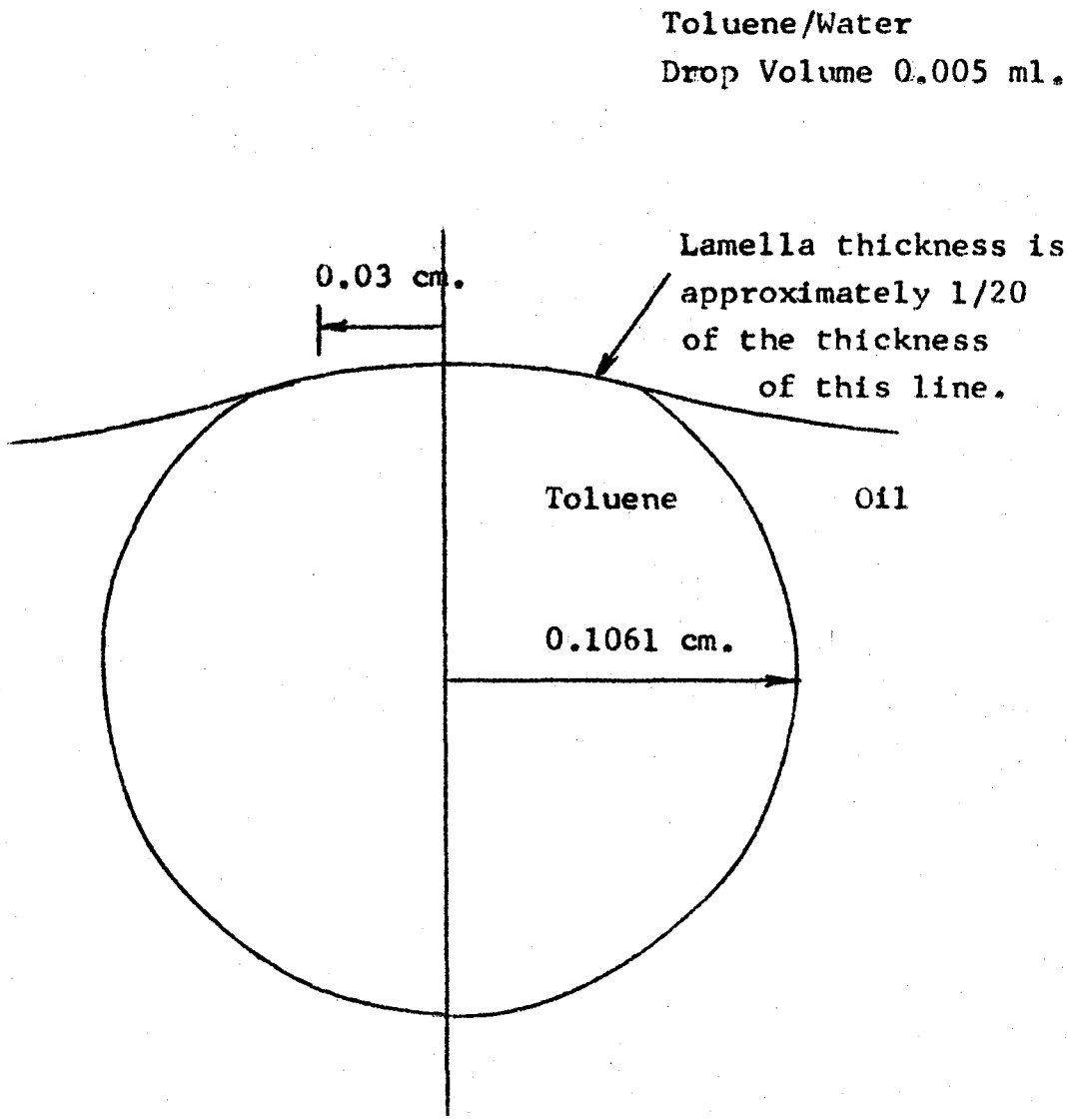

Figure 14. Algorithm for the Solution of the Coupled Equations

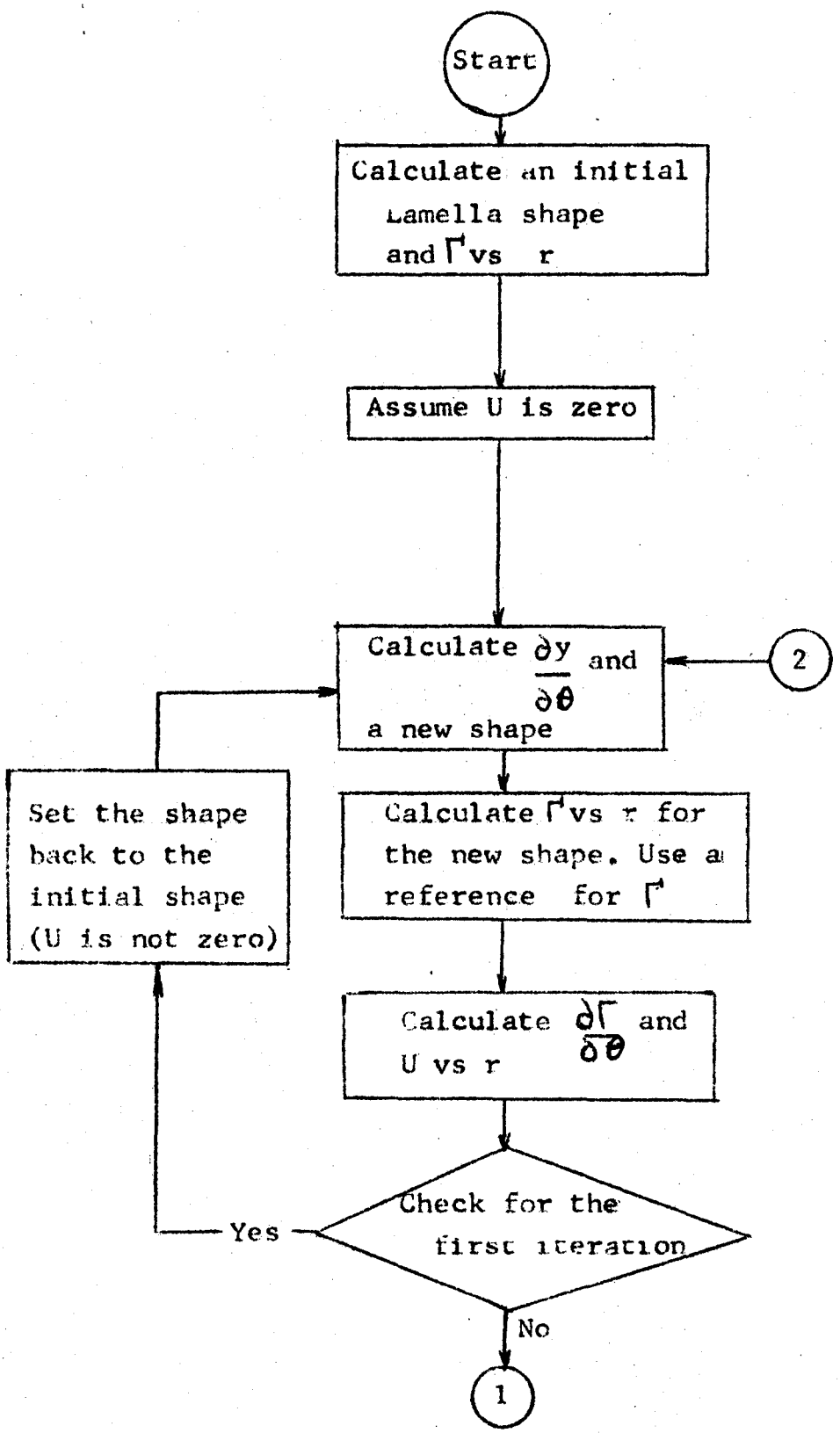

Figure 14 (cont'd)

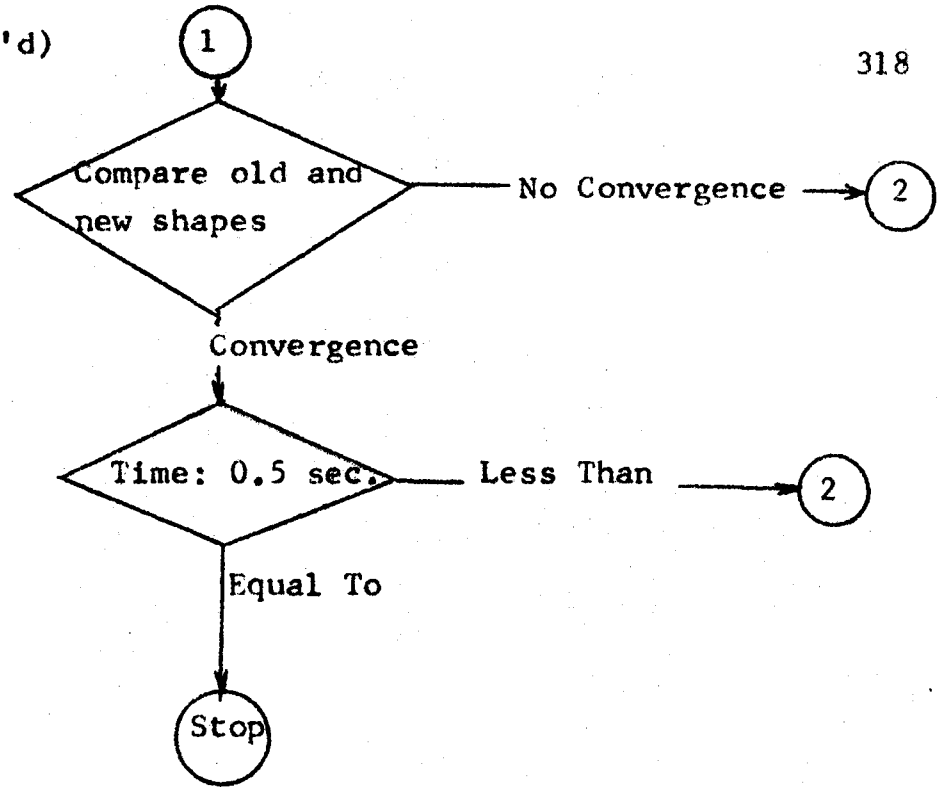

Figure 15a. Comparison of the Coupled Model with Barrier Ring Thinning Data

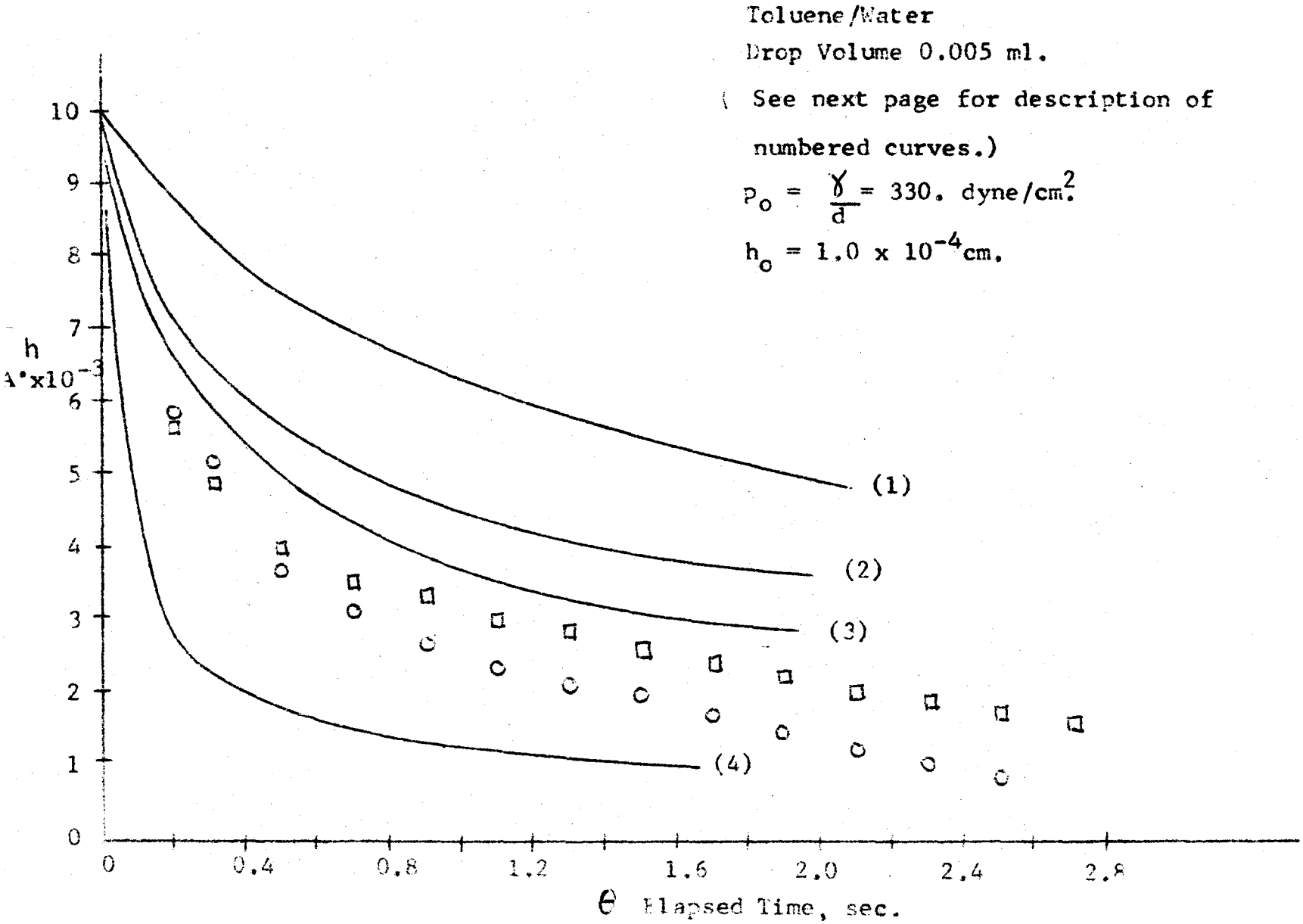

Notes on Figure 15a.

Curve (1) : Calculated from equation (50).

$k\Gamma_t = 0$

$R^2 = \frac{2 W g}{\pi p_o}$

Approximate model

Curve (2) : Calculated from equation (50).

$k\Gamma_t = 0$

$R^2 = \frac{W g}{\pi p_o}$

Equilibrium model

Curve (3) : Calculated from equation (49).

$k\Gamma_t = 0.01$ dyne/cm.

$R^2 = \frac{W g}{\pi p_o}$

$c = 0.0175$ cm.

Curve (4) : Calculated from equation (49).

$k\Gamma_t = 0.001$ dyne/cm.

$R^2 = \frac{W g}{\pi p_o}$

$c = 0.0175$ cm.

Figure 15b. Comparison of the Coupled Model with Barrier Ring Thinning Data

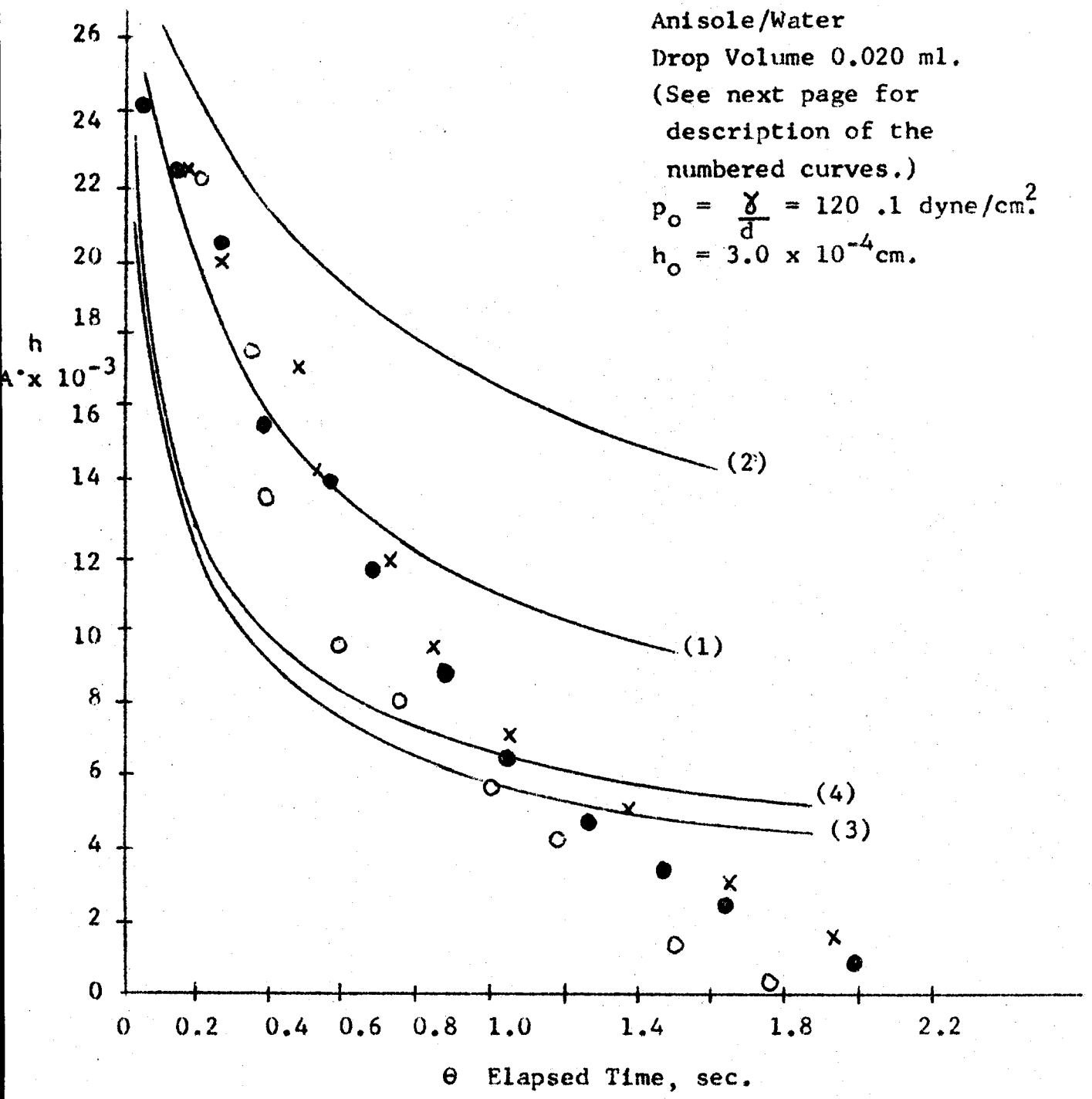

Notes on Figure 15b.

Curve (1) : $k\Gamma_t' = 0.001$ dyne/cm.

$$R^2 = \frac{2 W g}{\pi p_o}$$

$c = 0.020$ cm.

Curve (2) : $k\Gamma_t' = 0.01$ dyne/cm.

$$R^2 = \frac{2 W g}{\pi p_o}$$

$c = 0.020$ cm.

Curve (3) : $k\Gamma_t' = 0.001$ dyne/cm.

$$R^2 = \frac{W g}{\pi p_o}$$

$c = 0.020$ cm.

Curve (4) : $k\Gamma_t' = 0.01$ dyne/cm.

$$R^2 = \frac{W g}{\pi p_o}$$

$c = 0.020$ cm.

All curves calculated from equation (49).

Figure 16. Relative Lamella Thickness Profiles Predicted from the Coupled Model

Toluene/Water
Drop Volume 0.005 ml.
$k\Gamma_t = 0.001$ dyne/cm.
$R^2 = \frac{2 W g}{\pi P_o}$
Calculated from equation (49).

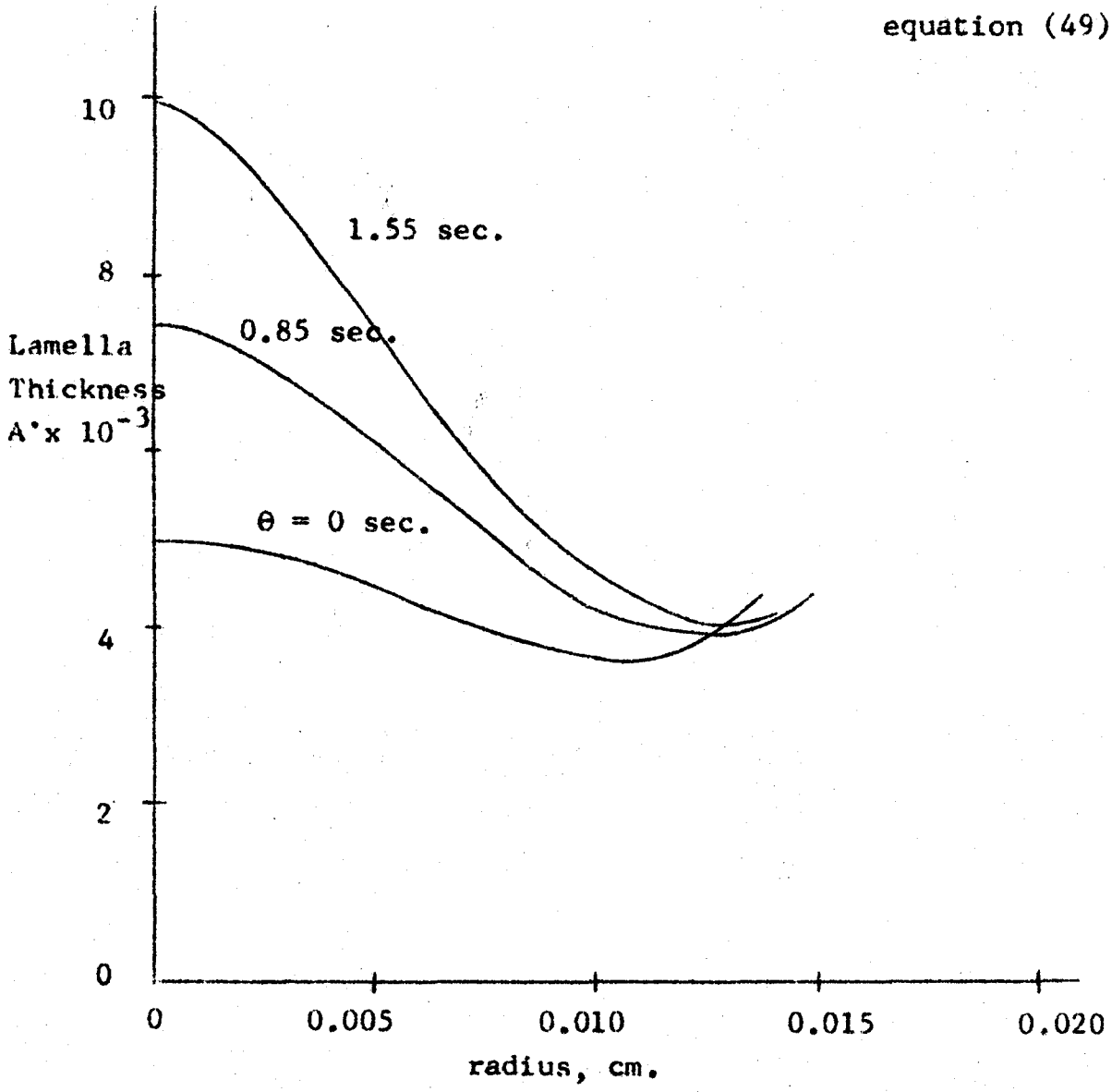

Figure 17. Bulk Interface Velocity versus Radius for the Initial Lamella Profile in Figure (16)

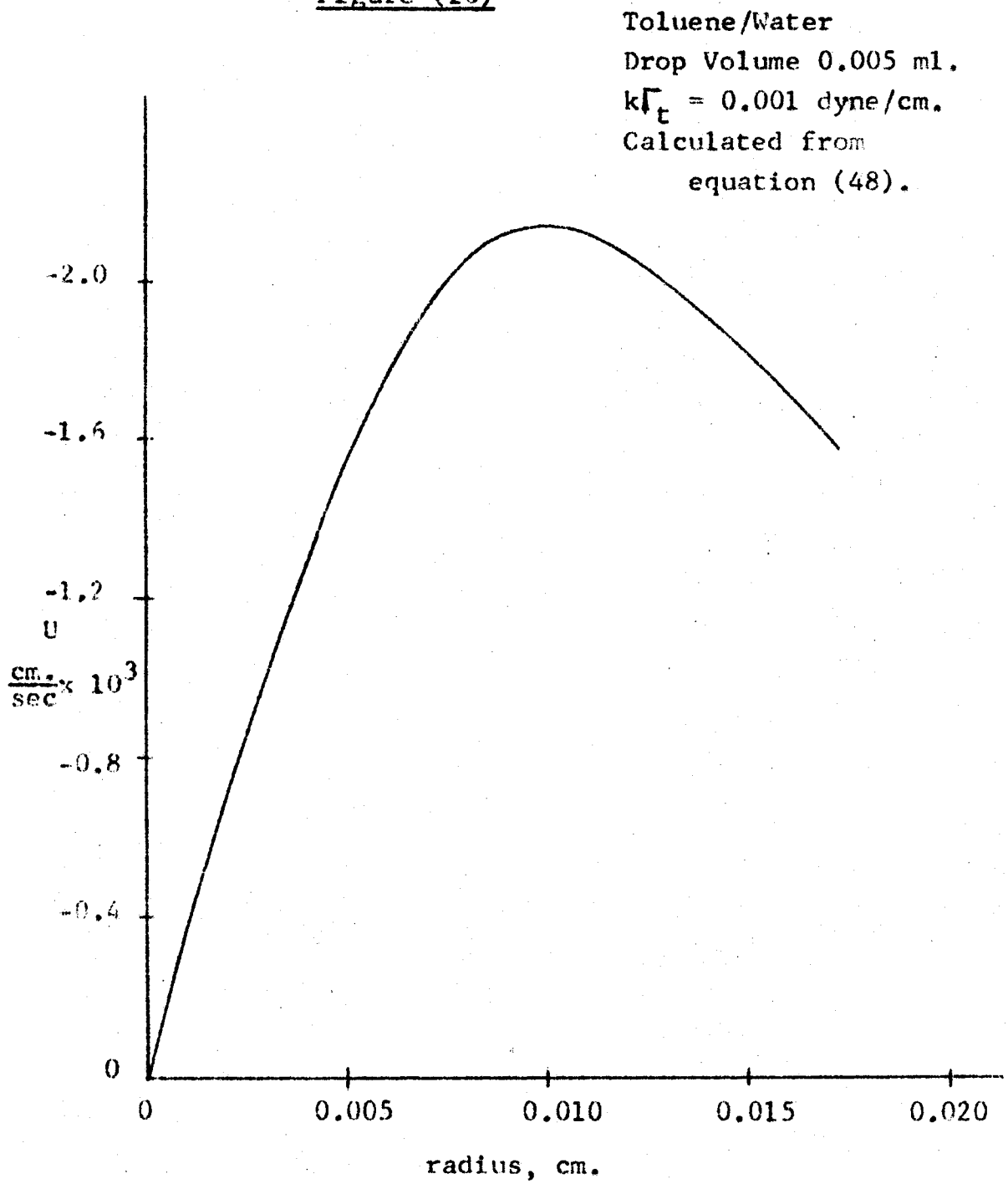

Figure 18. Interfacial Concentration of Surfactant versus Radius, for the Initial Lamella Profile in Figure (16)

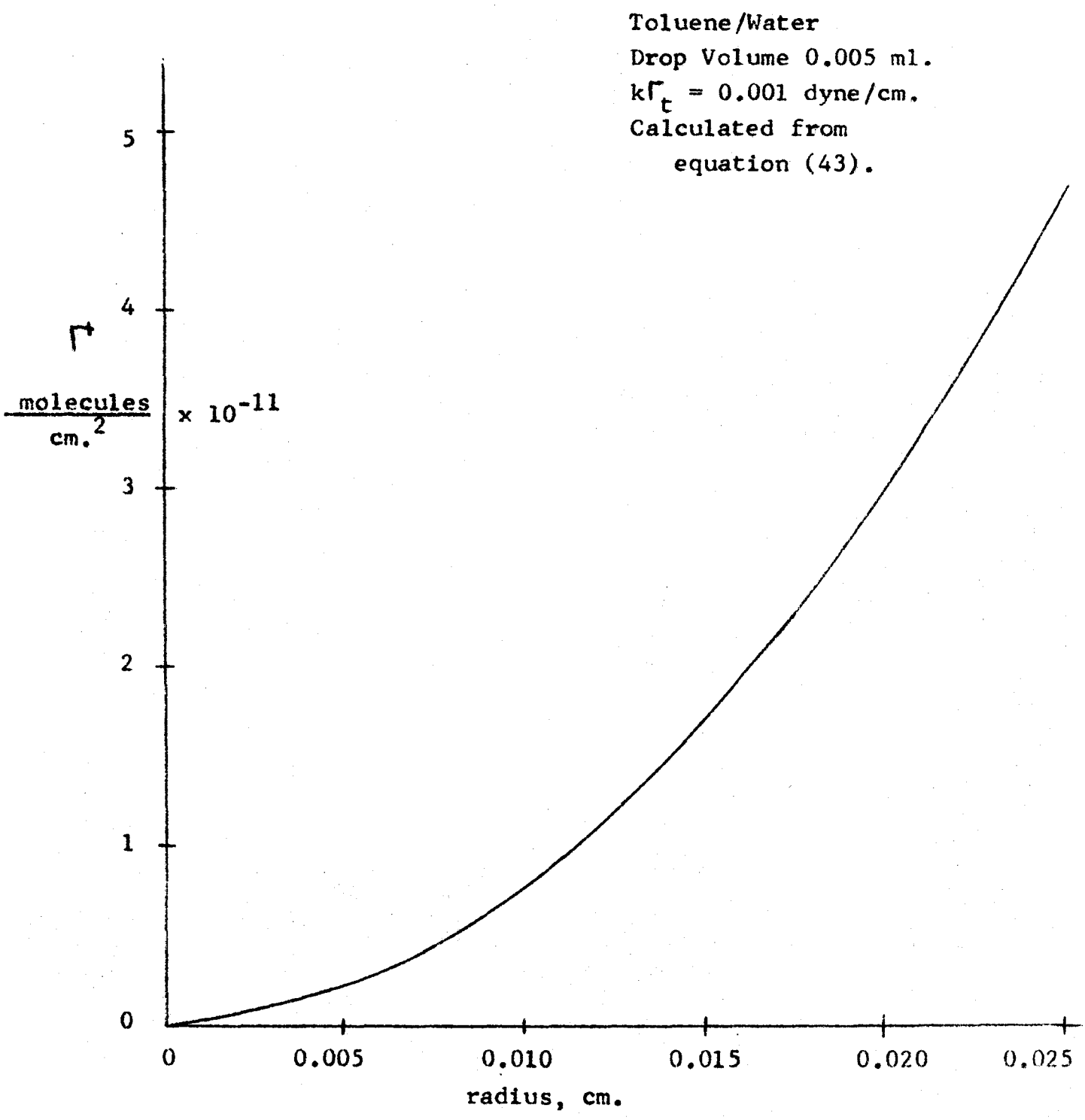

This curve is adjusted upward, as noted in chapter 4, part B.

Figure 19. The Effect of Initial Lamella Thickness and of Interfacial Surfactant Concentration on the Motion of the Lamella Center

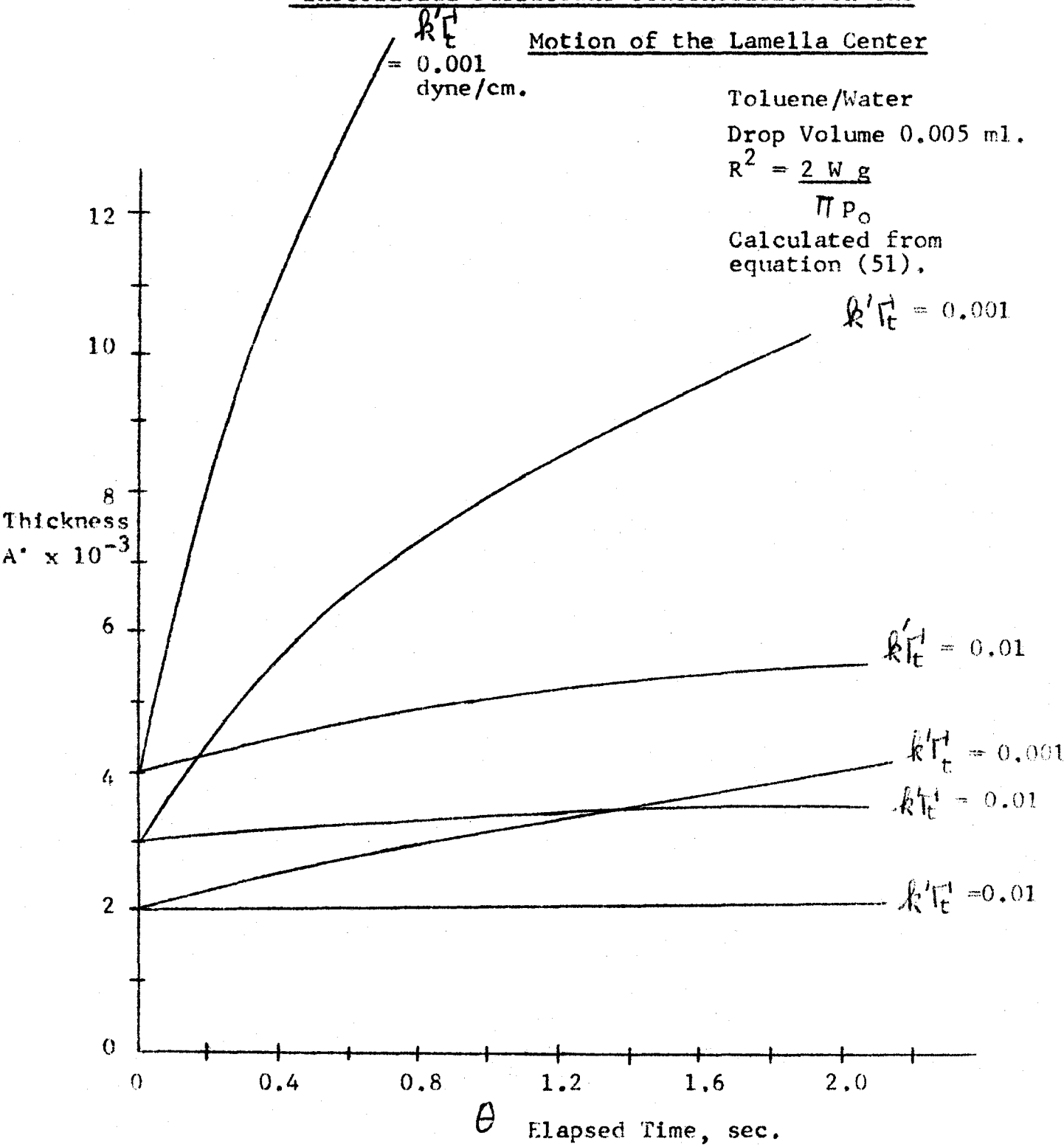

CHAPTER 5. CONCLUSIONS AND FUTURE WORK

Conclusions

Detailed conclusions are given in the conclusion sections of Chapter (2), (3), and (4). General conclusions, and the contributions of this work are:

(1) A simple, semi-empirical polynomial has been used to derive a general equation to calculate the profiles of the relative lamella thickness. This general equation is useful in the fitting of experimentally measured lamella profiles which were obtained over a wide range of drop size and oil/water system physical properties for both this work and for data presented in the literature. The original semi-empirical polynomial may then be used to calculate the dynamic pressure distribution in the lamella, the surface shear stress that the flowing lamella liquid exerts on the bulk interface, the interfacial tension gradient that exists in the bulk interface because of the surface shear stress exerted on it, and the radial gradient of the interfacial concentration of surfactant adsorbed at the bulk interface.

(2) All the light interference patterns produced by the lamellae of four oil/water systems could be simplified into five distinct mechanisms for the lamella behaviour. These mechanisms are:

1. rapid approach
2. dimple formation
3. slow even drainage
4. uneven drainage
5. lamella rupture

Each mechanism has been described and analyzed in detail. In particular, the use of the polynomial equation discussed in contribution No. 1 results in the formulation of a useful hypothesis to interpret the uneven drainage mechanism. This hypothesis is based on the results of calculations which have shown that the interfacial concentration of surfactant adsorbed at the bulk interface in the stressed region of the lamella may exceed the average interfacial concentration of surfactant adsorbed in the unstressed region of the bulk interface.

3.a) The simultaneous observation of drop rest-times and of light interference patterns has been extended to include four different oil/water systems. The oils used were toluene, anisole, cyclohexanol, and a cyclohexane-anisole mixture. One surfactant, sodium lauryl sulfate, with an aqueous phase concentration 0, 10^{-6}, 10^{-5}, 10^{-4}, 10^{-3}, and 10^{-2} grams/l., has been used in the study of rest-time and lamella behaviour for the toluene/water system. Concentrations of 10^{-6} and 10^{-4} grams/l. were employed in the studies of the other three oil/water systems. For the three low viscosity oils, no new drainage types could be added to those already observed by Hodgson and Woods. However, the lamella behaviour for the cyclohexanol/water system was unique and may serve as a "fifth" drainage type.

The changes in the lamella behaviour for increases in the interfacial concentration of S.L.S. resulted in a complex

distribution of drop rest-times with increasing interface age. These rest-time data have been qualitatively summarized in simple graphs of rest-time as a function of interface age, for the ranges of the bulk concentration of S.L.S. used.

3.b) A simple method has been devised to predict drop rest-times. The method employs a standard rest-time and uses the physical property dependence of lamella thinning models such as the Hodgson/Woods model and the parallel disc model to predict the drop rest-time for even drainage for the same interfacial concentration of adsorbed surfactant for any oil/water system. This analysis also shows that the effect of the oil/water system physical properties on drop rest-times cannot yet be accurately specified because the different physical property dependencies of the Hodgson/Woods model and the parallel disc model both give reasonably accurate estimates of drop rest-times.

4.) An experimental method has been modified to allow the measurement of the apparent thickness of the lamella when the rupture mechanism occurs. Despite the several assumptions which are necessary, the light intensity of the gray-black region of the light interference pattern was measured from light interference data recorded on colour ciné film. The lamella thickness at rupture was 200 - 400 A° for the 48 measurements made. These values agree with measurements made by other investigators who employed more sophisticated versions of this technique.

5. A theoretical consideration of lamella drainage has been made. This analysis solves a simplified form of the equations of motion, written in terms of the stream function. A simple exponential form of the dynamic pressure distribution in the lamella results, and allows a concise expression for the local rate of lamella thinning to be derived. This latter expression is solved with and without coupling of the motion of the bulk interface. The lateral motion of adsorbed surfactant molecules in the bulk interface has been taken into account by the consideration of both surface diffusion and of the bulk interface motion which results when the surface shear stress exerted on the bulk interface, changes with time. The lack of agreement between the observed lamella behaviour and the predicted behaviour suggests that the motion of the bulk interface has not been adequately described, particularly in the region of the lamella outside the barrier ring. The motion of the bulk interface in this region is expected to be complicated by expansion, as outlined in the discussion of the uneven drainage hypothesis. This expansion has not been taken into account in the mathematical analysis.

A simplified form of the mathematical analysis has been made by using the parallel disc model. A simple model results. This model shows that lamella drainage at the barrier ring and at the lamella center is a function of the interfacial concentration of adsorbed surfactant. This model seems more successful

than the complex analysis in the prediction of observed lamella behaviour.

A model has also been derived to account for barrier ring expansion. This model is based on the parallel disc model, and while it is only partially successful in accurately describing the observed barrier ring expansion over the entire range of lamella thickness, the model does allow an understanding of why barrier ring expansion occurs.

A final contribution of the theoretical analysis is that the analysis shows that lamella drainage is not a simple function of the oil/water system physical properties, and that the dependence of drainage on physical properties changes with the radial location in the lamella. The analysis shows how the physical property dependence of the Hodgson/Woods model arises, and shows that the rate of drainage at the barrier ring has the same physical property dependence as the parallel disc model.

Future Work

The problem of rest-time prediction in an industrial liquid/liquid system cannot be solved unless the degree of contamination of the industrial system is known. Since this information is likely to be difficult to obtain, any further work in coalescence studies will be of value only in the understanding that the work provides of problems caused by the existence of lamella drainage. Problems caused by the existence of foaming, and of stable emulsions, for example, are characterized by lamella drainage, or the lack of it, and by rupture. Further studies of the coalescence process therefore will be valuable if they can determine the effect of such variables as temperature, solid interfacial impurities, surfactant type, and surrounding droplets on the lamella drainage and lamella thickness at rupture.

More specifically, the following work is also suggested:

(1) The effect of the physical property variables such as the liquid/liquid system density difference, the interfacial tension, and discontinuous phase viscosity on the lamella drainage should be further investigated. The two oils, ethoxybenzene (phenetole), and propoxybenzene are part of the alkyl-phenyl-ether series and may be useful in a physical property study, especially since these two oil/water systems are expected to have a large change in interfacial tension for a small change

in density difference.

(2) Further mathematical modelling of lamella drainage should be done in order to specify further the effect of the oil/water system variables and of the interfacial concentration of adsorbed surfactant on lamella drainage.

(3) It may be worthwhile to continue the work of Vrij and Overbeek on the prediction of the apparent lamella thickness at rupture. This may be done by employing an inertial flow model for lamella drainage at rupture, instead of a viscous flow model. The use of an inertial flow model therefore dictates that the mobility of the interfaces must be taken into account. Mathematical modelling in this area would provide a bridge between lamella drainage and lamella rupture.

(4) The possibility of in situ measurements of the apparent lamella thickness at rupture would be valuable in allowing a confirmation of any results to come from modelling of the rupture process. The in situ measurements would require a new optical arrangement to be fabricated, similar to that employed by M. van den Temple, J. Coll. Sci. 13 125-133 (1958).

APPENDIX A1. ADDITIONAL DATA

Appendix A1

Additional data on drop rest-times and on lamella thickness are presented in this appendix. These data show the effect of surfactant type, of interface cleaning, of drop aging, and of a large oil viscosity on either drop rest-times or lamella drainage. A comparision between the light interference technique and the light intensity technique is also given.

A1.1. A Change in Surfactant Type

A non-ionic liquid surfactant, 2(2-ethoxy-ethoxy)-ethanol , abbreviated to 2-EEE, was also employed in this work.

The 2-EEE surfactant was water soluble, but it may be also partially soluble in the toluene phase because of its non-ionic nature. Lamella behaviour for the two aqueous phase concentrations may be compared with S.L.S. behaviour as follows: 0.05 ml. of 2-EEE + 0.01 N. KCl. gave the same lamella behaviour as 10^{-6} gm/l. S.L.S. + 0.01 N. KCl.

Rest-time data measured for these two surfactant concentrations for the toluene/water system are given in Tables (A1.1) and (A1.2).

For 0.50 ml/l. of this surfactant, local lamella depressions were present in some lamellae, especially for an aged interface. These depressions were observed only when a drop was at the interface. Lamella thicknesses were about 1000 A°

Table A1.1 Drop Rest-time Data for a Non-ionic Surfactant

Toluene/Water
0.05 ml. of 2-(2 ethoxy-ethoxy)ethanol/l.
+ 0.01 N.KCl

Drop Volume 0.005 ml.

t (min.)	$\hat{\tau}$ (sec.)	Drain-age
0	12.0	E
1	10.1	E
2	9.3	E
3	8.5	E
4	6.5	E
5	9.0	E
6	4.4	E
7	6.2	E
8	7.8	E
9	3.7	E
10	3.7	E
11	5.7	E
12	6.1	E
13	4.8	E
14	5.4	E
15	10.7	E→UE
16	5.1	E
17	10.0	E→UE
18	12.0	E→UE

Drop Volume 0.0025 ml.

t (min.)	$\hat{\tau}$ (sec.)	Drain-age
0	8.8	E
1	7.5	E
2	7.6	E
3	5.6	E
4	4.0	E
5	4.1	E
6	8.2	E→UE
7	6.9	E→UE

E = dimple formation
→ slow even drainage
→ rupture

E→UE = dimple formation
→ slow even drainage
→ uneven drainage
→ rupture

Drop not aged on the syringe.

Table A1.2 Drop Rest-time Data for a Non-ionic Surfactant

Toluene/Water
0.50 ml. of 2-(2 ethoxy-ethoxy)ethanol/1.
+ 0.01 N.KCl

Drop Volume 0.005 ml.

t (min.)	τ (sec.)
0	39.7
1½	11.7
2	12.2
3	17.5
4	11.2
5	7.4
6	10.5
7	9.9
8	9.8
9	7.6
10	11.6
18 hours	4.4
"	2.5
"	5.8
"	4.4
"	6.4

Drop Volume 0.0025 ml.

t (min.)	τ (sec.)
0	22.4
1	15.0
2	11.6
3	10.8
4	7.3
5	8.9
6	8.3
7	6.1
8	9.9
9	9.0
10	4.9

Lamella drainage is uneven for the data in both tables. Drop not aged on the syringe.

before these depressions were observed. Their width was estimated at 10 μ. for this surfactant. When the interface was cleaned, these depressions were seldom observed.

A1.2. The Effect of Interface Cleaning on Drop Rest-Times

Three consecutive sets of rest-time data for 0.020 ml. anisole drops for 10^{-6} gm/l. S.L.S. + 0.01 N. KCl. are presented to illustrate the effect of interface cleaning on drop rest-times. The data in Table (A1.3-c) are also given in Figure (18) of Chapter 3 and are representative of the effect on drop rest-times of S.L.S. at a 10^{-6} gm/l. concentration, 0.020 ml. volume drops, for this oil/water system. Local lamella depressions appear in some interference patterns. Rest-times for the occurrence of this phenomenon are marked with an asterisk, and are not included in Figure (18) of Chapter 3. The presence of depressions was seldom observed, and therefore the rest-times measured for the occurrence of depressions were not representative of the effect of only the S.L.S. bulk interface concentration.

The data in Table (A1.3) show that successive interface cleaning allows the interfacial concentration of surfactant to be reduced, since even drainage appears after the second and third cleaning.

Table A1.3 Effect of Interface Cleaning on Rest-times

Anisole/Water
10^{-6} gm/l. S.L.S. + 0.01 N.KCl
Drop Volume 0.020 ml.

(a)			(b)			(c)		
Cleaning No. 1			Cleaning No. 2			Cleaning No. 3		
t,min.	τ sec.	Drainage	t,min.	τ sec.	Drainage	t,min.	τ sec.	Drainage
0	46.6	E→UE	0	30.0	E	0	29.2	E
2	29.0		2	23.0	E	2	25.3	E
3½	24.0		3½	14.8	E→UE	3½	31.9	E→UE
5	23.9		4½	9.6*		5	17.9*	
6½	8.4*		5½	18.1		6½	33.5	
7½	19.8		7	27.5		8	24.8	
9	8.6*		9	23.8		9½	11.5*	
10	10.9		10½	28.0	E→UE	10½	25.4	
11	22.9					12½	13.6	
12	16.6					14	17.3	
13	14.5(dust)					15½	12.9*	
14	13.8*					16½	22.0	
15	20.5	E→UE				17½	14.4	
						18½	18.1	
						19½	16.7	E→UE

* = rest-time was affected by dust, dirt, or local lamella depression.

A1.3 The Effects of Surfactant Concentration and of Drop Aging on Drop Rest-Times

A small change in the aqueous concentration of S.L.S. should allow the effect of a more rapid surfactant adsorption on drop rest-times to be observed. The effect of aging the drop interface for 100 seconds while the drop was on the capillary tip has also been studied. Rest-time data for these two variables are given in Table (A1.4).

These data show that a slight increase in the aqueous concentration of S.L.S. has reduced the value of t_c. This is caused by a more rapid adsorption for a larger concentration of S.L.S. The interface mobility is reduced. The drop rest-times are also smaller for an increase in concentration of S.L.S. This is caused by a decrease in the time, τ', taken to form the dimple.

The aging of the drop interface also increased the time taken to form the dimple. Drop rest-times for an aged drop are therefore larger than for an unaged drop interface. A small interfacial tension gradient should be set up in the drop interface during the rapid approach of the drop to the interface. The contraction of the drop interface should add additional water to the lamella dimple. The rate of addition of water should be faster than for an unaged drop interface. However, the total time taken to form the dimple may or may not be less than for an unaged drop interface.

Table A1.4 Effect of the Aqueous Phase S.L.S. Concentration and of Drop Aging on Rest-time and Dimple

Toluene/Water — Formation Time

3×10^{-6} gm/l. S.L.S.+0.01 N.KCl

Drop Volume 0.005 ml.

(1)

Drop not aged			Drop aged 100 sec.		
t,min.	τ sec.	τ' sec.	t,min.	τ sec.	τ' sec.
0	1.3	1.3	0	0.7	0.7
1	10.5	6.5	2½	13.4	4.3
2	12.3	-	4½	11.2	2.7
3	9.6	5.2	6½	9.4	2.6
4	9.2	3.5	8½	10.4	2.2
5	10.2	2.5	10½	11.8	2.3
6	8.8	-	12½	8.9	2.0
7	9.9	1.9	14½	8.4	1.7
8	8.7	1.6	16½	8.4	1.4
9½	9.1	1.5	18½	6.6	1.1
10	7.1	1.0[e]	20½	7.1	1.0
11	7.8	1.0[e]	22½	6.9	1.0
12	-	-[e]	24½	6.8	< 1.0
13	8.3	1.2	26½	4.8	< 1.0
14	6.7	1.0	28½	6.4	< 1.0
15	5.6	< 1.0			
16	5.4	"			
17	5.6	"			
18	5.8	"			
19	5.8	"			
20	4.2	"			
21	5.7	"			

1. Drainage is even for all drops.
2. τ' is the time taken to form the dimple. It was measured from the instant that the drop reached the interface until the instant that the lamella reached its maximum thickness at the center.

Table A1.4 (continued)

Toluene/Water
1×10^{-6} gm/l. S.L.S.+ 0.01 N.KCl
Drop Volume 0.005 ml.

(2)

Drop not aged			Drop aged 100 sec.		
t,min.	τ sec.	τ' sec.	t,min.	τ sec.	τ' sec.
½	3.7	3.7	½	1.0	1.0
1	0.8	0.8	2	12.7	5.6
2	11.7	5.0	4	8.9	4.6
3	9.1	4.6	6	9.9	4.6
4	9.3	3.6	8	5.2	3.4
5	8.1	3.6	10	5.8	2.5
6	7.8	3.6	12	9.2	2.8
7	7.2	3.1	14	8.6	2.5
8	4.2	3.0	16	9.7	2.3
9	5.7	2.4	18	5.1	1.9
10	8.0	2.3	20	8.9	1.5
11	6.5	2.5	22	3.7	1.5
12	7.7	2.1	24	7.8	1.3
13	8.0	2.2	26	5.2	1.7
14	6.3	2.0	28	8.2	1.0
15	7.8	1.8	30	8.4	1.1
16	5.4	1.6	32	8.7	1.0
17	6.4	1.5	34	7.3	1.1
18	4.2	1.6	36	4.7	1.1
19	7.2	1.4			
20	7.4	1.2			
21	3.9	1.2			
22	7.6	1.1			
23	6.7	1.0			

Drainage is even for all drops.

A1.4. A Comparison of the Light Interference and Light Intensity Techniques

The data in Figure (A1.1) show the change in barrier ring thickness as a function of the elapsed time, θ, for two different drop sizes. Below 1000 A°, the lamella thickness was measured using the light intensity meter described in Appendix A.3. Despite some degree of subjectivity inherent in the measurement of lamella thickness from white light interference colours, and the use of the white light intensity as a measure of the lamella thickness, there is a smooth transition between the measurements produced by the techniques.

A1.5. Lamella Thickness Data for the Cyclohexanol/Water System

Lamella thickness data for the cyclohexanol/water system for 10^{-4} gm/l. S.L.S. + 0.05 N. KCl. for a 0.001 ml. drop are given in Figure (A1.2). The lamella behaviour during the first 60 seconds of elapsed time of the drop at the bulk interface is complex. However, after an elapsed time of 60 seconds, the lamella center thickness decreased linearly with time from 15000 A° to about 6000 A°. The barrier ring thickness decreased from 4000 A° until rupture occurred at less than 1000 A°.

There is a linear decrease in the center lamella thickness with an increase in time for the data in Figure (A1.2). This is contrary to the model proposed by Frankel and Mysels. The prediction of lamella thickness from this model is shown

Figure A1.1 Barrier Ring Thickness versus Elapsed Time

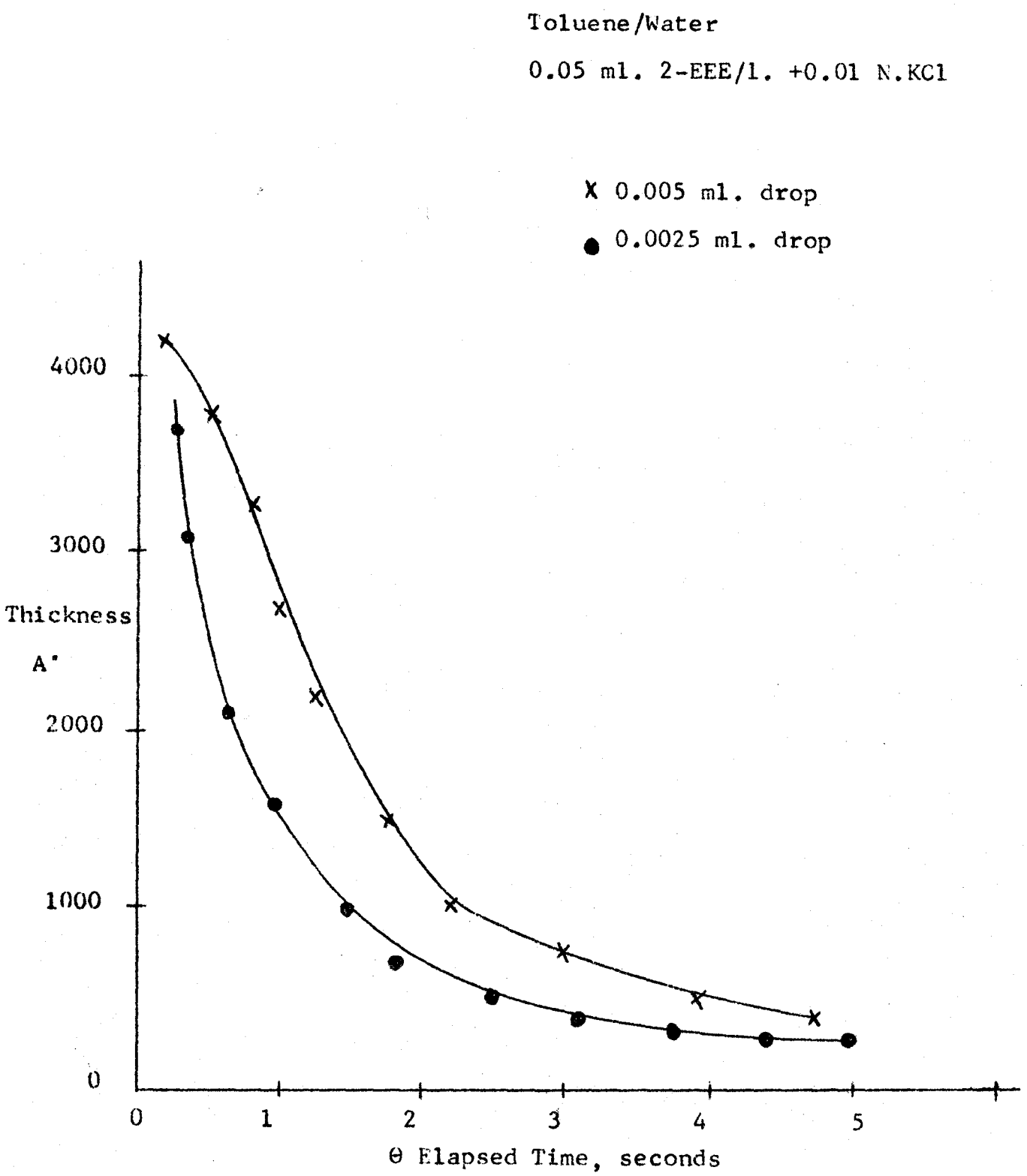

Figure A1.2 Dimple Center and Barrier Ring Heights for Cyclohexanol/Water - Even Drainage

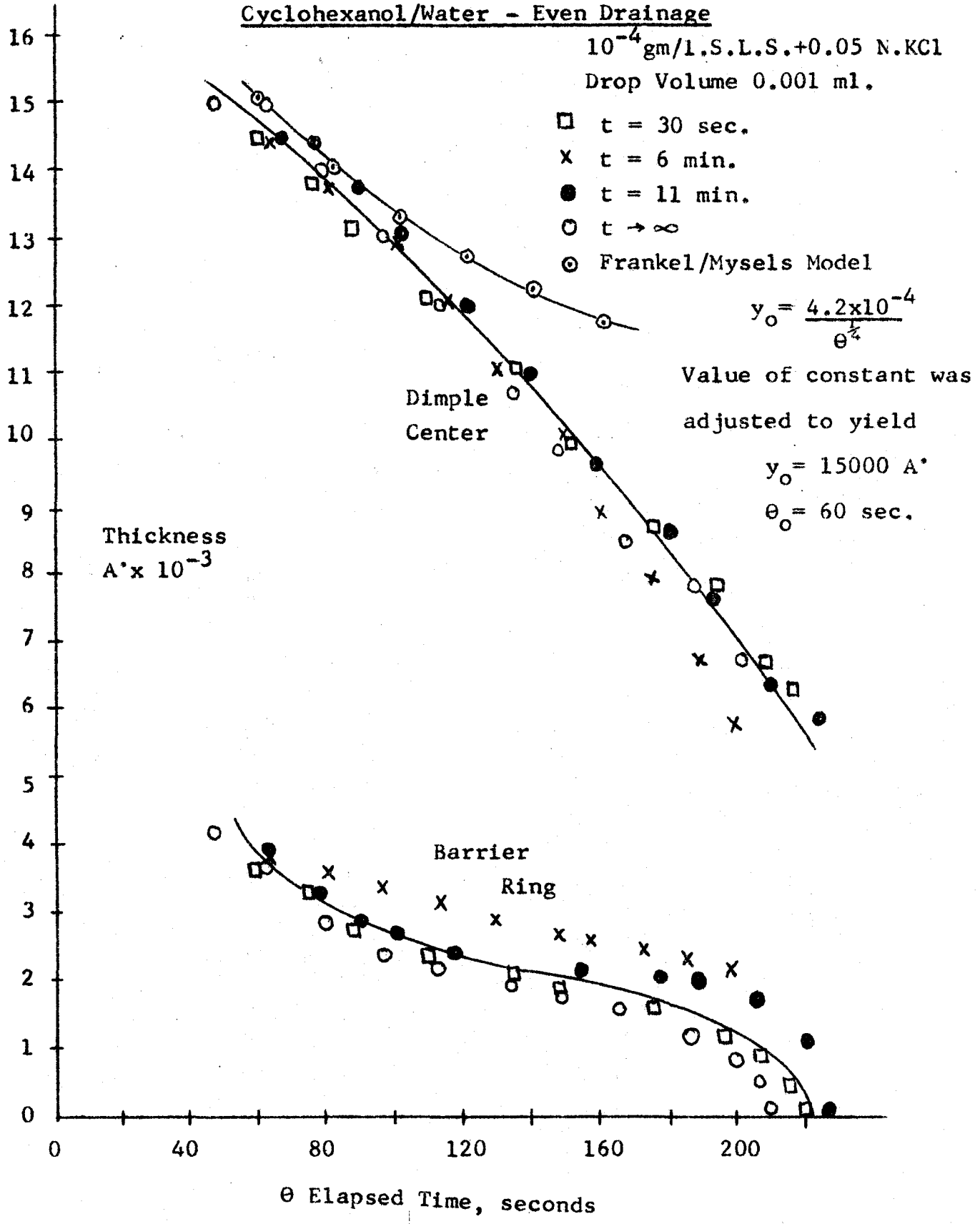

in the figure. There is also a reproducibility of data, regardless of the bulk interface age. This large viscosity of the cyclohexanol phase appears to dominate the motion of the bulk interface. For less viscous oils, the bulk interface concentration of surfactant controls the motion of the bulk interface. The dimple center may move upward to a maximum height which depends upon the interfacial motion of the bulk interface.

The profiles of lamella thickness for cyclohexanol/water given in Figure (11c) of Chapter (4) show that only one side of the barrier ring becomes thin. The remainder of the barrier ring height decreases more slowly. The black interference colour extended over an angle of about 30°, while the colour over the remaining 330° was amber or white. The colour in the black region becomes very intense shortly before rupture, and the lamella thickness in this region decreased very rapidly when the lamella thickness was less than 1000 A°. This is shown in Figure (A1.2). There is no apparent explanation for this type of uneven drainage behaviour.

The slowness of the lamella behaviour for the cyclohexanol/water system may be shown relative to the other low viscosity oil/water systems used. The data in Figure (A1.2) may be compared with that data given for toluene/water in Figure (A1.3). The lamella behaviour for the toluene/water system occurs an order of magnitude faster than the lamella behaviour of the cyclohexanol/water system.

Figure A1.3 Dimple Center and Barrier Ring Heights for Toluene/Water- Even Drainage

10^{-6}gm/l. S.L.S. +0.01 N. KCl
Drop Volume 0.005 ml.
Interface Age t = 11 min.

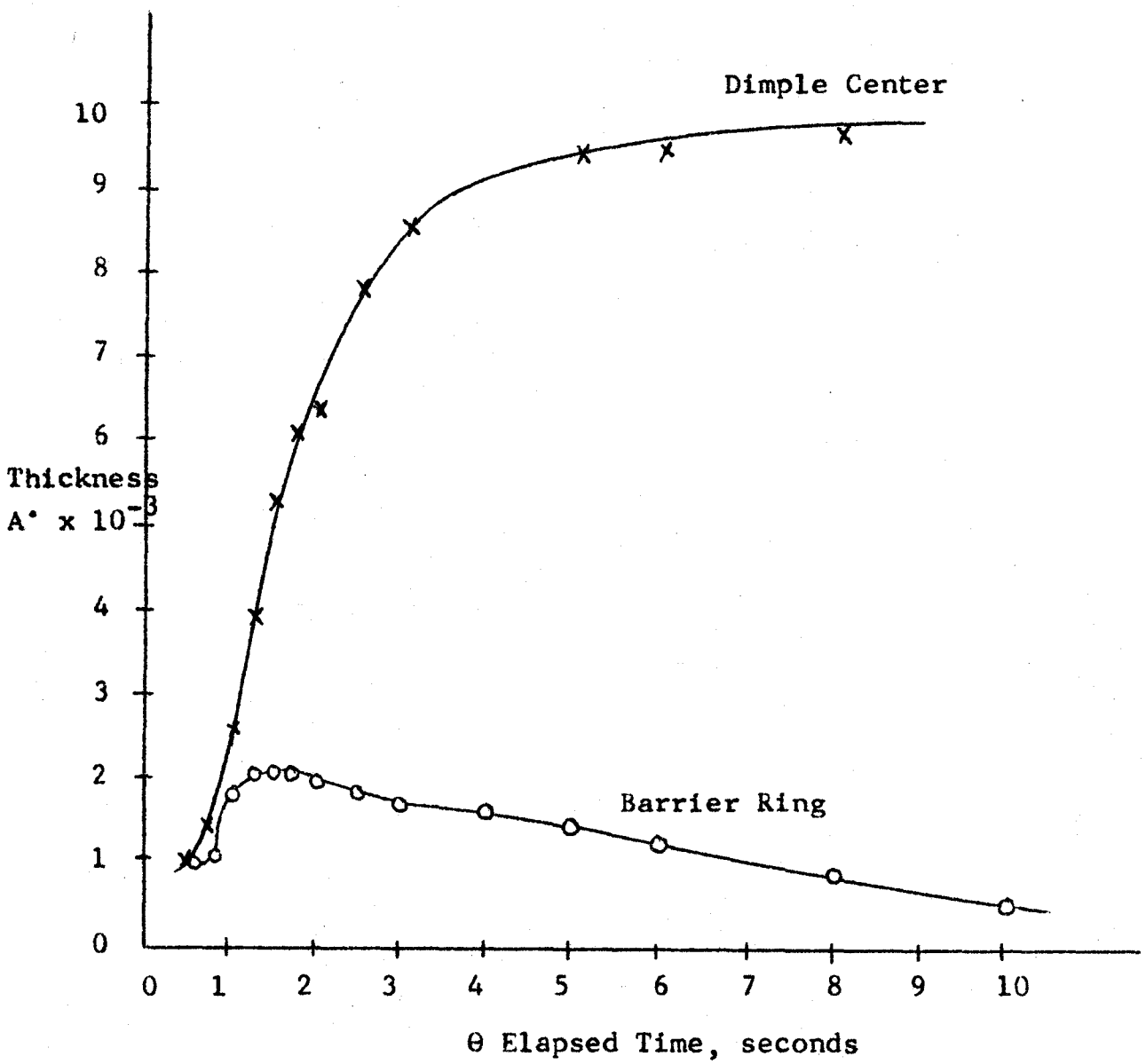

APPENDIX A2.

ADDITIONAL DERIVATIONS AND CALCULATIONS

Appendix A2

This appendix will give additional details on the derivation of the equations given in Chapter (4). Approximations which were made in Chapter (4) will also be discussed, and equations for the parallel disc model and for the expansion of the barrier ring will be derived.

A2.1 An Alternative Derivation of the Lamella Drainage Equation

The detailed derivation of the lamella thinning equation in Chapter (4) was necessary to show how the expression for lamella pressure was produced. The derivation is long and the assumptions made are obscured. This section will consider a much simpler derivation.

The equations of motion may be simplified by the following assumptions:

(1) Only flow in the r-direction is significantly large. (Figure (2) of Chapter 4 gives the geometry for this derivation.)

(2) $$\frac{\partial}{\partial r}\left(\frac{1}{r}\frac{\partial}{\partial r}(ru)\right) \ll \frac{\partial^2 u}{\partial z^2}$$

(3) Pseudo-steady state

(4) Creeping flow

(5) Axisymmetry

The application of these assumptions to the equations of motion

leads to the following result:

$$\frac{1}{\mu}\frac{\partial p}{\partial r} = \frac{\partial^2 u}{\partial z^2}$$

This equation may be integrated twice with respect to z to yield:

$$u = \frac{1}{2\mu}\frac{\partial p}{\partial r} z^2 + az+b$$

The application of boundary conditions:

B.C. 1	B.C. 2
$u = 0$	$\frac{\partial u}{\partial z} = 0$, $z = y$, $m = 1$
$z = 0$	$u = 0$, $z = y$, $m = 2$

gives:

$$u = \frac{1}{2\mu}\frac{\partial p}{\partial r}\left(z^2 - \frac{2}{m} yz\right) \qquad \ldots\ldots(1)$$

This equation may be substituted into the continuity equation, which may be written:

$$\frac{\partial u}{\partial r} + \frac{u}{r} + \frac{\partial w}{\partial z} = 0 \qquad \ldots\ldots(2)$$

The continuity equation is integrated with respect to z to give the final result:

$$\frac{\partial y}{\partial \theta} = \frac{(3-m)}{6m\mu}\frac{\partial^2 p}{\partial r^2} y^3 + \frac{1}{2m\mu}\frac{\partial p}{\partial r}\frac{\partial y}{\partial r} y^2 + \frac{(3-m)}{6m\mu}\frac{1}{r}\frac{\partial p}{\partial r} y^3 \qquad \ldots\ldots(3)$$

This expression is the same as that derived in Chapter (4), where the derivatives of p were evaluated from $p = p_o e^{-\lambda r^2}$.

If equation (26) of Chapter (4) is used:

$$p = -\frac{\gamma}{2}\left(\frac{\partial^2 y}{\partial r^2} + \frac{1}{r}\frac{\partial y}{\partial r} - \frac{2}{d}\right) \qquad \ldots\ldots(4)$$

then equation (3) becomes:

$$\frac{\partial y}{\partial \theta} = \frac{(3-m)}{6m\mu} y^3 \left(-\frac{\gamma}{2}\left(\frac{\partial^4 y}{\partial r^4} + \frac{1}{r}\frac{\partial^3 y}{\partial r^3} - \frac{2}{r^2}\frac{\partial^2 y}{\partial r^2} + \frac{2}{r^3}\frac{\partial y}{\partial r}\right)\right)$$

$$+ \frac{1}{2m\mu}\frac{\partial y}{\partial r} y^2 \left(-\frac{\gamma}{2}\left(\frac{\partial^3 y}{\partial r^3} + \frac{1}{r}\frac{\partial^2 y}{\partial r^2} - \frac{1}{r^2}\frac{\partial y}{\partial r}\right)\right)$$

$$+ \frac{(3-m)}{6m\mu} y^3 \left(-\frac{\gamma}{2}\left(\frac{1}{r}\frac{\partial^3 y}{\partial r^3} + \frac{1}{r^2}\frac{\partial^2 y}{\partial r^2} - \frac{1}{r^3}\frac{\partial y}{\partial r}\right)\right) \qquad \ldots\ldots(5)$$

There is a difficulty with the apparent indeterminacy of equation (5) at r = 0. Hartland has derived a similar equation for a drop at a flat plate (17), and he has assumed that a spherical cap exists at r = 0. This is not necessary since equation (5) is determinate at r = 0. To show this, the boundary conditions on y at r = 0 are considered first.

$$\left.\begin{array}{ll} \text{B.C. 1} & y \neq 0 \\ \text{B.C. 2} & \dfrac{\partial y}{\partial r} = 0 \\ \text{B.C. 3} & \dfrac{\partial^2 y}{\partial r^2} \neq 0 \\ \text{B.C. 4} & \dfrac{\partial^3 y}{\partial r^3} = 0 \end{array}\right\} \quad r = 0$$

Three groups of terms cause difficulty:

$$\text{Group (1)} = \frac{1}{r}\frac{\partial^3 y}{\partial r^3} = \frac{\partial^4 y}{\partial r^4} \quad \text{at } r = 0$$

The application of L'Hopital's Rule shows that Group one may be evaluated.

$$\text{Group (2)} = \frac{1}{r}\frac{\partial^2 y}{\partial r^2} - \frac{1}{r^2}\frac{\partial y}{\partial r} = ?$$

Since $\frac{\partial^2 y}{\partial r^2} \neq 0$ at $r = 0$.

This group of terms may be written:

$$(2) = \frac{1}{r}\left(\frac{\partial^2 y}{\partial r^2} - \frac{1}{r}\frac{\partial y}{\partial r}\right) \longrightarrow \frac{1}{r}\left(\frac{\partial^2 y}{\partial r^2} - \frac{\partial^2 y}{\partial r^2}\right)$$

as $r \longrightarrow 0$. With L'Hopital's Rule, these terms become

$$\frac{\partial^3 y}{\partial r^3} - \frac{\partial^3 y}{\partial r^3} = 0 = (2).$$

Group two may also be evaluated.

$$\text{Group (3)} = \frac{1}{r}\frac{\partial^3 y}{\partial r^3} - \frac{2}{r^2}\frac{\partial^2 y}{\partial r^2} + \frac{2}{r^3}\frac{\partial y}{\partial r} = ?$$

$$\frac{1}{r}\frac{\partial^3 y}{\partial r^3} \neq \frac{\partial^4 y}{\partial r^4} \quad \text{as } r \longrightarrow 0$$

The next two terms can be written as before:

$$(3) = \frac{\partial^4 y}{\partial r^4} - \frac{2}{r^2}\left(\frac{\partial^2 y}{\partial r^2} - \frac{1}{r}\frac{\partial y}{\partial r}\right)$$

$$= \frac{\partial^4 y}{\partial r^4} - \frac{1}{r}\left(\frac{\partial^3 y}{\partial r^3} - \frac{\partial^3 y}{\partial r^3}\right)$$

$$= \frac{\partial^4 y}{\partial r^4} - \left(\frac{\partial^4 y}{\partial r^4} - \frac{\partial^4 y}{\partial r^4} \right)$$

$$= \frac{\partial^4 y}{\partial r^4}$$

Therefore equation (5) may be written at the lamella center as follows:

$$\frac{\partial y}{\partial \theta} = - \frac{(3-m)}{4m} \frac{\gamma}{\mu} y^3 \frac{\partial^4 y}{\partial r^4} \qquad \ldots\ldots(6)$$

A2.2 Infinite Series Form of the Stream Function

Equation (8) of Chapter (4) used an infinite series to express the velocity derivative. An infinite series is necessary to satisfy all the boundary conditions, and is written explicitly in terms of r so that equation (8) may be integrated. A final difficulty is in the values of the index i to use in the series.

If i equals one, then:

$$\frac{1}{r} \frac{\partial}{\partial r} \left(r \frac{\partial w}{\partial r} \right) = f(z) + g(z)\, r$$

This expression may be integrated and the stream function found to be:

$$\Psi(r,z) = - \frac{r^5}{45} g(z) - \frac{r^4}{16} f(z) - \frac{r^2}{2} h(z) + c'$$

Since $\frac{\partial \Psi}{\partial z} = 0$ when $r = 0$, then $\frac{\partial c'}{\partial z} = 0$ and since c' is not a function of r, c' must be a constant. This constant may be set arbitrarily to zero. The above expression for Ψ may be substituted

into the equation:

$$\psi_{zzzz} + 2\psi_{rrzz} - \frac{2}{r}\psi_{rzz} = 0$$

to give:

$$-\frac{r^5}{45} g_{zzzz} - \frac{8}{9} r^3 g_{zz} + \frac{2}{9} r^3 g_{zz}$$

$$-\frac{r^4}{16} f_{zzzz} - r^2 f_{zz} - \frac{r^2}{2} b_{zzzz} = 0$$

Since r is not zero, then:

$$g_{zzzz} = 0$$

$$g_{zz} = 0$$

$$f_{zzzz} = 0$$

$$2f_{zz} + b_{zzzz} = 0$$

The derivative g_{zz} may be integrated to give:

$$g(z) = pz + q$$

The boundary conditions are:

$$\psi_z = 0, \quad z = 0, \quad \therefore p = 0$$

$$\psi_r = 0, \quad z = 0, \quad \therefore q = 0$$

Therefore, g(z) must be zero and there can be no odd power of r in the original infinite series. Therefore, i = 0, 2, 4,...

A2.3. Order of Magnitude Analysis of the Complete Stream Function Expression

For equation (13) in Chapter (4), the coefficients a'

and e' may be evaluated by using the boundary conditions on pressure. Since the following approximation may be written:

$$\frac{1}{\mu}\frac{\partial p}{\partial r} \doteq \frac{1}{r}\ \psi_{zzz} \qquad \text{.....(9a)}$$

then,

$$\frac{1}{\mu}\frac{\partial p}{\partial r} \doteq -\frac{e'r}{2} - \frac{a'}{16}r^3 \qquad \text{.....(9b)}$$

Equation (9b) represents a three term pressure polynomial whose coefficients are:

$$a' = -\frac{64p_o}{\mu R^4}\ ,\quad e' = \frac{8P_o}{\mu R^2}$$

where

$$R^2 = \frac{3\,Wg}{\pi P_o}$$

The boundary condition on $\psi(r,z)$ is: $\psi_z = 0,\ z = y$

or $\psi_{zz} = 0,\ z = y.$

Equation (9a) may be solved for ψ. The application of the above boundary conditions gives an expression which may be solved for the quantity b' in equation (13) of Chapter (4). When y is expressed in terms of an infinite series and is substituted into equation (13) and the coefficients of like powers of r are summed, an infinite number of equations results. The second equation of this infinite number, for the coefficients of r^2, may be solved for b'. The results are:

$$O(a') >> O(b') = O(e')$$

and $O(a' z^3) \doteq O(b' z^2)$

then,

$$O\left(\frac{2a' z^5}{120}\right) + O\left(\frac{2b' z^4}{24}\right) << O\left(\frac{-e' z^3}{6}\right) + O\left(\frac{-f' z^2}{2}\right)$$

Therefore, the stream function has the approximate form:

$$\Psi(r,z) \doteq -\frac{r^4}{16}\left(\frac{a' z^3}{6} + \frac{b' z^2}{2}\right) - \frac{r^2}{2}\left(\frac{e' z^3}{6} - \frac{f' z^2}{2}\right)$$

Only terms in z^3 and z^2 are significant.

A2.4. The Convergence of ln (1 + j)

Thomas (1960) has shown on page 807 of his text that the logarithmic series is:

$$\ln (1 + j) = j - \frac{j^2}{2} + \frac{y^3}{3} - \frac{j^4}{4} + \ldots$$

This equation becomes the series in Chapter (4) when j = 1. An alternating series converges conditionally even when the all-positive series diverges, but the following conditions must be valid:

(1) The series is alternating

(2) The n-th term tends to zero as n increases

(3) Each term is numerically less than the one before it. Therefore the series for ln (2) converges conditionally and the series in Chapter (4) has the value ln (2) = 0.693.

A2.5 Details of Solution Assumptions

Velocity derivatives in the r-direction will be first shown to be small relative to the velocity derivatives in the z-direction. Then, the pseudo-steady state and creeping flow assumptions will be considered.

$$\text{If,} \quad \Psi(r,z) = -\frac{z^3}{6} F(r) + \frac{z^2}{2} y F(r)$$

then,

$$u = \frac{1}{r}\frac{\partial \Psi}{\partial z} = -\frac{z^2}{2}\frac{F}{r} + zy\frac{F}{r}$$

and,

$$w = -\frac{1}{r}\frac{\partial \Psi}{\partial r} = -\frac{z^3}{6}\frac{1}{r}\frac{dF}{dr} + \frac{z^2 y}{2}\frac{1}{r}\frac{dF}{dr} + \frac{z^2 F}{2 r}\frac{\partial y}{\partial r}$$

Since,

$$F = \beta r^2 e^{-\lambda r^2}$$

and,

$$\beta = \frac{2\pi {P_o}^2}{\mu Wg}, \quad \lambda = \frac{\pi P_o}{Wg}$$

Then,

$$\mu = O(10^{-2})$$

$$Wg = O(10^{-1})$$

$$P_o = O(10^{-2})$$

$$r = O(10^{-2})$$

$$y = z = O(10^{-4})$$

$$\lambda = O(10^{3})$$

$$\frac{\partial y}{\partial r} = O(10^{-2})$$

$$\therefore \quad \beta = O(10^7)$$

$$\frac{dF}{dr} = O(10^5)$$

Therefore,

$$u = O(10^{-3})$$

$$w = O(10^{-5})$$

The derivative $\frac{\partial w}{\partial r}$ may be approximated by $\frac{w}{r}$, and $\frac{\partial^2 w}{\partial r^2}$ by $\frac{w}{r^2}$.

Then:

$$\frac{\partial^2 w}{\partial r^2} + \frac{1}{r}\frac{\partial w}{\partial r} = O(10^{-1})$$

since

$$\frac{\partial^2 w}{\partial z^2} = O(10^3)$$

Then,

$$\frac{1}{r}\frac{\partial}{\partial r}\left(r\frac{\partial w}{\partial r}\right) \ll \frac{\partial^2 w}{\partial z^2}$$

Similarly, for the velocity in the r-direction,

$$\frac{\partial}{\partial r}\left(\frac{1}{r}\frac{\partial}{\partial r}(ru)\right) = O(10^1)$$

$$\frac{\partial^2 u}{\partial z^2} = O(10^5)$$

$$\therefore \quad \frac{\partial}{\partial r}\left(\frac{1}{r}\frac{\partial}{\partial r}(ru)\right) \ll \frac{\partial^2 u}{\partial z^2}$$

The creeping flow assumption is valid if the Reynolds Number, which is the ratio of inertia terms to the viscous terms in the equation of motion, is much less than one.

For the z-direction,

$$N_{RE_z} = \frac{\rho\left(u\frac{\partial w}{\partial r} + w\frac{\partial w}{\partial z}\right)}{\mu\frac{\partial^2 w}{\partial z^2}} = \frac{O(10^{-6})}{O(10^{1})} = O(10^{-7})$$

and for the r-direction,

$$N_{RE_r} = \frac{\rho\left(u\frac{\partial u}{\partial r} + w\frac{\partial u}{\partial z}\right)}{\mu\frac{\partial^2 u}{\partial z^2}} = \frac{O(10^{-4})}{O(10^{3})} = O(10^{-7})$$

Convective acceleration terms may therefore be neglected.

The pseudo-steady state assumption requires that the time acceleration term be small relative to the viscous terms.

For the r-direction velocity,

$$\frac{\partial u}{\partial \theta} = \frac{z^2}{2r}\frac{\partial^2 F}{\partial \theta\,\partial r}\left(\frac{z}{3} - \frac{y}{m}\right) - \frac{z^2}{2rm}\frac{\partial F}{\partial r}\frac{\partial y}{\partial \theta}$$

$$- \frac{z^2}{2rm}\frac{\partial F}{\partial \theta}\frac{\partial y}{\partial r} - \frac{z^2}{2rm}F\frac{\partial^2 y}{\partial \theta\,\partial r}$$

$$\frac{\partial F}{\partial \theta} = r^2 e^{-\lambda r^2}\frac{\partial \beta}{\partial \theta} - \beta r^4 e^{-\lambda r^2}\frac{\partial \lambda}{\partial \theta}$$

$$\frac{\partial \lambda}{\partial \theta} = \frac{\pi}{Wg}\frac{\partial P_o}{\partial \theta}, \quad \frac{\partial \beta}{\partial \theta} = \frac{4\pi P_o}{\mu Wg}\frac{\partial P_o}{\partial \theta}$$

If these equations are used, and the values of parameters are found from the program solutions, it is found that:

$$\frac{\partial P_o}{\partial \theta} = O(10^2)$$

$$\frac{\partial \lambda}{\partial \theta} = O(10^3)$$

$$\frac{\partial \beta}{\partial \theta} = O(10^8)$$

$$\frac{\partial F}{\partial \theta} = O(10^4)$$

$$\frac{\partial^2 F}{\partial \theta \partial r} = O(10^6)$$

$$\frac{\partial y}{\partial \theta} = O(10^{-4})$$

$$\frac{\partial^2 y}{\partial \theta \partial r} = O(10^{-1})$$

$$\frac{\partial v}{\partial r} = O(10^{-1})$$

then,

$$\rho \frac{\partial u}{\partial \theta} = O(10^{-3})$$

and so,

$$\frac{\rho \frac{\partial u}{\partial \theta}}{\mu \frac{\partial^2 u}{\partial z^2}} = \frac{O(10^{-3})}{O(10^3)} = O(10^{-6})$$

For the velocity in the z-direction,

$$\rho \frac{\partial w}{\partial \theta} = \rho \frac{\partial^2 y}{\partial \theta^2} = O(10^{-3})$$

then: $$\frac{\rho \frac{\partial w}{\partial \theta}}{\mu \frac{\partial^2 w}{\partial z^2}} = \frac{O(10^{-3})}{O(10^{1})} = O(10^{-4})$$

The creeping flow assumption therefore appears to be valid.

The assumption of the arbitrary straightening of the lamella should be discussed. This assumption is valid if the curvature of the lamella is small relative to the lamella height. To show that the curvature has little effect on the solution, the difference must be small between the dynamic pressure that the lamella liquid exerts on the upper surface of the lamella when the lamella liquid is being constrained to follow a curved path and the dynamic pressure that exists when the lamella is not curved. Re-stated, the assumption requires that the increment in the dynamic pressure exerted on the upper lamella surface because of centrifugal force acting on the flowing lamella liquid must be negligible relative to the existing lamella pressure when the lamella is straight.

The centrifugal force per unit area may be written:

$$p_{C.F.} = m^* \frac{u^2}{\beta'}$$

where m* is mass per unit area in the lamella, u is radial velocity in lamella and β' is the radius of curvature of the lamella. If b is equal to $\frac{1}{\beta'}$, the constant b will be large for small β' and therefore measures the curvature. To find m*, the following approximation must be made.

lamella volume

= lamella area x average height

or: $V_L = A_L h$

ρ = density of lamella liquid

$\therefore m^* = \rho \frac{V}{A} = \rho h$

$p_{C.F.} = \rho bh\, u^2$

For the drops used in this study:

$\rho = O(10^0)$

$b = O(10)$

$h = O(10^{-4})$

and since $\rho bh = O(10^{-3})$

and, $u = O(10^{-3})$

then, $p_{C.F.} = O(10^{-9}) \quad \frac{dyne}{cm^2}$

The dynamic lamella pressure is of the order of 10^2. Therefore, the lamella may be arbitrarily straightened without significantly changing the fluid mechanical behaviour of the lamella.

A2.6 The Simplification of the Radii of Curvature Expressions

The linearized equations for the radii of curvature of the bulk and drop interfaces must be shown to hold at large lamella radii. This section will derive a simple expression that may be solved to allow a comparison between this more

accurate expression for the relative lamella thickness and the linearized expression used throughout this work.

The radii of curvature for the drop interface are:

$$\frac{1}{\beta_1} = \frac{\frac{d^2h}{dr^2}}{\left(1+\left(\frac{dh}{dr}\right)^2\right)^{3/2}}$$

and

$$\frac{1}{\beta_2} \quad \frac{\frac{dh}{dr}}{r\left(1+\left(\frac{dh}{dr}\right)^2\right)^{\frac{1}{2}}}$$

where h is the height of the drop interface above the horizontal reference axis, as shown in Figure (3) of Chapter (2). The height of the bulk interface, k, may be similarly defined and employed to express the radii of curvature of the bulk interface at any radial location r.

When a force balance is performed at any radial location r in the lamella,

$$p = \frac{2\gamma}{d} + \gamma\left(\frac{1}{H_1}\frac{d^2h}{dr^2} + \frac{1}{H_2 r}\frac{dh}{dr}\right)$$

$$= -\gamma\left(\frac{1}{K_1}\frac{d^2k}{dr^2} + \frac{1}{K_2 r}\frac{dk}{dr}\right) \qquad \text{.....(1)}$$

where

$$H_1 = \left(1+\left(\frac{dh}{dr}\right)^2\right)^{3/2}$$

$$H_2 = \left(1+\left(\frac{dh}{dr}\right)^2\right)^{\frac{1}{2}}$$

$$K_1 = \left(1+\left(\frac{dk}{dr}\right)^2\right)^{3/2}$$

$$K_2 = \left(1+\left(\frac{dk}{dr}\right)^2\right)^{\frac{1}{2}}$$

Since $h = k - y$, and $\frac{dk}{dr} \ll 1$, as shown in Chapter (2) for the toluene/water system for a 0.005 ml. toluene drop, then:

$$\frac{dh}{dr} \doteq \frac{dy}{dr} \qquad \text{and} \qquad \frac{d^2h}{dr^2} \doteq \frac{d^2y}{dr^2} .$$

These approximations become more accurate as the radial distance outside the barrier ring is increased, because $\frac{dk}{dr} \longrightarrow 0$ and $\frac{dh}{dr} \longrightarrow \infty$.

Before the substitution for $\frac{dh}{dr}$ and $\frac{d^2h}{dr^2}$ is made in terms of y, the accurate forms,

$$\frac{dh}{dr} = \frac{dk}{dr} - \frac{dy}{dr} \quad \text{and} \quad \frac{d^2h}{dr^2} = \frac{d^2k}{dr^2} - \frac{d^2y}{dr^2}$$

are used and are substituted into the numerators of equation (1) to yield:

$$p = \frac{2\gamma}{d} + \gamma\left(\frac{1}{H_1}\frac{d^2k}{dr^2} + \frac{1}{H_2 r}\frac{dk}{dr}\right)$$

$$- \gamma\left(\frac{1}{H_1}\frac{d^2y}{dr^2} + \frac{1}{H_2 r}\frac{dy}{dr}\right)$$

$$= -\gamma\left(\frac{1}{K_1}\frac{d^2k}{dr^2} + \frac{1}{K_2 r}\frac{dk}{dr}\right)$$

Therefore:

$$\gamma\left(\left(\frac{1}{H_1}+\frac{1}{K_1}\right)\frac{d^2k}{dr^2}+\left(\frac{1}{H_2}+\frac{1}{K_2}\right)\frac{1}{r}\frac{dk}{dr}\right)$$

$$=-\frac{2\gamma}{d}+\gamma\left(\frac{1}{H_1}\frac{d^2y}{dr^2}+\frac{1}{H_2 r}\frac{dy}{dr}\right) \qquad \ldots\ldots(2)$$

Equation (2) is an exact force balance, but the equation is difficult to use in this form. As was done in Chapter (2), the left-hand-side of equation (2) may be set equal to -2 p. This is an approximation.

Then:

$$\frac{1}{H_1}\frac{d^2y}{dr^2}+\frac{1}{H_2 r}\frac{dy}{dr}-\frac{2}{d}=-\frac{2p}{\gamma} \qquad \ldots\ldots(3)$$

wher e H_1 and H_2 may be approximated by:

$$H_1 \doteq\left(1+\left(\frac{dy}{dr}\right)^2\right)^{3/2}$$

$$H_2 \doteq\left(1+\left(\frac{dy}{dr}\right)^2\right)^{\frac{1}{2}}$$

Equation (3) is a more accurate form of the force balance than was used in Chapter (2). The effect of the H_1 and H_2 factors on the relative lamella shape calculated from equation (3) may be evaluated by employing the following steps:

(1.) The factors H_1 and H_2 are assumed to be unity. The value of y is calculated as a function of r for an arbitrarily specified polynomial distribution of the lamella pressure, p.

(2.) The factors H_1 and H_2 are evaluated and y is again determined as a function of r.

(3.) Step (2) is repeated until the convergence of the relative lamella shape is achieved. These calculations were made for the toluene/water and anisole/water systems for an arbitrary distribution of the lamella pressure. The results are shown in Tables (A2.1,2).

The calculations were started at the barrier ring, since at less than this radius, the value $\frac{dh}{dr}$ much less than 1 is expected. The data in the tables show that the percentage change in the lamella height at R is 1 - 3% for both systems. No further calculations have been done, since this small change in the relative lamella shape when a more accurate form of the force balance is used should not alter the conclusion that $\Gamma_{max.} > \Gamma_t$ for some of the lamella profiles shown in Figure (8) of Chapter (3).

Also, an approximation was used for the L.H.S. of equation (2). Since the use of H_1 and H_2 in equation (3) does not significantly alter the relative lamella shape, the use of H_1 and H_2 in the L.H.S. of equation (2) should not radically alter the percentage change in relative lamella shape when compared with the shape calculated from the linearized equations. Both K_1 and K_2 approach unity as r approaches R. These factors will not affect the calculations adversely.

Table A2.1 Effect of Linerization of the Radii of Curvature Expressions on the Calculated Relative Lamella Thickness Profiles

Toluene/Water
Drop Volume 0.005 ml.

	Radius cm.	Linearized Results A°	First Iteration A°	Converged Result A°	
	0	15,500	15,500	15,500	
	0.0069	15,154	15,154	15,154	←Barrier Ring
	0.0104	15,658	15,656	15,656	
	0.0202	32,959	32,953	32,953	
	0.0302	106,773	107,019	107,021	
	0.0400	277,719	280,799	280,869	
R	0.0489	532,208	546,174	546,913	% Change is 2.76%

1. Convergence was reached at the fourth iteration.
2. $p_o = 339.88 \text{ dyne/cm}^2 = \frac{\gamma}{d} + 10.$
3. $p = p_o - \frac{3\,p_o r^2}{R^2} + \frac{3\,p_o r^4}{R^4} - \frac{p_o r^6}{R^6}$
4. $R^2 = \frac{4\,W\,g}{\pi\,p_o}$

Table A2.2 Effect of Linearization of the Radii of Curvature Expressions on the Calculated Relative Lamella Thickness Profiles

Anisole/Water
Drop Volume 0.020 ml.

	Radius cm.	Linearized Results, A°	First Iteration A°.	Converged Results A°	
	0	15,500	15,500	15,500	
	0.0099	14,341	14,341	14,341	←Barrier Ring
	0.0150	16,308	16,307	16,307	
	0.0201	25,194	25,192	25,192	
	0.0300	78,919	79,015	79,016	
	0.0351	133,434	133,845	133,847	
R	0.0424	245,979	247,781	247,807	% Change is 0.74%

1. Convergence was reached at the third iteration.
2. $p_o = 131.88$ dyne/cm. $= \frac{\gamma}{d} + 10.$
3. The same form of pressure distribution as used in the calculation of the results in Table A2.1 was used for this calculation.

A2.7 The Pressure Polynomial Work

The work in Chapter (2) on the application of the pressure polynomial to the description of dimple shapes is reasonably complete. This section will compare the calculations of dimple shapes given in Chapter (2) from the semi-empirical polynomial pressure model with the shapes calculated from the theoretical exponential pressure model, derived in Chapter (4).

A comparison of the prediction of these models relative to the same experimental lamella shape used in the polynomial work of Chapter (2) is given in Figures (A2.1),(2) and (3). The most distinctive difference among these figures is in the location of the barrier ring. The exponential pressure model predicts narrow barrier ring radii. This is because the experimental lamella pressure does not decay as rapidly as the exponential model predicts.

This comparison also suggests an important conclusion. The theory derived in Chapter (4) is not adequate to describe experimental lamella shapes. This may be caused by the limitation of the assumptions used. The assumptions simplified the problem to permit the analytical treatment, but there is a loss of accuracy.

A final conclusion that may be made is that the semi-empirical polynomial pressure model should still be used if an accurate description of the lamella shape and pressure is desired.

Figure A2.1 Observed Relative Lamella Thickness Profile

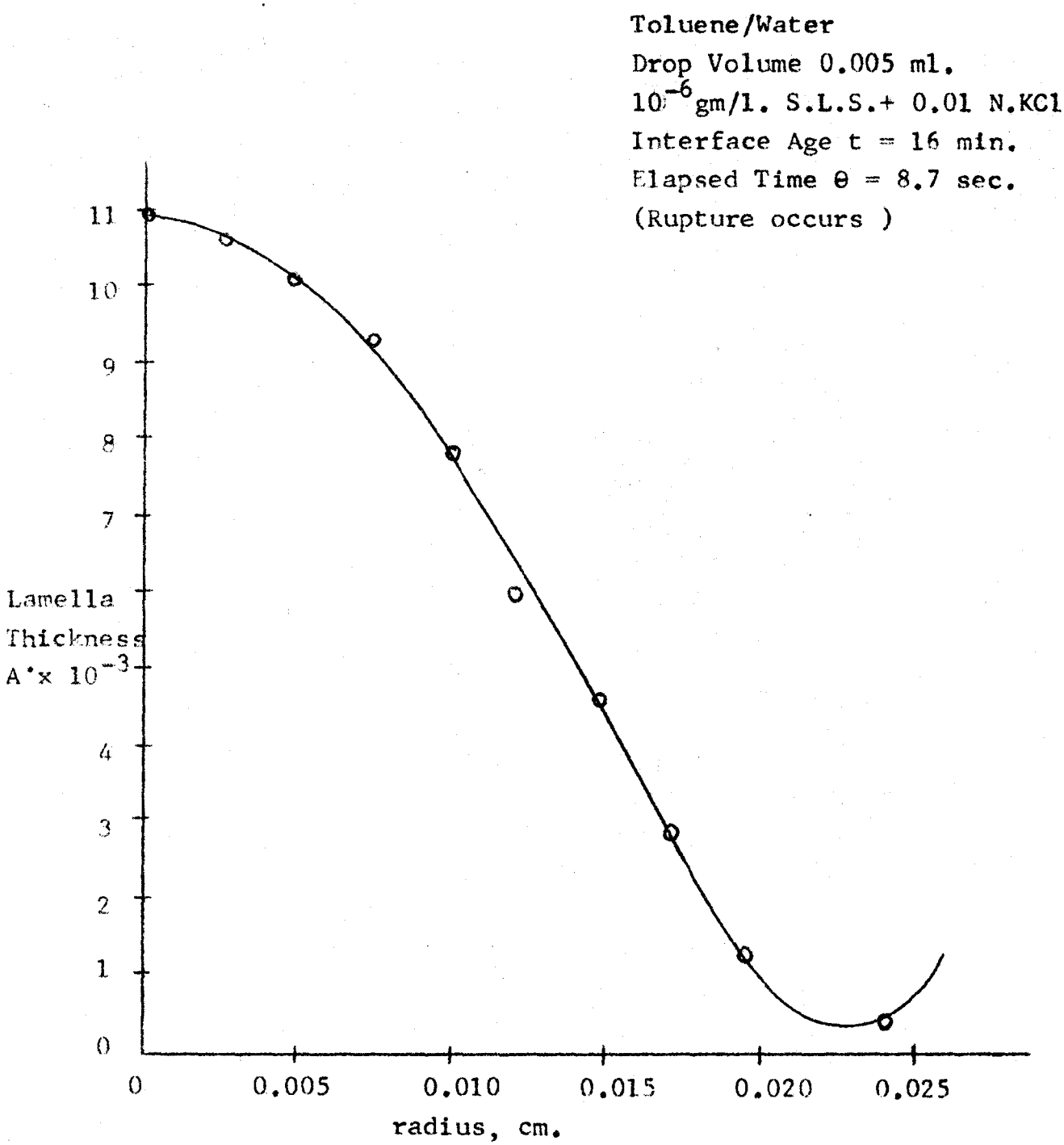

Figure A2.2 Semi-Empirical Prediction of the Relative Lamella Thickness Profile

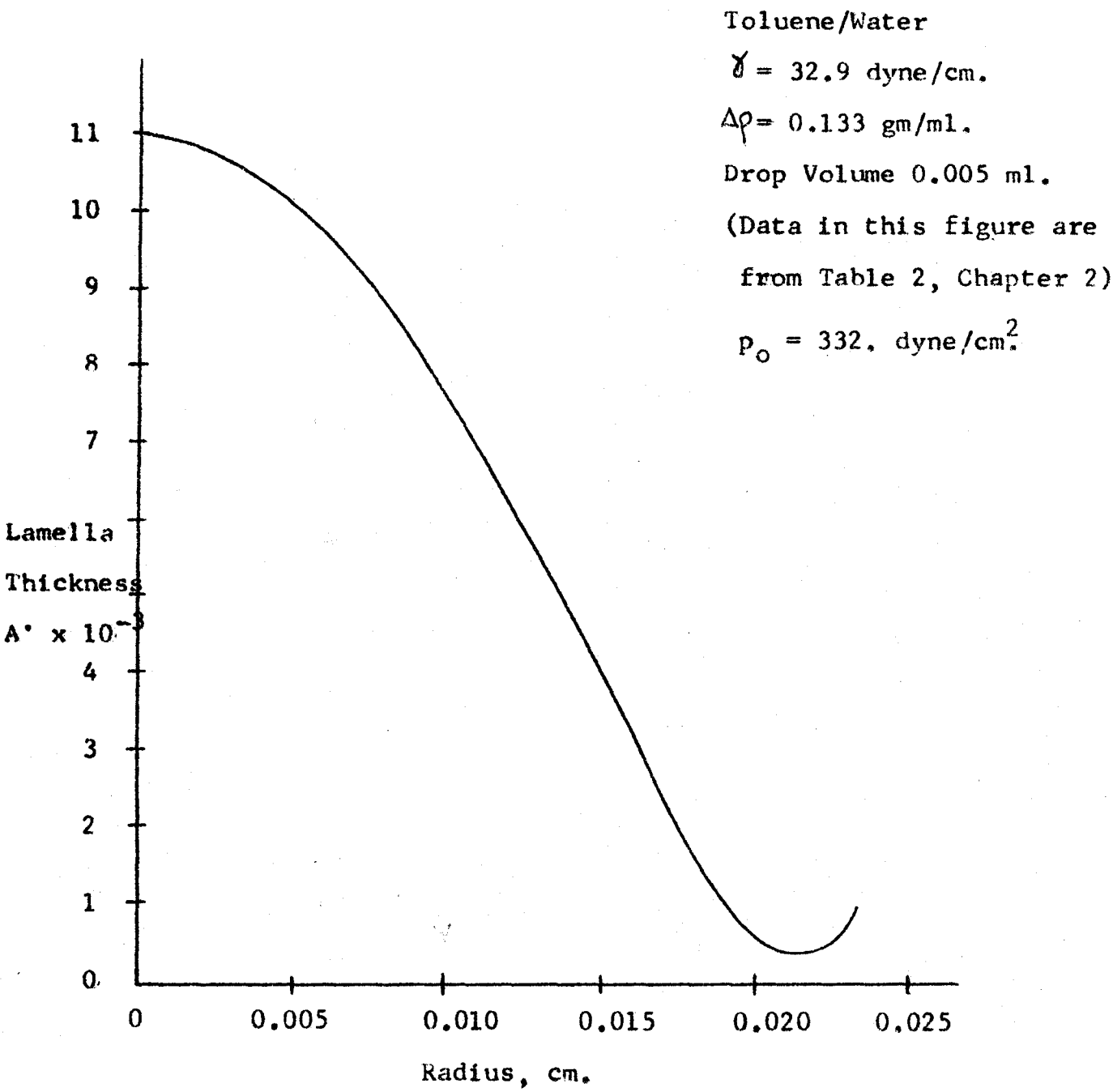

Figure A2.3 Exponential Model Prediction of the Relative Lamella Thickness Profile

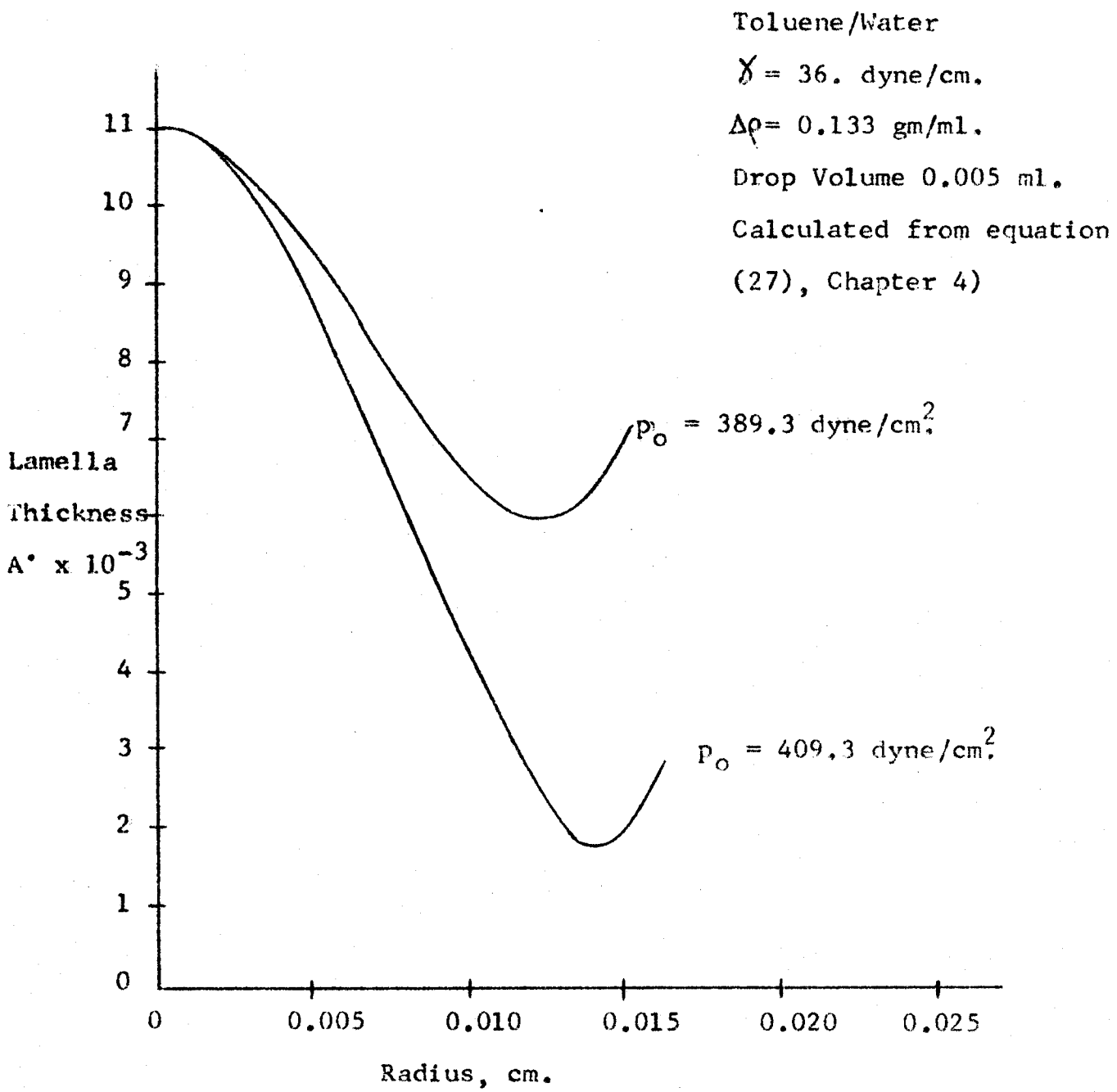

A2.8 The Series Type Pressure Polynomial

The pressure polynomial proved to be extremely valuable because the lamella shape, the lamella pressure, and the interfacial distribution of adsorbed surfactant could be predicted as functions of the radius. An analytical form is known for the lamella pressure, but the use of the polynomial is the only means by which an analytical method can be used to calculate the interfacial distribution of adsorbed surfactant. This will be outlined in section A2.9.

The a_i in equation (18) of Chapter 4 can be evaluated from the polynomial expression for the pressure distribution. To illustrate how the a_i of equation (18) in Chapter 4 were found, the coefficients are determined when equation (18) is truncated after five terms. Equation (18) becomes:

$$\frac{p}{\mu} \doteq \frac{p_o}{\mu} + \frac{a_1 r^2}{4} + \frac{a_2 r^4}{64} + \frac{a_3 r^6}{576} + \frac{a_4 r^8}{2304} \qquad \ldots\ldots(7)$$

Sufficient boundary conditions are chosen so that the a_i can be found in terms of a radius R. The value of R is defined as that radius at which the lamella pressure is zero. For equation (7), the boundary conditions on pressure may be written:

$$\left.\begin{array}{ll} p = 0 & \dfrac{\partial^2 p}{\partial r^2} = 0 \\ \dfrac{\partial p}{\partial r} = 0 & \dfrac{\partial^3 p}{\partial r^3} = 0 \end{array}\right\} \quad r = R$$

A fifth boundary condition is that the lamella pressure must balance the drop buoyancy force. The equation is:

$$\int_0^R 2\pi r p \, dr = Wg \qquad \ldots\ldots(8)$$

For the first four boundary conditions, the four resultant equations from equation (7) are solved simultaneously to yield:

$$a_1 = \frac{-16\, a_0}{R^2}$$

$$a_2 = \frac{384\, a_0}{R^4}$$

$$a_3 = \frac{-2304\, a_0}{R^6}$$

$$a_4 = \frac{2304\, a_0}{R^8}$$

and the fifth boundary condition then yields:

$$R^2 = \frac{5\, Wg}{\mu \pi a_0}$$

where $a_0 = \frac{P_o}{\mu}$.

If more terms are used in equation (7), more boundary conditions on the pressure derivatives at R are used. Table (A3.3) shows the results when a various number of terms in equation (7) are used.

Clearly R^2 approaches infinity as an infinite number

Table A2.3 Coefficients in Series-Type Polynomial

Coefficient	Number of Unknown a_i and Their Value			
	2	3	4	5
a_1	$-\frac{8\,a_0}{R^2}$	$-\frac{12\,a_0}{R^2}$	$-\frac{16\,a_0}{R^2}$	$-\frac{20\,a_0}{R^2}$
a_2	$\frac{64\,a_0}{R^4}$	$\frac{192\,a_0}{R^4}$	$\frac{384\,a_0}{R^4}$	$\frac{640\,a_0}{R^4}$
a_3		$-\frac{576\,a_0}{R^6}$	$-\frac{2304\,a_0}{R^6}$	$-\frac{5760\,a_0}{R^6}$
a_4			$\frac{2304\,a_0}{R^8}$	$\frac{11520\,a_0}{R^8}$
a_5				$-\frac{6400\,a_0}{R^{10}}$
Value of R^2	$\frac{3\,W\,g}{\mu\pi a_0}$	$\frac{4\,W\,g}{\mu\pi a_0}$	$\frac{5\,W\,g}{\mu\pi a_0}$	$\frac{6\,W\,g}{\mu\pi a_0}$

of terms are taken. To find the values of the a_i as an infinite number of terms are taken, general expressions are needed for a_i in terms of the number of unknowns. If n is the number of unknowns, then:

$$a_1 = \frac{-4n a_o}{R^2}$$

and since, $$R^2 = (n+1)\frac{Wg}{\mu\pi a_0}$$

$$a_1 = \frac{-4n}{(n+1)}\left(\frac{\mu\pi a_0^2}{Wg}\right)$$

Since, $n \longrightarrow \infty$

Then, $$a \longrightarrow -4\left(\frac{\mu\pi a_0}{Wg}\right) a_0$$

For the second unknown,

$$a_2 = 32n(n-1)\frac{a_0}{R^4}$$

and so,

$$a_2 \longrightarrow 32\left(\frac{\mu\pi a_0}{Wg}\right)^2 a_0$$

And for the third term,

$$a_3 = -96\frac{n(n-1)(n-2)}{(n+1)^3}\left(\frac{\mu\pi a_0}{Wg}\right)^3 a_0$$

$$a_3 \longrightarrow -96\left(\frac{\mu\pi a_0}{Wg}\right)^3 a_0$$

Similarly for a_4 and a_5:

$$a_4 \longrightarrow 96\left(\frac{\mu\pi a_0}{Wg}\right)^4 a_0$$

$$a_5 \longrightarrow \frac{-160}{3}\left(\frac{\mu\pi\, a_0}{Wg}\right)^5 a_0$$

More values of a_i may be found if more terms are used in the polynomial expression for ρ. This method shows how the a_i in equation (18) of Chapter (4) may be evaluated.

A2.9 The Derivation of an Expression for the Interfacial Distribution of Adsorbed Surfactant

The product of the series polynomial expression for the radial pressure gradient and the series expression for the relative lamella thickness defines $\frac{\partial \Gamma}{\partial r}$ as a function of r. These series are obtained from the following expressions:

$$p = a_0 + a_2 r^2 + a_4 r^4 + a_0 r^6$$

and $$y = y_o + b_2 r^2 + b_4 r^4 + b_6 r^6 + b_8 r^8$$

where: a_0 = center lamella pressure

$$a_2 = \frac{-3a_0}{R^2}$$

$$a_4 = \frac{+3a_0}{R^4}$$

$$a_6 = -\frac{a_0}{R^6}$$

$$R^2 = \frac{4Wg}{\pi\, a_0}$$

and y_o = center lamella height

$$b_2 = \left(\frac{1}{2d} - \frac{a_0}{2\gamma}\right)$$

$$b_4 = \frac{3}{8}\frac{a_0}{\gamma R^2}$$

$$b_6 = -\frac{a_0}{6\gamma R^4}$$

$$b_8 = \frac{a_0}{32\gamma R^6}$$

The interfacial gradient of adsorbed surfactant may be written for a mobile drop interface as in equation (11) of Chapter (3):

$$-\frac{k'\partial\Gamma}{\partial r} = y\frac{\partial p}{\partial r}$$

where Γ is the interfacial concentration of adsorbed surfactant at any radial distance r, and k' is a constant used in the isotherm for interfacial tension. This isotherm is:

$$\gamma = \gamma_0 - k'\Gamma$$

If y and $\frac{\partial p}{\partial r}$ are found from the polynomials, then equation (1) is written:

$$y\frac{\partial p}{\partial r} = c_2 r + c_4 r^3 + c_6 r^5 + \ldots c_{14} r^{13} \qquad \ldots\ldots(2)$$

where the c_i must be found from a term-by-term multiplication of the polynomials.

Equation (2) may be integrated with respect to r to yield:

$$\Gamma = \Gamma_0 - \frac{2}{k'}\left(\frac{c_2 r^2}{2} + \frac{c_4 r^4}{4} + \ldots \frac{c_{14} r^{14}}{14}\right) \qquad \ldots\ldots(3)$$

where the boundary condition $\Gamma = \Gamma_0$ at $r = 0$ has been used to evaluate the integration constant.

The interfacial distribution of adsorbed surfactant may be calculated from equation (3).

A2.10 The Parallel Disc Model

A derivation of the parallel disc model is presented in this thesis for the sake of completeness. The derivation closely follows the derivation given by Hodgson (1966).

If all the simplifying assumptions discussed in Chapter (4) are valid, the equations of motion may be written as:

$$\mu \frac{\partial^2 u}{\partial z^2} = \frac{\partial p}{\partial r} \qquad \ldots\ldots(1)$$

This equation may be integrated twice with respect to z. If the bulk and drop interfaces are both immobile, the resulting equation is:

$$u = \frac{(z^2 - hz)}{2\mu} \frac{\partial p}{\partial r} \qquad \ldots\ldots(2a).$$

If only the drop interface is mobile, the result is:

$$u = \frac{(z^2 - h^2)}{2\mu} \frac{\partial p}{\partial r} \qquad \ldots\ldots(2b)$$

The volume flux across any perpendicular plane may now

be evaluated at any radius r. The equation for this flux is:

$$Q = \int_0^h 2\pi r u \, dz$$

where Q is the volume of water which passes through the vertical plane located at r = r

h is lamella thickness.

This equation may be solved when either equation (2a) or (2b) is used. For both cases, the result is:

$$Q = -\frac{(3-m)^2}{6\mu} \pi r \frac{\partial p}{\partial r} h^3 \qquad \ldots\ldots(3)$$

where m is the number of immobile interfaces.

A mass balance for the water in the lamella may now be made on a ring of elemental volume. Since the following equality must hold:

mass into the ring - mass out = the change in mass in the ring

The following partial differential equation results:

$$\frac{(3-m)^2}{12\mu}\left(\frac{\partial^2 p}{\partial r^2} + \frac{1}{r}\frac{\partial p}{\partial r}\right) = \frac{\partial h}{\partial \theta} \qquad \ldots\ldots(4)$$

Before equation (4) can be solved, the pressure gradients must be evaluated. To find an expression for the pressure in the lamella, the continuity equation is written in terms of velocity. This equation is:

$$\frac{\partial u}{\partial r} + \frac{u}{r} = \text{constant} = W'$$

This equation may be integrated with respect to r to yield:

$$u = \frac{1}{2} W'r \qquad \ldots\ldots(5)$$

where the boundary condition: u is finite at r equal to zero has been used to evaluate the integration constant.

If equation (5) is equated to either equation (2a) or (2b), the result is:

$$\frac{\partial p}{\partial r} = K_z r \qquad \ldots\ldots(6)$$

Equation (6) may be integrated to yield:

$$p = \frac{K_z}{2} (r^2 - R^2) \qquad \ldots\ldots(7)$$

where the boundary condition: $p = 0$ at $r = R$ has been used. Since the pressure force in the lamella must balance the drop weight, equation (8) may be written as:

$$\int_0^R 2\pi r\, p\, dr = Wg \qquad \ldots\ldots(8)$$

If equation (7) is substituted into equation (8) and the result is integrated, it is found that:

$$K_z = -\frac{4\,Wg}{\pi R^4}$$

Therefore:

$$\frac{\partial p}{\partial r} = -\frac{4\,Wg}{\pi R^4} r$$

and $$\frac{\partial^2 p}{\partial r^2} = -\frac{4 Wg}{\pi R^4}$$

The partial differential equation, equation (4), may be written in final form as:

$$\frac{\partial h}{\partial \theta} = -\frac{2(3-m)^2 Wg\, h^3}{3\mu \pi R^4} \qquad \ldots\ldots(9)$$

If the average lamella pressure for the parallel disc is $\frac{2\gamma}{d}$, a force balance may be made to find R.

Since: $$\frac{2\gamma}{d} \pi R^2 = Wg$$

then: $$R = d^2 \sqrt{\frac{2 \Delta\rho\, g}{3\gamma}} \qquad \ldots\ldots(10)$$

When equation (10) is substituted into equation (9) and the result is integrated with respect to r, the integrated form of the parallel disc model is:

$$\left(\frac{1}{h_o^2} - \frac{1}{h^2} \right) = -\frac{4(3-m)^2 \gamma^2 (\theta-\theta_0)}{d^5 \mu \Delta\rho\, g} \qquad \ldots\ldots(11)$$

A2.11 Barrier Ring Expansion

An expression for the expansion of the barrier ring radius is derived as a function of barrier ring height in this section. The derivation of the equation provides insight into the mechanism responsible for barrier ring expansion.

To begin the analysis, in section (A2.10), an expression

for the rate of lamella drainage at the barrier ring is of the form: (from equation 9 of A2.10)

$$\frac{\partial h_c}{\partial \theta} = - \alpha h_c^3 \qquad \ldots\ldots(1)$$

where h_c is the barrier ring height, θ is time, and where α is a constant to be defined later. Equation (1) corresponds to the parallel disc model.

Outside the barrier ring, the rate of lamella drainage may be written as:

$$\frac{\partial h}{\partial \theta} = - \alpha h^3 - \beta h^2 \frac{\partial h}{\partial r} \qquad \ldots\ldots(2)$$

Equation (2) is equation (3) of section (A2.1) of this appendix, simplified by the assumption of a parabolic type pressure distribution, but with the assumption that the lamella thickness is no longer constant with radius outside the barrier ring. The parameter β is a constant to be defined later, and h is the thickness of the lamella at any radius outside the barrier ring.

Since the slope of the lamella shape must be evaluated in equation (2), the shape of the lamella must be found. From equation (27) of Chapter (4), the lamella thickness may be written as:

$$h = h_0 + a_1 r^2 + a_2 r^4 + \ldots$$

where $h = h_0$

$r = 0$

and a_1, a_2, are constants.

At the barrier ring, $h = h_c$ when $r = c$, therefore:

$$h_c = h_0 + a_1 c^2 + a_2 c^4 + \ldots$$

Therefore:

$$h = h_c + a_1(r^2-c^2) + a_2(r^4-c^4) + \ldots$$

If r is written as $c+\Delta$, and the third term in the above equation is included, then:

$$h \doteq h_c + 2c\Delta a_1 + 4c^3\Delta a_2 + 4c^2\Delta^2 a_2 + 2c\Delta^3 a_2$$

This equation defines the shape of the lamella outside the barrier ring. Also, from the above equation, the slope may be written:

$$\frac{\partial h}{\partial r} = 2c\,(a_1 + 2c^2 a_2 + 4c\Delta a_2)$$

since, $\Delta = r - c$.

Figure A2.4 shows the geometry for the problem, in the upper graph.

The mechanism for the expansion of the barrier ring may be postulated as follows. All the factors in equations (1) and (2) are positive, therefore, all lamella thicknesses outside the barrier ring are decreasing at a greater rate than at the barrier ring. Therefore it is possible that at a point close to and outside of the barrier ring, the lamella thickness may equal the barrier ring thickness. This postulate is shown

Figure A2.4 Lamella Geometry for the Derivation of an Expression for Barrier Ring Expansion

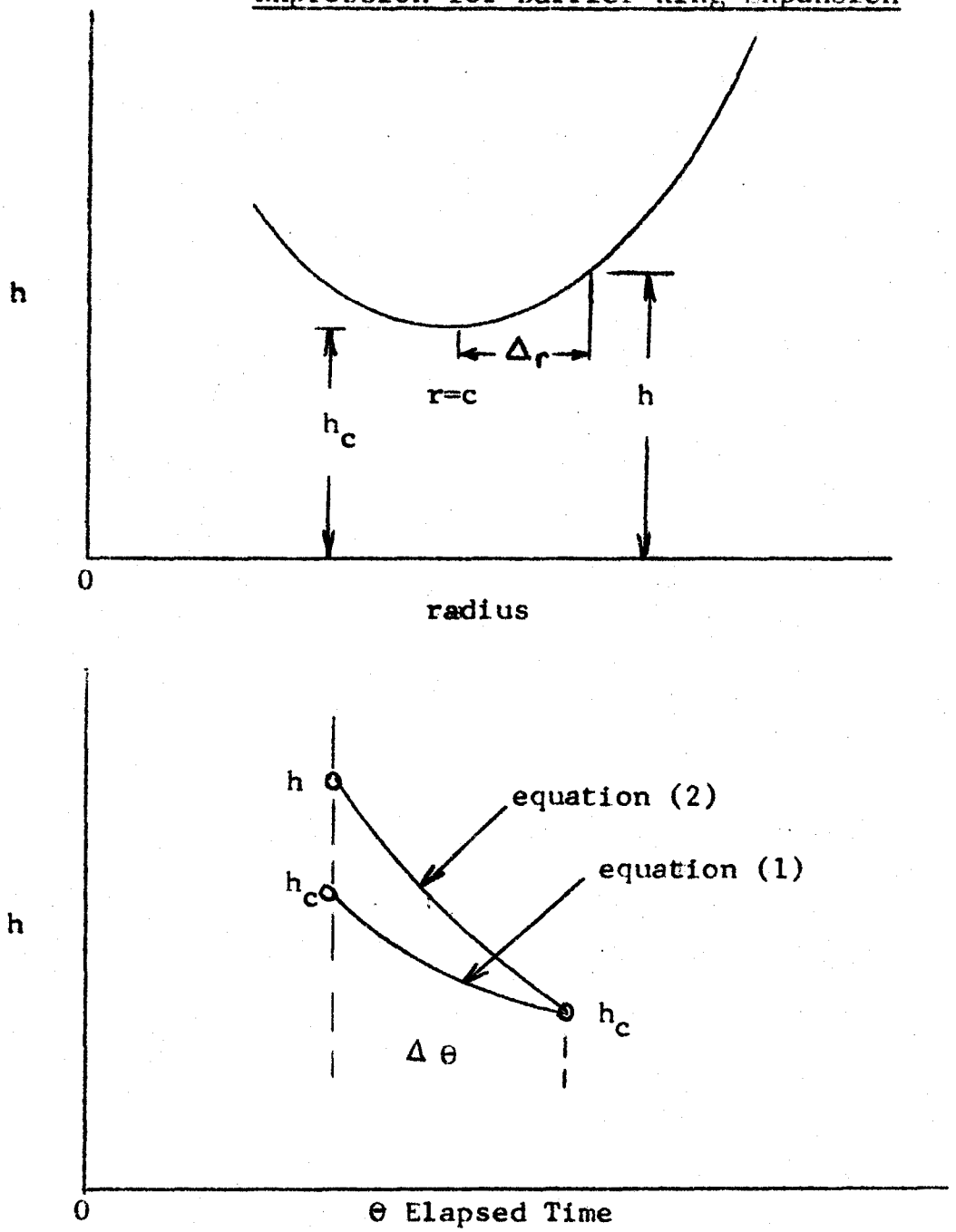

graphically in the second graph in Figure A2.4.

Based on this postulate the following equation may be written:

$$h_c + \frac{dh_c}{d\theta}\,\Delta\theta = h_c + \frac{1}{2}\frac{\partial^2 h_c\,\Delta^2}{\partial r^2} + \frac{\partial h}{\partial \theta}\,\Delta\theta$$

or, in the following form:

$$\Delta\theta = \frac{\frac{1}{2}\frac{\partial^2 h_c}{\partial r^2}\Delta^2}{\frac{dh_c}{d\theta} - \frac{\partial h}{\partial \theta}} \qquad \ldots\ldots(4)$$

From equations (1) and (2), the denominator of equation (4) may be written as:

$$\frac{dh_c}{d\theta} - \frac{\partial h}{\partial \theta} = \beta h_c^2 \frac{\partial h}{\partial r}$$

Since h^2 approximately equals h_c^2, then equation (4) may be written as:

$$\Delta\theta = \frac{\frac{1}{2}\frac{\partial^2 h_c}{\partial r^2}\Delta^2}{\beta h_c^2 \frac{\partial^2 h_c}{\partial r^2}\Delta}$$

Since Δ is equal to the change in the barrier ring radius, Δc, in time $\Delta\theta$, and Δc is approximately zero, then,

$$\frac{\Delta c}{\Delta\theta} \longrightarrow \frac{dc}{d\theta} = \frac{\beta h_c^2 \frac{\partial^2 h_c}{\partial r^2}\Delta}{2\frac{\partial^2 h_c}{\partial r^2}\Delta}$$

$$= \frac{1}{2}\beta h_c^2$$

The differential equation which describes the expansion of the barrier ring, therefore may be written:

$$\frac{dc}{d\theta} = \frac{1}{2}\beta\, h_c^2 \qquad \ldots\ldots(5)$$

The value of β must now be defined. Equation (3) of section A2.1 is the partial differential equation which may be used to define β as:

$$\beta = \frac{-1}{2\mu}\frac{\partial p}{\partial r} \quad \text{for a mobile drop interface.}$$

In section A2.10, an expression was derived for $\frac{\partial p}{\partial r}$ for the parallel disc model. This pressure gradient may be used. It was found that:

$$\frac{\partial p}{\partial r} = -\epsilon r$$

where $\epsilon = \frac{4\,Wg}{\pi R^4}$

Therefore, $\beta = \frac{\epsilon r}{2\mu}$

Since $r \doteqdot c$, equation (5) may be written as:

$$\frac{1}{c}\frac{dc}{d\theta} = \frac{\epsilon h_c^2}{4\mu} \qquad \ldots\ldots(6)$$

Similarly, α may be obtained from the parallel disc model, derived in section A2.10. The value of α is:

$$\alpha = \frac{8\,Wg}{3\mu\pi R^4} \quad \text{for a mobile drop interface.}$$

Equation (1) may be integrated to yield:

$$\left(\frac{1}{h_c^2} - \frac{1}{h_{c_o}^2}\right) = 2\alpha(\theta-\theta_o) \qquad \ldots\ldots(7)$$

where $h_c = h_{c_o}$

$\theta = \theta_o$

If equation (7) is solved for h_c^2 and the result is substituted into equation (6), and the equation is integrated, the following expression results:

$$\frac{4\mu}{\epsilon} \ln\left(\frac{c}{c_o}\right) = \int_{\theta_o}^{\theta} \frac{h_{c_o}^2 \, d\theta}{2\alpha h_{c_o}^2 \theta + (1 - 2\alpha h_{c_o}^2 \theta_o)} \qquad \ldots\ldots(8)$$

where $c = c_o$

$\theta = \theta_o$

If $\theta_o \neq 0$ when $h_c = h_{c_o}$, equation (8) may be integrated to yield:

$$\frac{4\mu}{\epsilon} \ln\left(\frac{c}{c_o}\right) = \frac{1}{2\alpha} \ln(2\alpha h_{c_o}^2 \theta + 1)$$

Since:

$$2\alpha\theta = \frac{1}{h_c^2} - \frac{1}{h_{c_o}^2}$$

Then:

$$\frac{4\mu}{\epsilon} \ln\left(\frac{c}{c_o}\right) = \frac{1}{\alpha} \ln\left(\frac{h_{c_o}}{h_c}\right)$$

This equation may be re-written in final form as:

$$\frac{c}{c_o} = \left(\frac{h_{c_o}}{h_c}\right)^{\frac{\epsilon}{4\alpha\mu}} \qquad \ldots\ldots(9)$$

Equation (9) may be further simplified if the exponent is evaluated for specific cases. Three cases may be distinguished:

(1) Both drop and bulk interfaces are immobile, then:

$$\alpha = \frac{\epsilon}{6\mu}$$

This results simply by using m = 2 in equation (9) of section A2.10.

(2) The drop interface is mobile, then:

$$m = 1$$

and

$$\alpha = \frac{2\epsilon}{3\mu}$$

(3) For the coupled model of Part B of Chapter (4), equation (49) of that chapter may be simplified by letting

$$k' \Gamma_t \longrightarrow 0.$$

For this case, $\alpha = \frac{4\epsilon}{3\mu}$

For these three cases, the exponent on equation (9) becomes:

Case (1), $\frac{\epsilon}{8\alpha\mu} = 3/4$ $\left(\beta = \frac{-1}{4\mu}\frac{\partial p}{\partial r}\right.$ for an immobile drop interface)

Case (2), $\frac{\epsilon}{4\alpha\mu} = 3/8$

Case (3), $\frac{\epsilon}{4\alpha\mu} = 3/16$

Equation (9) has been solved for the values of the exponents given in all the above cases. The results are given in

Figure (A2.5) and they may be compared with a line for anisole/water which was measured experimentally. This line describes the locus of the barrier ring radius for a 0.020 ml. anisole drop.

An exponent of 3/4 for equation (9) results in a predicted curve which deviates from the expermental curve. An exponent of 3/16 obtained from the coupled model for $k' \Gamma_t$ equal to zero, and used to evaluate equation (9), results in a predicted curve for barrier ring expansion which closely describes the observed expansion at large lamella thicknesses. A curve, calculated from equation (9) for an exponent of 1/4 is also shown in Figure (A2.5).

The close agreement between the results of this simple model for barrier ring expansion and the experimental data supports the mechanism for barrier ring expansion that has been proposed.

Figure A2.5 Comparison Between the Predicted and Observed Expansion of the Barrier Ring

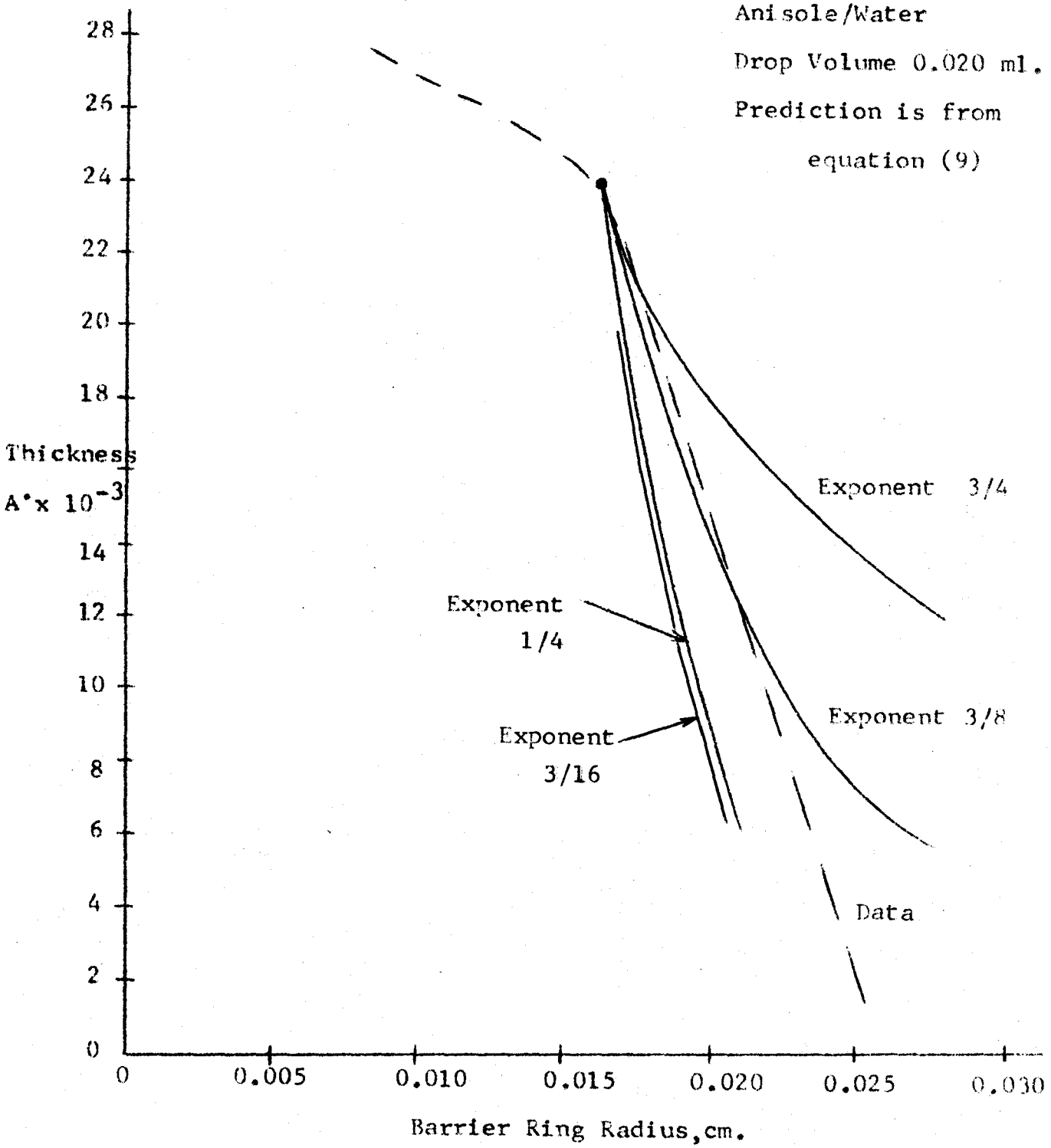

Program Listings for Solution of Equations in Chapter (4):

(1) Solution of Equation (23)

(2) Solution of Equations (28) (31) and (32a)

(3) Solution of Equation (49)

```
C
C     PROGRAM TO NUMERICALLY EVALUATE THE
C     CHANGE IN DIMPLE SHAPE WITH TIME
C     FROM SOLUTION OF THE EQUATIONS OF MOTION
C
C++++ ++++++++++++++++++++++++++++++++++++++++++++++++++++++++++++++++++++++++++
C     SYMBOL DEFINITIONS- ALL PARAMETERS ARE IN C.G.S. UNITS
C     R-RADIAL DISTANCE ARRAY
C     Y-DIMPLE HEIGHT ARRAY
C     YTEMP-TEMPORARY STORAGE FOR NEW Y VALUES
C     VIS-VISCOSITY OF THE CONTINUOUS PHASE
C     SIG-SYSTEM INTERFACIAL TENSION (NO SURFACTANT)
C     BUOY-SYSTEM DENSITY DIFFERENCE
C     GRAV-GRAVITATIONAL CONSTANT
C     RAD-DROP RADIUS
C     VOL-DROP VOLUME
C     WG-NET DROP WEIGHT
C     PI-CONSTANT
C     PO-CENTER DIMPLE PRESSURE
C     YO-CENTER DIMPLE HEIGHT
C     XLAM,BETA,-PARAMETERS
C     R2-A CONVENIENT DEFINITION OF POINT WHERE PRESSURE IS APPROX. ZERO
C     K,KK,N,NN,N2,-COUNTERS
C     T-TIME
C     DELT-TIME INCREMENT
C     DELR-DISTANCE INCREMENT
C     DYDR,D2YDR2,-SLOPE OF THE DIMPLE AND GRADIENT OF THE SLOPE
C     EXP-COMPUTER LIBRARY SUBROUTINE NAME FOR EXPONENTIAL FUNCTION
C++++ ++++++++++++++++++++++++++++++++++++++++++++++++++++++++++++++++++++++++++
C
      DIMENSION R(201),Y(201),YTEMP(201)
C     DEFINE PARAMETERS
C
C     ANISOLE-WATER SYSTEM
C
      VIS=.00894
      SIG=20.5
      BUOY=.0097
      RAD=.1682
      VOL=.020
      GRAV=981.
      WG=VOL*BUOY*GRAV
      PI=3.1416
      K=1
C
C     MOBILITY CRITERION
C     M=2, TWO IMMOBILE INTERFACES
C     M=1, ONE IMMOBILE INTERFACE
C
      M=1
C
      PO=150.
      YO=1.5E-04
      XLAM=PI*PO/WG
      BETA=2.*XLAM*PO/VIS
C
      R2=3.*WG/(PI*PO)
C
      N=200
```

```
      NN=N+1
      N2=N/2
      T=0
      DELT=1.0E-04
      KK=100
C
C     CALCULATE RADIUS ARRAY
C
      DELR=SQRT(R2)/FLOAT(N)
      R(1)=0
      DO 10 J=1,N
      R(J+1)=R(J)+DELR
   10 CONTINUE
C
C     CALCULATE INITIAL SHAPE
C
      FACT1=(1./RAD-PO/SIG)/2.
      FACT2=PO/(2.*XLAM*SIG)
      Y(1)=YO
      DO 11 J=2,NN
      X=XLAM*(R(J)**2)
      Y(J)=YO+FACT1*(R(J)**2)+FACT2*(X**2/4.-X**3/18.+X**4/96.)
   11 CONTINUE
C
      DO 302 J=2,N2,2
      J1=J+N2
      PRINT 201,R(J),Y(J),R(J1),Y(J1)
  302 CONTINUE
C
      PRINT 202
C
C     NOW PROCEED TO A NEW SHAPE
C
  101 CONTINUE
C
      DO 12 J=1,NN
      IF(J.LE.1)GO TO 13
      IF(J.GE.(N+1))GO TO 15
      DYDR=(Y(J+1)-Y(J-1))/(DELR*2.)
      GO TO 14
   15 CONTINUE
      D2YDR2=(Y(NN)-2.*Y(N)+Y(N-1))/(DELR**2)
      DYDR=(Y(NN)-Y(N-1))/(2.*DELR)
      DYDR=DYDR+D2YDR2*DELR
      GO TO 14
   13 DYDR=0
   14 CONTINUE
      ARGU=XLAM*(R(J)**2)
      FACT3=(Y(J)**2)*BETA/(EXP(ARGU)*FLOAT(M))
      FACT4=-Y(J)*2./(3.*FLOAT(M))
      FACT5=ARGU*Y(J)*2./(3.*FLOAT(M))
      FACT6=-R(J)*DYDR/2.
      DYDT=FACT3*(FACT4+FACT5+FACT6)
      YTEMP(J)=Y(J)+DYDT*DELT
   12 CONTINUE
C
      DO 301 J=1,NN
      Y(J)=YTEMP(J)
```

```
  301 CONTINUE
C
C
C     RECALCULATE CENTRE PRESSURE AND PARAMETERS
C
      D2YDR2=2.*(Y(2)-Y(1))/(DELR**2)
      PO=((1./RAD)-D2YDR2)*SIG
      XLAM=PI*PO/WG
      BETA=2.*XLAM*PO/VIS
C
      T=T+DELT
      IF(T.GT..5)GO TO 300
      K=K+1
      IF(K.GT.KK)GO TO 100
      GO TO 101
C
C     PRINTOUT
C
  100 CONTINUE
      PRINT 200,T
  200 FORMAT(10X,6H TIME=,F7.4,///)
C
      DO 102 J=2,N2,2
      J1=J+N2
      PRINT 201,R(J),Y(J),R(J1),Y(J1)
  201 FORMAT(4(10X,E13.5))
  102 CONTINUE
      PRINT 203,R(NN),Y(NN)
  203 FORMAT(46X,2(10X,E13.5))
C
      PRINT 202
  202 FORMAT(1H1)
C
      K=1
      GO TO 101
  300 CONTINUE
      STOP
      END
*        6400 END RECORD
*        6400 END FILE
```

```
C
C     PROGRAM TO SOLVE TWO COUPLED NON-LINEAR P.D.E. NUMERICALLY.
C     FOR THE CHANGE IN DIMPLE SHAPE WITH TIME                    396
C
C+++++++++++++++++++++++++++++++++++++++++++++++++++++++++++++++++++++++++++++
C     -ARRAY DEFINITIONS
C     R-RADIAL DISTANCE ARRAY
C     Y-DIMPLE HEIGHT ARRAY
C     U-SURFACE VELOCITY
C     DUDR-GRADIENT OF SURFACE VELOCITY
C     DYDT-CHANGE IN DIMPLE SHAPE
C     DYSTOR-TEMPORARY STORAGE OF THE CHANGE IN DIMPLE SHAPE
C     GAM-S.A.A. SURFACE CONC,N
C     GAMT-TEMPORARY STORAGE OF S.A.A. SURFACE CONC,N
C     YTEMP-TEMPORARY STORAGE OF DIMPLE SHAPE
C     DGDT-CHANGE IN S.A.A. SURFACE CONC,N
C     DDGDT- CHANGE IN S.A.A. SURFACE CONC,N DUE TO SURFACE DIFFUSION
C
C     SYMBOL DEFINITIONS- ALL PARAMETERS ARE IN C.G.S. UNITS
C     VIS-VISCOSITY OF THE CONTINUOUS PHASE
C     SIG-SYSTEM INTERFACIAL TENSION (NO SURFACTANT)
C     BUOY-SYSTEM DENSITY DIFFERENCE
C     GRAV-GRAVITATIONAL CONSTANT
C     RAD-DROP RADIUS
C     VOL-DROP VOLUME
C     WG-NET DROP WEIGHT
C     PI-CONSTANT
C     PO-CENTER DIMPLE PRESSURE
C     YO-CENTER DIMPLE HEIGHT
C     XLAM,BETA,-PARAMETERS
C     R2-A CONVENIENT DEFINITION OF POINT WHERE PRESSURE IS APPROX. ZERO
C     K,KK,N,NN,N2,-COUNTERS
C     T-TIME
C     DELT-TIME INCREMENT
C     DELR-DISTANCE INCREMENT
C     DYDR,D2YDR2,-SLOPE OF THE DIMPLE AND GRADIENT OF THE SLOPE
C     EXP-COMPUTER LIBRARY SUBROUTINE NAME FOR EXPONENTIAL FUNCTION
C     DS-SURFACE DIFFUSION COEFFICIENT
C     GAME-AVERAGE S.A.A. SURFACE CONC,N AT THE INSTANT CONSIDERED
C     - IN THIS PROBLEM
C     XK- CONVERSION FACTOR IN THE LINEAR ISOTHERM
C     TOL- A TOLERANCE USED IN CONVERGENCE OF A LOOP
C     NCOUNT- A COUNTER
C     MAX- MAXIMUM ALLOWABLE VALUE OF NCOUNT
C+++++++++++++++++++++++++++++++++++++++++++++++++++++++++++++++++++++++++++++
      DIMENSION R(201),Y(201),U(201),DUDR(201),DYSTOR(201),DYDT(201)
      DIMENSION GAM(201),GAMT(201)
      DIMENSION YTEMP(201),DGDT(201)
      DIMENSION DDGDT(201)
C
C     ANISOLE-WATER SYSTEM
C     DEFINE PARAMETERS
C
      DELT=1.0E-04
      DS=1.0E-05
      GAME=5.0E+12
      XK=1.4E-14
      VIS=.00894
      SIG=20.5
```

```
      BUOY=.0097
      VOL=.020
      RAD=.1682
      GRAV=981.
      WG=VOL*BUOY*GRAV
      PI=3.1416
      K=1
      KK=100
      TOL=.01
      NCOUNT=1
      MAX=10
      N=200
      NN=N+1
      N2=N/2
      T=0
C
      PO=150.
      YO=1.0E-04
      XLAM=PI*PO/WG
      BETA=2.*XLAM*PO/VIS
C
C     MOBILITY CRITERION
C     M=2,TWO IMMOBILE INTERFACES
C     M=1,ONE IMMOBILE INTERFACE
C
      M=1
C
      R2=3.*WG/(PI*PO)
      R2=R2/2.
C
C     CALCULATE THE RADIUS ARRAY
C
      DELR=SQRT(R2)/FLOAT(N)
      R(1)=0
      DO 10 J=1,N
      R(J+1)=R(J)+DELR
   10 CONTINUE
C
C     CALCULATE THE INITIAL SHAPE
C
      FACT1=(1./RAD-PO/SIG)/2.
      FACT2=PO/(2.*XLAM*SIG)
      Y(1)=YO
      DO 11 J=2,NN
      X=XLAM*(R(J)**2)
      Y(J)=YO+FACT1*(R(J)**2)+FACT2*(X**2/4.-X**3/18.+X**4/96.)
   11 CONTINUE
C
      PRINT 204,R(1),Y(1)
  204 FORMAT(2(10X,E13.5))
C
      DO 302 J=2,N2,2
      J1=J+N2
      PRINT 201,R(J),Y(J),R(J1),Y(J1)
  201 FORMAT(4(10X,E13.5))
  302 CONTINUE
C
      PRINT 202
```

```
  202 FORMAT(1H1)
C
C     DEFINE THE INITIAL SURFACTANT DISTRIBUTION
C
      TERM1=-PO*Y(1)
      TERM2=.346*WG*PO/(PI*SIG)
      TERM3=-WG/(2.*PI*RAD)
C
      TERM4=(TERM1+TERM2+TERM3)/XK
      GAMO=GAME+TERM4
C
      IF(GAMO.GT.0)GO TO 107
      PRINT 205,GAMO
  205 FORMAT(10X,24H SURFACE CONC,N NEGATIVE,E13.5)
      GO TO 104
C
  107 CONTINUE
C
      GAM(1)=GAMO
      DGDRO=0
      DO 16 J=2,NN
      X=XLAM*(R(J)**2)
      FACTOR=BETA*VIS/XK
      DGDR=FACTOR*Y(J)*R(J)/EXP(X)
      SLOPE=(DGDRO+DGDR)/2.
      GAM(J)=GAM(J-1)+SLOPE*DELR
      DGDRO=DGDR
   16 CONTINUE
C
      PRINT 204,R(1),GAM(1)
C
      DO 109 J=2,N2,2
      J1=J+N2
      PRINT 201,R(J),GAM(J),R(J1),GAM(J1)
  109 CONTINUE
C
      PRINT 203,R(NN),GAM(NN)
C
      PRINT 202
C
C
C     ASSUME SURFACE VELOCITY IS EVERYWHERE ZERO
C     -CALCULATE CHANGE IN SHAPE
C     -SET SURFACE VELOCITY TO TO ZERO AT T=0
C
      DO 12 J=1,NN
      U(J)=0
      DUDR(J)=0
   12 CONTINUE
C
  100 CONTINUE
C
C     CALCULATE THE CHANGE IN DIMPLE SHAPE
C
      DO 23 J=1,NN
C
      IF(J.LE.1)GO TO 17
      IF(J.GE.NN)GO TO 18
```

```
      DYDR=(Y(J+1)-Y(J-1))/(DELR*2.)
      FACT7=-Y(J)*U(J)/R(J)
      GO TO 19
   18 CONTINUE
      D2YDR2=(Y(NN)-2.*Y(N)+Y(N-1))/(DELR**2)
      DYDR=(Y(NN)-Y(N-1))/(2.*DELR)
      DYDR=DYDR+D2YDR2*DELR
      FACT7=-Y(J)*U(J)/R(J)
      GO TO 19
   17 DYDR=0
      FACT7=-Y(J)*DUDR(J)
   19 CONTINUE
      X=XLAM*(R(J)**2)
      FACT3=(Y(J)**2)*BETA/(EXP(X)*FLOAT(M))
      FACT4=-Y(J)*2./(3.*FLOAT(M))
      FACT5=X*Y(J)*2./(3.*FLOAT(M))
      FACT6=-R(J)*DYDR/2.
      FACT8=-Y(J)*DUDR(J)
      DYDT(J)=FACT3*(FACT4+FACT5+FACT6)
      DYDT(J)=DYDT(J)+FACT7+FACT8
   23 CONTINUE
C
C     KNOWING THE INITIAL SURFACTANT SURFACE DISTRIBUTION,
C     CALCULATE VALUES FOR THE SURFACE VELOCITY
C     USING THE SURFACTANT MASS BALANCE EQUATION
C
C
C     CALCULATE NEW SURFACE DISTRIBUTION OF SURFACTANT
C     AND THEN THE REQUIRED SURFACE VELOCITIES
C     -USE GAM(NN) AS A REFERENCE
C
      DO 20 J=1,NN
      YTEMP(J)=Y(J)+DYDT(J)*DELT
   20 CONTINUE
C
C     CALCULATE OUTSIDE SLOPE FIRST
C
      X=XLAM*(R(NN)**2)
      DGTEMO=BETA*VIS*YTEMP(NN)*R(NN)/(EXP(X)*XK)
      ENDSLO=DGTEMO
      DGDT(NN)=0
      GAMT(NN)=GAM(NN)
C
      DO 21 J=1,N
      JM=NN-J
      X=XLAM*(R(JM)**2)
      DGTEMP=BETA*VIS*YTEMP(JM)*R(JM)/(EXP(X)*XK)
      GAMT(JM)=GAMT(JM+1)-(DGTEMP+DGTEMO)*DELR/2.
      DGTEMO=DGTEMP
      DGDT(JM)=(GAMT(JM)-GAM(JM))/DELT
   21 CONTINUE
C
C     MODIFY THE CALCULATION OF SURFACTANT TIME CHANGE
C     BY CONSIDERING SURFACE DIFFUSION
C
      CONST=BETA*VIS/XK
C
      DO 24 J=1,NN
```

```
      IF(J.LE.1)GO TO 25
      IF(J.GE.NN)GO TO 26
      DYDR=(Y(J+1)-Y(J-1))/(DELR*2.)
      GO TO 27
C
   26 CONTINUE
      D2YDR2=(Y(NN)-2.*Y(N)+Y(N-1))/(DELR**2)
      DYDR=(Y(NN)-Y(N-1))/(2.*DELR)
      DYDR=DYDR+D2YDR2*DELR
      GO TO 27
C
   25 DYDR=0
   27 CONTINUE
      X=XLAM*(R(J)**2)
      D2GDR2=CONST*(R(J)*DYDR+Y(J)-2.*XLAM*Y(J)*(R(J)**2))/EXP(X)
C
      IF(J.GT.1)GO TO 28
      DGDR=D2GDR2
      FACT9=DGDR
      GO TO 29
C
   28 CONTINUE
      DGDR=CONST*Y(J)*R(J)/EXP(X)
      FACT9=DGDR/R(J)
C
   29 CONTINUE
      DDGDT(J)=DS*(D2GDR2+FACT9)
      DGDT(J)=DGDT(J)-DDGDT(J)
   24 CONTINUE
C
C     KNOWING THE SURFACTANT CHANGE WITH RADIUS AND TIME,
C     NOW CALCULATE NEW VALUES FOR SURFACE VELOCITIES
C
      DUDR(1)=-DGDT(1)/(2.*GAM(1))
      U(2)=U(1)+DUDR(1)*DELR
C
      DO 22 J=2,N
      DGDR=(GAM(J+1)-GAM(J-1))/(DELR*2.)
      TERM10=U(J)*DGDR
      TERM11=U(J)*GAM(J)/R(J)
      DUDR(J)=(-DGDT(J)-TERM10-TERM11)/GAM(J)
      U(J+1)=U(J)+DUDR(J)*DELR
   22 CONTINUE
C
      TERM10=U(NN)*ENDSLO
      TERM11=U(NN)*GAM(NN)/R(NN)
      DUDR(NN)=(-TERM10-TERM11)/GAM(NN)
C
C     NOW CHECK FOR RECALCULATION OF THE CHANGE IN SHAPE
C     WITH NEW SURFACE VELOCITY COMPONENTS
C     -STORE LAST DYDT VALUES
C
      IF(T.GT.0)GO TO 102
      IF(NCOUNT.GT.1)GO TO 102
      DO 13 J=1,NN
      DYSTOR(J)=DYDT(J)
   13 CONTINUE
      NCOUNT=2
```

```
      GO TO 100
C
  102 CONTINUE
      CONVER=ABS((DYDT(NN)-DYSTOR(NN))/DYDT(NN))
      VALUE=DYSTOR(NN)
      IF(CONVER.LE.TOL)GO TO 101
      NCOUNT=NCOUNT+1
C
      DO 14 J=1,NN
      DYSTOR(J)=DYDT(J)
   14 CONTINUE
C
      IF(NCOUNT.LE.MAX)GO TO 100
C
      PRINT 103,CONVER,VALUE,DYDT(1)
  103 FORMAT(10X,15H NO CONVERGENCE,3E13.5)
      GO TO 104
C
C     CALCULATE THE NEW SHAPE AND CHECK FOR PRINTOUT
C
  101 CONTINUE
C
      DO 15 J=1,NN
      Y(J)=Y(J)+DYDT(J)*DELT
      GAM(J)=GAMT(J)
   15 CONTINUE
C
C     RECALCULATE CENTRE PRESSURE AND PARAMETERS
C
      D2YDR2=2.*(Y(2)-Y(1))/(DELR**2)
      PO=(1./RAD-D2YDR2)*SIG
      XLAM=PI*PO/WG
      RETA=2.*XLAM*PO/VIS
C
      T=T+DELT
      IF(T.GT..5)GO TO 104
      K=K+1
      IF(K.GT.KK)GO TO 105
      NCOUNT=1
      GO TO 100
C
  105 CONTINUE
      PRINT 200,T
  200 FORMAT(10X,6H TIME=,F7.4,///)
C
      PRINT 204,R(1),Y(1)
C
      DO 106 J=2,N2,2
      J1=J+N2
      PRINT 201,R(J),Y(J),R(J1),Y(J1)
  106 CONTINUE
C
      PRINT 203,R(NN),Y(NN)
  203 FORMAT(46X,2(10X,E13.5))
C
      PRINT 202
C
      K=1
```

```
      GO TO 100
C                                                                    402
  104 CONTINUE
      STOP
      END
```

```
C
C     RATE OF FILM THINNING AND DIMPLE FORMATION
C     GIVEN BY COUPLED MODEL-PARALLEL DISC MODEL                    403
C
C     -ARRAY DEFINITIONS
C++++++++++++++++++++++++++++++++++++++++++++++++++++++++++++++++++++++++++++++
C
C     R-RADIAL DISTANCE ARRAY
C     Y-LAMELLA THICKNESS ARRAY
C     U-SURFACE VELOCITY ARRAY
C     GRAV-GRAVITATIONAL CONSTANT
C     VOL-DROP VOLUME
C     RAD-DROP RADIUS
C     SIG-INTERFACIAL TENSION
C     WG-DROP BUOYANCY FORCE
C     VIS-WATER VISCOSITY
C     XK-A CONSTANT
C     XKT-INTERFACIAL TENSION LOWERING
C     K,KK,KN,KNN-COUNTERS
C     N-NUMBER OF RADIAL INTERVALS
C     T-TIME
C     DELT-TIME INTERVAL
C     PO-CENTER LAMELLA PRESSURE
C     YO-CENTER LAMELLA HEIGHT
C     RE-RADIUS WHE-E P=0
C     DELR-RADIAL DISTANCE INCREMENT
C
C++++++++++++++++++++++++++++++++++++++++++++++++++++++++++++++++++++++++++++++
C
      DIMENSION R(101),Y(101)
      DIMENSION U(101)
C
C     CALCULATE CONSTANTS
C
C     TOLUENE/WATER
C
      U(1)=0.
      GRAV=981.
      VOL=.005
      BUOY=.133
      RAD=.1061
      SIG=35.
      PI=3.1416
      WG=VOL*BUOY*GRAV
      K=1
      KK=50
      KN=17
      KNN=0
      VIS=.00894
      XK=1.4E-14
      XKT=.001
      T=0.
      DELT=1.0E-03
C
      PO=1.05*SIG/RAD
      N=100
      NN=N+1
      N2=N/2
      YO=5.0E-05
```

```
C
   21 CONTINUE
      R2=2.*WG/(PI*PO)
      RE=SQRT(R2)
      R4=R2**2
      ETA=4.*WG/(PI*R4)
      A=2.*ETA/(3.*VIS)
      B=(ETA**2)*R2/(3.*VIS*XKT)
      C=-2.*WG/(PI*R4*XKT)
      IF(T.GT.0.)GO TO 20
C
C     CALCULATE RADIUS ARRAY
      DELR=RE/(2.*FLOAT(N))
      R(1)=0
      DO 10 J=1,N
      R(J+1)=R(J)+DELR
   10 CONTINUE
C
C     CALCULATE THE INITIAL SHAPE
C
      CON1=1./(2.*RAD)-PO/(2.*SIG)
      CON2=PO/(8.*S+G*R2)
      Y(1)=YO
      DO 11 J=2,NN
      R22=R(J)**2
      Y(J)=YO+CON1*R22+CON2*(R22**2)
   11 CONTINUE
C
C     LOCATE THE BARRIER RING
C
   20 CONTINUE
      DO 12 J=1,N
      IF(Y(J+1).GT.Y(J))GO TO 13
   12 CONTINUE
C
   13 CONTINUE
      IF(J.LE.1)GO TO 14
      IF(J.GE.NN)GO TO 14
      GO TO 15
C
   14 CONTINUE
      PRINT 100,J
  100 FORMAT(10X,11H MINIMUM J=,I5)
      GO TO 200
C
C     CALCULATE CHANGE AT THE BARRIER RING
C
   15 CONTINUE
      KJ=J
      STOREH=Y(KJ)
C
C    CALCULATE THE SURFACE VELOCITY DISTRIBUTION
C
      FACT1=ETA*R2*(STOREH**2)
      FACT2=2.*XKT*STOREH
      FACT3=3.*VIS
      FACT4=ETA*(STOREH**2)
      FACT5=STOREH*ETA/(2.*XKT)
```

```
      DO 23 M=2,NN
      FACT6=1./EXP(FACT5*(R(M)**2))
      FACT7=1.-FACT6
      U1=-FACT7*(FACT1+FACT2)/(FACT3*R(M))
      U2=FACT4*R(M)/FACT3
      U(M)=U1+U2
   23 CONTINUE
C
      IF(T.LE.0.)GO TO 26
      GO TO 27
C
   26 CONTINUE
      DO 28 J=2,N2
      J1=J+N2
      PRINT 103,R(J),Y(J),R(J1),Y(J1)
   28 CONTINUE
C
      PRINT 104,R(NN),Y(NN)
C
   27 CONTINUE
C
      CC=C*(R(KJ)**2)
      FUNC1=EXP(Y(KJ)*CC)
      FUNC2=FUNC1-2.
      DHDT=A*FUNC2*(Y(KJ)**3)+B*FUNC1*(Y(KJ)**4)
      Y(KJ)=Y(KJ)+DHDT*DELT
C
C     CALCULATE CHANGES AT REMAINING POINTS
C
      XH3=STOREH**3
      XH4=STOREH**4
      DO 16 J=1,NN
      IF(J.EQ.KJ)GO TO 16
      CC=C*(R(J)**2)
      FUNC1=EXP(CC*Y(J))
      FUNC2=FUNC1-2.
      DHDT=A*FUNC2*XH3+B*FUNC1*XH4
      Y(J)=Y(J)+DHDT*DELT
   16 CONTINUE
C
      T=T+DELT
      K=K+1
      IF(K.GT.KK)GO TO 17
      GO TO 18
C
C     PRINTOUT
C
   17 CONTINUE
C
      KNN=KNN+1
      K=1
      IF(KNN.GE.KN)GO TO 25
      GO TO 18
C
   25 CONTINUE
      KNN=0
      KN=14
      PRINT 106,PC
```

```
  106 FORMAT(10X,10H PRESSURE=,E13.5,//)
      PRINT 101,T
  101 FORMAT(//,10X,6H TIME=,E13.5,//)
  103 FORMAT(4(10X,E13.5))
  104 FORMAT(46X,2(10X,E13.5))
  105 FORMAT(1H1)
C
C
      DO 24 J=2,N2
      J1=J+N2
      PRINT 103,R(J),Y(J),R(J1),Y(J1)
   24 CONTINUE
C
      PRINT 104,R(NN),Y(NN)
      PRINT 105
C
   18 CONTINUE
      IF(T.GT.1.55)GO TO 200
      GO TO 21
C
  200 CONTINUE
      STOP
      END
```

APPENDIX A3. EXPERIMENTAL DETAIL

A3 Experimental Detail

More experimental detail is given in this appendix to aid the understanding of the experimental techniques used in this work.

A3.1 Finding Lamella Thickness from the Light Interference Colour

An equation is derived to relate the lamella thickness to the observed light interference colour. This derivation shows the theory required to understand the mechanics of light interference. The photographic aspects are then detailed.

A3.1-1 Theory of Light Interference

Consider Figure (A3.1). What colour of light will an observer at X see when white light is reflected off a lamella of thickness d? To answer this question, reference is made to a derivation given by Vasicek, (1960). When light reaches a surface where there is a change in refractive index in going from medium 1 to medium 2, a fraction of the incident light, AB, is reflected along the path BC. This fraction for normally incident light reflected is given by Fresnel's Law:

$$f = \frac{(n_1 - n_2)^2}{(n_1 + n_2)^2}$$

where n_1, n_2 are the refractive indices of media 1 and 2, respectively, the remainder of the light follows path BD to the second surface where a fraction of this light is reflected along DE to the first surface. Some light is reflected back

Figure A3.1 Geometry of Light Interference

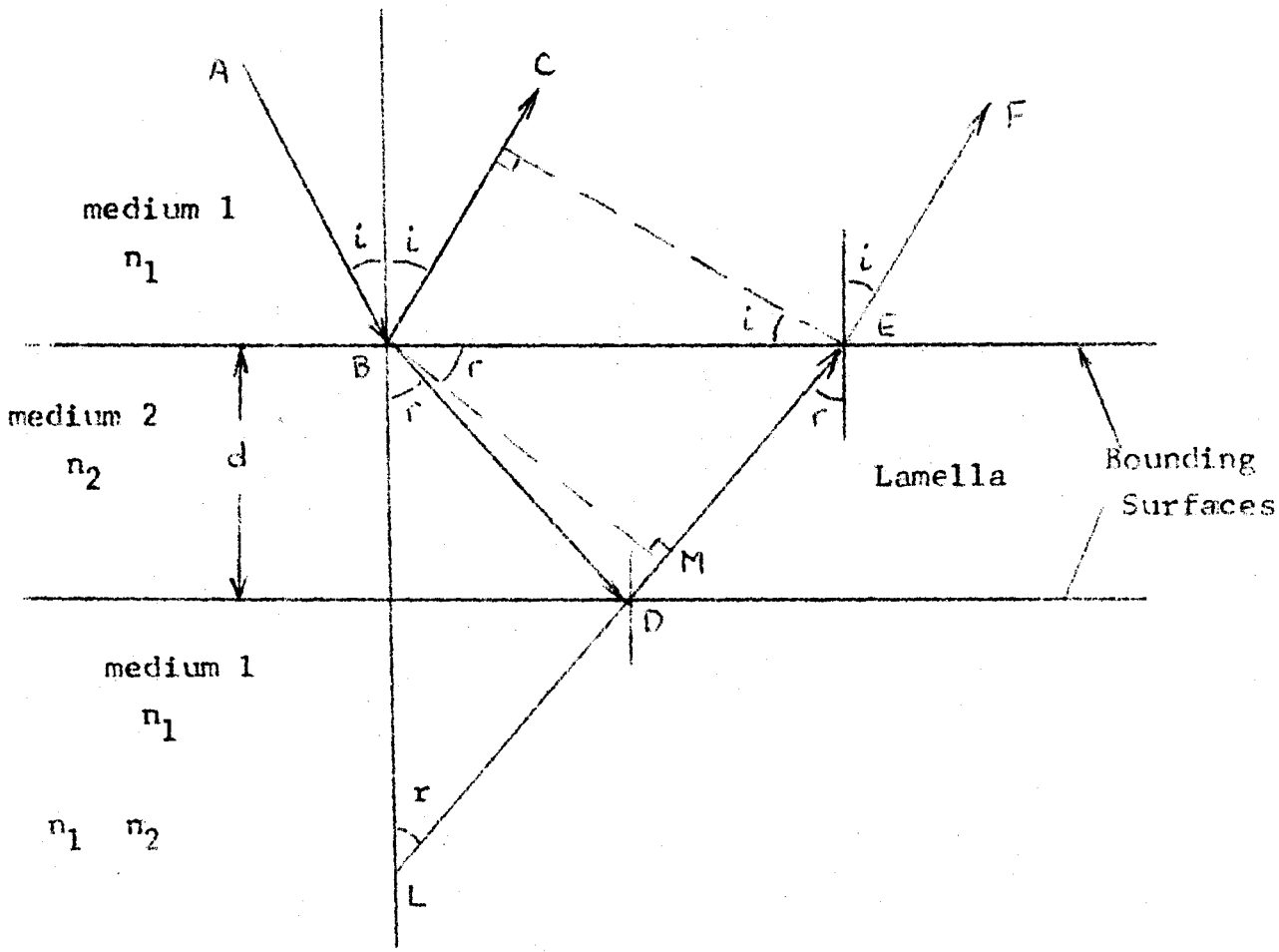

into the lamella, but the majority continues along path EF. An observer at X will see a mixture of light made up of rays BC and EF. Since light ray EF has traversed the lamella twice, we expect rays BP and EF to either constructively or destructively interfere with each other.

The geometrical path difference is given by BD + DE - BP = LM + ME - BP. A problem arises, however, since the velocity of light in medium 1 is different from that in medium 2. The time to travel LM + ME in medium 2 is

$$\frac{LM + ME}{v_2} \quad \text{seconds}$$

and to travel BP in medium 1 is

$$\frac{BP}{v_1} \quad \text{seconds}$$

where v_1, v_2 are the velocities of light in media 1 and 2, respectively. If the wave length of one segment of the light spectrum is λ_o in a vacuum, and velocity is v_0, we know that since $\frac{\lambda_o}{v_0}$ = frequency, then λ_2 must be smaller than λ_o since $v_2 < v_0$, and the frequency remains constant, independent of the medium.

Now then, light in medium 2 will travel a distance:

$$\frac{(LM + ME)/v_2}{\lambda_2/v_2} = \frac{LM + ME}{\lambda_2} \quad \text{wavelength}$$

and in medium 1, will traverse:

$$BP/\lambda_1 \quad \text{wavelength}$$

since, $n_1 = \frac{v_o}{v_1}$, $n_2 = \frac{v_o}{v_2}$

then, $n_1 = \frac{\lambda_o}{\lambda_1}$, $n_2 = \frac{\lambda_o}{\lambda_2}$

therefore, light in medium 2 will traverse:

$$\frac{n_2}{\lambda_o} \text{ (LM + ME) of a wavelength}$$

and in medium 1:

$$\frac{n_1}{\lambda_o} \text{ (BP) of a wavelength}$$

The difference in wavelengths travelled between the rays at P and E is therefore:

$$\frac{n_2}{\lambda_o} \text{ (LM + ME)} - n_1 \frac{BP}{\lambda_o}$$

or

$$\frac{n_2}{n_1 \lambda_1} \text{ (LM + ME)} - \frac{BP}{\lambda_1}$$

Now, since $\sin(i) = \frac{BP}{EB}$

and $\sin(r) = \frac{ME}{EB}$

and since the ratio $\frac{\sin(i)}{\sin(r)} = \frac{BP}{ME}$

is also the ratio of refractive indices as given by Snell's Law of Refraction:

$$\frac{\sin(i)}{\sin(r)} = \frac{n_2}{n_1} = \mu_{21}$$

Then: $$\frac{BP}{ME} = \frac{n_2}{n_1} = \mu_{21}$$

and so: $$\frac{1}{\lambda_1}\left(\frac{BP}{ME}\right)(LM + ME) \quad \frac{-BP}{\lambda_1} = \frac{1}{\lambda_1} \quad \frac{n_2}{n_1} \quad (LM)$$

By trigonometry, LM = 2d cos (r), so the difference in wavelength at P and E is just

$$\frac{2d}{\lambda_1} \quad \frac{n_2}{n_1} \quad \cos\ (r)$$

When light reflects off a surface because of a change in refractive index between two media separated by that surface, there is a change in phase of one-half wavelength. This is true only if the light will pass into a more optically dense medium (larger refractive index). Therefore, the rays at P and E will be different in phase by the phase change $\frac{\lambda_1}{2}$ and by the path difference. The light intensity is a maximum for the observer at X when the phase change is just balanced by the difference in path across the lamella. This condition is then:

$$\frac{2d}{\lambda_1} \quad \frac{n_2}{n_1} \quad \cos\ (r) \quad = \quad \frac{1}{2}$$

and since the maximum also occurs for an even number of half wave-lengths k :

$$2\ \mu_{21}\ d \quad \cos(r) - \frac{\lambda_1}{2} \quad = \quad k \quad \frac{\lambda_1}{2} \qquad \ldots.(1)$$

This derivation yields a working equation which can be used to calculate d if all other parameters are known.

If cos (r) $\doteqdot$ 1.0 and j = k + 1, then equation (1) becomes:

$$\mu_{21}\, d = \frac{j\lambda_1}{4} \qquad \ldots.(2)$$

A maximum in intensity occurs at X for j = 1, 3, 5.... and a minimum for j = 2, 4, 6.... . To calculate the expected interference colour for lamella thickness d, consider first the table of wavelengths for different segments of the visible light spectrum, Table (A3.1).

For a soap film in air:

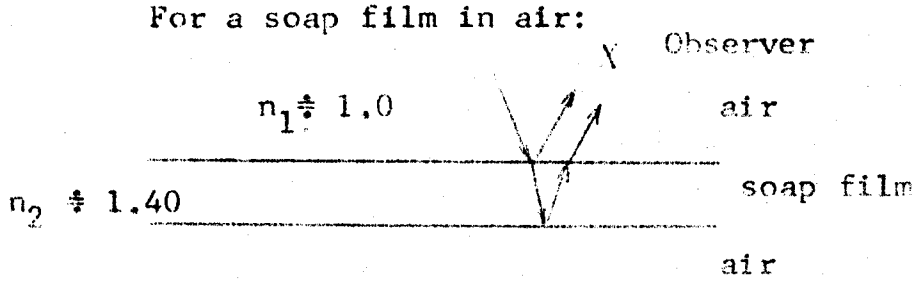

By employing equation (2), a table of maxima and minima for various wavelengths may be constructed. Results are summarized in Table (A3-2). This table shows that for a soap film thickness of 715-1250 Å, the five components of white light all run through their maximum in intensity. While theoretically the lamella should take on each individual colour, experiments indicate that only white light is observed. In the range 1430-1970 Å, violet, blue, and green run through their minimum. At d = 2140 Å, yellow is at a minimum, but violet is at a maximum, so the lamella appears violet in colour. This is observed. Again, it is not apparent what colour the lamella should appear, in the range 1430-1970 Å. Experimentally, the

Table A3.1 Light Wave-Length versus Colour

Colour	Wave-Length in vacuum, λ_o A°	
	Range	Nominal Value
Violet	4000 to 4300	4000
Blue	4300 to 4900	4500
Green	4900 to 5700	5500
Yellow	5700 to 6050	6000
Red	6050 to 8000	7000

Table A3.2 Maxima and Minima for Various Wave-Lengths

$$d = \frac{j\ \lambda_o}{1.40 \times 4}$$

j- odd, maximum
j- even, minimum

d = soap film thickness for a maximum or minimum

j	Violet 4000 A° A°	Blue 4500 A° A°	Green 5500 A° A°	Yellow 6000 A° A°	Red 7000 A° A°
1	715	820	980	1070	1250
2	1430	1600	1970	2140	2500
3	2140	2420	2950	3210	3750
4	2860	3220	3930	4290	5000
5	3580	4020	4910	5350	6250
6	4300	4830	5890	6430	7500
7	5000	5640	6870	7500	8750

$\mu_{21} = 1.40$

lamella appears a yellow-red colour, and then a violet-red. However, when j = 3, the colours seen should be, in increasing order of thickness: violet, blue, green, yellow, and red. This is observed, and makes up the "second order" of interference colours. The third order should be blue, green, yellow, and red, for j = 5. These calculations may be continued to produce a table of lamella interference colour versus lamella thickness. A table for a water lamella (n_2 = 1.33) surrounded by oil (n_1 = 1.50) may be calculated from the table given by Lawrence (1929) on page 137 by noting $n_1\lambda_1 = \lambda_0$, and so equation (2) is written:

$$n_2 \, d = j\frac{\lambda_0}{4}$$

For the same $j\frac{\lambda_0}{4}$ (same interference colour),

$$1.40 \, d_1 = 1.33 \, d_2$$

So the values of d_2 in Table (A3-3) are calculated from Lawrence's soap film thickness by $\times\frac{1.40}{1.33}$. The first four orders show many variations in interference colour which appear to be washed out as the lamella thickness increases. Eventually, at large lamella thicknesses, the red and green colours predominate.

A3.1-2 Photographic Details

A Bolex 16 mm. movie camera with electric motor was used with Kodak Ektachrome EF colour film to record the changing light interference patterns. Illumination was with a 30 watt Galileo light source adapted to the Olympus Model MR Metallurgical

Table A3.3 Interference Colour Versus Water Lamella Thickness

Colour	Thickness(A°)	Colour	Thickness (A°)
1st order		4th order	
black	100	grass green	6290
white	1000	green	6680
amber	1580	yellow green	7180
magenta	2120	carmine	7850
2nd order		5th order	
violet	2280		
blue	2640	green	8320-8860
green	3050	pink	9400-9950
yellow	3400		
orange	3660	6th order	
crimson	3910		
		green	10,500-11,000
3rd order		pink	11,600-12,100
purple	4170	7th order	
blue	4330		
blue	4500	green	12,750-13,000
emerald green	4900	pink	13,850-14,400
yellow green	5300	8th order	
carmine	5700	green	15000
bluish red	6090	pink	15800

Microscope. No lens was used on the camera. The camera was positioned over the empty vertical tube of the microscope and only the 10X microscope objective lens was used to focus the interference pattern on the film. Camera speeds of 16-32 pictures per second (p.p.s.) were adequate to capture the rapidly changing interference pattern.

A Hycam high speed 16mm. movie camera was also used to record the rapid approach of the drop to the interface for one set of experimental conditions. When a 100 watt quartz iodide projector bulb was used as the light source, frame rates of 300 p.p.s. could be used with Kodak Ektachrome EF.

Film was analyzed using a Kodak 16 mm. Analyzer projector. When projected at a lens-to-screen distance of 88 inches, a photograph of a graduated 1 mm. scale gave a magnification of 625X. This was sufficiently large to enable accurate measurements of lamella shape to be made.

Bolex camera frame rates were checked by photographing an electric Cenco timer. Results are summarized in Table (A3-4). Data given in Chapter 4 for change in lamella shape with time are corrected for this difference in nominal frame rates.

A3.2 Light Intensity Measurements

By employing the relationship of relative light intensity to lamella thickness given in Chapter 3, the colour movies could be used with a light intensity meter to measure the lamella thickness at rupture. The schematic diagram for

Table A3.4 Bolex Camera Calibration

Nominal Camera Speed pps	Measured Camera Speed pps
16	-
24	20
32	28

Figure A3.2 Schematic Diagram for the Light Intensity Meter

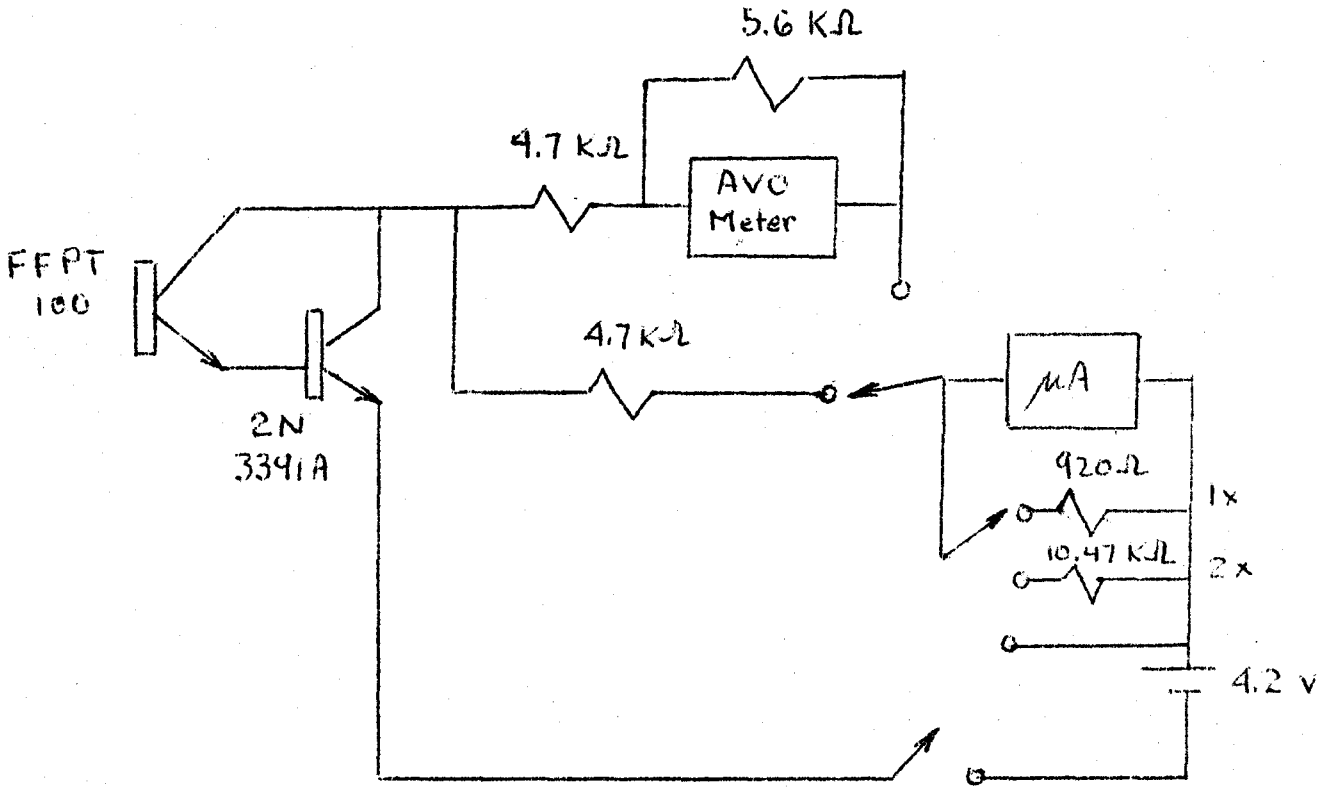

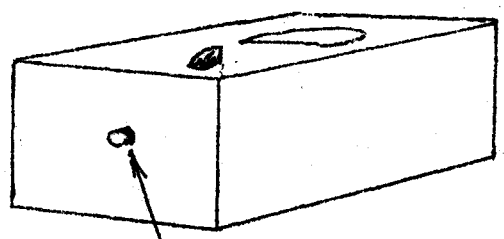

Perspective

Photo-transistor protrudes slighty from the box.

such a meter is given in Figure (A3-2).

A small (2mm. dia.) phototransistor was used with a current amplifying transistor to drive a microammeter or an A.V.O. meter on the ammeter scale. To record meter output, a small resistor was used in place of the A.V.O. meter, and the voltage drop across the resistor measured using a Honeywell strip chart recorder.

A small hole was placed in a white Bristol-board screen and the phototransistor put through the hole from behind the screen. A 5 mm. long black plastic tube was placed around the phototransistor so that only light normal to the screen reached the phototransistor. By projecting the film at about 1-4 p.p.s. in a completely dark room at a lens to screen distance of about 100 inches, the recorder pen traced out the voltage reading versus time. A typical trace is shown in Figure (A3-3).

The maximum voltage is taken as proportional to I_0. This intensity is assumed to be produced by white light given off at the lamella thickness of 1000 $\mathring{A}$. Knowing the voltage at rupture, equation (4) in Chapter 3 is used to calculate lamella thickness at rupture. For the sample data given in Figure (A3-3), rupture occurs at about 330 $\mathring{A}$. Curves of minimum lamella thickness versus elapsed time of the drop at the interface may also be obtained right down to rupture. Much of the time the drop is at the interface, the minimum lamella thickness is lessthan 1000 $\mathring{A}$ and thicknesses cannot be accurately

Figure A3.3 Typical Trace of Light Intensity Meter

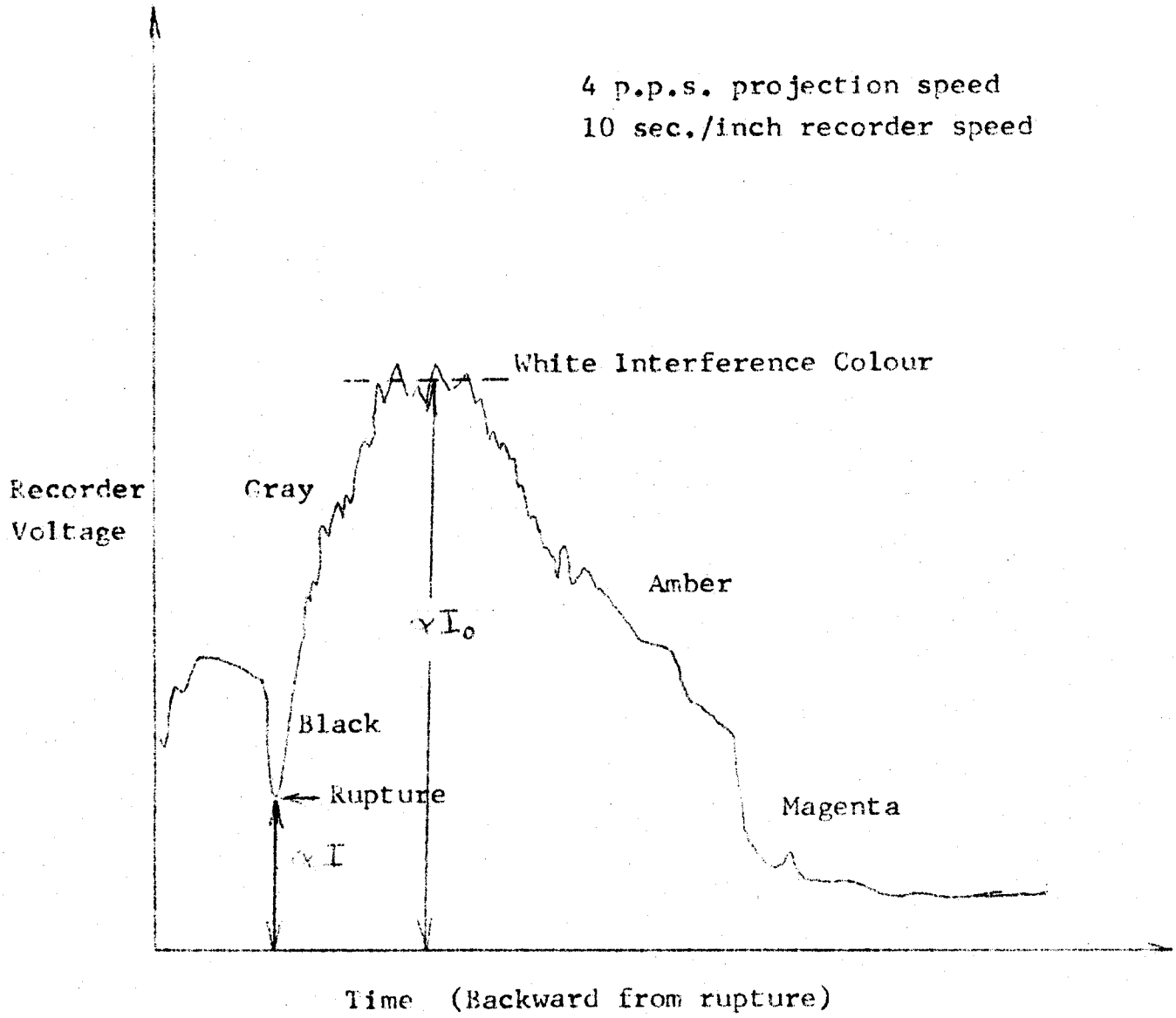

determined by any means other than light intensity measurements.

One major difficulty ensues with this technique. Previously, investigators have mounted a photo-multiplier tube directly in the light interference equipment and taken in situ measurements in the black region. These workers appeared to work, however, with lamellae whose entire thickness was in the black region. For the present work, the black region extended over a width of less than 20μ, and even when magnified 10X by the microscope objective, this region is far too small to be used with a 2 mm. diameter phototransistor. Thus the interference colour must be recorded on film. The difficulty is in not being able to accurately reproduce on a screen the light intensity produced by the lamella in the coalescence cell. For example, there is obviously a limit to the "blackness" of the dye on a clear celluloid film base, and just by increasing the projector bulb voltage, the black region on the film can be made translucent. Part of the answer lies in photographing a black object and requiring the light intensity meter to register zero current. A developed strip of unexposed colour film duplicated this condition of zero light and the meter did not register current. Therefore, for the experimental conditions used in this work, film translucence isn't a problem. Another part of the problem is that the light intensity produced by the lamella in the coalescence cell is not just due to lamella thickness, but also due to reflected light from the cell components. This is background light. Background light could not

be measured, because one of the prime causes of reflected light is the drop itself.

Therefore, the extent to which the light intensity method used in this work is capable of accurately determining lamella thickness at rupture depends upon seemingly unmeasurable factors. The influence of these factors must still be determined before the results of the light intensity method used in this work can be accepted.

One final point concerns the linearity of the light intensity meter. Ohm's Law holds for voltage drop generated by a current passing through a constant resistance, so it is assumed that the voltage-current relationship is linear. However, as the light intensity falling on the phototransistor is increased, a linear relationship must be proven between phototransistor current and light intensity.

A simple approach was taken to this problem. In photography, for film exposure times greater than approximately 0.001 second, the reciprocity law holds. This law says that the product of light intensity and film exposure time must be a constant, once a reference exposure is established. For example, halving the exposure time means light intensity must by doubled to still achieve proper exposure of the light-sensitive film emulsion.

Based on this line of argument, an Asahi Pentax Spotmeter was used to calibrate the light intensity meter. Results are given in Figure (A3-4). The abscissa shows the

Figure A3.4 Light Intensity Meter Calibration

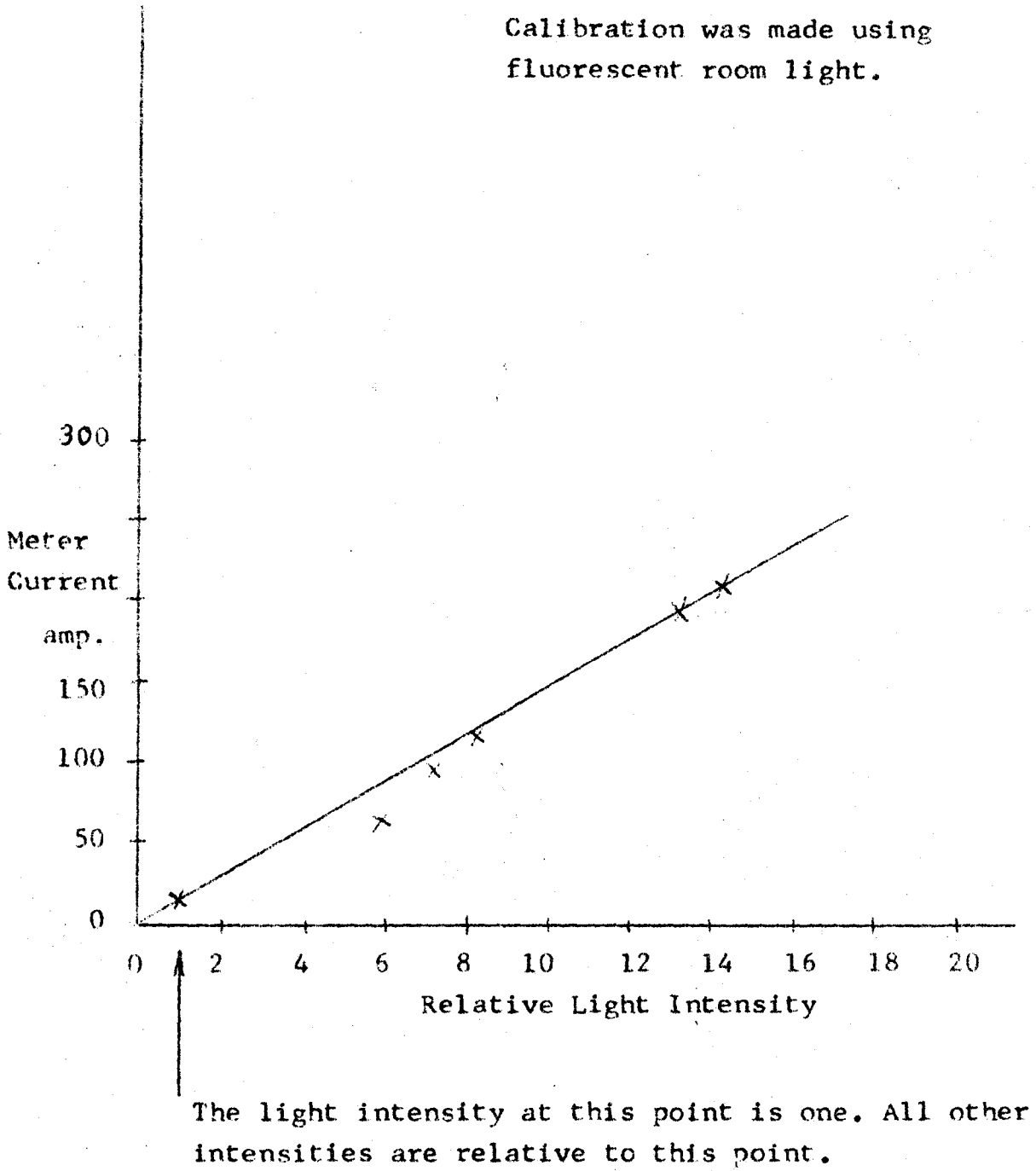

multiple increase in light intensity based on an arbitrary reference of the minimum intensity observed. This calibration is linear, i.e.:

$$\text{current} = k \times \text{Intensity}$$

where k is a constant.

APPENDIX A4. PHYSICAL PROPERTY DETERMINATION

A4. Physical Property Determination

The two most important physical properties, as they affect coalescence, were measured and are compared with the literature values, where possible, in Tables (A4-I, 2). Since literature temperatures and the temperature at which the properties were measured in this work (25°C) are different, no conclusions on the agreement can be made.

For the sake of completeness, the data in Tables (A4-I, 2) are accompanied by the procedures used in their determination.

A4.1 Density Difference

Although the standard 1 or 2 ml. pycknometer bottle may yield specific gravities with a reasonable degree of accuracy, subtraction of two densities obtained for an oil and water, for example, yields a small difference with a large error. Therefore, standard glass 50 ml. volumetric flasks with ground glass stoppers were used to increase the magnitude of the weight difference between an oil and water, and hence decrease the relative error.

The procedure for obtaining the desired density difference is straight-forward. A flask is weighed empty, and weighed completely full of either water or the oil used. The weights of each liquid for the same volume may then be divided to give a specific gravity. By knowing the liquid temperature (25°C $\pm$0.5°C) and the density of water at 25°C, the density of the oil for the same volume may be calculated

Table A4.1 Experimentally Determined Density Differences

25° C.

Oil/Water System	$\Delta\rho$ gram/ml.	Approx. Error	% Error	Literature Values
Toluene/Water	0.136	$\pm$0.001	$\pm$0.7	$0.133^{20°C}$
Anisole/Water	0.0097	$\pm$0.0002	$\pm$2.0	$0.00645^{20°C}$
Cyclohexanol/ Water	0.051	$\pm$0.0004	$\pm$0.8	-
CA/Water	0.053	$\pm$0.0004	$\pm$0.8	-

Notes on Table A4.1

1.) CA is 0.84 mole fraction anisole and 0.16 m.f. cyclohexane.

2.) The oil and the water are mutually saturated.

3.) The experimental error is determined from two separate weighings. This error is approximate only.

4.) The literature value for the anisole/water system is from the International Critical Tables, at the superscripted temperature indicated.

5.) The value for the toluene/water system is found by taking the difference of pure densities at 20°C., as given by the Handbook of Physics and Chemistry.

Table A4.2 Experimentally Determined Interfacial Tensions

25° C.

Oil/Water System	γ dyne/cm.	Approx. Error	% Error	Literature Values
Toluene/Water	35.0	± 0.5	± 1.6	$36.1^{25°C}$
Anisole/Water	20.5	± 1.3	± 6.5	$25.82^{20°C}$
Cyclohexanol/ Water	3.93	± 0.09	± 2.4	$3.92^{16.2°C}$
CA/Water	28.9	± 0.72	± 2.5	--

1.) The oil and water are mutually saturated.

2.) The literature values were measured at the superscripted temperature indicated. Values are from the International Critical Tables.

3.) For this work, the surface tension of pure water in air at 25°C was = 71.13 ± 0.92 dynes/cm. The air was not saturated with water vapour.

from the specific gravity. This entire procedure was repeated once more and the resulting density difference was averaged with the first to yield the value given in Table (A4-1). The experimental error in Table (A4-I) is the difference between the two density difference measurements, and is only an approximate measure of the experimental error.

A4.2 Interfacial Tension

Figure (A4-1) shows the apparatus used to measure interfacial tension. It is based on the design used by Hodgson (1966).

The principle upon which the apparatus is based is very simple. When the net weight of liquid in a drop formed on the end of a smooth ground-glass capillary tip exceeds the surface tension force holding the drop to the tip, the drop separates from the tip at the point of minimum cross-sectional area. The volume of the drop may be easily measured, and if the liquid/liquid system density difference is known, the surface tension may be calculated. This method is called the drop-volume approach.

The steps involved in an interfacial tension measurement are:

1.) Fill the glass apparatus with water (since water will wet the clean glass capillary tip in preference to oil), and fill the flask partially full of oil. When the flask is wedged on the rubber stopper, the capillary tip should be submerged in the oil.

Figure A4.1 Interfacial Tension Apparatus

after Hodgson (1966)

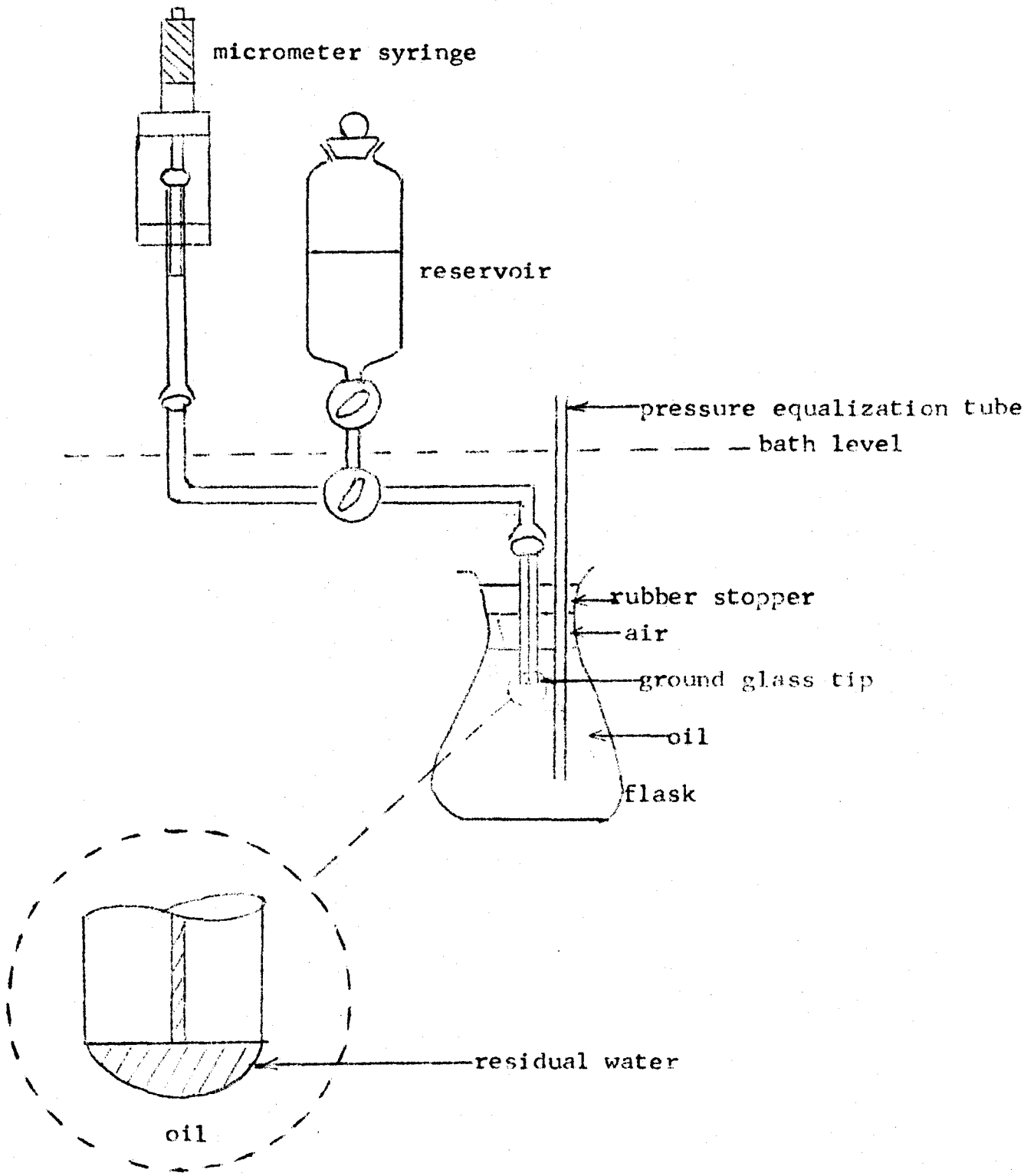

2.) Water is forced into the capillary by the syringe to form the first drop. This drop is slowly forced off the tip.

3.) There are two ways of proceeding from this point. If the "residual water" shown in Figure (A4-1) is sucked back into the capillary so that oil wets the capillary tip, then the volume of each drop when it falls off the tip may be determined. Another method is to assume that the volume of the "residual water" on the tip remains constant. This was the method used. This latter method was necessary since small oil drops often would remain on the tip when the residual water was sucked back into the capillary and a new drop formed. When a new drop is formed, the oil drops prevent the water from wetting the tip and may interfere with the drop weight/interfacial tension force balance.

4.) To calculate the surface tension, several measurements are made of the drop volume and an average taken. The surface tension is calculated for both the mean volume and the volume falling farthest from the mean. This defines the experimental error as employed in this appendix.

The following equation is used to calculate the interfacial tension once drop weight is known:

$$\gamma = \frac{Wg}{2\ rf\left(\frac{r}{\sqrt[1/3]{V}}\right)}$$

where $f\left(\frac{r}{\sqrt[1/3]{V}}\right)$ is a correction factor presented by W. D. Harkins (1952).

Wg is drop buoyancy force

r is capillary tip radious

γ is interfacial tension

V is drop volume

Bibliography for Appendices

Harkins, W. D., "The Physical Chemistry of Surface Films", Reinhold, New York (1952) pg. 76-77.

Hodgson, T. D., Ph.D. Thesis, Swansea (1966).

Lawrence, A. C. S., "Soap Films", Bell, London (1929).

Vasicek, A., "Optics of Thin Films", North Holland Pub., Amsterdam (1960).

Thomas, G.B., "Calculus and Analytic Geometry", Addison-Wesley, Reading (1960).